Cranfield University

Konstantinos I. Tifkitsis

Simulation and monitoring in composites manufacture under uncertainty

School of Aerospace, Transport and Manufacturing

PhD
Academic Years: 2015 - 2018

Supervisor: Dr Alex Skordos
January 2019

Cranfield University

Konstantinos I. Tifkitsis

Simulation and monitoring in composites manufacture under uncertainty

School of Aerospace, Transport and Manufacturing

PhD
Academic Years: 2015 - 2018

Supervisor: Dr Alex Skordos
January 2019

Abstract

This study focuses on the development of an inversion procedure based on Markov Chain Monte Carlo (MCMC) integrating composites process monitoring with simulation to provide real time probabilistic estimations of process outcomes. The simulation incorporates material and boundary condition uncertainty. Quantification of resin viscosity uncertainty showed a variability of 30% in initial values, introducing variations of an equivalent magnitude in the filling stage of Liquid Composite Moulding (LCM). A surrogate model based on Kriging was developed to enable the use of process models iteratively within a stochastic simulation or optimisation loop. The Kriging model reduces run times by 99% compared to finite element simulation, introducing only an error below 2%. A dielectric sensor appropriate for flow and cure monitoring in the presence carbon reinforcement was developed overcoming limitations of electrical sorting and interference with the electric field. The sensor functionality was demonstrated in both flow and cure LCM trials. Real time flow monitoring was integrated with simulation into an inverse algorithm achieving on line estimation of unknown variables and of the resulting flow field with an error lower than 5%, compared to visual measurements. The inversion was also used in curing, by combining thermal monitoring with simulation to identify the thermal conductivity and heat transfer coefficient probabilistically, leading to estimation of cure duration and final degree of cure with an error below 1%. A stochastic multi-objective optimisation methodology has been developed as a first step towards model based stochastic control of composite manufacturing. The method, which is based on Genetic Algorithms (GA), is capable of identifying process settings that optimise process objectives and their variance. In the case of cure of thick composites, the optimisation identifies cure profiles which achieve 40% reduction in temperature overshoot and process duration compared to standard profiles, whilst achieving increased process robustness through minimisation of the variance.

Keywords: Thermosetting composites; Liquid Composite Moulding; Inverse problems; Stochastic simulation; Markov Chain Monte Carlo; Uncertainty quantification; Dielectric monitoring; Surrogate model; Cure; Filling.

"Και όταν η ψυχή σού μιλά, καλύτερα εσύ να σιωπάς. και σκύψε όσο μπορείς να την ακούσεις, γιατί η φωνή της είναι πάντα ψίθυρος, για να μην ενοχλεί την επιθυμία σου"

Άγιος Σιλουανός ο Αθωνίτης

Acknowledgements

I am deeply grateful to my supervisor Dr Alex Skordos for his technical and moral support, guidance, patience and continuous effort to improve this piece of work. I would like to thank Mr Jim Hurley for the technical assistance that made part of the experimental work possible. I would also like to thank Assistant Professor Anestis Kalfas for giving me the opportunity to study at Cranfield University.

I would like to express my gratitude to Charoula for her limitless patience, encouragement and moral support.

I am grateful for my parents Ioannis and Marianthi and my sisters Chrysoula, Zacharoula and Olymbia for their continuous moral support and inspiration.

I am very grateful for my good friend and housemate Stavros for his moral support and continuous encouragement for the last three years. He was always giving me the motivation to push myself and withstand the arisen difficulties.

I would especially like to thank my old friends Kleanthis, Minos and Alexandros for their constant support in every step in my life.

I also sincerely thank my colleagues and friends Giacomo and Tasso for their valuable contributions and for their willingness to share their knowledge and expertise.

I would especially like to thank my friends Thanasis Pouchias, Alexandros Chasoglou, Konstantinos Arvanitopoulos, Maria Kazakou, Nikos Polyzos, Mavroudis Kavvalos, Dimitris, Gabrielle, Kostas Magkoutas, Sotirios Theodorou, and Panagiotis Tsiftsidis for their constant encouragement and moral support.

Table of Contents

List of Tables

List of Figures

Notation

A. Nomenclature

A_1	Pre-exponential factor of the nth order term
A_2	Pre-exponential factor of the autocatalytic term
A_d	Pre-exponential factor of diffusion
A_{cfc_p}	Carbon fibre specific heat capacity model slope
A_e	Constant phase element coefficient
A_{gfc_p}	Glass fibre specific heat capacity model slope
A_{rc_p}	Resin specific heat capacity model slope
AS	Artificial sensor response
A_h	Heat transfer coefficient level variability
A_t	Tool temperature level variability
b	Exponent of diffusion term
B_{cfc_p}	Carbon fibre specific heat capacity model intercept
B_{gfc_p}	Glass fibre specific heat capacity model intercept
B_{rc_p}	Resin specific heat capacity model intercept
B_{tcf}	Carbon fibre transverse thermal conductivity
B_{tgf}	Glass fibre transverse thermal conductivity
B_h	Heat transfer coefficient volatility
B_{ti}	Tool temperature amplitude of cosinusoidal fit
c_p	Composite specific heat capacity
C_{rc_p}	Resin specific heat capacity model step breadth parameter
C_{sd}	Dipolar relaxation capacitance
C_{id}	Induced dipoles capacitance
CM	Heat flux sensor calibration multiplier
d	Distance between sampling and untrained points
$\mathbf{d}$	Spatial coordinates of heat transfer model boundaries
D	Temperature dependence coefficient
D	Heat transfer model boundary model

E	Activation energy of Arrhenius function
E_1	Activation energy of the nth order term
E_2	Activation energy of the autocatalytic term
E_d	Activation energy of diffusion
f_v	Equilibrium free volume
f	Regression model basis function
g	Equilibrium free volume model intercept
h	Surface heat transfer coefficient
H	Heat flux sensor output
H_{tot}	Total enthalpy of the curing reaction
$\mathbf{K}$	Thermal conductivity tensor
$\boldsymbol{\varkappa}$	Permeability tensor
K_{33}	Composite thermal conductivity in transverse direction
K_{Ri}	Equivalent race tracking permeability
K_1	Longitudinal permeability
K_2	Transverse permeability
K_x	Preform permeability in x direction
K_y	Preform permeability in y direction
k_5	Resin thermal conductivity model quadratic coupling coefficient
k_4	Resin thermal conductivity model coupling constant
k_3	Resin thermal conductivity model linear temperature coefficient
k_2	Resin thermal conductivity model quadratic conversion coefficient
k_1	Resin thermal conductivity model linear conversion coefficient
k	Resin thermal conductivity model intercept
k_{tot}	Total number of data batches
k_{lag}	Autocorrelation structure lag
L	Length of the lineal dielectric sensor
L_w	Sensor length covered with resin
m	Autocatalytic reaction order
M	Total number of MCMC iterations
N_k	Total number of process monitoring data

N_{η}	Total number of rheology data
N_{exp}	Tool temperature experimental data
N_{MC}	MC realisations
N	Number of initial sampling points
$\mathbf{n_{sv}}$	Surface vector of heat transfer model
n	Surrogate model dimensionality
n_{CPE}	Constant phase element order coefficient
n_{ch}	Number of parallel chains
n_p	Number of unknown stochastic parameters
n_s	MCMC iterations for swap algorithm initiation
n_1	Reaction order of the nth order term
n_2	Reaction order of the autocatalytic term
P	Pressure gradient
$\dot{Q}$	Heat flux
q	Prescribed heat flux
r	Cross-correlation vector
r	Heat ramp rate
$r_{k_{lag}}$	Autocorrelation function
R	Correlation matrix of unknown point and sampling points
$\boldsymbol{\mathcal{R}}$	Correlation matrix of sampling points
R_{sd}	Dipolar relaxation resistance
R_m	Migration charges resistance
S_{OU}	OU process
S	Lineal dielectric sensor response
S	Initial sample matrix
$\mathbf{s_x}$	Sampling points input matrix
$\mathbf{s_y}$	Sampling points responses matrix
t	Time
t_{cure}	Cure duration
t_{fill}	Filling duration
T	Temperature

T_{air}	Air temperature in the oven
T_b	Prescribed temperature
T_g	Glass transition temperature
T_{g0}	Glass transition temperature of uncured material
$T_{g\infty}$	Glass transition temperature of fully cured material
T_{mid}	Temperature at mid-thickness
TM	Heat flux sensor temperature multiplication factor
T_{ref}	Temperature reference
T_s	Surface temperature
T_{top}	Temperature at the top surface
T_{pt}	Parallel tempering temperature parameter
T_∞	Temperature at the convection boundary
v_f	Fibre volume fraction
$\mathbf{v_{fl}}$	Darcy velocity
$\mathbf{V}$	MCMC proposed sample vector
$\mathbf{x}$	Surrogate model input vector
w	Equilibrium free volume model slope
W_t	Brownian motion
$\mathbf{y}$	Tool temperature experimental response
y_h	Standard normal variable
y_w	Admittance per unit length of wetted part of the lineal sensor
y_{wg}	Admittance per unit length of filled gaps of the lineal sensor
y_{dg}	Admittance per unit length of dry gaps of the lineal sensor
y_c	Admittance per unit length of the sensor coating of the lineal sensor
y_d	Admittance per unit length of the dry part of the lineal sensor
y_w	Admittance per unit length of the wetted part of the lineal sensor
$\mathbf{Y_{exp}}$	Process monitoring matrix
Y_m	Surrogate model response
Y	Measured admittance
Y_o	Admittance of the dry sensor

z	Parallel tempering parameter
$Z^{"}$	Imaginary impedance
$Z^{"}_{m}$	Material imaginary impedance

Greek symbols

a	Acceptance criterion
α	Degree of cure
α_0	Initial degree of cure
α_{fmin}	Final minimum degree of cure
$\boldsymbol{\beta}$	Regression parameters vector
$\boldsymbol{\gamma}$	Correlation term parameters vector
γ	Viscosity model coefficient
Δ_{rc_p}	Resin specific heat capacity model step
Δt	Dwell duration
ΔT_{max}	Maximum temperature overshoot
$\boldsymbol{\varepsilon}$	Gaussian variable
η	Resin viscosity
η_0	Initial reference viscosity
η_{ref}	Resin reference viscosity
θ	Anisotropy parameter vector
$\boldsymbol{\lambda_{OU}}$	Speed of reversion control parameter
$\boldsymbol{\mu_{OU}}$	OU process long term mean
ρ	Composite density
ρ_r	Resin density
ρ_{cf}	Carbon fibre density
ρ_{gf}	Glass fibre density
σ_r	Resin specific heat capacity model step shift parameter
σ_y	Tool temperature sample data variance
σ^2	Predictor Gaussian process variance
σ_{exp}	Likelihood distribution standard deviation
σ_{OU}	OU process volatility
$\boldsymbol{\sigma_{prior}}$	Prior distribution standard deviation vector

$\boldsymbol{\sigma_\varepsilon}$	Gaussian variable standard deviation vector
ω	Angular velocity
ω_{ti}	Angular frequency of cosinusoidal fit

Subscripts and superscripts

i	Surrogate model index
j	Index for MCMC iterations
k	Index for monitoring data batches
l	Index for swap chain in parallel tempering
m	Index for surrogate initial sampling points
n	Index for autocorrelation structure
o	Index for unknown stochastic parameters
p	Number of basis functions
q	Index for surrogate model dimensionality

B. Abbreviations

ABS	Acrylonitrile Butadiene Styrene
CDF	Cumulative Density Function
CV/FE	Control Volume/Finite Element
CPE	Constant Phase Element
DSC	Differential Scanning Calorimetry
FE	Finite Elements
FFT	Fast Fourier Transformation
FPR	Carbon/epoxy composite Flat Panel with Recessed edge
FP	Carbon/epoxy composite Flat Panel
GA	Genetic Algorithm

GFP	Glass/epoxy composite Flat Panel
IIM	Imaginary Impedance Maximum
K-L	Karhunen-Loève
LCM	Liquid Composites Moulding
MC	Monte Carlo scheme
MCMC	Markov Chain Mote Carlo method
OU	Ornstein Uhlenbeck process
PCA	Principal Component Analysis
PDF	Probability Density Function
PID	Proportional Integral Derivative
RTM	Resin Transfer Moulding
SM	Surrogate Model
SSFEM	Spectral Stochastic Finite Element Method
TFP	Thick carbon/epoxy composite Flat Panel
VARTM	Vacuum Assisted Resin Transfer Moulding
VOF	Volume Of Fluid method

1. Introduction

1.1. Motivation and contribution

The utilisation of continuous fibre composites has grown and expanded in different applications in the last decades due to their high specific stiffness and strength. In the aerospace industry, the use of thermosetting composite materials is attractive since the low weight results in significant savings in fuel consumption. Boeing 787 Dreamliner is made of 50% of composite materials with average weight savings of about 20% [1], whilst the Airbus A350 XWB is the first aircraft with both the wings and fuselage made primarily from composites exceeding 50% of its total weight [2]. However, the high cost of composite materials due to the complex and multi stage manufacturing process is still a major challenge related to the achievement of high quality within sort process cycles. The lack of full automation and the inherent uncertainty involved in composites manufacture increase process complexity introducing variations of process outcomes. Conservative processes are selected to prevent risks associated with input parameters uncertainty resulting in increased manufacturing costs.

Figure 1.1 A350 XWB wing lower cover (© Airbus S.A.S.) [3].

The continuous demand for cost reduction and accomplishment of the desired final part quality with zero defects has motivated the development of predictive simulation tools, process monitoring and automation of composites manufacture. The main objectives of designing a composite manufacturing process are the minimisation of process duration and manufacturing cost and the delivery of the desirable product quality. Part quality is characterised by fulfilment of design tolerances, surface state and absence of process-induced defects. Typical examples of composites manufacturing processes are autoclave processing, pultrusion, filament winding and LCM. Resin Transfer Moulding (RTM) is an LCM variant, in which resin impregnates a dry preform under pressure in a sealed rigid mould followed by curing at elevated temperature. Processing decisions such as inlet and outlet locations, injection pressure, and cure profile are crucial for the quality of the final part.

Process simulation can be used to model each stage of the manufacturing process, and to select process parameters to optimise the final part quality and eliminate potential defects. Process models are capable to provide accurate estimations of process outcomes such as permeability distribution after draping, dry spots formation, process duration, degree of cure and temperature gradients within the part. However, deterministic models treat material properties and boundary conditions as fully defined, without considering the presence of uncertainty. Stochastic simulation can be performed to investigate the input variability influence on process outcomes. Uncertainties in material properties and boundary conditions introduce significant variations in manufacturing process inducing potential defects such as dry spots, temperature overshoots and undercure. Stochastic simulation provides process outcome estimations with high uncertainty resulting in selection of conservative process cycles to prevent potential risks associated with inherent input variability.

Process monitoring is used to acquire data for the manufacturing process state, such as flow front position, reaction progress and temperature distribution. Process monitoring can be useful by detecting unexpected defects during manufacturing process, such as race tracking, dry spots, exotherms, undercure and potentially triggering actions to avoid process failure. Process monitoring in industrial scale applications of carbon fibre composites presents significant challenges as the conductive reinforcement causes disturbances in the signal of sensors based on monitoring of the electromagnetic or optical

response of the measured material. The integration of process monitoring and process modelling into an inverse algorithm can provide estimations of input material properties and boundary conditions. Process monitoring results can be fed into an inverse solver, which can be used to minimise the difference between process simulation and monitoring results. Using an inversion scheme, local monitoring results can give accurate predictions of the temperature and degree of cure evolution during cure process [4]. However, material or parameter identification problems are often ill-posed and because of that, deterministic approximation is either unstable, or has to rely on considerable amount of data, which makes the whole process inefficient. Furthermore, the considerable computational time, required for process models based on Finite Element (FE) analysis to run, lead to off line implementation of the inversion schemes. Against this background a gap can be identified on the topic of utilisation of real time monitoring signals to drive stochastic simulation resulting in low uncertainty estimations related to composites manufacturing process.

1.2. Aim and objectives

The aim of this study is to develop a predictive simulation tool integrating stochastic simulation with process monitoring systems for the probabilistic prediction of composites manufacture process outcomes. To accomplish this, the following objectives have to be met:

- Uncertainty quantification of material properties, such as high specification epoxy resin viscosity and thermal boundary conditions, such as surface heat transfer coefficient and tool/air temperature.
- Development of stochastic objects representing the variability of material properties and boundary conditions.
- Development of fast surrogate process models based on FE process simulation models for the LCM filling and curing stage.
- Development and validation of process monitoring sensors for the continuous flow front monitoring in the filling stage and resin reaction progress monitoring in the curing stage applicable to the processing of carbon reinforced thermosetting composites.

- Integration of real time flow monitoring signals with stochastic filling simulation through an inverse scheme that takes into account process variability.
- Inverse solution of the cure problem under uncertainty by integrating real time cure monitoring with cure simulation.
- Development of a stochastic multi-objective optimisation methodology applied to the curing of composites.

1.3. Project setting

This work was supported by the EU through the Clean Sky 2 project Simulation tool development for a Composite manufacturing process Default prediction integrated into a Quality control system (SimCoDeQ) and EPSRC project Robustness-Performance Optimisation for Automated Composites Manufacture (RPOACM). SimCoDeQ integrates three approaches to provide a unified integrated simulation tool combining predictive modelling, variability propagation and process monitoring. The objectives related to SimCoDeQ and addressed in the present study focus on the development of the simulation tool combining sensing system signals with process simulation for the probabilistic estimation of input parameters and process outcomes. The SimCoDeQ project team included three organisations, Cranfield University, TWI and the University of Stuttgart, and was managed by Airbus Spain. RPOACM focused on the development of stochastic simulation of composites manufacturing and its combination with process monitoring and optimisation. The elements addressed in this study related to RPOACM are the development of an efficient process sensing system monitoring the flow and cure process in the presence of carbon fibre reinforcement and of a stochastic multi-objective optimisation methodology incorporating stochastic simulation into an optimisation algorithm for the minimisation of process duration and defects formation with respect to variability. The RPOACM consortium included Cranfield University, University of Nottingham and University of Bristol and was supported by Coriolis Composites SA and the ESI Group.

1.4. Thesis road map

The present thesis is organised into 12 chapters. Chapter 2 summarises the state of the art on stochastic simulation, inverse problem solutions and multi-objective optimisation of composites manufacture and application of process monitoring to the manufacturing of

carbon fibre composites. This chapter also identifies the gaps in literature related to the developments in this work. Chapter 3 describes the experimental and numerical methods used. Experimental methods include the characterisation of variability and the execution of manufacturing trials. Numerical developments encompass standard finite element models of filling and curing, fast surrogate models, inverse problem solution through Markov Chain Monte Carlo and multi-objective optimisation using Genetic Algorithms (GAs). Chapter 4 reports the constitutive material models used in process simulation, the results of uncertainty quantification and the corresponding stochastic objects of process parameters and material properties. Chapter 5 reports the sensor development and validation addressing the filling and curing of carbon fibre reinforced composites using impedance monitoring. Chapters 6 and 7 present the results of inverse solution of the RTM filling problem under uncertainty for two characteristic components, addressing application of the development within a slow and a fast filing process. Chapter 8 presents the inverse solution of the curing problem under uncertainty. Chapter 9 presents the results of the stochastic multi-objective optimisation methodology applied to curing of a thick composite flat panel. Chapter 10 presents an overall discussion of the findings of this study, whilst chapters 11 and 12 provide lists of the main conclusions of the work and of recommendations for further development and investigation.

2. Literature review

2.1. Introduction

This chapter presents the state of the art of stochastic simulation, inverse problems solution, and multi-objective optimisation applied to composites manufacturing processes as well as process monitoring techniques for carbon reinforced composites. The existence of uncertainty in the draping/forming, filling and curing stages of composites manufacture has motivated the development of stochastic process simulation [5]. The stochastic simulation methodologies developed, and their findings are presented providing an insight of the significance of input variations in each stage. The integration of process monitoring in composites manufacture can provide useful information regarding the process outcomes. The techniques developed so far have found limited application in industrial environments. One of the reasons for this is their limited applicability to carbon reinforced composites manufacture due to the interaction of carbon with electromagnetic fields. The current state of the art of this topic is reviewed here. The integration of simulation with process monitoring requires successful use of inverse solution schemes. This is an emerging area, in which activity has mainly focused on property identification. The complexity of composites manufacturing and design is reflected in the existence of different trade-offs manufacturing engineers come across when developing or adapting a process. Work on composites manufacturing optimisation has recently entered this area of investigation through the development of multi-objective optimisation methodologies which are reviewed here.

2.2. Stochastic simulation of composites manufacturing

The manufacturing of thermosetting matrix composite materials incorporates multiple stages, such as draping/forming, filling/consolidation, curing/cooling, which involve considerable variations in material properties and boundary conditions. These variations induce uncertainty into the manufacturing process affecting the outcomes of the process. This uncertainty can also initiate process defects resulting in significant amounts of rejected parts associated with considerable cost. For these reasons, stochastic simulation has been developed to address the variability in manufacturing process and to investigate its influence on process outcomes such as process time, geometrical distortion and temperature overshoot. The classification and quantification of process parameters

uncertainty is very critical for the development of reliable stochastic models expressing the associated variability.

Variations are usually created during production, storage and handling of all forms of textile reinforcement and are related to fibre misalignment, tow geometry variations, distribution of fibres inside the tow and resin content variations [6]. A likely source of tow waviness (Figure 2.1) is due to wrinkles caused by the way that the fabric is wrapped on to a drum during storage [7]. Variations in fibre architecture of textiles may induce significant uncertainty in permeability and in thermal properties affecting subsequent processing steps such as impregnation/consolidation and curing.

Permeability plays a significant role in the impregnation stage of LCM processes. Variations of permeability of dry reinforcement are caused by shear deformation during the draping stage, fibre architecture variability and nesting effects during lay-up. Furthermore, preform volume fraction variations can also induce uncertainty in the impregnation stage [5].

The cure process is a thermo-mechanical phenomenon in which the thermosetting polymer resin reacts exothermically and is transformed from an oligomeric liquid to a glassy solid. Curing involves several sources of variability related to environmental/boundary conditions and material properties [5]. These uncertainties can initiate undesirable defects into the part, such as excessive residual stress, geometrical distortion, low degree of cure or temperature overshoot.

2.2.1. Forming/draping stage

Variability in fibre architecture such as tow orientation of dry textiles may affect the outcome of the draping/forming stage resulting in uncertainty in permeability, thermal and elastic properties which in turn introduces variability in outcomes of subsequent process stages [8]. Fibre direction variations within a non-crimp fabric affect localised buckling and wrinkling during forming stage [9]. Uncertainty quantification experiments - using images processing - uncovered the presence of strong spatial correlated random fields in fibre tows direction of woven fabrics [10]. Fibre orientation variability represented by a Gaussian distribution [10-12] with a spatial autocorrelation over several unit cells of the fabric [10, 13, 14] affects the minimum and average wrinkling strain introducing a coefficient of variation in the range of 10-20% [10]. Boundary conditions, such as blank holder force and forming speed [15] or the frictional behaviour of the fabric

[16] affect the forming stage. Apart from fibre architecture variability and its consequences in draping, the manual work character of the draping stage and the lack of a standard procedure may also lead to potential variations [6, 17]. Mechanical conditioning of fabrics before draping results in an increased repeatability of forming results, since a balance of tow tension due to weaving can be achieved [17]. Uncertainty in fibre architecture and in forming process parameters should be considered in the development of draping/forming models acquiring an accurate view of the process and minimising the variability of process outcomes.

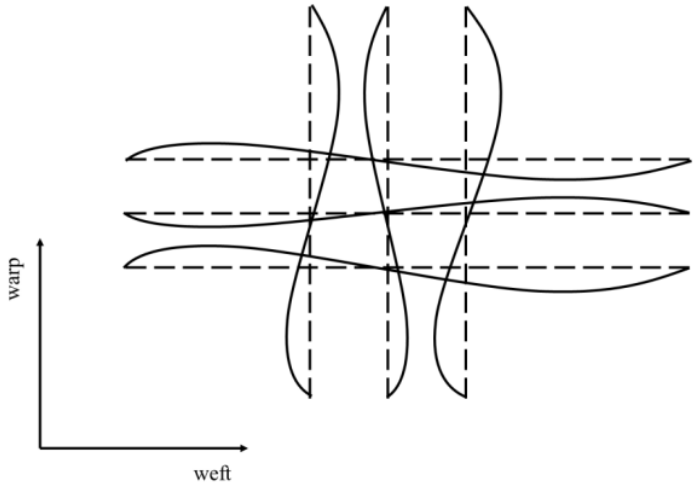

Figure 2.1 Tow waviness in warp and weft direction.

2.2.2. Filling stage

The impregnation stage of LCM processes presents considerable variations in boundary conditions and material properties [5]. The variability can lead to significant variations in filling duration and initiate process defects such as dry spots, non-uniform filling and voids, resulting in rejected parts. The permeability of textiles is a crucial material property that controls the filling step in LCM processing. Evaluating the permeability of fabrics and its variability is critical as this parameter controls the occurrence of potential problems during impregnation [18]. Variations in fibre architecture due to handling and storage, nesting effects during lay-up, fibre misplacement in the mould affect significantly permeability values and introduce variability [19-21]. Permeability can

show significant variations at the macro and micro scale [11, 22] with coefficients of variation reaching 20% [12, 21, 23].

Uncertainty hypothetically assigned to LCM process parameters such as the resin viscosity, preform permeability and length of the distribution medium can introduce a coefficient of variation of about 20% in filling duration [24, 25]. Potential imperfect placement of woven fabric plies during the lay-up stage results in local variations in through thickness permeability. Figure 2.2 illustrates two potential scenarios; i) nesting effects in which the fibre tows cover the tows spaces of the layer above or below and ii) by-pass paths formed as channels at the intersections of fibre tows. These heterogeneities play a significant role in processes in which the presence of distribution media accelerates the in-plane flow and the filling is performed predominantly in the through thickness direction. It has been observed that variations in through thickness permeability result in high scatter in the formation of dry spots [26]. Nesting effects can be represented by an equivalent permeability value treated as a random field with spatial correlation [27]. Stochastic simulation has demonstrated that nesting effects variations result in significant levels of voids formation in VARTM (Vacuum Assisted Resin Transfer Moulding) filling [28]. Furthermore, the utilisation of distribution media with higher permeability values in the VARTM process increases the average level of voids [29]. Stochastic modelling of in-plane permeability as a random field shows that there is a significant dependence of filling duration variability on permeability correlation length [30]. Variations of tow spacing and fibre angle represented by random fields have shown strong influence on the variability of overall part filling duration [31]. The coefficient of variation of the complete filling duration can reach up to 20% in the case where the standard deviation of fibre angles is about 10° [32]. Local variations of preform thickness due to potential wrinkles influence the flow front evolution, increasing the filling duration by up to 40% [33].

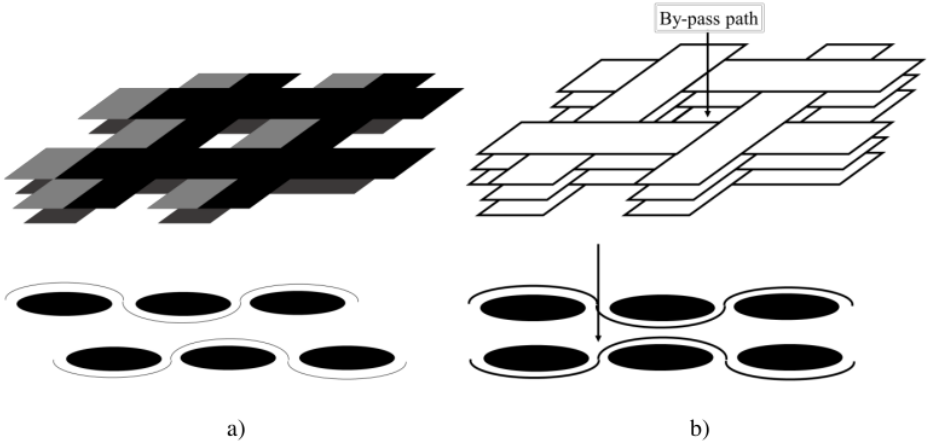

Figure 2.2 a) Nesting effects; b) by-pass-paths.

Race tracking, potentially occurring at the edges of LCM tooling, is caused either unintentionally by imperfect placement of the preform in the mould cavity or intentionally by introducing flow channels in the tool to accelerate the filling process. Flow channels are usually applied to the fabrication of large scale composites reducing the number of inlet/outlet ports needed. Careful consideration is required since flow channels may lead to uncomplete filling or formation of dry regions. Channels with high permeability can be unintentionally formed along the tool edges, resulting in high local flow front rate [34]. Race tracking effects can be represented by race tracking strength, which is the ratio of equivalent race tracking permeability over principal permeability [35]. The permeability values caused by race tracking effects can be represented by a Weibull [34] or normal distribution [36]. The measured variations of race tracking permeability highlight the stochastic nature of edge effects and their influence on filling introducing significant variability in resin flow front patterns [36]. However, only permeability variations have been quantified experimentally, whilst for viscosity which plays a dominant role in flow processes only assumptions have been made related to its variability [24, 25]. This is important for the comprehensive investigation of input parameters variability influence on filling stage outcomes.

2.2.3. Curing stage

Curing involves different sources of uncertainty such as tool/air temperature, heat transfer coefficient and cure kinetics behaviour [5, 37, 38]. The statistical modelling of these

variations provides a quantitative understanding of the influence of variability on process outcomes such as cure time or distortion. The estimation of process outcomes confidence intervals allows the selection of design process parameters which reduce the likelihood of potential defects formation such as under cure, temperature overshoot and distortion. However, this leads to selection of conservative process setups with long durations and consequently increased cost. Uncertainty in high specification fabrics, such as fibre misalignments, introduces variability in residual stresses and higher estimated average level compared to the nominal value resulted by deterministic analysis [8]. Furthermore, qualitative variations in geometrical distortions of thin L shape composite parts can be introduced by geometrical imperfections in the perform architecture. A stochastic simulation introducing artificial variations of up to 5% on cure kinetics model variables and tool temperature has shown that among these input parameters, the tool temperature causes greater variability on cure duration reaching up to 7% [39]. However, the quantification of cure kinetics variability of a high performance epoxy resin has shown greater variations in cure kinetics, especially in initial degree of cure affecting significantly the curing stage and resulting in a coefficient of variation of about 30% in exothermic effects in the case of thick composite parts [37]. Variability is pronounced in boundary conditions of the cure process [38]. Consideration of boundary conditions and cure kinetics variations indicates significant variability in cure time reaching approximately 22% [38]. The magnitude of uncertainty also affects the outcome of process optimisation problems. Higher levels of uncertainty increase the optimal cure time [40].

2.2.4. Stochastic simulation methods

Conventional Monte Carlo (MC) is usually applied for the implementation of stochastic simulation in composites manufacture calculating the statistical moments of process outcomes with generating random samples of input stochastic variables from their respective statistical distributions [8-10, 37-39, 41]. The simplicity of this non-intrusive method - treating the corresponding model as independent - allows its application in different process models of draping, filling and curing stage. However, MC operates as a random sampler and in cases of high dimensionality a large number of model evaluations is required to ensure convergence of average and standard deviation. This increases significantly the computational cost. The Spectral Stochastic Finite Element Method

(SSFEM) is an intrusive method, which involves reformulation of the deterministic model equations, based on the Karhunen-Loève (K-L) expansion for the discretisation of input random fields and polynomial chaos expansion for the representation of the outcome variables using a set of orthogonal functions [42]. The probability space is incorporated in the solution domain resulting in a system of equations larger than that of the deterministic model requiring additional computational resources [43] similar to the MC simulation. Stochastic simulation based on the Probabilistic Collocation Method (PCM) which is an intermediate between of MC and SSFEM [25, 37, 38] reduces the CPU time by 95% in stochastic simulation compared to MC.

Stochastic simulation can provide probabilistic estimation for a given set of input statistical properties. However, the confidence intervals of process outcomes estimation are wide and, in some cases, reach up to 30%. This information leads to more conservative process cycles in order to prevent the extreme events predicted by stochastic simulation.

2.3. Process monitoring in carbon fibre reinforced composites manufacturing

Process monitoring techniques have been developed to provide information during the filling stage of LCM processes and the curing step of all variants of composites manufacturing identifying potential defects and monitoring the progress of each stage. The production of high quality parts with zero defects requires comprehensive control of the manufacturing process. The monitoring of filling provides an insight in cases of two sided closed tools related to flow front progression and to the occurrence of discrepancies compared to the predicted filling pattern. Monitoring of cure can be applied to all composite manufacturing processes. The implementation of monitoring systems within the manufacturing assembly faces several challenges in terms of sensors sensitivity, manufacturing integrity and the level of intrusiveness in the composite. In the case of carbon reinforcement, the electromagnetic behaviour of the fabric is an additional challenge for techniques that are based on monitoring the electrical or optical response of the material.

2.3.1. Flow monitoring

The main types of sensors implemented for flow monitoring in the manufacture of fibrous composites can be grouped into two main categories; lineal and local sensors. Lineal

sensors are based on dielectrics [44], fibre optics [45], electric time domain reflectometry (E-TDR) [46] and Direct Current (DC) measurements [47, 48] and are usually placed across the potential flow path. These sensors monitor continually the flow front position mainly in the presence of glass fibre reinforcement. However, high specification parts, which are the primary target of monitoring methodologies, usually involve carbon fibres. The conductive nature of carbon fibres introduces measurement issues in cases where the sensing system operation is based on measuring the electromagnetic or optical response of the resin system.

A lineal flow dielectric sensor consisting of two parallel electrodes and placed between two polymeric films (Figure 2.3) can monitor continuously the resin flow front but only with non-conductive reinforcement as the presence of carbon disturbs the electric field around the electrodes [44]. An approach to overcome these disturbances is based on the utilisation of the conductive reinforcement as one of the electrodes of the sensing system [49]. However, this solution involves significant practical complexity as it requires electrical insulation of the reinforcement from the tooling assembly. Lineal flow sensors based on the E-TDR method [46] face the same monitoring limitations since the measured reflections in the impedance transmission line are disrupted by the carbon fibres. The utilisation of porous shield coaxial cables, as the conductors of the lineal sensor, provides insulation against carbon fibre reinforcement but increases the intrusiveness of the sensor [50]. Furthermore, the electric field around the conductors is formed only within the shielding resulting in potential differences between the material monitored and the material in the area of interest.

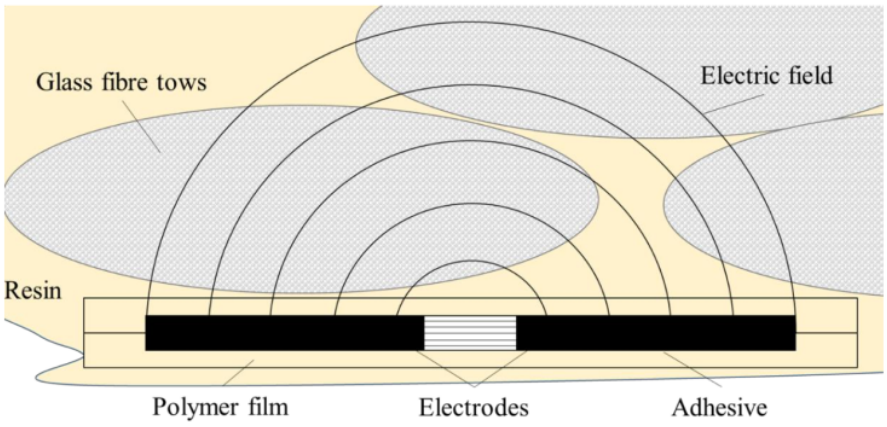

Figure 2.3 Lineal flow dielectric sensor design and electric field.

Lineal fibre optical sensors have been used for the monitoring of flow front evolution [51, 52]. In this method, light is transmitted through the optical fibre with part of the cladding around the core removed. This results in partial reflection of the transmitted light in the etched cladding region where an evanescence field is formed. The loss between the incident and the received signal depends on the refractive index of the medium (air or resin) in contact with the evanescence field. Optical fibres based on Fresnel reflection have been implemented for the monitoring of the through thickness resin flow front in a Resin Film Infusion (RFI) process [53]. The embedded optical fibre sensors are local, detecting resin arrival at the fibre-end/medium interface due to the significant differences in refractive index of resin and air. However, the use of optical fibres in the presence of carbon fibre reinforcement faces potential limitations since the light is absorbed by carbon. The careful placement of optical fibres to prevent contact between fibre-end interface and carbon increases the complexity and is currently unrealistic in the context of practical processing. The use of fibre optics as sensing system has some more disadvantages related to the high cost of the overall monitoring system and the complexity in preparation/installation of fibre optical sensors.

Vacuum sensors [53], pressure sensors [54], ultrasonic [55] or thermal probes [56] are not affected by the presence of carbon fibre, and thus can be utilised for this purpose. The implementation of pressure transducers within the mould provides local information regarding the resin arrival [57], whilst 2-D pressure sensors allow the mapping of pressure distribution within the mould cavity area and thus the resin filling pattern. However, the accuracy of the measured flow front depends on the sensitivity of the monitoring system [58, 59]. Furthermore, the implementation of 2-D pressure sensors requires significant adjustments and modifications of the mould cavity, increasing the monitoring system complexity. An intermediate element such as a long needle can be used between the pressure sensors and the resin, which has been shown to be effective in vacuum assisted processes [60]. A similar approach uses hollow metal probes embedded within the preform, mounted at individual vacuum reservoirs, identifying resin arrival at specific locations from the vacuum pressure drop in the reservoir [61]. However, the intrusiveness of metal probes and needles is considerable, introducing local deformation in the preform. The utilisation of thermocouples placed in discrete positions within the part for monitoring of resin arrival does not depend on fabric type, but it is limited only to cases

in which there are high temperature differences between resin and the mould [56, 62]. Furthermore, the integration of thermocouples within the preform induces local disturbances in preform architecture.

The though thickness flow in non-crimped carbon fibre preforms has been monitored by a sensing system based on ultrasound transmission by placing a sound source and an ultrasound receiver on the bottom and upper mould plate respectively [55]. The difference in speeds of acoustic waves in resin and air affects the time required for the wave to propagate from the sound source to the receiver as a function of the flow front position. This method faces practical implications in complex geometries, whilst the presence of potential through the thickness imperfections may result in internal reflection of the acoustic waves introducing measurement errors.

Local sensors implemented in the filling stage can instantly provide information of resin arrival, whilst the technology applied is in a mature stage for integration in industrial applications. However, the local character of these sensors makes them not appropriate to monitor continuously the flow front, whilst the implementation of multi point sensor arrays at sufficient resolution within the tooling assembly is cumbersome in practice and increases the intrusiveness of the monitoring system.

2.3.2. Cure monitoring

Cure monitoring systems are based on tracking the evolution of a physical quantity connected either directly or indirectly to the cure state. Near-infrared [63-65] and infrared spectroscopy [66, 67] provide direct chemical information on cure evolution. Application of infrared techniques is usually performed in the near-infrared region of the spectrum providing correlation of observed peaks with the chemical behaviour of the resin [64]. The correlation between fluorescence and viscosity has been used as the basis for monitoring of the cure [68-70]. The refractive index is directly related to the density of the resin and can be used for cure monitoring through fibre optic sensors based on the densification occurring during cross linking [52, 71]. Consideration of the optical fibre core refractive index is required to select a fibre with an index slightly larger than that of the resin system for the effective monitoring of the cure process. Selection of an optical fibre with refractive index far larger than that of the resin index results in negligible dispersion of the transmitted light.

Dielectric cure monitoring methods are based on the dependence of the electric and dielectric properties on the chemo-structural properties of the resin and have been used successfully to follow the degree of cure, viscosity and vitrification [72-79]. The underlying phenomena occurring in a thermoset system by the application of an AC electric field are: i) dipolar relaxation ii) migrating charges conduction and iii) electrode polarisation. Dipolar relaxation is manifested as a step change in the permittivity spectrum and a bell-shaped curve in the dielectric loss spectrum due to the dipole orientation mechanism under AC excitation. The migration charges mechanism involves the mobility of extrinsic charge carriers such as sodium and chloride present in thermosets as well as intrinsic carriers mainly through a proton transfer [80]. The mobility of migrating charges is related to material state of the resin. Electrode polarisation effects occur around the electrodes forming a thin layer with low conductivity and permittivity due to diffusion limitations of charge discharging on the sensor electrodes. Interfacial polarisation, which is a mechanism similar to electrode polarisation, occurs due to differences in dielectric constant and conductivity between the phases in multiphase epoxy resins. This mechanism involves the accumulation of charges at an interface between the different phases within the material when an electric excitation is applied. Monitoring of interfacial polarisation has been utilised for the identification of phase separation occurred in curing of modified epoxy resins [81].

The implementation of monitoring techniques in processes using carbon fibre as reinforcement is problematic. The use of optical fibres correlating changes of the resin refractive index with reaction progress [82] faces significant limitations in the presence of carbon fibre reinforcement since potential contact between the measuring area and the carbon results in absorption of the transmitted light. Dielectric cure sensors have been successfully tested in the fabrication of carbon fibre composites when they are covered with a permeable non-conductive material such as thin porous PTFE film [72], glass cloth [78] or a peel ply [83] preventing the contact with conductive carbon fibres. However, these solutions reduce the reliability of the sensor since the intermediate medium increases the discrepancy between the material in the region of interest and the material in contact with sensors. Monitoring based on impedance/dielectric spectroscopy is considered advantageous due to the high sensitivity of sensor response, the robustness

and low cost of the measurement setup and the capability for easy incorporation in tooling.

Some monitoring methods are independent of fibre type of the composite. The sensitivity of ultrasonic wave propagation (i.e. sound velocity, attenuation) to macroscopic polymer structure, viscosity and modulus has been used to capture the evolution of the curing reaction [84-86]. The strong dependence of ultrasonic velocity on temperature changes may cause difficulties in identifying the vitrification time in cases of non-isothermal curing, in contrast with the gelation time which is pronounced with a step change in ultrasound velocity [87]. The acoustic wave can be transmitted/received using one [88] or two probes [87, 89]. In the latter case, an ultrasound source is integrated into a RTM tool generating ultrasonic waves received by an embedded ultrasonic sensor. The use of direct transmission of ultrasound requires significant tool modifications, since the transmitter and the receiver need to be integrated into the two sides of the tool. This causes practical limitations in cases of complex geometries i.e. double curvature where the accessibility for the sensing system installation can be limited. Remote ultrasound sensing is performed using as an intermediate element such as optical fibres [90] or rod shaped waveguides [91] to guide the propagated wave from transmitter to receiver. However, this approach results in high noise to signal ratio compared to conventional ultrasound measurements.

Thermal monitoring systems based on heat flux sensors [92-95] can provide local information regarding the heat generated during the cure process without the signal being affected by the presence of carbon fibre reinforcement. In this technique, the thermal properties of the composite are assumed to be constant during the curing so that all changes in the sensor signals can be attributed to the exothermic reaction of the resin. However, this approach may face potential limitations since thermal properties depend on reaction progress.

2.4. Inverse problems in composites manufacturing

An inverse problem of a physical model is defined as the process where physical observations are used to estimate unknown model parameters. Inverse problems are often ill-posed in nature. A problem is stated as ill-posed if at least one of the following conditions of well-posedness is violated: i) a solution exists, ii) the solution is unique and iii) the solution behaviour changes continuously and smoothly with the initial conditions.

Inversion schemes have been developed in composites manufacture to characterise material properties integrating monitoring data with process models. In the filling stage, inversion schemes based on error minimisation methods have been implemented for the estimation of preform permeability combining numerical flow models with process monitoring data [96, 97]. Most of the conventional methods for estimation of preform permeability are carried out off-line, without considering potential non-uniformity in permeability values due to perform imperfections. Local reinforcement permeability has been estimated on-line using least squares combined with visual and pressure sensor monitoring data [98, 99]. An interpolation algorithm has been used to integrate monitoring data from pressure sensors, placed at discrete positions within the tool cavity, with a numerical 2-D flow model for the prediction of flow front progression in RTM filling [54]. The use of local sensors provides limited information regarding the flow process resulting in estimation inaccuracies when unexpected local flow disturbances occur outside the measurable area of local sensors. Inverse schemes have been implemented in the curing stage for identification of cure kinetics model parameters [100] and thermal properties such as thermal conductivity and specific heat capacity [4, 101] using experimental data acquired by thermocouples placed in composites parts. The methods used are based on error minimisation such as the Gauss-Newton algorithm [101] or the Levenberg–Marquardt algorithm [100] and zero order algorithms such as GAs [4]. Direct error minimisation or zero order algorithms cannot deal fully with the potential ill posedness of inverse composites manufacturing problems. In the filling stage, the problem involves a free boundary due to the moving flow front. Partial monitoring of flow front evolution may result in potential inverse solution discontinuities violating the third condition of well-posed problems. Curing involves a highly non-linear heat transfer problem, which can present ill-posedness in cases where the boundary conditions cannot be fully defined and/or there is limited access for placing monitoring sensors on the domain boundaries. Regularisation methods, such as the Tikhonov regularisation [102], are usually applied to deal with ill-posedness, giving accurate approximate solutions by including an additional term in the error minimisation function that ensures that the solution is either smooth or not too far from an expected value. Unlike deterministic approaches where only single estimates are obtained, Bayesian inference operates as a sampler providing probabilistic estimations of the problem. The Markov Chain Monte

Carlo method based on Bayesian inference addresses ill-posed problems through the regularisation of the solution by the use of a prior estimate [103-107]. MCMC operates as a sampler computing the uncertainty associated with the estimation by incorporating measurements and modelling into the inverse scheme. An application of Bayesian inference has been performed for the real time estimation of perform permeability in a simple 1-D filling problem [108]. The Bayesian posterior was numerically approximated using the regularising ensemble Kalman algorithm (REnKA) for the probabilistic estimation of volume fraction and permeability within the preform in a RTM filling [107]. The coupling of the inversion scheme with control actions in real-time has been performed in a 1-D problem to correct potential disturbances of the target flow front [109]. However, the use of conventional FE models representing 2-D or 3-D filling causes significant computational challenges since inversion schemes based on Bayesian inference require a large number of model evaluations to ensure convergence and thus they cannot be applied to real time applications.

2.5. Multi-objective optimisation in composite manufacture

Composites manufacturing involves complex interdependencies of different stages and physics, which cause complicated trade-off in process outcomes that need to be addressed during process design. In the filling stage, the selection of filling strategy i.e. location of injection ports and vents, governs the filling patterns, duration and dry spots formation. The use of many injection ports and high injection pressure results in acceleration of the flow, although potential dry spots or voids can be formed. In curing of thick components, severe temperature overshoots can be observed due to the heat generated during exothermic reaction of the resin. These can affect considerably the quality of the manufactured component. The risks associated with temperature overshoots in thick components are dealt with by adopting conservative cure cycles. This in turn results in long processing times and high manufacturing costs. The inherent trade-off between defects formation and process duration arises the need of exploration of potential solution that can balance the requirements of fast cycles combined with minimum defects formation.

The optimisation of the manufacturing of continuous fibre thermosetting matrix composites is critical for minimising cost and the likelihood of occurrence of process failures defects. The optimisation of composites manufacturing has been addressed as

single objective optimisation problems considering one [110, 111] or multiple objectives merged in a weighted sum [112, 113]. In the latter case, the optimal solutions obtained are dependent on the weights assigned to the different objectives which imply a relative prioritisation between the different objectives. Multi-objective optimisation can overcome this limitation by treating the objectives independently. In this case, the set of optimal points forms an efficient frontier and the set of potential solutions forms the Pareto set. The efficient frontier constitutes the boundary of the feasible region of solutions as illustrated in Figure 2.4. The optimal trade-off between maximum absolute shear angle and the average shear angle in draping has been identified in a multi-objective optimisation problem considering as design parameters the pre-shear, drape starting point and draping direction [114]. An optimisation of RTM filling has been performed to find the optimal solutions resulting in minimisation of both filling duration and dry spots formation [115]. A two objectives optimisation problem based on filling duration and the presence of dry regions has provided optimal solutions where the competitive nature of the objects leads to an L-shape Pareto front [116]. In pultrusion processing, optimisation of heating system parameters i.e. number and dimensions of heaters and temperature along the die, has been addressed using a multi-objective optimisation scheme to maximise pulling speed and minimise energy consumption using constraints related to the maximum temperature and minimum final degree of cure [117-119]. A multi-objective optimisation based on GAs has been used to address cure time and temperature overshoot minimisation in thick parts. with optimal solutions achieving improvements of about 50% with respect to both cure time and overshoot compared to standard cure profiles [120].

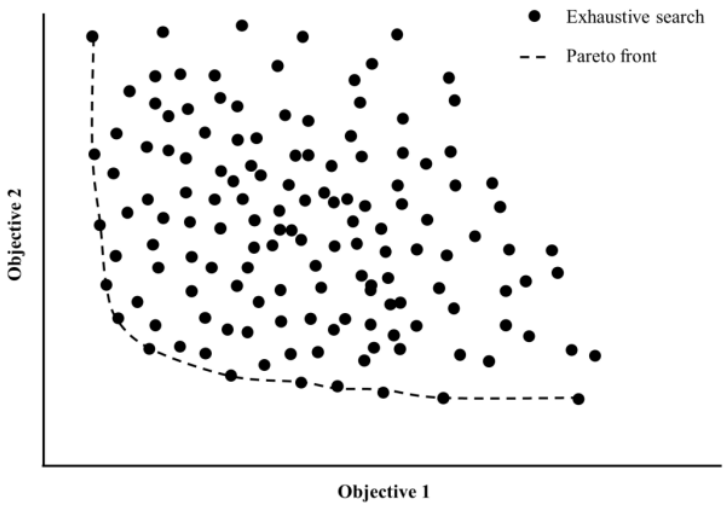

Figure 2.4 Pareto set frontier against exhaustive search results.

The benefits offered by the exploration of the design space by numerical optimisation can be accompanied by relative instability of some of the solutions with respect to perturbations of nominal process parameters leading to potential risks. The potential lack of stability of optimised solutions can be addressed by the combination of multi-objective optimisation with stochastic simulation aiming to address simultaneously efficiency and robustness.

2.6. Overview

Composites fabrication comprises different stages such as draping/forming, filling and curing and a wide range of physical phenomena. The accurate representation of these phenomena is performed by process models capable to estimate process outcomes such as shear angles, filling patterns, process duration, voids formation, temperature and degree of cure distributions and distortion. Stochastic simulation methods have been developed to investigate the influence of input parameters variations i.e. preform permeability, cure kinetics and thermal boundary conditions on process outcomes. The implementation of stochastic simulation is performed off-line the manufacturing process resulting in estimations with high uncertainty.

Process sensing systems based on dielectrics or optical fibres can monitor the flow and cure process effectively. However, these methods are problematic in monitoring of carbon reinforced parts since the conductive carbon disturbs the electromagnetic field.

The proposed solutions, covering the sensor with a permeable nonconductive medium, are also problematic due to the increased intrusiveness of the covered sensor and potential measurements differences caused by the increased distance between sensor and material in the region of interest.

The identification of unknown process parameters such as preform permeability or thermal properties has been performed integrating process monitoring data and process models into inverse algorithms. Algorithms based on error minimisation cannot be applied to more complex problems with potential ill-posedeness, whilst the real time implementation of inversion schemes faces limitations due to the computational expensive FE models.

The selection of multiple objectives in an optimisation problem results in optimal solutions that balance the different objectives. However, optimal solutions based on deterministic multi-objective optimisation approaches may present instability in the presence of input parameters variations affecting the optimality of the solution.

The gaps identified in literature are summarised as follows:

- Resin viscosity variability has been only modelled hypothetically so far in the literature. This is an important gap since viscosity plays a significant role in the filling stage. The lack of experimental data related to the resin viscosity is tackled here by conducting uncertainty quantification tests of high performance resin viscosity which are presented in chapter 4.
- Current flow monitoring systems applied to industrial scale processes either provide local information related to the resin arrival or are only applicable to non-conductive reinforcement. The solutions provided to prevent the contact between sensors and the conductive carbon increase the intrusiveness of the sensing system and the mismatch between the material in contact with sensors and the material in the area of interest. The identified gap is addressed by developing a new dielectric sensor capable for effective monitoring in presence of carbon fibres, which is presented in chapter 5.
- The integration of process monitoring signals with process modelling into an inverse algorithm has focused on the estimation of unknown input parameters such as perform permeability, resin thermal properties and boundary conditions. These approaches have not estimated process outcomes, whilst the

implementation has been performed off line. In order to fill this gap an inversion scheme is developed, which is presented in chapters 6-8, integrating process models with process monitoring data for the real time probabilistic estimation of input parameters and the corresponding process outcomes.

- Multi-objective optimisation schemes applied to composites manufacture provide optimal solutions without considering the inherent uncertainty in material properties and boundary conditions. This leads to solutions highly sensitive to potential variations of material properties and boundary conditions. The lack of stability in deterministic optimal solutions is addressed by developing a stochastic multi-objective optimisation scheme, which is presented in chapter 9, optimising process objectives with respect to variability.

3. Methodology

3.1. Introduction

This chapter covers the methodological approaches followed in this work. The experimental methods employed for material characterisation and variability quantification for material properties and boundary conditions are presented. Validation tests of process monitoring sensors performed by conducting a series of LCM process trials are described. The materials used in the characterisation and manufactural trials are also specified. Process simulation models representing the filling and cure stage of LCM processing are presented and a procedure for the development of their surrogate equivalents based on Kriging is also described. An inversion scheme based on MCMC utilised to integrate on line process monitoring with stochastic process models for the real time probabilistic estimation of process outcomes is presented. A stochastic multi-objective optimisation framework combining stochastic simulation with a multi-objective Genetic Algorithm used to address process design is detailed.

3.2. Materials

The resin utilised in this work was the Hexcel HexFlow® RTM6 epoxy system [121]. RTM6 epoxy resin is a premixed monocomponent resin, which is widely used in RTM processes for aerospace industry applications. At ambient temperature, it is a brown translucent high viscosity liquid, whilst its service temperature lies between -60 °C up to 180 °C. Two carbon fibre fabrics were utilised: (i) Hexcel HexForce® G0926, which is a 5H satin weave of HexTow® 6K AS4 carbon fibres tows evenly distributed in the warp and weft direction with areal density of 375 g/m^2 [122] and; (ii) Hexcel HexForce® G1157 D1300, which is a pseudo unidirectional fabric with Tenax® E HTA40 E13 6K carbon fibre tows [123] in the warp direction and EC9 34 Z40 1383 glass fibre tows of about 400 filaments in the weft direction with a 97% and 3% weight fraction respectively and an areal density of 277 g/m^2 [124]. The G1157 UD carbon fabric was used in the simulation of VARTM cure processing of thick laminates, whilst the G0926 woven carbon fabric was utilised in experimental RTM filling of flat laminates and in the simulation of RTM filling of typical composite parts such as a C spar. The E-TX1769 (BTI Europe) tri-axial E-glass fabric with a surface density of 1770 g/m^2 [125] was used for the simulation of RTM cure processing of thin flat panels.

Flow and cure dielectric sensors were fabricated using a 136-AWP solid copper wire with polyurethane enamel coating with the diameter of 127 μm [126]. Acrylonitrile Butadiene Styrene (ABS) was utilised to make a miniature loom used for the construction of woven dielectric cure sensor.

3.3. Characterisation techniques

Rheology was employed for the characterisation of RTM6 epoxy resin viscosity and its variability. The variability of thermal boundary conditions was quantified in a series of experiments using an apparatus mimicking LCM process thermal conditions in an oven. The quality of signals acquired by cure dielectric sensors, proposed in this work, was established during isothermal runs of neat epoxy resin using a heated copper cell.

3.3.1. Rheology

Rheology tests of RTM6 epoxy resin were carried out using a TA Instrument AR200ex rheometer. A plate and a 2° cone with a diameter of 40 mm and a truncation depth of 54 μm were used. The gap between the cone and the plate was set to be identical to the truncation of the cone ensuring constant strain rate of the resin sample across the plate radius. An amount of about 0.5 g of resin was placed on the lower heating plate filling the gap between the cone and the plate once the upper cone was positioned in place. The excess resin around the cone/plate edge was carefully removed with the straight edge of a spatula ensuring a well-defined and reliably repeatable sample amount in the measuring system. The resin viscosity was characterised using a recently proposed rheology test applying a cyclic thermal profile [127]. This profile combines isothermal and non-isothermal segments to capture both the dependence of resin viscosity on temperature and time effects due to the cure. The thermal profile - illustrated in Figure 3.1 - includes cooling/heating cycles applied periodically during an isothermal experimental at a constant temperature of 120 °C. The amplitude of the cooling/heating cycles was 40 °C resulting in a minimum temperature of 80 °C, whilst the ramp rate for both the heating and cooling phases was 10 °C/min.

Samples from four different batches were utilised for the uncertainty quantification of RTM6 epoxy resin viscosity. All batches were within the shelf life of the material at the time of testing stored in the fridge as recommended by the manufacturer [121]. According to the recommendation, the resin is allowed to remain at ambient temperature for up to

15 days and at -18 °C for up to 9 months. Two resin samples of each batch were tested at the 1st and the 15th day of ambient temperature exposure to investigate potential variations in resin viscosity due to differences in storage conditions.

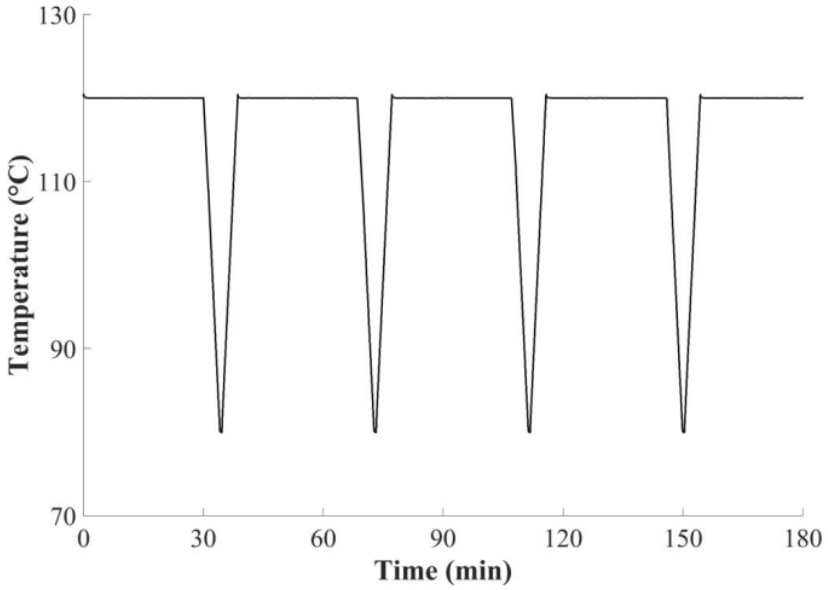

Figure 3.1 Cyclic thermal profile used in rheology tests for RTM6 epoxy resin viscosity characterisation.

3.3.2. Thermal boundary conditions

The variability of thermal boundary conditions variability of processing in an oven was quantified in a series of 10 experimental runs. The experimental set-up employed is depicted in Figure 3.2. A 5 mm carbon/epoxy composite flat panel was used to create thermal conditions similar to those during VARTM cure of a composite part. The matrix system of the panel was RTM6 epoxy resin and the reinforcement G1157 UD carbon fabric. The composite part was placed on an aluminium tooling plate with 10 mm thickness inside a Caltherm E9321V2 oven with a Eurotherm 2408P4 PID controller. The part was covered with N64PS-x VAC Innovation peel ply fabric, whilst a VAC slip 10P1-1420 PTFE coated glass fabric was used as flow media. A nylon xR1.2 VAC Innovation vacuum bag was placed on top of the assembly and sealing was achieved with VACsealY sealant tape to ensure vacuum conditions. Two K-type thermocouples were mounted on

the tool surface to measure the tool temperature, and a third one was placed outside the thermal boundary layer and close to the surface to measure the air temperature. Two heat flux sensors were placed on the vacuum bag to measure the convection heat flux and its variability.

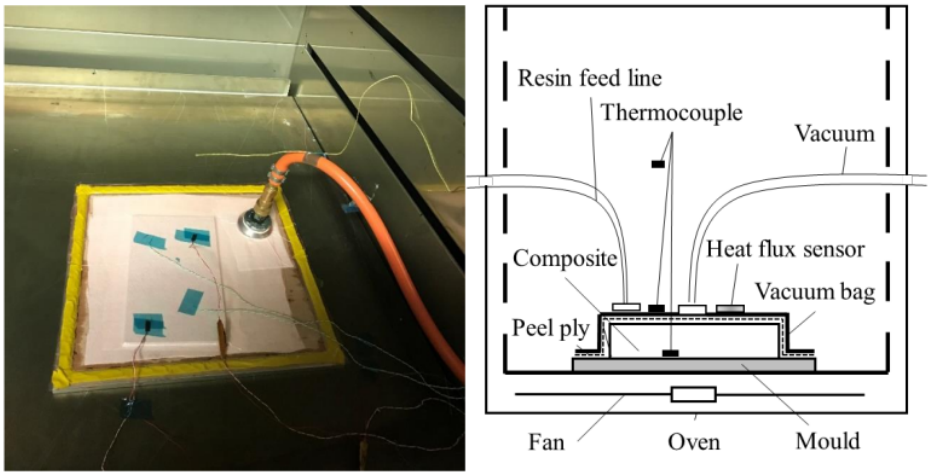

a) b)

Figure 3.2 Instrumented VARTM set up a) VARTM process within the oven of carbon/epoxy composite flat panel; b) Schematic representation of experimental set-up.

The micro-foil heat flux sensors used output a voltage signal which is proportional to the heat flux with the proportionality coefficient determined individually per sensor by the supplier [128]. The heat flux $\dot{Q}$ is given as follows:

$$\dot{Q} = \frac{H}{CM\ TM} \tag{3.1}$$

where H is the sensor output voltage, whilst CM and TM are a calibration multiplier and a temperature multiplication factor respectively. The sensors used in this study have a calibration multiplier of 0.15 $\mu V/W/m^2$. The temperature multiplication factor is a function of temperature as illustrated in Figure 3.3. The surface heat transfer coefficient is calculated using the temperatures of the surface (T_s) and air in the oven (T_{air}) and the measured heat flux ($\dot{Q}$) as follows:

$$h = \frac{\dot{Q}}{T_s - T_{air}} \tag{3.2}$$

The temperature was set at 160 °C during all runs. Cranfield Measurement and Control, which is an in house LabVIEW software, was used for data acquisition. The data acquisition frequency was 0.8 Hz and its duration was 20 min and 30 min after the oven temperature controller reached a plateau at 160 °C for the surface heat transfer coefficient and tool temperature measurements respectively.

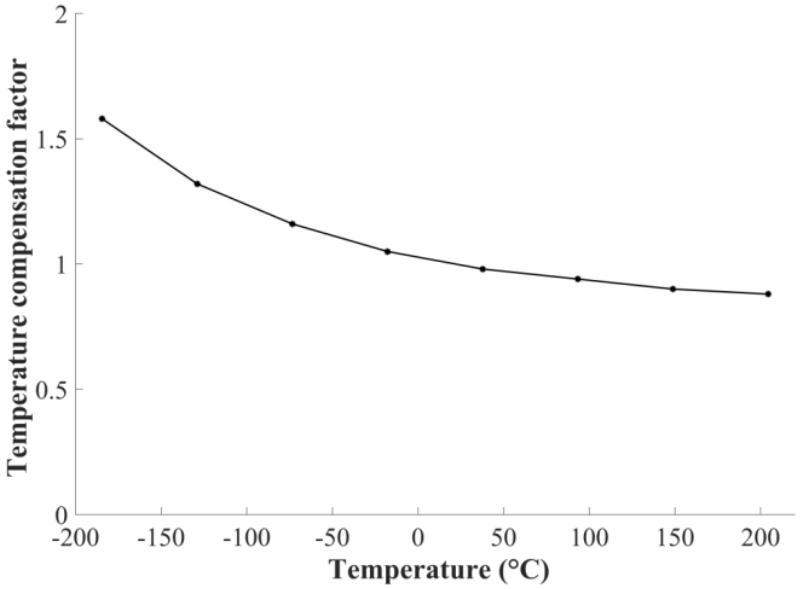

Figure 3.3 Micro-foil heat flux sensor output compensation factor as a function of surface temperature [128].

3.3.3. Cure monitoring

A cure dielectric sensor, which is presented in chapter 5, was developed to monitor reaction progress during the curing stage of carbon fibre composites manufacture. The cure sensor signal was evaluated in isothermal curing experiments of neat RTM6 epoxy resin using the set-up illustrated in Figure 3.4. The setup comprises a Eurotherm 2408 controller and an 235 W Acim Jouanin Nozzle Band Heater [129] with 38 mm height and 38 mm diameter mounted on a hollow copper cylinder. The cylinder has an outer diameter of 36 mm and inner 12 mm. The dielectric cure sensor was fully immersed in a glass tube with internal diameter of 10 mm and depth of 50 mm, containing the liquid resin and subsequently placed in the heated copper cylinder. A control thermocouple was attached

in the copper cylinder, and a second thermocouple was placed in the tube to measure the actual thermal profile the resin follows during cure. RS Pro Brown RG179B/U thin coaxial cables were used for the connection between the cure sensor and a Solartron 1260 Impedance Analyser. Impedance data were acquired over 31 frequencies swept logarithmically over the 1 Hz - 1 MHz range. The analyser communicates with a computer via an IEEE interface, whilst Cranfield Measurement and Control was utilised to drive the measurements and acquire the data.

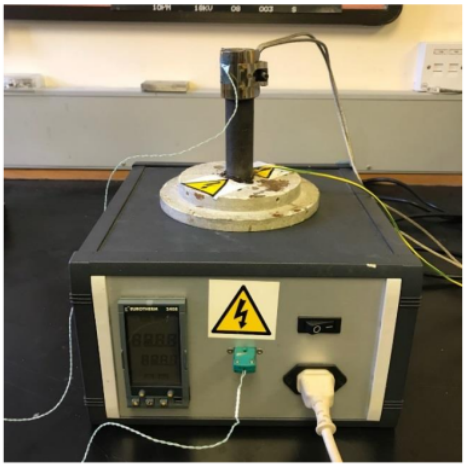

Figure 3.4 Experimental apparatus for isothermal curing of RTM6 epoxy resin.

3.4. Manufacturing trials

LCM processing was carried out to evaluate process monitoring sensors and the inversion procedure performance under industrial manufacturing conditions. RTM processing was employed for the fabrication of carbon/epoxy composite flat panels to test the flow monitoring capabilities in the presence of carbon reinforcement of a lineal dielectric sensor, which is presented in chapter 5, and to validate the real time inversion scheme developed in this work. The cure dielectric sensor was evaluated during the VARTM process of a carbon/epoxy composite flat part.

3.4.1. RTM manufacturing trials

The RTM facility illustrated in Figure 3.5 was utilised for the manufacturing of carbon/epoxy composite flat panels. The RTM tool includes a rectangular cavity with dimensions of 900×330×3.3 mm. The sides of the cavity are sealed with silicone rubber,

whilst a glass plate is placed on the top of the mould enabling the visual monitoring of the flow front during mould filling. The RTM tool is connected with an ISOJET Equipements injection system based on a piston with 2 l capacity actuated by a brushless motor driven by a servo controller. This system is used to heat up, stir, degas and inject the resin into the RTM tool cavity.

Figure 3.5 Instrumented RTM facility.

Two different part configurations were selected for RTM processing. The first configuration comprises a rectangular composite flat panel and is denoted as FP, with dimensions 800×330 mm and thickness of 3.3 mm. Two carbon/epoxy composite flat panels, denoted as FP_1 and FP_2, were manufactured using the RTM tool to validate the lineal dielectric sensor in two different injection pressures. The lineal flow sensor with a length of 800 mm was placed in the centre of cavity of the RTM tool as illustrated in Figure 3.6 and was connected to the Impedance Analyser. Impedance data were acquired at seven frequencies selected logarithmically over the range of 100 Hz – 100 KHz.

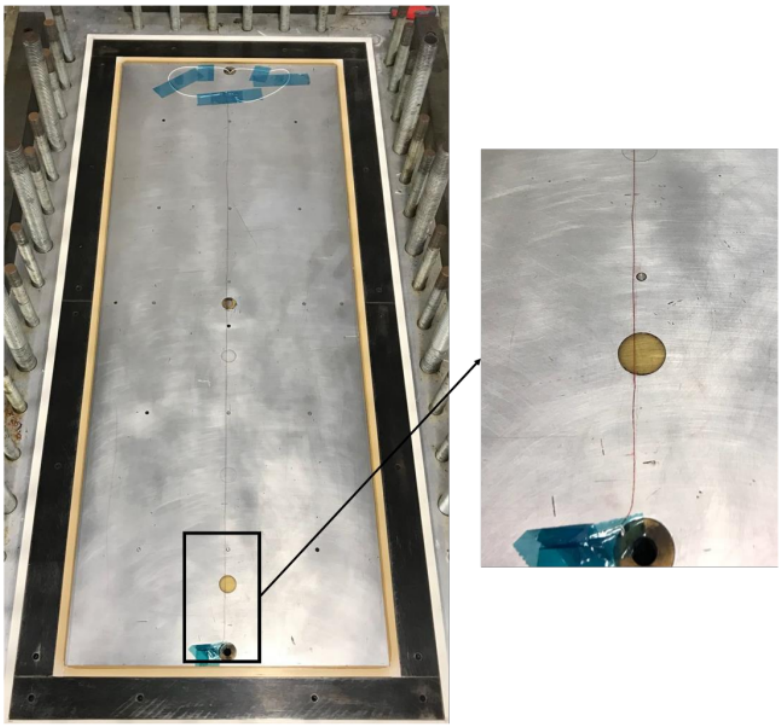

Figure 3.6 Lineal flow sensor placed at the centre of the tool cavity; Inset: detailed view.

The second configuration is a rectangular flat panel with a rectangular recessed edge denoted as FPR. The FPR part, illustrated in Figure 3.7, is 780 mm long and 330 mm wide with a thickness of 3.3 mm. The length of the recessed edge is 400 mm and the width 165 mm. A carbon/epoxy composite part based on this design was fabricated using the RTM tool to evaluate the performance of the inversion procedure developed in this work during the filling stage. Lineal flow dielectric sensors were embedded in different positions in the mould cavity for the monitoring of the flow front evolution. Three lineal flow sensors were utilised placed on the lower surface of the mould cavity as illustrated in Figure 3.7. Two sensors were placed across the straight and recessed edges of the mould to monitor potential race tracking effects, and one sensor was placed in the main flow path along the filling evolution in the main rectangle of the geometry. A Keithley 7001 switch system was used as an intermediate system between the three sensors and the Impedance Analyser. Thin coaxial cables passed through the outlet port were utilised to connect the sensors with the switch system. The switch system was connected with the impedance analyser via an IEEE interface, whilst Cranfield Measurement and Control

was adapted for the switching actions between the channels. In this set-up the channels are scanned in a serial manner; the flow sensor impedance data are acquired over three frequencies 10, 31.6 and 100 KHz and the multiplexer switches to the next channel. The duration of the activation/deactivation process for each channel is around 20 s.

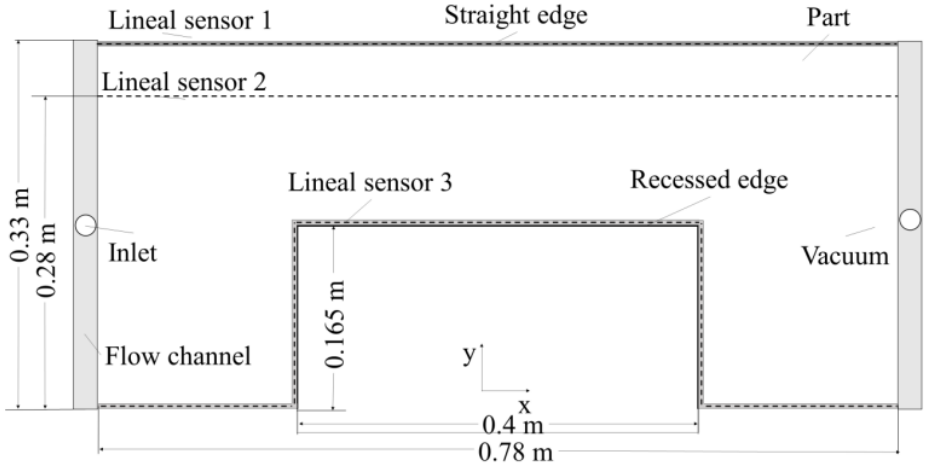

Figure 3.7 Mould cavity geometry and lineal dielectric sensors positions of FPR composite part.

Table 3.1 RTM manufacturing trials specification.

	RTM manufacturing trials		
	FP_1	**FP_2**	**FPR**
Preform	G0926 fabric	G0926 fabric	G0926 fabric
Plies	9	9	9
Lay up	$[(0/90)_2/0/(90/0)_2]$	$[(0/90)_2/0/(90/0)_2]$	$[(0/90)_2/0/(90/0)_2]$
Matrix	RTM6	RTM6	RTM6
Filling temperature	120 °C	120 °C	120 °C
Vacuum level	10 mbar	10 mbar	10 mbar
Injection pressure	2 bar	3 bar	2 bar
Cure temperature	160 °C	160 °C	160 °C
Cure duration	2 h	2 h	2 h
Frequency range	100 Hz – 100 KHz	100 Hz – 100 KHz	10 KHz -100 KHz
Number of points	7	7	3

Table 3.1 summarises the details of RTM manufacturing trials. In all trials the reinforcement material was G0926 woven carbon fabric, whilst the matrix system was RTM6 epoxy resin. The preforms comprised nine fabric layers in a $[(0F/90F)_2/0F/(90F/0F)_2]$ sequence resulting in a volume fraction of 57%. The filling was carried out at a constant temperature of 120 °C under a pressure of 2 bar for FP_1 and FPR cases and 3 bar for FP_2, with the simultaneous application of vacuum at 10 mbar. The curing was performed after the end of filling at 160 °C for 2 h. A digital camera was placed on the top of RTM tool for visual measurement of flow front evolution.

3.4.2. VARTM manufacturing trial

The dielectric cure sensor performance was assessed during VARTM processing of a carbon/epoxy composite flat part. The preform, with in-plane dimensions of 150×75 mm, comprised six plies of G0926 woven carbon fabric in a $[0F/90F]_3$ layup sequence resulting in a total thickness of 2.2 mm and fibre volume fraction of 57%. Infusion with RTM6 epoxy resin was carried out at 120 °C under vacuum and cure at 160 °C for 2 h. A flow media was placed on top of the preform to assist the flow of the resin. The cure sensor and a K-type thermocouple were placed on the tool cavity in contact with the fabric to monitor the reaction progress and temperature evolution during the process. The cure sensor was connected to the Impedance Analyser for the acquisition of impedance data over 31 frequencies selected logarithmically in the range of 1 Hz – 1 MHz.

3.5. Process simulation

Process simulation models of the different composite parts have been developed to represent the filling and curing stages of LCM processing. The process simulation models were used for the development of numerous computational methods i.e. stochastic simulation, inverse solution and stochastic multi-objective optimisation.

3.5.1. Flow modelling

The filling stage of composite manufacture can be modelled using Darcy's law expressing the viscous flow of a liquid through porous media as follows:

$$\mathbf{v_{fl}} = -\frac{\boldsymbol{\varkappa}\nabla\mathbf{P}}{\eta} \tag{3.3}$$

where $\mathbf{v_{fl}}$ is the Darcy velocity, $\boldsymbol{\varkappa}$ the permeability tensor, η resin viscosity and **P** the pressure gradient. The resin velocity is driven by the applied pressure gradient and is affected by material properties such as resin viscosity and preform permeability. Liquid resin is considered as incompressible, and thus in order to preserve the balance of resin mass the velocity is expressed as follows:

$$\nabla \mathbf{v_{fl}} = 0 \tag{3.4}$$

The modelling of filling was carried out using the Control Volume/Finite Element (CV/FE) solver PAM-RTM®. PAM-RTM® solves Eq. (3.3) using non-conforming elements, whilst the flow progression is computed with the volume of fluid (VOF) method. The flow models presented in this section have small thickness compared to their in plane dimensions. Therefore, the through thickness flow can be assumed to be negligible and the problem can be solved using three noded linear shell elements. User defined subroutines, written in Visual Studio C++ 2015, were used to incorporate a resin viscosity model expressing the evolution of rheological properties during the process. The modelling approach was implemented for the RTM filling of the carbon/epoxy composite flat panel with recessed edge (FPR) and a C spar.

3.5.1.1. Filling simulation of RTM of the flat panel with recessed edge (FPR)

A flow simulation model was developed to represent the filling of the FPR. The model illustrated in Figure 3.8 comprises 5,700 elements. A rectangular flow channel with an injection port and a vent located at the left and the right edge of the part respectively results in a linear filling. The boundary conditions used were a prescribed injection pressure of 2 bar applied to the nodes of the left edge - where the flow channel is - and vacuum applied to the outlet port. A constant temperature of 120 °C was applied to all nodes, representing isothermal filling. The model was divided into seven zones with different permeability values; one representing the main flow in the preform and the other six the flow across the part edges to simulate potential race tracking effects. Race tracking effects were modelled by assigned an equivalent permeability K_{Ri} value [130] to each of the six edges as shown in Figure 3.8, In the case of the main flow zone, the preform permeability values K_x and K_y of each element were aligned to the longitudinal (x) and transverse (y) direction of the mould.

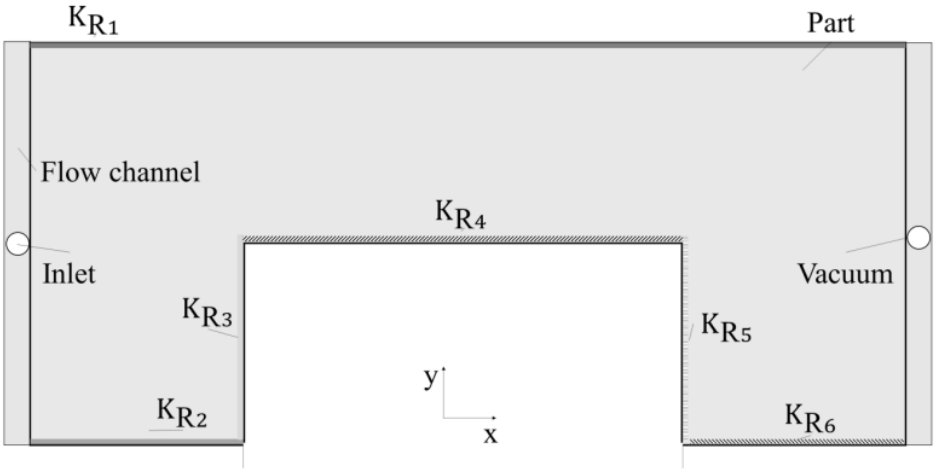

Figure 3.8 Schematic representation of the flow model of FPR composite part.

3.5.1.2. Filling simulation of RTM process of a carbon/epoxy composite C spar

A flow model was developed representing the filling of a carbon/epoxy composite C spar. The flow model is illustrated in Figure 3.9. The part thickness is equal to 2 mm, the total length is equal to 900 mm, the width 100 mm and the height of the two side flanges 50 mm. The model comprises 1,900 elements. A prescribed injection pressure of 2 bar was applied to the central injection port and vacuum to the six outlet ports located at the two edges corner of the C spar flanges. A flow channel across the top surface of the part accelerates the resin flow. The filling temperature applied to all nodes was constant and equal to 120°C. The reinforcement consisted of 6 plies of G0926 woven carbon fabric corresponding to a 62% volume fraction. The preform layers were considered to be aligned to the C-spar direction so that warp tows are parallel to the x direction in Figure 3.9. The flow model comprises two zones assigned with different permeability values; one representing the main flow and the flow across the channel where a relative high permeability K_R value was assigned.

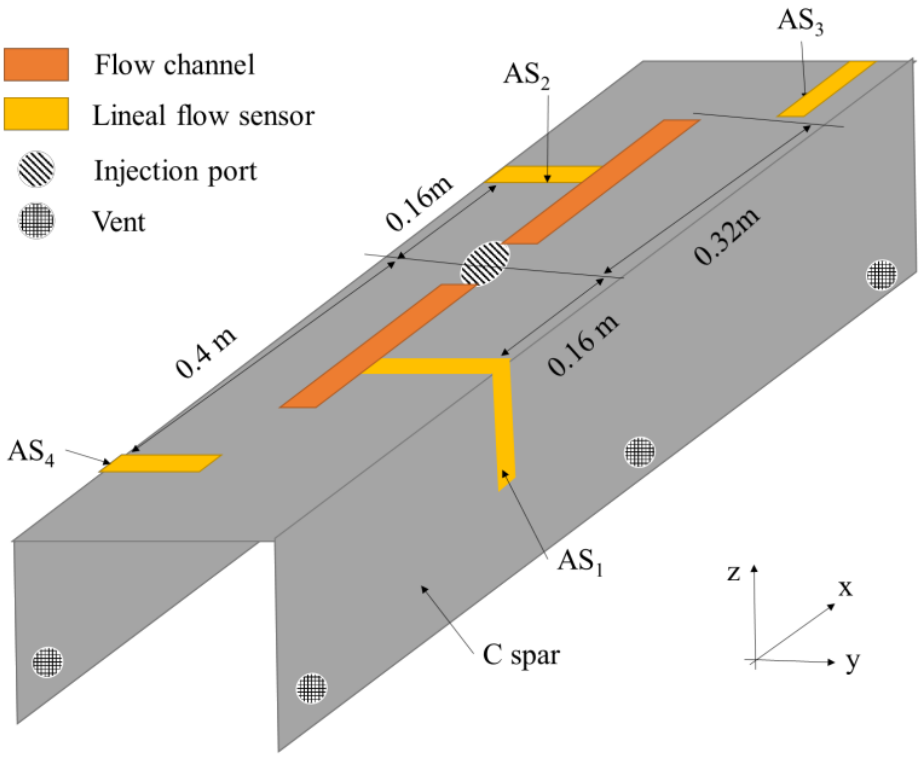

Figure 3.9 Flow model of RTM filling of carbon/epoxy composite C spar.

Four artificial lineal sensors were considered, placed in the assembly to acquire flow monitoring data during the filling stage used in the application of inversion scheme. Figure 3.9 depicts the location of each of the artificial sensors in the part. Artificial sensors 1 (AS_1) and 2 (AS_2) were placed symmetrically at a distance of 160 mm from the injection port. AS_1 is 75 mm long placed on the C spar top surface in parallel to the weft direction also covering a half of the C spar flange. AS_2 has a length of 50 mm placed on the C spar top surface parallel to the y direction. Artificial sensor 3 (AS_3) is 75 mm long and alligned parallel to the x direction to acquire monitoring data sensitive to longitudinal permeability. Artificial sensor 4 (AS_4) was placed 400 mm from the injection port parallel to the y direction and has a length of 50 mm.

3.5.2. Cure modelling

The heat transfer mechanism governing cure after completion of filling/consolidation is heat conduction, since convection due to buoyancy flow plays only a negligible role. The governing energy balance is:

$$\rho c_p \frac{\partial T}{\partial t} = \nabla \mathbf{K} \nabla T + (1 - v_f)\rho_r H_{tot} \frac{d\alpha}{dt} \tag{3.5}$$

where ρ is the density of the composite, c_p is the specific heat capacity, T the temperature, $\mathbf{K}$ the thermal conductivity tensor, v_f the fibre volume fraction, ρ_r the resin density, H_{tot} the total heat of the curing reaction, and α the degree of cure. The left-hand side of Eq. (3.5) expresses the rate of change of volumetric enthalpy. The first term of the right-hand side of Eq. (3.5) represents heat conduction, whilst the second term heat generated due to the exothermic resin reaction.

Three types of boundary conditions can be applied to the general case: i) prescribed temperature ii) convection iii) prescribed heat flux. The prescribed temperature boundary condition is expressed as follows:

$$T(\mathbf{d}, t) = T_b(\mathbf{d}, t), \qquad \mathbf{d} \in D_1 \tag{3.6}$$

where $\mathbf{d}$ denotes the spatial coordinates at the boundary D_1, whilst T_b is the prescribed temperature. The convection boundary condition is:

$$-\mathbf{n_{sv}} \mathbf{K} \nabla T(\mathbf{d}, t) = h(T(\mathbf{d}, t) - T_\infty), \qquad \mathbf{d} \in D_2 \tag{3.7}$$

where $\mathbf{n_{sv}}$ denotes the surface vector at the boundary D_2, h the surface heat transfer coefficient, and T_∞ the ambient temperature. The prescribed heat flux (q) condition is expressed as follows:

$$-\mathbf{n_{sv}} \mathbf{K} \nabla T(\mathbf{d}, t) = q(\mathbf{d}, t), \qquad \mathbf{d} \in D_3 \tag{3.8}$$

where

$$D_1 \cup D_2 \cup D_3 = D \tag{3.9}$$

where D is the boundary of the whole domain, and D_1, D_2, D_3 the corresponding parts of the boundary at which the prescribed temperature, convection and prescribed heat flux conditions apply respectively.

The simulation of cure process was performed using the Finite Element solver MSC.Marc [131]. The modelling approach is based on 3-D iso-parametric eight-node composite brick elements (175 MSC.Marc element type [132]) for thermal analysis. These elements allow the modelling of laminates with layers of different material properties, fibre orientations and thicknesses. Each element includes four integration points used for numerical integration based on Gaussian quadrature [132]. The parts used for cure modelling consists of rectangular flat panels with uniform thickness and are symmetrical in the in-plane directions. Assuming uniform heating across the tool cavity, the heat transfer problem is one-dimensional -in the through the thickness direction- requiring the use of only one element across the in-plane dimensions. A perfect insulation boundary condition is implied at the sides of each element to represent the symmetry of the geometry. User defined subroutines written in FORTRAN 90 [133] were used for the incorporation of constitutive material properties and boundary conditions in the cure model. More specifically, the UCURE subroutine was used for the computation of cure kinetics and heat of reaction. In the cure model, the degree of cure is calculated for each element at each simulation increment. The specific heat capacity model was incorporated into the model using subroutine USPCHT calculated at each integration point of each element. Subroutine ELMVAR is called to extract degree of cure information at each element integration point to incorporate the dependence of specific heat capacity on temperature and degree of cure. The thermal conductivity matrix is calculated using subroutine ANKOND. Considering the one-dimensional nature of the heat transfer problem only the through thickness thermal conductivity (K_{33}) was computed. The ELMVAR subroutine is also incorporated into ANKOND in order to acquire the degree of cure at each integration point. In the case of boundary conditions, subroutine FORCDT was used for the time dependent prescribed temperature and UFILM for the convection applied. The initial degree of cure and temperature were implemented using subroutine USINC. PLOTV calls ELMVAR to acquire the degree of cure values of each element and writes the minimum value in the post file. The UPSTNO subroutine calls the NODVAR

subroutine to extract nodal temperature values in order to calculate and save in the post file the maximum temperature overshoot in the case of thick composite parts.

3.5.2.1. Cure simulation of RTM process

A thermal cure simulation model was developed, based on model presented in [4], to simulate the RTM cure of a glass/epoxy composite flat panel used for the development of the inversion procedure. Figure 3.10 illustrates a schematic representation of the model geometry. The model comprises two parts; a glass/epoxy composite flat panel, denoted as GFP, and the glass top plate of the RTM tool. The thermal properties of the glass top plate are reported in Table 3.2. The composite part comprises two layers of E-TX1769 (BTI Europe) tri-axial E-glass fabric and total layup sequence of [+45°/-45°/0°/0°/-45°/+45°] resulting in fibre weight fraction of 62% at a thickness of 3.3 mm. The model is built using six elements representing one ply of E-glass with 0.55 mm nominal thickness. The prescribed thermal profile assigned to the nodes of the lower element of the model includes an initial dwell at 120 °C for 30 min to ensure equilibration of the temperature gradient in the thickness direction. A heating ramp of 1.5 °C/min was applied from 120 °C to 160 °C followed by a 90 min dwell. A natural convection boundary condition was applied on the top surface of the upper element. The initial degree of cure in the model was 2%. User subroutine UPSTNO was used to extract the temperatures evolution with time at the mid-thickness and at the top surface of the cure model which correspond to the thermocouples responses during RTM curing of the part.

Table 3.2 Glass top plate thermal properties [4].

Properties	Value	Units
Density	2.7	gcm^{-3}
Specific heat capacity	0.84	$Jg^{-1}°C^{-1}$
Thermal conductivity	0.78	$Wm^{-1}°C^{-1}$
Heat transfer coefficient	8.5	$Wm^{-2}°C^{-1}$

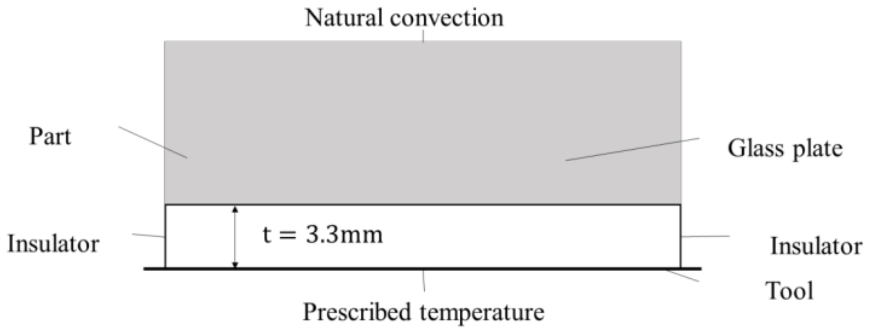

Figure 3.10 Cure model of RTM curing of glass/epoxy composite flat panel (GFP).

3.5.2.2. Simulation of oven cure

A heat transfer cure simulation model was developed to represent the cure of a carbon/epoxy thick flat panel, denoted as TFP, in an oven. The cure model was used for the assessment of the stochastic multi-objective optimisation framework. Figure 3.11 illustrates a schematic representation of the model. The model includes 26 elements representing a 15.6 mm thick laminate. Each element represents two layers of G1157 UD carbon fabric with a thickness of 0.3 mm each and total sequence of $[0/90]_{26}$. A prescribed temperature profile was applied to the lower boundary of composite flat panel, whilst forced air convection was applied to the top surface as specified in section 3.4.2. The initial temperature assigned to all nodes was 120 °C and the initial degree of cure applied to all elements was 0.02.

Subroutines PLOTV and UPSTNO were used to compute and save in post files the cure time and the maximum temperature overshoot used as objectives in the optimisation. Cure time is defined as the time at which the minimum degree of cure of the part is greater than 88%, which is the degree of cure that RTM6 epoxy resin reaches in an isothermal cure at 180 °C as determined by Differential Scanning Calorimetry (DSC) [134]. When the degree of cure reaches this threshold the simulation ends. The maximum temperature overshoot is defined as the maximum difference between the prescribed tool temperature and the temperature in the composite during the process.

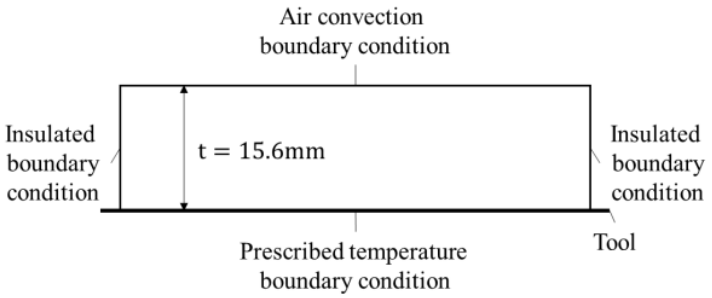

Figure 3.11 Cure model of VARTM curing of carbon/epoxy thick composite flat panel (TFP).

3.6. Surrogate models

Process simulation using FE analysis is computationally expensive. Conventional computing resources are inadequate to handle large number of function evaluations of an FE model required by computational methods such as stochastic simulation, inverse solutions and stochastic multi-objective optimisation. Therefore, surrogate models were developed using the Kriging method to overcome this issue by substituting the FE solution for the filling and curing stage of the manufacturing process. Kriging allows the unbiased estimation of untried parameter values to be made with minimum variance and more accurately in comparison to low order polynomial regression [135]. Figure 3.12 illustrates the procedure of surrogate model development adopted in this work. Kriging requires a set of sampling points at which the model response is known. Latin Hypercube Sampling (LHS) [136] was utilised for generating a large sample of N points, whilst the filling and cure FE models were used to compute the response at these points.

The Kriging metamodel expresses the model response $Y_m(\mathbf{x}) \in \mathbb{R}$ for the input vector $\mathbf{x} \in \mathbb{R}^n$ as follows:

$$\mathbf{Y_m(x)} = \mathbf{f(x)^T\beta} + \mathbf{r(x)^T\gamma^*} \tag{3.10}$$

where term $\mathbf{f(x)^T\beta}$ corresponds to a 2nd order regression model expressing the output variable as a linear combination of p basis functions $f_i(\mathbf{x})$: $\mathbb{R}^p \longmapsto \mathbb{R}$ expressed as:

$$\mathbf{f(x)^T\beta} = \beta_1 f_1(\mathbf{x}) + \cdots + \beta_p f_p(\mathbf{x}) \tag{3.11}$$

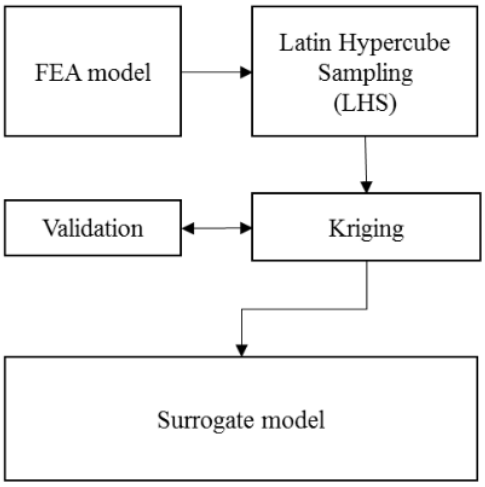

Figure 3.12 Surrogate model methodology

Here $\boldsymbol{\beta} \in \mathbb{R}^{p}$ is the vector of regression parameters computed using generalised least squares and p is:

$$p = \frac{(n+1)(n+2)}{2} \tag{3.12}$$

with n the dimensionality of the model.

Term $\mathbf{r}(\mathbf{x})$ corresponds to a vector of cross-correlations between input point $\mathbf{x}$ and each of N sampling points ($\mathbf{s_x} \in \mathbb{R}^{n}$):

$$\mathbf{r}(\mathbf{x}) = [R(\boldsymbol{\theta}, \mathbf{x}, \mathbf{s_x^1}), \dots, R(\boldsymbol{\theta}, \mathbf{x}, \mathbf{s_x^N})]^{\mathbf{T}} \tag{3.13}$$

Here $R(\boldsymbol{\theta}, \mathbf{x}, \mathbf{s_x^m})$ denotes the correlation between input point $\mathbf{x}$ and sampling point $\mathbf{s_x^m}$ and depends on the parameter vector $\boldsymbol{\theta} \in \mathbb{R}^{n}$ and the distance between them. A Gaussian function was chosen for the correlation structure as follows:

$$\mathbf{R}(\boldsymbol{\theta}, \mathbf{x}, \mathbf{s}) = e^{-\theta_q d_q}, \qquad d_q = x_q - s_q, \qquad q = 1, \dots, n \tag{3.14}$$

The parameter vector $\boldsymbol{\theta}$ allows the correlation function to represent anisotropy in the correlation across different directions of the model. The optimal correlation parameter vector $\boldsymbol{\theta}$ can be estimated by solving the following minimisation problem [137]:

$$\boldsymbol{\theta} = \arg\ \min\left(|\mathcal{R}|^{\frac{1}{N}}\sigma^2\right) \tag{3.15}$$

where $|\mathcal{R}|$ is the determinant of the correlation matrix $\boldsymbol{\mathcal{R}} \in \mathbb{R}^{N\times N}$ of all sampling points involved in the model and σ^2 is the predictor Gaussian process variance, expressed as follows [138]:

$$\sigma^2 = \frac{1}{N}\left[s_y^1 - \mathbf{f}(\mathbf{s_x^1})^T\boldsymbol{\beta} \quad \dots \quad s_y^N - \mathbf{f}(\mathbf{s_x^N})^T\boldsymbol{\beta}\right]\boldsymbol{\mathcal{R}}^{-1}\begin{bmatrix} s_y^1 - \mathbf{f}(\mathbf{s_x^1})^T\boldsymbol{\beta} \\ \vdots \\ s_y^N - \mathbf{f}(\mathbf{s_x^N})^T\boldsymbol{\beta}\end{bmatrix} \tag{3.16}$$

The minimisation problem in Eq. (3.15) is combined with the estimation of the regression coefficients ($\boldsymbol{\beta}$) in Eq. (3.11) and of the process variance (σ^2) based on maximising the likelihood of responses $s_y^1, \dots, s_y^N$ at sampling points $\mathbf{s_x^1}, \dots, \mathbf{s_x^N}$ respectively.

Vector $\boldsymbol{\gamma}^* \in \mathbb{R}^N$ is computed as follows:

$$\boldsymbol{\gamma}^* = \boldsymbol{\mathcal{R}}^{-1}\begin{bmatrix} s_y^1 - \mathbf{f}(\mathbf{s_x^1})^T\boldsymbol{\beta} \\ \vdots \\ s_y^N - \mathbf{f}(\mathbf{s_x^M})^T\boldsymbol{\beta}\end{bmatrix} \tag{3.17}$$

Surrogate models were constructed utilising Eqs. (3.10)-(3.17) to represent process outcomes and the response of dielectric sensors and thermocouples integrated into the RTM filling and RTM/VARTM curing stage as a function of stochastic and/or unknown variables. The inputs and the corresponding responses of each of the surrogate models are summarised in Table 3.3. Four surrogate models were constructed based on the flow model described in section 3.5.1.1, denoted as FPR SM, representing the RTM filling of the FPR composite. FPR SM_1, FPR SM_2 and FPR SM_3 describe the response of the three lineal dielectric sensors, specified in section 3.4.1, as a function of stochastic parameters i.e. preform permeability, resin viscosity, race tracking permeability and time. FPR SM_4 calculates the duration of the filling stage for a given set of stochastic parameters. Five surrogate models, denoted as C spar SM were built based on the model representing the artificial RTM filling of composite C spar presented in section 3.5.1.2. C spar SM_1 - C spar SM_4 express the response of the four artificial flow sensors as a function of stochastic parameters such as principal permeability and resin viscosity, whilst C spar SM_5 computes the duration of the filling stage.

Table 3.3 Surrogate models inputs and outputs parameters.

	Kriging parameters	
Surrogate models (SM)	Response: **Y**	Inputs **x**
FPR SM_1 FPR SM_2 FPR SM_3	Sensor 1 response Sensor 2 response Sensor 2 response	Preform permeabilities Race tracking permeability Initial resin viscsoity Filling time
FPR SM_4	Filling duration	Preform permeabilities Race tracking permeability Initial resin viscosity
C spar SM_1 C spar SM_2 C spar SM_3 C spar SM_4	Artificial sensor 1 response Artificial sensor 2 response Artificial sensor 3 response Artificial sensor 4 response	Principal permeabilities Initial resin viscsoity Filling time
C spar SM_5	Filling duration	Principal permeabilities Initial resin viscosity
GFP SM_1 GFP SM_2	Thermocouple 1 response Thermocouple 2 response	Heat transfer coefficient Resin thermal conductivity Cure time
GFP SM_3	Final minimum degree of cure	Heat transfer coefficient Resin thermal conductivity
TFP SM_1 TFP SM_2	Cure duration Maximum overshoot	Cure profile parameters Cure kinetics parameters Heat transfer coefficient Tool temperature

In the case of RTM curing of a glass/epoxy flat panel (GFP), described in section 3.5.2.1, three surrogate models were developed denoted as GFP SM_1, GFP SM_2 and GFP SM_3. GFP SM_1 and GFP SM_2 represent the outputs of thermocouples as a function of unknown thermal properties and boundary conditions. GFP SM_3 estimates the final minimum degree of cure for a given set of unknown input parameters. The surrogate models of FPR, C spar and GFP are used for the development of the inversion scheme. Two surrogate models were developed for the stochastic multi-objective optimisation of cure based on

the model described in section 3.5.2.2. The surrogate models, denoted as TFP SM_1 and TFP SM_2, calculate the cure time and maximum temperature overshoot for a given set of inputs which include cure profile parameters, cure kinetics parameters and boundary conditions parameters.

The estimation problem corresponding to Eqs. (3.10)-(3.17) was implemented and solved using the MATLAB® toolbox for Kriging modelling [139]. The estimated Kriging coefficients vectors of regression and correlation model ($\boldsymbol{\beta}$ and $\boldsymbol{\gamma}^*$), the optimal correlation parameter vector ($\boldsymbol{\theta}$) and the initial sample matrix ($\mathbf{S}$) were utilised for the implementation of the predictor in Eq. (3.10). The surrogate model predictors expressed by Eq. (3.10) were implemented in Visual Studio C++ 2015.

3.7. Stochastic simulation

A Stochastic simulation methodology is developed to model input parameters uncertainty in order to investigate its effect on filling and curing process outcomes. The Ornstein-Uhlenbeck (OU) process is used for the modelling of residuals of the de-trending of periodic signals. The Monte Carlo scheme was used for stochastic simulation to account for the influence of process parameters variability on the uncertainty of process outcomes for the filling and curing stages.

3.7.1. Ornstein-Uhlenbeck process

The OU process is an autoregressive second order stationary Gaussian process used for modelling of mean reverting processes. These processes tend to drift towards a long term mean with a rate proportional to the distance from it. In composite manufacture the OU process has been employed to model autocorrelation structures of random fields such as imperfections in fibre architecture [8, 10] and residuals after de-trending applied to tool and air temperature periodic signal [38]. An OU process can be expressed as follows [140]:

$$dS_{OU} = \lambda_{OU}(\mu_{OU} - S_{OU})dt + \sigma_{OU}dW_t \tag{3.18}$$

where S_{OU} is the OU process, W_t a Brownian motion following a normal distribution with mean 0 and standard deviation 1 so that $W_t \sim N(0,1)$, whilst dW_t follows a normal distribution with mean 0 and standard deviation $\sqrt{dt}$ so that $W_t \sim N(0, \sqrt{dt})$, λ_{OU} controls

the speed of mean reversion to the long term average of the process, σ_{OU} is the process volatility and μ_{OU} is the long term mean of the stochastic process. The analytical solution of Eq. (3.18) has been used in this study to develop the stochastic objects of tool and air temperature and can be written as follows [140]:

$$S_{OU} = e^{-\lambda_{OU}dt} S_{OU-1} + \left(1 - e^{-\lambda_{OU}dt}\right)\mu_{OU} + \sigma_{OU}\sqrt{\frac{\left(1 - e^{-2\lambda_{OU}dt}\right)}{2\lambda_{OU}}} W_t \qquad (3.19)$$

where dt is the time increment. The parameters of Eq. (3.19) are calculated using the experimental data acquired for the tool and air temperature based on maximisation of the likelihood function [140].

3.7.2. Monte Carlo scheme

The stochastic simulation carried out in this work is based on the MC scheme involving the generation of N_{MC} realisations of random input stochastic variables using the Mersenne Twister random number generator [141]. In each realisation, the deterministic model is executed calculating the process outcomes and subsequently computing the first and second statistical moments using the overall set of realisations up to the current point. The outputs of the stochastic simulation are the average and standard deviation of relevant process outcomes. The total number of deterministic model realisations depends on the convergence of first and second statistical moments. The Cholesky decomposition was applied to transform stochastic variables which present strong correlation to the set of uncorrelated random variables.

The MC scheme is applied to the RTM filling of the FPR and C spar part described in sections 3.5.1.1 and 3.5.1.2 respectively to investigate the influence of stochastic flow parameters on the filling duration. In curing, MC is implemented in the case of the GFP composite part described in section 3.5.2.1 examining the variability of final minimum degree of cure due to variations of material properties and boundary conditions. The stochastic multi-objective optimisation scheme, which is presented in chapter 9, incorporates the MC scheme in order to calculate the average and standard deviation of cure process outcomes specified in 3.5.2.2 considering the variability of input parameters.

3.8. Inversion scheme using Markov Chain Monte Carlo

An inversion scheme was developed integrating monitoring data in real time with the process models for the probabilistic prediction of the unknown stochastic parameters and

the process outcomes. The inversion scheme illustrated in Figure 3.13, utilised the Markov Chain Monte Carlo method. MCMC is based on Bayes' theorem and is utilised in many inverse problems due to its simplicity [104–106]. Bayesian inference operates as a sampler and addresses potential ill-posedness of inverse problems by incorporating prior knowledge about the parameters values. MCMC draws a series of parameter realisations with a probability of acceptance proportional to the conditional incremental likelihood of process monitoring data. The accepted realisations constitute the solution of the inverse problem in the form of a probabilistic estimate of process outcomes. According to Bayes' theorem, the monitoring data matrix $\mathbf{Y_{exp}}(t) \in \mathbb{R}^{n_{exp} x n_{set}}$ is linked to the corresponding surrogate model responses $\mathbf{Y_m}$ as follows:

$$P(\mathbf{Y_m}|\mathbf{Y_{exp}}) \propto P(\mathbf{Y_{exp}}|\mathbf{Y_m})P(\mathbf{Y_m}) \tag{3.20}$$

where $P(\mathbf{Y_m}|\mathbf{Y_{exp}})$ denotes the posterior probability, $P(\mathbf{Y_{exp}}|\mathbf{Y_m})$ the likelihood distribution and $P(\mathbf{Y_m})$ the prior distribution. Eq. (3.20) expresses the probability of model response $\mathbf{Y_m}$ for a given set of unknown stochastic parameters $\mathbf{V}$ conditional to process monitoring data $\mathbf{Y_{exp}}$. MCMC utilises Bayes' theorem to accept or reject the proposed set of input samples which in this case are the unknown stochastic parameters. The random walk Metropolis Hastings algorithm was utilised to generate samples $\mathbf{V_j} \in \mathbb{R}^{\mathbf{n_p}}$ where n_p is the number of unknown stochastic input parameters from a symmetric normal proposal distribution $q(\mathbf{V_j}|\mathbf{V_{j-1}})$ resulting in a simplified draw of new samples. Due to symmetry, the new sample $\mathbf{V_j}$ is calculated using an incremental step drawn from the multivariate Gaussian variable $\boldsymbol{\varepsilon} \in \mathbb{R}^{\mathbf{n_p}}$ with mean value 0 and standard deviation $\boldsymbol{\sigma_\varepsilon} \in \mathbb{R}^{\mathbf{n_p}}$, applied to sample $\mathbf{V_{j-1}}$ from the previous step. An acceptance criterion is applied to each of the samples generated and by accepting or rejecting it the posterior probability converges to the target distribution $P(\mathbf{Y_m}(\mathbf{V}, t)|\mathbf{Y_{exp}}(t))$. The algorithm operates as shown in Table 3.4 and the procedure is repeated M times, where M is the number of MCMC iterations.

The likelihood distribution is expressed as:

$$P(\mathbf{Y_{exp}}(t)|\mathbf{Y_m}(\mathbf{V_j}, t)) = \prod_{k=1}^{N_k} N(\mathbf{Y_{exp}}(t_k); \mathbf{Y_m}(\mathbf{V_j}, t_k), \sigma_{exp}) \tag{3.21}$$

where N_k denotes the total number of experimental data acquired by time t_k. The likelihood incorporates all the distributions which are computed with experimental data $\mathbf{Y_{exp}}$ using a normal distribution with the model values $\mathbf{Y_m}(\mathbf{V_j}, t_k)$ as a mean and a standard deviation σ_{exp}. The prior distribution of input vector $\mathbf{V_j}$ including the unknown stochastic variables is computed in a similar way:

$$P(\mathbf{V_j}) = \prod_{o=1}^{n_p} N(V_j^o; \mu_{prior}^o, \sigma_{prior}^o) \tag{3.22}$$

where $\boldsymbol{\mu_{prior}} \in \mathbb{R}^{n_p}$ and $\boldsymbol{\sigma_{prior}} \in \mathbb{R}^{n_p}$ are the mean and standard deviation of the prior distributions.

Table 3.4 Metropolis Hastings algorithm.

Algorithm 1 Metropolis Hastings algorithm

Initialise $\mathbf{V_0}$

for $j = 1$ to M

Draw a sample $u \sim U(0,1)$ from a uniform distribution.

Draw sample $\boldsymbol{\varepsilon} \sim N(\mathbf{0}, \boldsymbol{\sigma_\varepsilon}) \longrightarrow \mathbf{V_j} = \mathbf{V_{j-1}} + \boldsymbol{\varepsilon}$

Calculate acceptance probability $a = \min\left\{1, \frac{P(\mathbf{Y_{exp}}(t)|\mathbf{Y_m}(\mathbf{V_j}, t))P(\mathbf{V_j})}{P(\mathbf{Y_{exp}}(t)|\mathbf{Y_m}(\mathbf{V_{j-1}}, t))P(\mathbf{V_{j-1}})}\right\}$

if $u \leq a$ then

accept $\mathbf{V_j}$

else

$\mathbf{V_j} = \mathbf{V_{j-1}}$

end if

end for

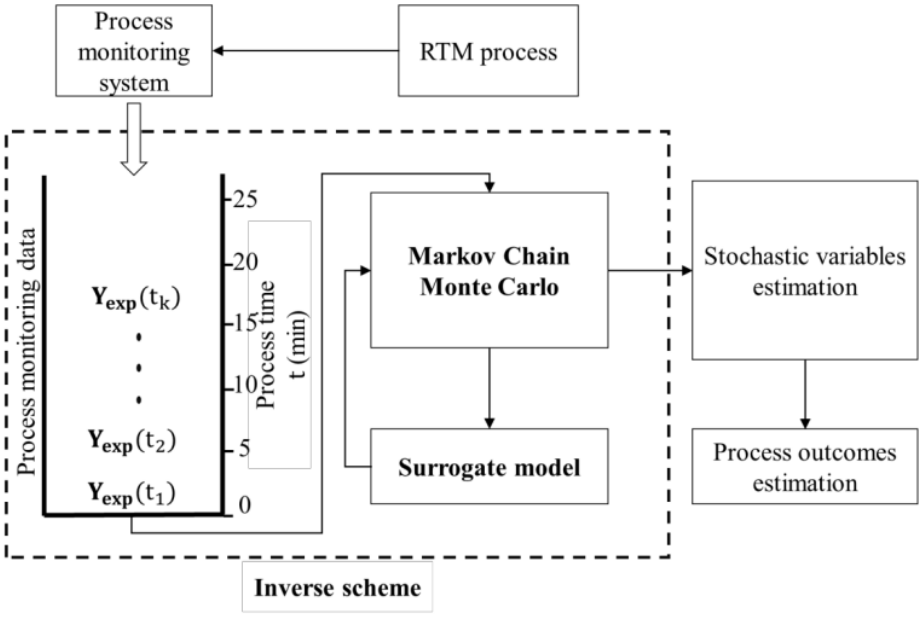

Figure 3.13 Inversion procedure framework

Simulations of a single chain may be trapped in a local mode. Parallel tempering was applied to address this problem. In this method a temperature parameter T_{pt} with the property $1 \leq T_{pt} \leq \infty$ is introduced where $T_{pt} = 1$ corresponds to the desired target distribution and is referred to as cold sample. Values with $T_{pt} \gg 1$, which are referred to as hot samples, flatten the target distribution and allow the acceptance of a wider range of proposed parameters. Hence, these distributions explore a wider parameter region. In parallel tempering a parameter defined as $z = 1/T_{pt}$ is assigned to the likelihood term as follows:

$$\pi\left(\mathbf{Y_T}(\mathbf{V_j}, t)\middle|\mathbf{Y_{exp}}(t), w\right) = P\left(\mathbf{Y_{exp}}(t)\middle|\mathbf{Y_T}(\mathbf{V_j}, t)\right)^z P(\mathbf{V_j}) \text{ for } 0 < z < 1 \qquad (3.23)$$

This tempering posterior distribution is calculated using Eq. (3.20). A different discrete value of z is assigned to each of the n_{ch} chains resulting in a ladder with different temperatures. After a certain number of iterations (n_s) a parameter swap algorithm is initiated which exchanges parameters between two chains, if $U_1 \sim U[0,1] \leq 1/n_s$ with U_1 being a random number drawn from a uniform distribution. If the swap occurs, a chain

l is randomly selected to swap the parameter set with the chain $l+1$. A swap is accepted if $a_{pt} \geq U_2$ where $U_2 \sim U[0,1]$ and a_{pt} is the acceptance probability expressed as:

$$a_{pt} = \min\left\{1, \frac{\pi\left(\mathbf{Y_m}(\mathbf{V_j^{l+1}}, t)\middle|\mathbf{Y_{exp}}(t), z_m\right)\pi\left(\mathbf{Y_m}(\mathbf{V_j^{l}}, t)\middle|\mathbf{Y_{exp}}(t), z_{l+1}\right)}{\pi\left(\mathbf{Y_m}(\mathbf{V_j^{l}}, t)\middle|\mathbf{Y_{exp}}(t), z_m\right)\pi\left(\mathbf{Y_m}(\mathbf{V_j^{l+1}}, t)\middle|\mathbf{Y_{exp}}(t), z_{l+1}\right)}\right\} \quad (3.24)$$

Chains with higher temperatures can explore different modes, whilst chains within the ladder allow the possibility to refine these sets. Only the results of the cold chain corresponding to the target distribution are considered for the final sample, whilst the results from the remaining chains are disregarded [142].

The inversion scheme was implemented in real time in the RTM filling of the FPR composite part and composite C spar using flow monitoring data acquired by lineal dielectric and artificial flow sensors. The monitoring matrix ($\mathbf{Y_{exp}}$) at time t_k comprises the flow front position S_{1-3}^k and AS_{1-4}^k of each of the flow dielectric and artificial flow sensors. The inversion procedure was also used in a cure heat transfer problem integrating temperature signals for the manufacturing of a glass/epoxy composite flat panel, which is described in chapter 8, with cure models for the estimation uncertainty of thermal properties and boundary conditions. In this case, $\mathbf{Y_{exp}}$ includes the thermocouples response T_{mid}^k and T_{top}^k up to time t_k placed in the middle and on the top of the glass/epoxy composite flat panel. The response vector ($\mathbf{Y_m}$) calculated using the models corresponds to estimations of monitoring sensors and process outcomes using the drawn sample of unknown stochastic parameters $\mathbf{V}$ as an input. Standard deviation σ_{exp} is utilised in the likelihood distribution in Eq. (3.21) to express the accuracy of the experimental data. Table 3.5 summarises the main parameters of the MCMC for each of the three case studies. The standard deviation vector $\boldsymbol{\sigma_\varepsilon}$ defines the size of the sampling step of the chain [143] and needs to be adjusted before the initiation of the inversion procedure. A short sequence of MCMC iterations is carried out at the beginning of the inverse algorithm to tune the vector of $\boldsymbol{\sigma_\varepsilon}$ of the algorithm targeting an acceptance probability between 30% and 50% [143].

Table 3.5 Inversion scheme parameters for each implementation.

	Filling stage		Curing stage
	FPR	**C spar**	**GFP**
Monitoring matrix $\mathbf{Y_{exp}}(t_k)$	$\begin{bmatrix} S_1^1 & \cdots & S_3^1 \\ \vdots & \ddots & \vdots \\ S_1^k & \cdots & S_3^k \end{bmatrix}$	$\begin{bmatrix} AS_1^1 & \cdots & AS_4^1 \\ \vdots & \ddots & \vdots \\ AS_1^k & \cdots & AS_4^k \end{bmatrix}$	$\begin{bmatrix} T_{mid}^1 & T_{top}^1 \\ \vdots & \vdots \\ T_{mid}^k & T_{top}^k \end{bmatrix}$
Number of sensors (n_{set})	3	4	2
Type of sensors	Lineal dielectric flow	Artificial lineal flow	Thermocouples
Number of points (N)	96	19	220
Model response $\mathbf{Y_m}(\mathbf{V_j}, t_k)$	Response of sensors Filling duration	Response of sensors Filling duration	Response of sensros Final minimum degree of cure
Unknowns ($\mathbf{V_j}$)	Preform permeability Race tracking permeabilit Resin viscosity	Principal permeability Resin viscosity	Thermal properties Boundary conditions
Standard deviation: (σ_{exp})	10 mm	10 mm	1 °C [144]

3.9. Stochastic multi-objective optimisation

A stochastic multi-objective optimisation scheme was developed integrating the Monte Carlo scheme described in section 3.7.2 with a GA for multi-objective optimisation [120].

The stochastic multi-objective optimisation framework illustrated in Figure 3.14 was implemented in Visual Studio C++ 2015. In this, the GA begins with the generation of the first population of individuals corresponding to a solution of design space. The individuals correspond to the average and standard deviation of the optimisation objective parameters calculated using the MC simulation. A fitness function, which evaluates the goodness of a solution, is assigned to each individual. Individuals are compared with others within the population and a dominance rank is formed by decreasing dominated individuals rank by a fixed value where in this case is five. A sharing ranking is also applied to ensure evenly distributed optimal points. This includes the penalisation by one of an individual which is within a defined radius of another one. When the ranking process completes the individuals of the population are sorted according to their fitness value. The best individuals are sent to the next generation, whilst the others compete in a tournament procedure. Four individuals called parents are selected through a tournament selection to generate new offsprings. In this selection process, which the selection probability increases with the increased fitness, four individuals are compared and the best among these is selected as first parent. Following the same procedure, the four selected individuals (parents) generate four individuals through two operators: uniform cross-over and mutation. These operations are repeated until a new population has been generated. The output of the GA is the Pareto set of optimal design parameters and the corresponding objective values; the average and the standard deviation. The algorithm accepts as inputs the number of generations, the number of individuals in each generation, the reproduction, the elite number and the size of the optimal Pareto front, the number of objectives, the number of the optimisation parameters and their ranges, and the probability of cross-over and mutation. The algorithm stops when a maximum number of generations has been met.

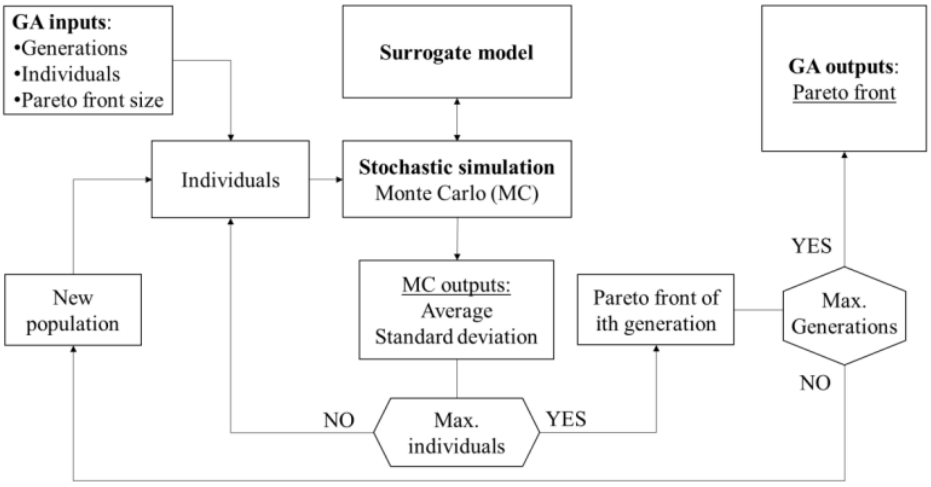

Figure 3.14 Stochastic multi-objective optimisation methodology.

The stochastic multi-objective optimisation was implemented in the case of the cure process of a carbon/epoxy thick composite flat panel described in section 3.5.2.2. In this case, four minimisation objectives were considered for the stochastic optimisation problem; the cure time (t_{cure}) and the maximum temperature overshoot (ΔT_{max}) mean values and their corresponding standard deviations. The design parameters are the parameters of the two-dwell cure profile illustrated in Figure 3.15, such as the temperature of first (T_1) and second dwell (T_2), the duration of the first dwell (Δt_1) and the heat ramp rate (r). The second dwell time is not considered as a design parameter in the optimisation due to the definition of cure time. The stochastic variables for the integrated MC simulation were the cure kinetics parameters and thermal boundary conditions i.e. tool temperature and heat transfer coefficient.

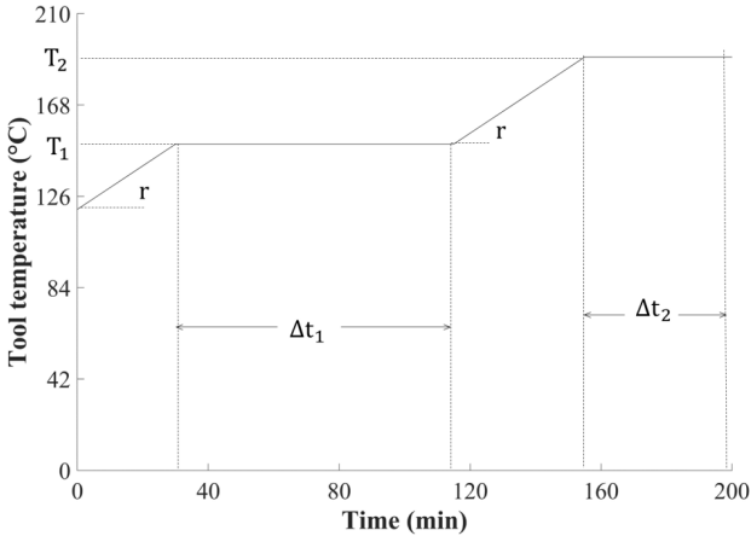

Figure 3.15 Two-dwell cure profile for the cure process of thick carbon/epoxy composite flat panel.

3.10. Overview

This chapter reports all methodological aspects of the work, detailing both experimental and computational methods. The rheology set-up presented in this chapter is used for the characterisation of the RTM6 epoxy resin viscosity and the quantification of its variability in chapter 4. The apparatus for isothermal curing of neat resin is used for the assessment the accuracy of the cure dielectric sensor developed and described in chapter 5. Process simulation models representing the filling and curing stage of LCM processing form the basis for the construction of surrogate models used for inversion and process optimisation in chapters 6-9. The stochastic processes presented in this chapter are used for the development of stochastic objects representing material properties and boundary conditions variability. The stochastic simulation based on MC is applied to the filling stage of FPR which is presented in chapter 6. The use of surrogate models results in reducing of computational time, allowing the real time application of the inversion scheme in the RTM filling and curing stage which is presented in chapters 6-8. The implementation of stochastic multi-objective optimisation - which is presented in chapter 9 - is performed for the cure of a thick composite part with the use of surrogate models to address the high computational cost of the stochastic simulation integration into the GA.

4. Material models and uncertainty quantification

4.1. Introduction

In the present chapter, the constitutive models of material properties such as cure kinetics, specific heat capacity and thermal conductivity are specified for their integration into the process models described in section 3.5. The results of uncertainty quantification tests of resin viscosity and thermal boundary conditions described in sections 3.3.1 and 3.3.2 respectively are presented, whilst stochastic objects are developed based on the methodological approach presented in section 3.7 representing the corresponding variability. The stochastic variables such as preform permeability, cure kinetics and race tracking considered in the stochastic simulation of filling and cure are specified as well.

4.2. Constitutive material models

The filling stage of composites manufacture involves the flow of a thermosetting resin through a preform under the application of pressure. This process can be described by Darcy's law presented in Eq. (3.3), where the volume rate of flow is proportional to preform permeability and inversely proportional to resin viscosity. The resin viscosity is strongly affected by the material state and temperature.

A constitutive material model representing resin viscosity has been developed based on rheology results, and cure kinetics, glass transition temperature development and thermal properties models such as specific heat capacity and thermal conductivity of carbon fabric and epoxy resin are presented based on literature data.

4.2.1. Resin viscosity

Figure 4.1 illustrates the applied cyclic thermal profile and the corresponding resin viscosity results obtained following the procedure described in section 3.3.1. The viscosity increases exponentially with time due to the increasing cross-linking density of the thermosetting material and is a decreasing function of temperature. Raising the temperature results in higher mobility of resin molecules reducing the energy required for their movement and consequently the viscosity.

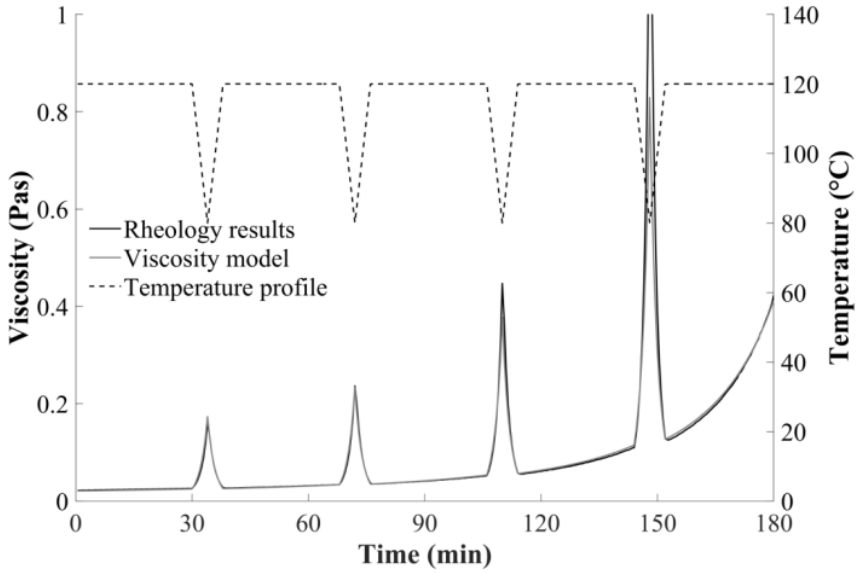

Figure 4.1 RTM6 epoxy resin viscosity model fitting.

For the representation of RTM6 epoxy resin viscosity a model was implemented utilising the viscosity η_{ref} at a reference temperature T_{ref} as a state variable [127]. The reference viscosity follows its own kinetics and can be expressed as:

$$\frac{d\ln\eta_{ref}}{dt} = Ae^{-\frac{E}{RT}}(\ln\frac{\eta_{ref}}{\gamma})^m \quad (4.1)$$

The rate of change of the reference viscosity in Eq. (4.1) follows an Arrhenius dependence on temperature where A is the pre-exponential factor and E is the activation energy of Arrhenius factor. The dependence of the rate of change on the logarithm of reference viscosity has an autocatalytic behaviour with m denoting the order of this dependence and γ a coefficient. The viscosity at any temperature can be estimated, using the reference viscosity calculated by the integration of Eq. (4.1), as follows:

$$\eta = \eta_{ref}Ae^{-D(\frac{1}{T}-\frac{1}{T_{ref}})} \quad (4.2)$$

where D is the temperature dependence coefficient.

Parameters A, E, γ, m, D in Eqs. (4.1) and (4.2) and the initial reference viscosity η_0 were estimated using the hybrid Genetic Algorithm implemented in the Solver of Microsoft Excel [145]. The reference temperature was set equal to the lowest temperature of cyclic

thermal profile 80 °C. The overall viscosity model parameters were obtained by conducting an overall fitting, using published values for the resin system of this study as initial guess [127]. The error minimisation indicator for model fitting is expressed as follows:

$$\text{Error} = \sum_{i=1}^{N_\eta} (\log\eta_{exp} - \log\eta_{mod})^2 \tag{4.3}$$

where N_η denotes the number of viscosity experimental data, η_{exp} the experimental measured viscosity and η_{mod} the viscosity as computed by the model. Table 4.1 summarises the results of RTM6 epoxy resin viscosity model fitting of a fresh sample of the 3rd resin batch. The average fitting error in this case is equal to 0.003.

Table 4.1 RTM6 resin viscosity model fitting parameters.

Parameter	Symbol	Value
Initial reference viscosity	η_0	0.13 Pas
Temperature dependence coefficient	D	6,500 1/K
Pre-exponential factor	A	171,508 1/s
Activation energy of Arrhenius function	E	70,485 J/mol
Coefficient	γ	0.059 Pas
Reaction order	m	1.31

4.2.2. Cure kinetics

The cure kinetics model for the resin system of RTM6 epoxy resin is a combination of an n^{th} order term and an autocatalytic term [146]:

$$\frac{d\alpha}{dt} = k_1(1-\alpha)^{n_1} + k_2(1-\alpha)^{n_2}\alpha^m \tag{4.4}$$

where α is the instantaneous degree of cure, m, n_1, n_2 the reaction orders and k_1 and k_2 the reaction rate constants defined as follows:

$$\frac{1}{k_i} = \frac{1}{k_{i,C}} + \frac{1}{k_d}, \qquad i = 1,2 \tag{4.5}$$

Here $k_{i,C}$ are Arrhenius functions of temperature for the chemical reaction and k_d is a diffusion rate constant, which expresses the deceleration of the reaction as the instantaneous glass transition of the curing material approaches the cure temperature. These are expressed as follows:

$$k_{i,C} = A_i e^{(-E_i/RT)}, \quad i = 1, 2 \tag{4.6}$$

$$k_d = A_d e^{(-E_d/RT)} e^{(-b/f_v)} \tag{4.7}$$

where A_i, A_d are pre-exponential factors, b is a fitting parameter, E_i and E_d the activation energy for the chemical reactions and diffusion process respectively, R the universal gas constant and f_v the equilibrium free volume, which is expressed as follows:

$$f_v = w(T - T_g) + g \tag{4.8}$$

Table 4.2 Parameters values for the RTM6 resin cure kinetics and glass transition temperature models [37]**.**

Parameter	Symbol	Value
Pre-exponential factor of the nth order term	A_1	$19{,}000\ s^{-1}$
Pre-exponential factor of the autocatalytic term	A_2	$22{,}080\ s^{-1}$
Pre-exponential factor of diffusion	A_d	$6.76\ 10^{18}\ s^{-1}$
Activation energy of the nth order term	E_1	$72{,}900\ Jmol^{-1}$
Activation energy of the autocatalytic term	E_2	$57{,}820\ Jmol^{-1}$
Activation energy of diffusion	E_d	$138{,}000\ Jmol^{-1}$
Autocatalytic reaction order	m	1.29
Reaction order of the nth order term	n_1	1.97
Reaction order of the autocatalytic term	n_2	1.53
Exponent of diffusion term	b	0.452
Equilibrium free volume model slope	w	$0.00048\ K^{-1}$
Equilibrium free volume model intercept	g	0.025
Glass transition temperature of uncured material	T_{g0}	262.15 K
Glass transition temperature of fully cured material	$T_{g\infty}$	479.15 K
Glass transition temperature convexity constant	λ	$0.435\ Jg^{-1}K^{-2}$

Here w and g are constants and T_g is the instantaneous glass transition temperature following the Di Benedetto equation [147]:

$$T_g = T_{g0} + \frac{(T_{g\infty} - T_{g0})\lambda\alpha}{1-(1-\lambda)\alpha} \quad (4.9)$$

where $T_{g\infty}$ and T_{g0} are the glass transition temperature of the fully cured and uncured material respectively and λ is a parameter controlling the convexity of the dependence. Model constants of Eqs. (4.4)-(4.9) are reported in Table 4.2 [37].

4.2.3. Composite specific heat capacity

The specific heat capacity of the composite is computed making use of the rule of mixtures as follows:

$$c_p = v_f c_{pf} + (1 - v_f) c_{pr} \quad (4.10)$$

where w_f is the fibre weight fraction, c_{pf} the fibre specific heat capacity and c_{pr} the specific heat capacity of the resin. The specific heat capacity of the resin and the fibre are computed using the models [120]:

$$c_{pf} = A_{fc_p} T + B_{fc_p} \quad (4.11)$$

$$c_{pr} = A_{rc_p} T + B_{rcp} + \frac{\Delta_{rc_p}}{1 + e^{C_{rc_p}(T - T_g - \sigma_r)}} \quad (4.12)$$

where A_{fc_p}, B_{fc_p} control the linear dependence of fibre specific heat capacity on temperature, A_{rc_p}, B_{rc_p} describe the linear dependence of the specific heat capacity of the uncured epoxy on temperature and Δ_{rc_p}, C_{rc_p}, and σ_r are the strength, width and temperature shift of the specific heat capacity step occurring at resin vitrification. The values of the parameters involved for the resin system of this study in Eqs. (4.10)-(4.12) are reported in Table 4.3 [120]. The densities of RTM6 epoxy resin ρ_r, Tenax® E HTA40 E13 6K carbon fibre ρ_{cf} and E-TX1769 (BTI Europe) E-glass fibre ρ_{gf} used in manufacturing trials and process simulation are reported in Table 4.3 [121, 123, 125].

4.2.4. Composite thermal conductivity

The thermal conductivity of the anisotropic composite material in the transverse direction is calculated as follows [148]:

$$K_{33} = v_f K_r \left(\frac{K_{tf}}{K_r} - 1\right) + K_r \left(\frac{1}{2} - \frac{K_{tf}}{2K_r}\right) K_r \left(\frac{K_{tf}}{K_r} 1\right) + \sqrt{v_f^2 - v_f + \frac{\left(\frac{K_{tf}}{K_r} + 1\right)^2}{\left(\frac{2K_{tf}}{K_r} - 2\right)^2}} \quad (4.13)$$

where K_{tf} is the thermal conductivity of the fibre in the transverse direction. The thermal conductivity of the carbon fibre in the transverse direction can be expressed as:

$$K_{tf} = B_{tf} \quad (4.14)$$

where B_{tf} is a constant.

Table 4.3 Model parameters values for the specific heat capacity of RTM6 epoxy resin [120] and density values for epoxy resin [121], Tenax® E HTA40 E13 6K carbon fibre [123] and E-TX1769 (BTI Europe) E-glass fibre [125].

Parameters	Symbol	Value
Carbon fibre specific heat capacity model slope	A_{cfc_p}	$0.0023\ Jg^{-1}°C^{-2}$
Carbon fibre specific heat capacity model intercept	B_{cfc_p}	$0.765\ Jg^{-1}°C^{-2}$
E-glass fibre specific heat capacity model slope	A_{gfc_p}	$0.0014\ Jg^{-1}°C^{-2}$
E-glass fibre specific heat capacity model intercept	B_{gfc_p}	$0.841\ Jg^{-1}°C^{-2}$
Resin specific heat capacity model slope	A_{rc_p}	$0.0025\ Jg^{-1}°C^{-2}$
Resin specific heat capacity model intercept	B_{rc_p}	$1.8\ Jg^{-1}°C^{-2}$
Resin specific heat capacity model step	Δ_{rc_p}	$-0.25\ Jg^{-1}°C^{-2}$
Resin specific heat capacity model step breadth parameter	C_{rc_p}	$1.1\ °C^{-1}$
Resin specific heat capacity model step shift parameter	σ_r	$16.5\ °C$
Resin density	ρ_r	$1.11\ gml^{-1}$
Carbon fibre density	ρ_{cf}	$1.76\ gml^{-1}$
E-glass fibre density	ρ_{gf}	$2.54\ gml^{-1}$

The thermal conductivity for the epoxy resin system RTM6 is a function of degree of cure and temperature and is expressed as [4]:

$$K_r = k_5 T\alpha^2 - k_4 T\alpha - k_3 T - k_2\alpha^2 + k_1\alpha + k \quad (4.15)$$

Here $k_5, k_4, k_3, k_2, k_1, k$ are coefficients of the polynomial function. The parameters of the thermal conductivity model are reported in Table 4.4 [4].

Table 4.4 Model parameters values for thermal conductivity constitutive models of RTM6 epoxy resin [4], Tenax® E HTA40 E13 6K carbon fibre [4] and E-TX1769 (BTI Europe) E-glass fibre [125].

Thermal conductivity parameters	Symbol	Values
Carbon fibre transverse thermal conductivity	B_{tcf}	$0.84\ Wm^{-1}{}^{\circ}C^{-2}$
E-glass fibre transverse thermal conductivity	B_{tgf}	$1.03\ Wm^{-1}{}^{\circ}C^{-2}$
Resin model quadratic coupling	k_5	$0.0008\ Wm^{-1}{}^{\circ}C^{-2}$
Resin model coupling constant	k_4	$-0.0011\ Wm^{-1}{}^{\circ}C^{-2}$
Resin model linear temperature constant	k_3	$-0.0002\ Wm^{-1}{}^{\circ}C^{-2}$
Resin model quadratic conversion constant	k_2	$-0.0937\ Wm^{-1}{}^{\circ}C^{-2}$
Resin model linear conversion constant	k_1	$0.22\ Wm^{-1}{}^{\circ}C^{-2}$
Resin model intercept	k	$0.12\ Wm^{-1}{}^{\circ}C^{-2}$

4.3. Uncertainty quantification of resin viscosity

Rheology results of resin sample of different batches and storage conditions are presented in Figure 4.2. All curves present the same qualitative behaviour as observed in characterisation results of resin viscosity described in section 4.2.1. The isothermal segments of thermal profile result in an increase of resin viscosity attributed to material state changes, whilst short term temperature drops/rises cause considerable changes of resin viscosity manifested as spikes in Figure 4.2.

Significant variability can be observed in both the comparison across batches and material exposed at ambient temperature for different durations. The samples used in this study were taken from four different resin batches (A, B, C, D) at the 1st (fresh) and 15th day of exposure at ambient temperature as described in section 3.3.1. Batches B and D present similar quantitative viscosity behaviour for both fresh samples and samples kept at ambient temperature for 15 days. However, the viscosity evolution of batches A and C presents significant differences in comparison to that of B and D. The batch to batch variability can be attributed to variations of thermal history due to different resin handling/storage conditions. Resin batches B and D have been defrosted several times within a certain time of period for different applications, whilst the utilisation of batches A and C resin was limited, whilst all batches were within their self-life. Samples tested at

the 1st day of exposure at ambient temperature present an initial resin viscosity in the range of 0.02–0.024 Pas. In contrast, the initial viscosity range of samples left for 15 days at ambient conditions is in the range of 0.025-0.042 Pas.

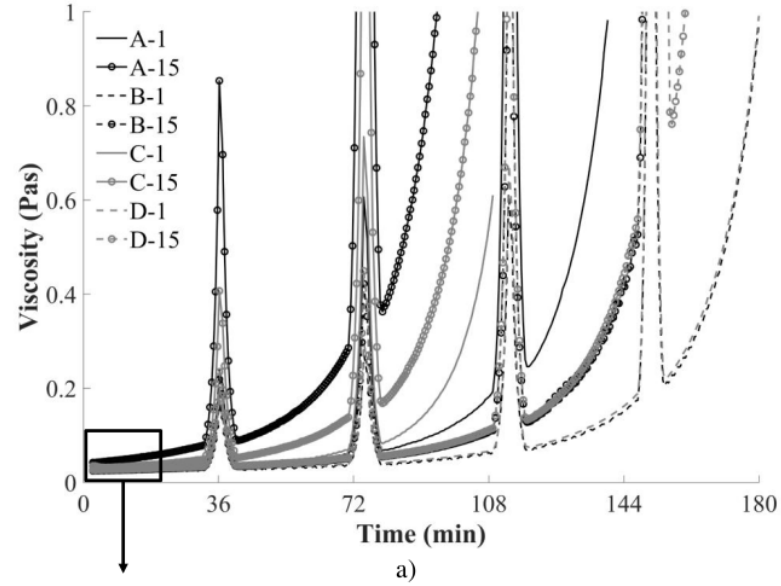

a)

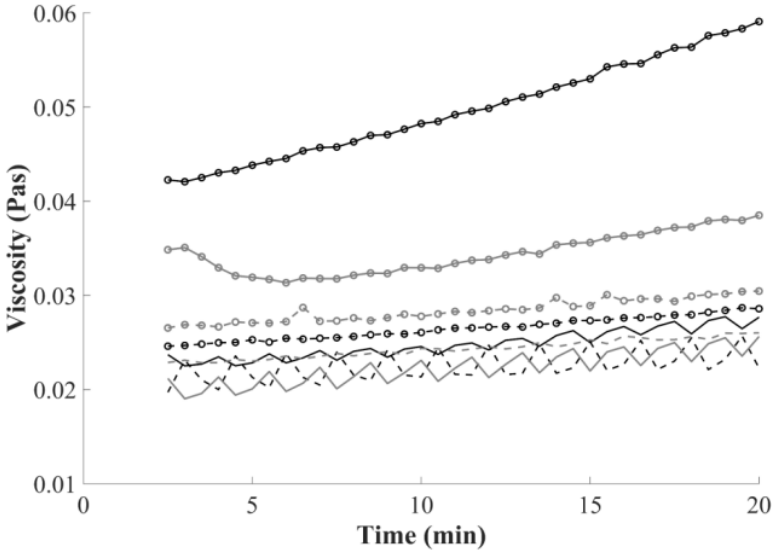

b)

Figure 4.2 a) Viscosity uncertainty quantification results for RTM6 epoxy resin samples at 1st (A-1, B-1, C-1, D1) and 15th day (A-15, B-15, C-15, D-15) of exposure at ambient temperature; b) detailed view of initial stages of viscosity evolution.

The initial resin viscosity increases by 25-40% within the 15 days exposure in the case of batches A and C that have undergone limited defrosting cycles. In the case of batches B and D that have undergone a greater number of defrosting cycles, the initial viscosity increase is more pronounced in the 65-80% range indicating a strong influence of storage conditions on initial material state. In addition, the resin viscosity of samples left for 15 days at ambient temperature increases faster with time than that of fresh samples. This behaviour is attributed to the autocatalytic character of the epoxy resin curing reaction in which the reaction rate is accelerated as the process progresses.

The procedure presented in section 4.2.1 was followed for the identification of viscosity model parameters using fitting for the different batches and samples. The model parameters values of Eqs. (4.1) and (4.2) were calculated for each resin sample providing an estimation of average and standard deviation of each model parameter. Figure 4.3 illustrates the viscosity model fitting. The model follows closely the rheology results with some slight discrepancies in the cooling/heating segments. The overall average squared absolute logarithmic error reported in Eq. (4.3) of the model fitting is 0.5. Table 4.5 summarises the average and standard deviation values of the viscosity model parameters as estimated by the overall fitting. Initial. The initial reference viscosity presents the highest variability with a coefficient of variation of about 29%. In contrast, the coefficient of variation of the rest of the parameters is below 6%. Considerable variations of about 18% have also been observed in the initial degree of cure of RTM6 epoxy resin [37]. The difference in variability of resin initial material state is attributed to the fact that the resin storage conditions have not been considered in cure kinetics uncertainty quantification tests and to the nonlinear dependence of viscosity on cure state.

Table 4.5 Statistical properties and sensitivity analysis results for RTM6 resin viscosity.

Parameter	μ	σ	μ/σ (%)
η_0 (Pas)	0.17	0.05	28.6
D (1/K)	6,800	371.5	5.5
A (1/s)	370,379	8456	2.3
E (J/mol)	70,309	336	0.5
γ (Pas)	0.061	0.004	6.2
m	1.34	0.07	5

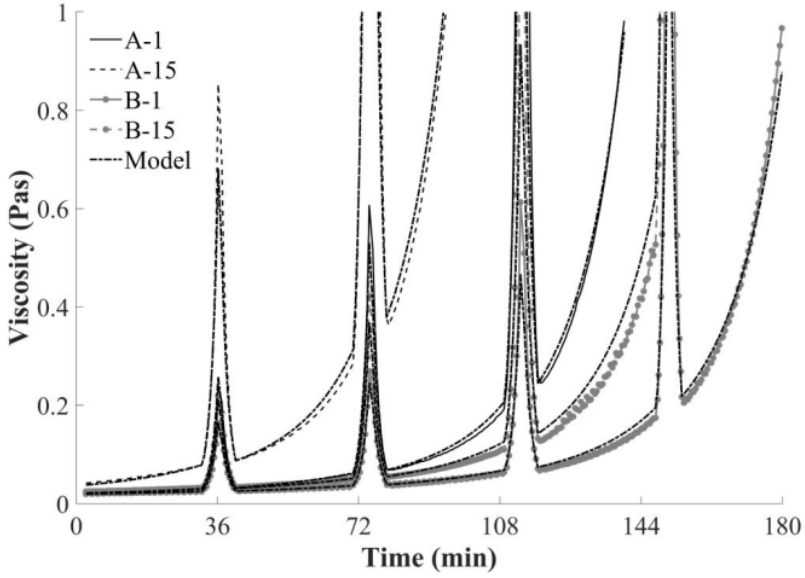

a)

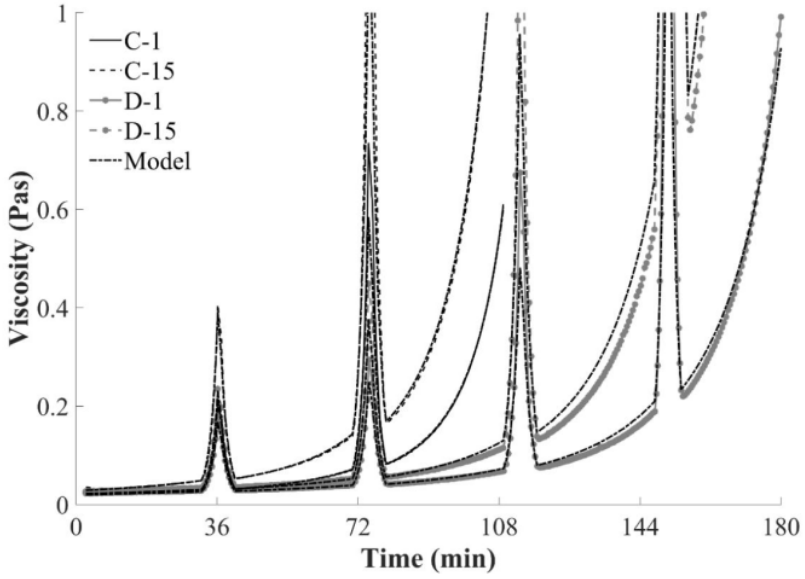

b)

Figure 4.3 Viscosity model fitting for different batches and samples for RTM6 epoxy resin; a) batches A and B at 1st (A-1, B-1) and 15th (A-15, B-15) day of exposure at ambient temperature; b) batches C and D at 1st (C-1, D-1) and 15th (C-15, D-15) day of exposure at ambient temperature.

Table 4.6 Sensitivity analysis results for RTM6 epoxy resin viscosity model parameters.

Parameter	Filling duration (sec)		Average relative absolute difference
	Realisation 1 $\mu + \sigma$	Realisation 2 $\mu - \sigma$	
η_0 (Pas)	149.2	289	**29%**
D (1/K)	219	193	5.7%
A (1/s)	216.4	208.6	1.7%
E (J/mol)	211.2	214.0	0.6%
γ (Pas)	218.4	208.1	2.3%
m	211.8	212.4	0.1%
Nominal case	212		

A sensitivity analysis was carried out using the RTM6 epoxy resin viscosity model to determine which of the model parameters should be considered in stochastic analysis. Each parameter of Eqs. (4.1) and (4.2) was varied by one positive and one negative (-σ) standard deviation around the average and inserted as an input in the PAM-RTM® model of the carbon/epoxy composite C spar described in section 3.5.1.2, whilst the rest of the model parameters were set equal to their mean values. The relative absolute difference of filling durations of realisations 1 (μ+σ) and 2 (μ-σ) with the filling duration of the nominal case (i.e. model parameters set equal to their mean values) was calculated. The average relative absolute difference of the two realisations was used as an indication of the model sensitivity to the level of variability of each of the model parameters. Table 4.6 reports the realisation viscosity model parameters values and the corresponding results. The nominal case illustrated in Figure 4.4 corresponds to the viscosity model with coefficients set to mean values. The average filling duration is 212 sec. The extreme cases of the 50% confidence intervals of initial reference viscosity sensitivity analysis are illustrated in Figure 4.5. The filling duration is affected significantly by initial reference viscosity variations resulting in an average relative difference of about 30%. Uncertainty of the other viscosity model parameters does not introduce significant variations in filling duration with the average relative differences being below 6%. Therefore, the main source of uncertainty in the experimental results is the variability in the initial reference viscosity and was considered as stochastic. The distribution of the stochastic variable η_0 can be

treated as uniform on the interval 0.1–0.22 Pas assuming that the probability of resin usage within the permitted time range is constant.

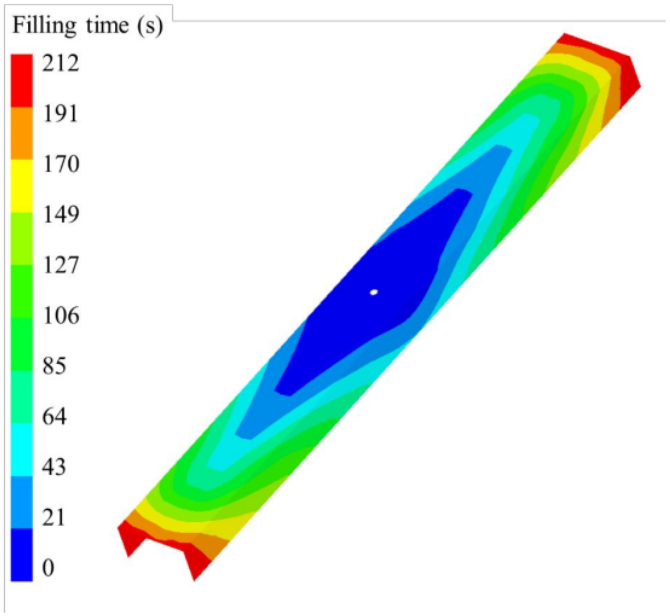

Figure 4.4 Nominal filling time of carbon/epoxy composite C spar.

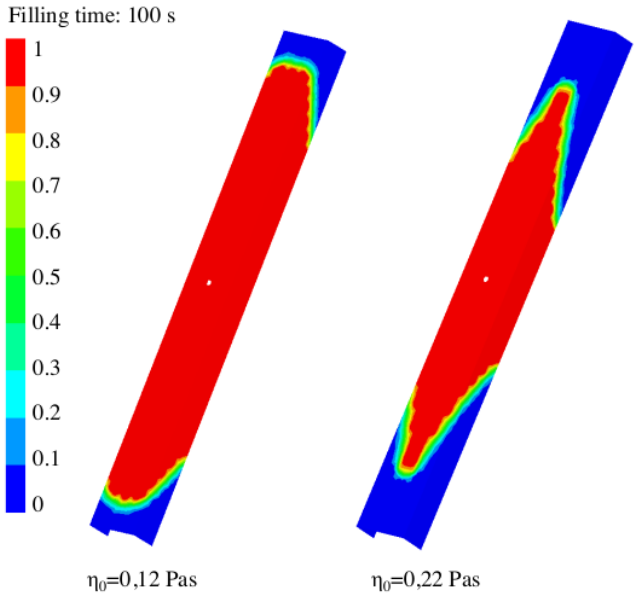

Figure 4.5 Extreme cases of initial reference viscosity sensitivity analysis of carbon/epoxy composite C spar.

4.4. Uncertainty quantification of tool temperature and surface heat transfer coefficient

The uncertainty of tool temperature and surface heat transfer coefficient in LCM processing of carbon/epoxy composite flat panel has been quantified in a series of experiments. Ten experiments were carried out utilising the experimental setup described in section 3.3.2. Figures 4.6 and 4.7 illustrate the results of surface heat transfer coefficient and tool temperature evolution variability experiments. Both parameters present two types of variation: (i) short term variability over time, and (ii) level variability across the different experiments. The air streams inside the oven produced by its fan cause forced convection at the carbon/epoxy composite part top surface. Short term variability of the heat transfer coefficient can be attributed to the continuous air movement caused by buoyancy forces arisen by air density differences due to temperature variations within the oven. The forced convection results in higher values of heat transfer coefficient in comparison to natural convection which is in the range of 10-15 $W/m^2/°C$ [38]. The level variability across different experimental runs for both the surface heat transfer coefficient and tool temperature can be attributed to the varying conditions within the oven. The average surface heat transfer coefficient for each run is in the range of 15–20 $W/m^2/°C$ is illustrated in Figure 4.6b. The tool temperature presents a periodic behaviour with time around the setting value, which is attributed to the action of the PID temperature controller of the oven. The corresponding periodic fluctuation is in the range of 2 °C around the set temperature. The same tool temperature periodic behaviour is also presented in a contact heating process [38] where a PID controller was also utilised.

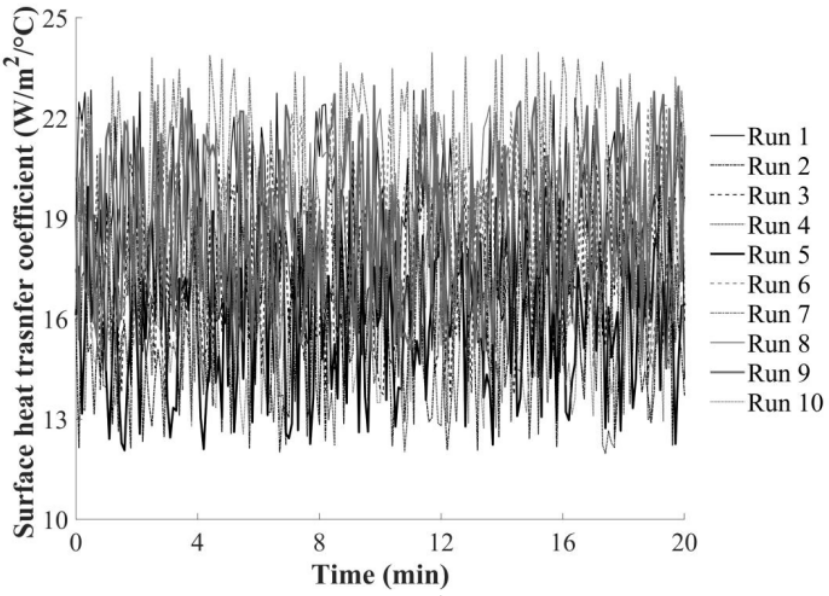

a)

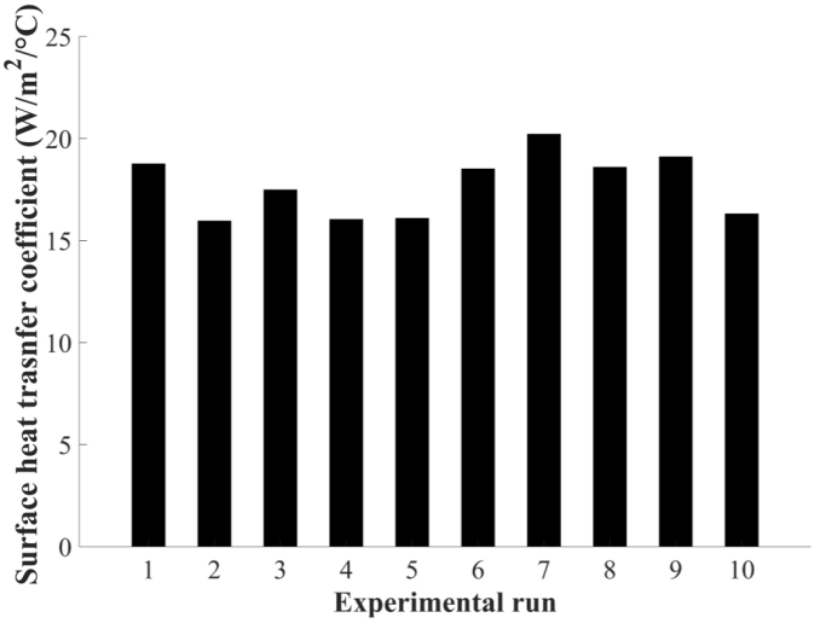

b)

Figure 4.6 a) Surface heat transfer coefficient evolution with time for different experimental runs of LCM process of carbon/epoxy composite flat panel in an oven; b) surface heat transfer coefficient mean value across different experimental runs.

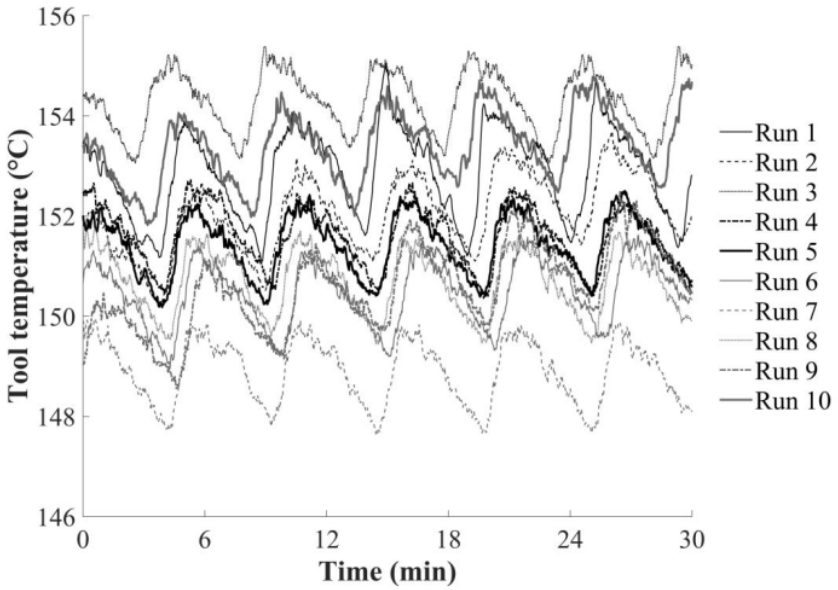

Figure 4.7 Tool temperature evolution with time for different experimental runs of LCM process of carbon/epoxy composite flat panel in an oven.

The autocorrelation structure of tool temperature illustrated in Figure 4.8 was calculated using the autocorrelation function $r_{k_{lag}}$ for lag k_{lag} as follows [149]:

$$r_{k_{lag}} = \frac{1}{N_{exp}\sigma_y} \sum_{n-1}^{N_{exp}-k_{lag}} (y_n - \bar{y})(y_{n+k_{lag}} - \bar{y}) \tag{4.16}$$

where $y_1, y_2, \ldots, y_{N_{exp}}$ denote the experimental measurements, $\bar{y}$ the average, σ_y the sample variance of the experimental run and N_{exp} the number of measurements. The tool temperature autocorrelation structure presents a periodic trend including negative values as a result of a long term periodic trend, implying that there is strong autocorrelation with time resulting in a non-stationary process. Consequently, de-trending needs to be applied to generate a stationary process in which the autocorrelation structure decays to zero in short time lag.

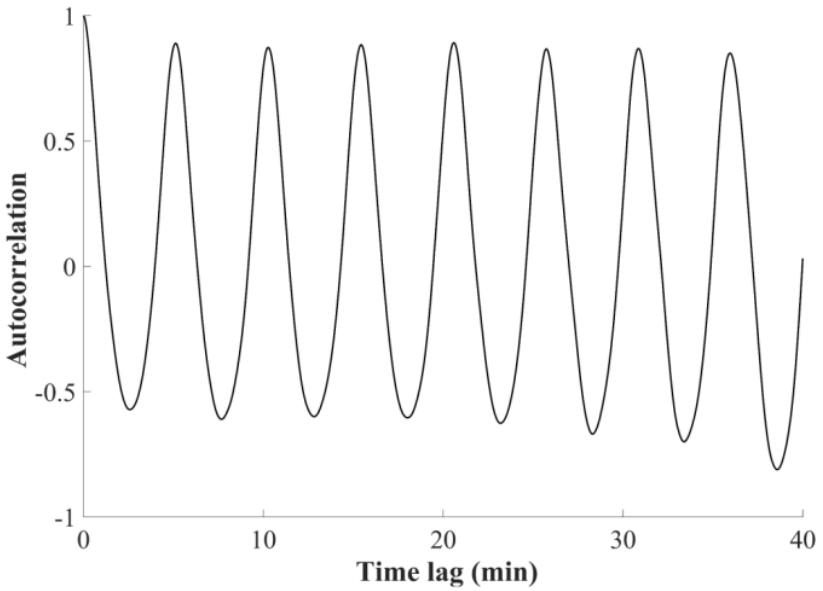

Figure 4.8 Autocorrelation structure of tool temperature of LCM process of carbon/epoxy composite flat panel in an oven.

Fast Fourier Transformation (FFT) implemented in MATLAB [150] was utilised to calculate the spectrum of the periodic component of the tool temperature signal. FFT transforms the experimental signal from time domain into a representation of frequency domain. Figure 4.9 depicts the spectrum over the 0-0.1 Hz frequency range. The amplitude decays to values below 0.1 after the third discrete frequency component. Therefore, only the first three components were considered for the representation of the tool temperature series. The three frequency components occur at multiples of a principal signal frequency of 0.0028 Hz. Figure 4.10 illustrates the cosinusoidal fitting for one of the experimental runs. The number of frequency components in FFT analysis depends on temperature controller operation and type of heating as a different setup using contact heating for infusion and curing showed only one principal frequency driving the temperature periodic behaviour [38].

The residuals from the de-trending process were modelled using the Ornstein-Uhlenbeck process (OU) described in section 3.7.1. This procedure was repeated for each of the ten experimental runs. Overall, the stochastic process of tool temperature can be expressed as follows:

$$T_{tool} = A_t + \sum_{i=1}^{3} B_{ti}\cos(i\omega_t t) + S_{OU} \quad (4.17)$$

where A_t is the level of each experimental curve, B_{ti} and ω_{ti} the i^{th} amplitude and angular frequency of the cosinusoidal fit respectively, and S_{OU} the mean reverting stationary stochastic process (OU) expressed using Eq. (3.19). Figure 4.11 illustrates the autocorrelation structure for a time lag of 6 min after de-trending and the simulated residuals generated by the OU process. It can be observed that the OU process reproduces the decay of the autocorrelation structure successfully. The same procedure was applied to all experimental runs. The average and standard deviation of each parameter of Eq. (4.17) are reported in Table 4.7.

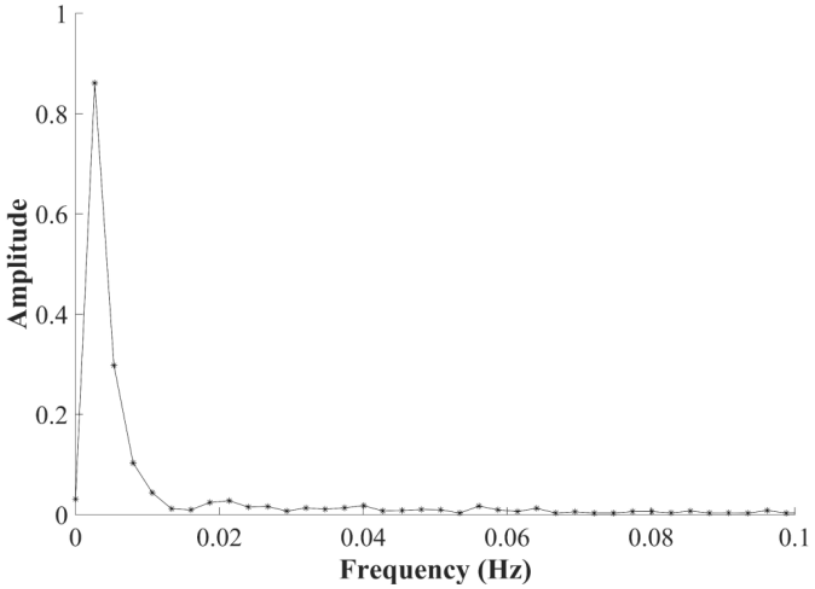

Figure 4.9 FFT single-sided amplitude spectrum of tool temperature of LCM process of carbon/epoxy composite flat panel in an oven.

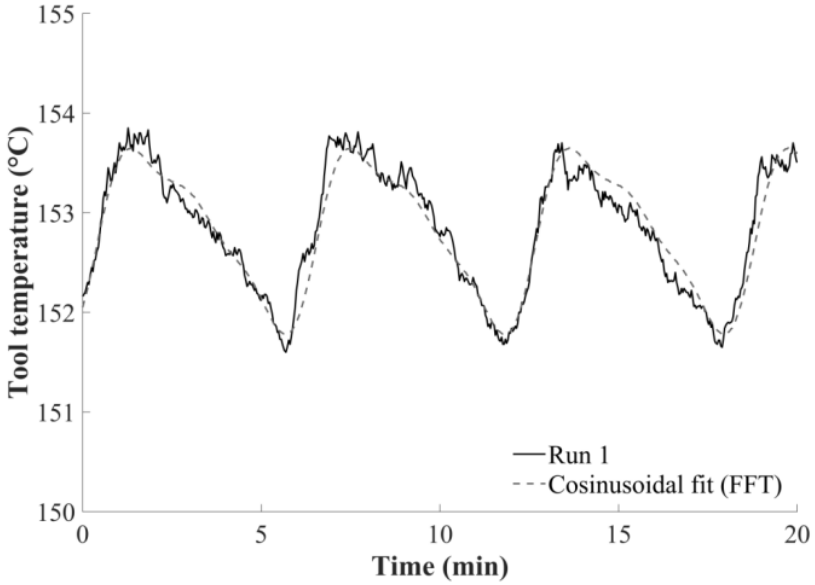

Figure 4.10 Cosinusoidal fit of tool temperature of LCM process of carbon/epoxy composite flat panel in an oven.

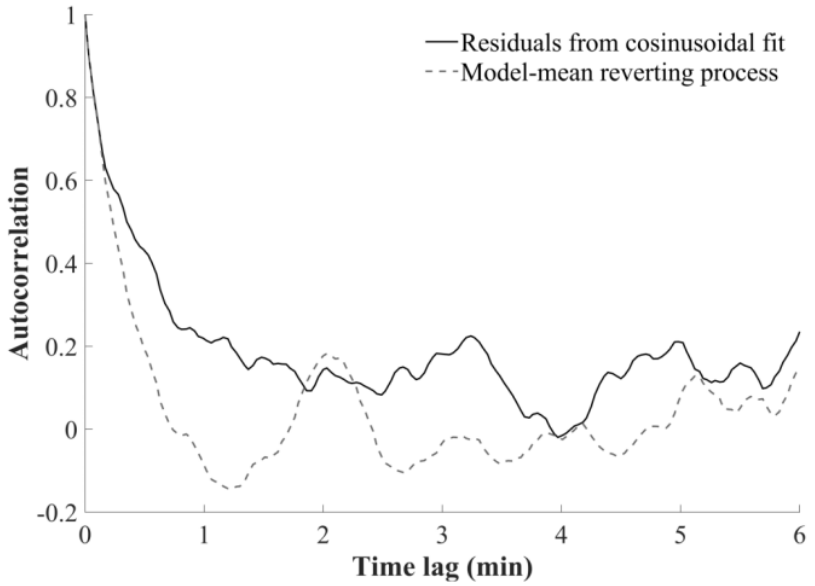

Figure 4.11 Autocorrelation structure of the residuals after the de trending of periodic trend of tool temperature of LCM process of carbon/epoxy composite flat panel in an oven.

The same periodic behaviour and level variability as in the case of tool temperature is also observed in the case of air temperature (T_{air}) in the oven illustrated in Figure 4.12. Therefore, the same statistical properties as those reported in Table 4.7 for tool were considered. The air temperature data of each experimental run were utilised in order to estimate the heat transfer coefficient value as described in section 3.3.2.

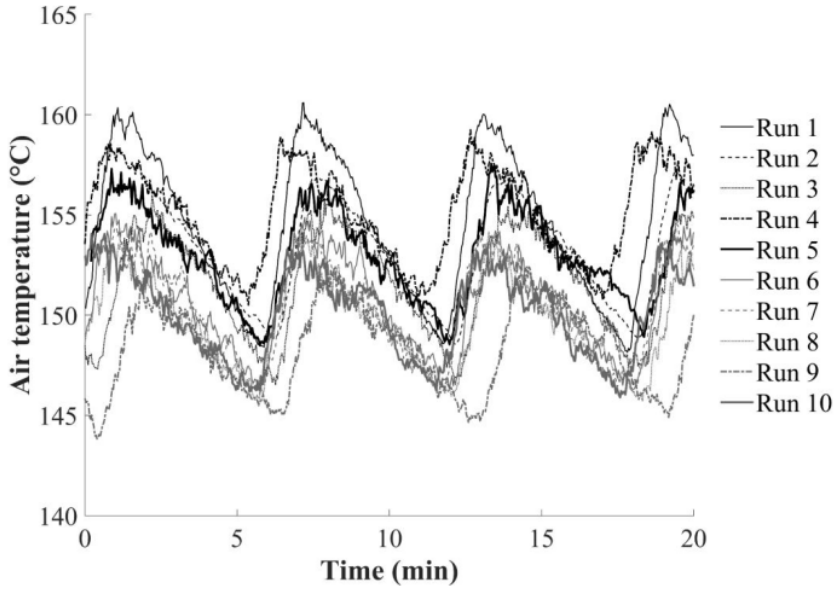

Figure 4.12 Air temperature evolution with time for different experimental runs of LCM process of carbon/epoxy composite flat panel in an oven.

The surface heat transfer coefficient does not involve a periodic trend since the autocorrelation structure decays relative fast to zero as illustrated in Figure 4.13. Therefore, it can be modelled as a realisation of a random scalar variable as follows:

$$h = A_h + B_h y_h \tag{4.18}$$

where A_h is the level, B_h the volatility of the process for each run, and y_h is a standard normal variable. The coefficients A_h and B_h were calculated for all experimental runs and their statistical properties are reported in Table 4.7.

Table 4.7 Statistical properties of boundary conditions.

Boundary conditions	Stochastic model parameter	Average	Standard deviation
h	A_h ($W/m^2/°C$)	17.8	1.33
	B_h ($W/m^2/°C$)	2.1	0.1
T_{tool}, T_{air}	A_{t1} (°C)	151.8	1.63
	B_{t1} (°C)	0.79	0.084
	B_{t2} (°C)	0.28	0.079
	B_{t3} (°C)	0.11	0.027
	ω_t (rad/s)	0.017	$9.8\ 10^{-11}$
	λ_t (°C)	1.14	0.82
	σ_t (°C)	0.4	0.04
	μ_t (°C)	0.025	0.055

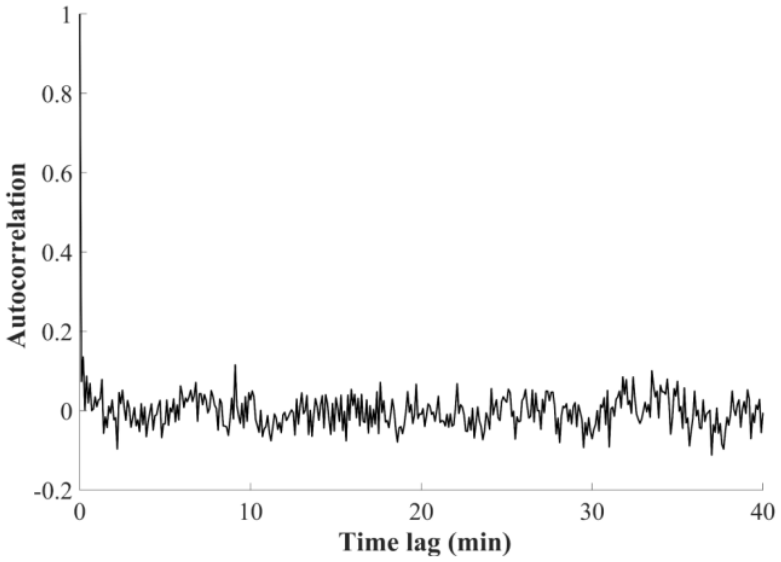

Figure 4.13 Autocorrelation structure of heat transfer coefficient of LCM process of carbon/epoxy composite flat panel.

4.5. Influence of short term variability of boundary conditions

The stochastic objects of tool and air temperature and surface heat transfer coefficient described by Eqs. (4.17) and (4.18) were used to investigate the influence of short term variability on cure time and maximum temperature overshoot of the cure process of the thick carbon/epoxy composite flat panel described in section 3.3.2. The FE cure model of the thick carbon/epoxy composite flat panel described in section 3.5.2.2 was utilised using a time increment of 2 sec to represent accurately short-term temperature variations. A standard thermal profile for the resin system of this study was utilised as the prescribed temperature boundary condition. The profile comprises one dwell at 160°C and a second dwell at 180 °C with dwell time of 75 min, and a heating ramp of 1.5 °C/min. The short term variability was investigated using constant tool temperature level A_t equal to the cure temperature and a convection coefficient level A_h equal to the estimated mean value of 17.8 W/m^2/°C. Ten FE cure model evaluations were carried out. The values of stochastic model parameters B_h, B_{ti}, ω_t, λ_t, μ_t, and σ_t were randomly selected using the Mersenne Twister random number generator [141] from normal distributions using their statistical properties.

The influence of the short term variability is illustrated in Figures 4.14 - 4.16. The periodic temperature trend as depicted in Figure 4.14 is diffused relatively quickly through the part thickness, appearing less pronounced at 3 mm distance from the tool surface. The short term variability of the surface heat transfer coefficient introduces weak temperature variations only at the top surface of the part without affecting the through thickness temperature evolution, as illustrated in Figure 4.15. Figure 4.16 shows the cure profile applied on the lower surface of the composite and the temperature evolution at the location of maximum temperature overshoot, which occurs at a height of 12.6 mm from the lower surface of the flat panel, as calculated by the deterministic cure model and one realisation of the stochastic cure simulation. Table 4.8 summarises the details of the deterministic and stochastic model realisation and the corresponding results. The deterministic model predicts a cure duration and temperature overshoot of 115 min and 40 °C respectively. The mean values of the cure duration and temperature overshoot of the ten stochastic cure models realisations are 114.9 min and 39.6 °C, whilst the corresponding standard deviations are equal to 0.07 min and 0.3 °C. Figure 4.17 compares the conversion evolution for the lower surface and the location corresponding to the

maximum temperature overshoot. It can be observed that the stochastic model parameters corresponding to short term variability introduce negligible differences in process outcomes. The coefficient of variation is about 0.06% and 0.8% for the cure time and maximum temperature overshoot respectively. Consequently, stochastic simulation can be carried out considering only the variability of the level of tool and air temperature and surface heat transfer coefficient. The influence of forced convection short term variability is similar to that of natural convection [38]. Eqs. (4.17) and (4.18) can be expressed as follows:

$$h = A_h \tag{4.19}$$

$$T_{tool}, T_{air} = A_t \tag{4.20}$$

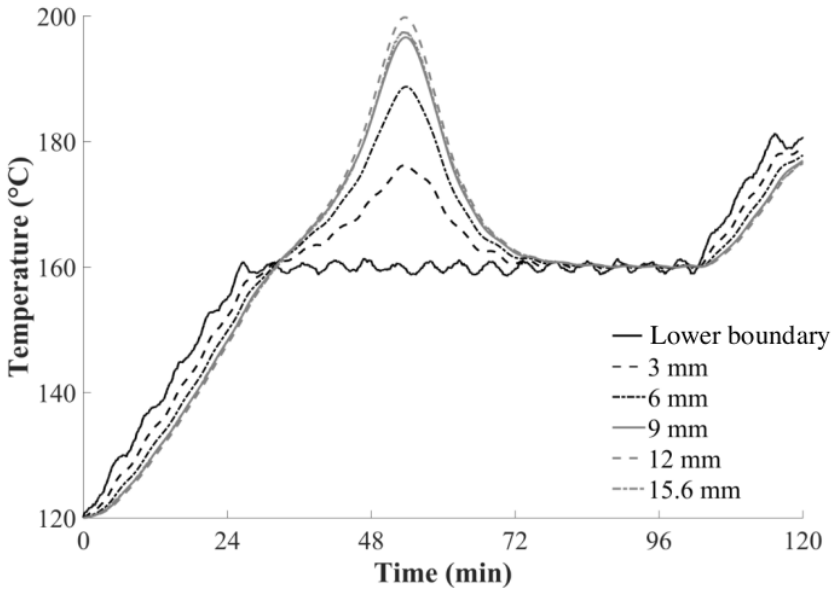

Figure 4.14 Short term variability of tool and air temperature influence on temperature distribution through the thickness of a thick carbon/epoxy composite flat panel (TFP) curing.

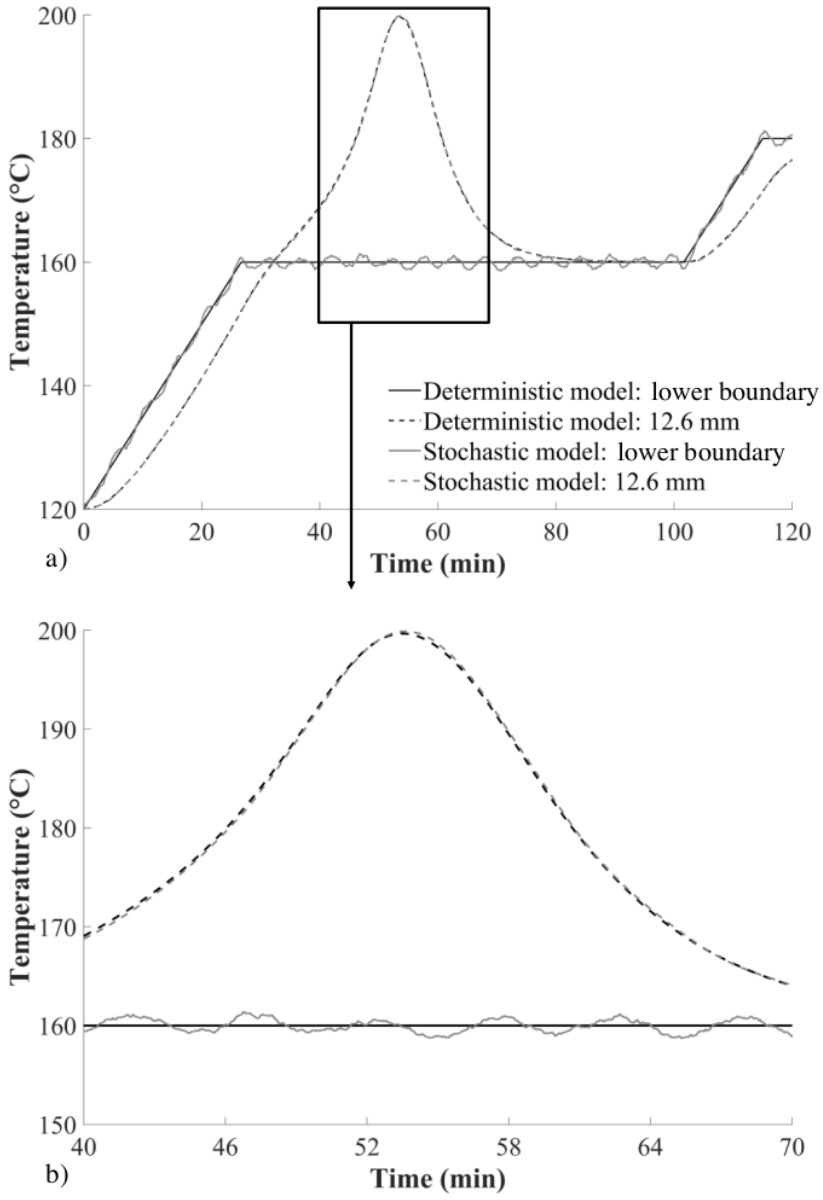

Figure 4.15 Short term variability of heat transfer coefficient influence on temperature distribution through the thickness of a thick carbon/epoxy composite flat panel (TFP) curing; inset: detailed view of temperature overshoot region.

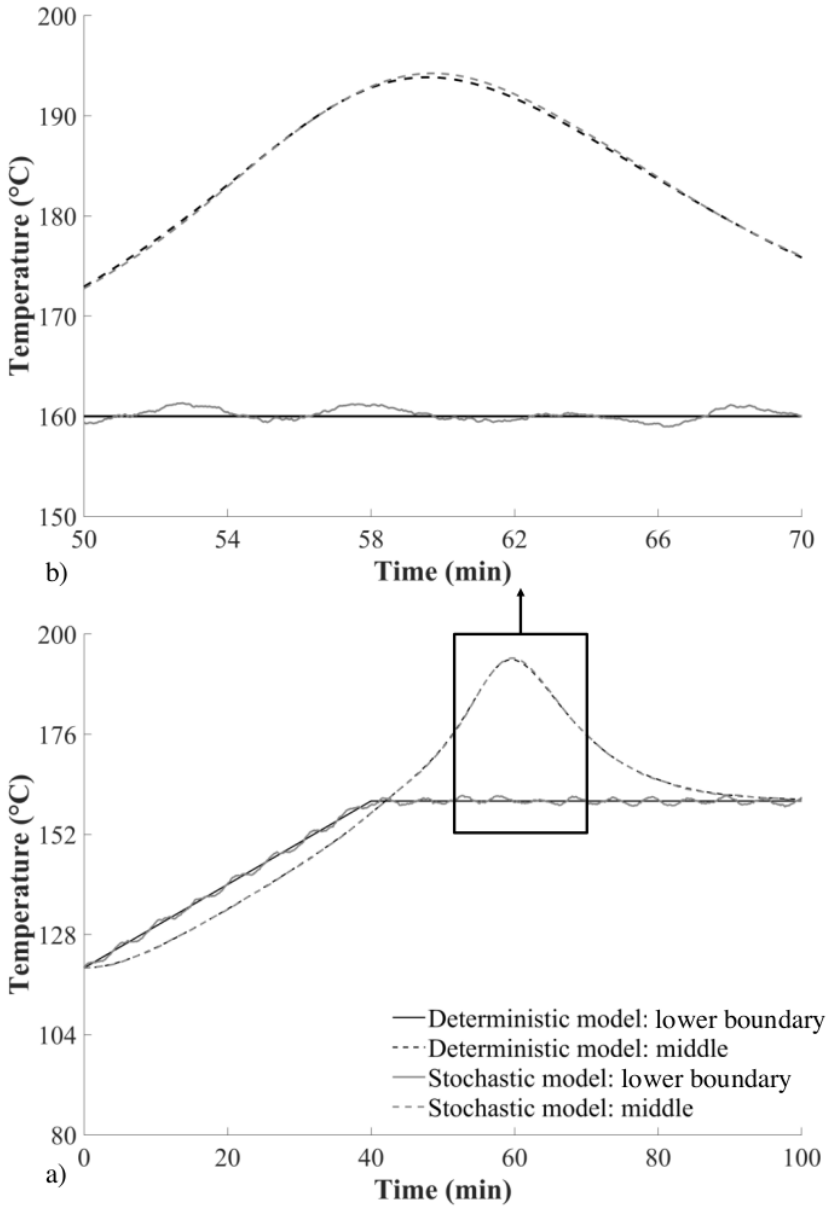

Figure 4.16 Short term variability of boundary conditions influence on temperature overshoot of curing of thick carbon/epoxy composite flat panel (TFP) curing; inset: detailed view of temperature overshoot region.

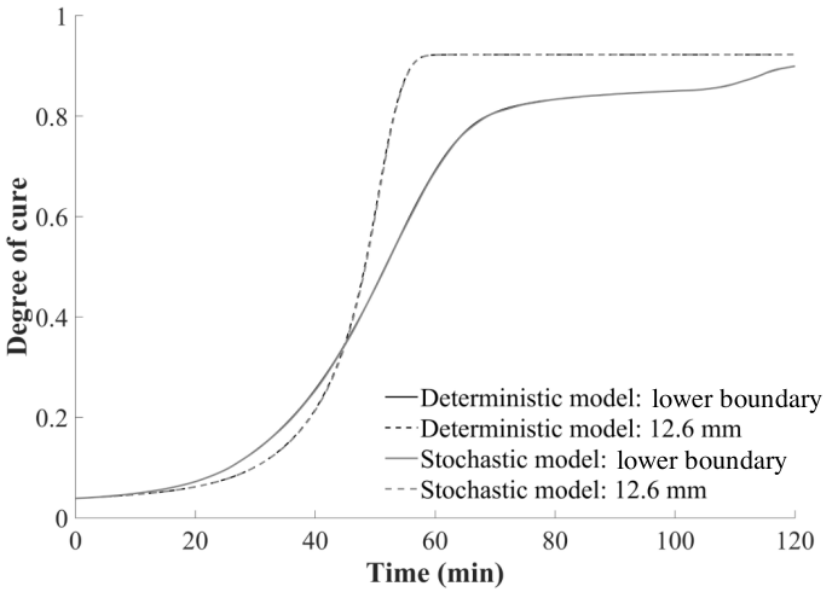

Figure 4.17 Short term variability of boundary conditions influence on degree of cure of thick carbon/epoxy composite flat panel (TFP) curing.

Table 4.8 Boundary conditions parameters values and cure process outcomes for deterministic and stochastic cure model of thick carbon/epoxy composite flat panel (TFP).

Model parameter/outcome	Deterministic model	Stochastic model realisation
A_h (W/m^2/°C)	17.82	17.82
B_h (W/m^2/°C)	-	2.2
B_{t1} (°C)	-	0.082
B_{t2} (°C)	-	0.077
B_{t3} (°C)	-	0.026
ω_t (1/s)	-	$9.9\ 10^{-11}$
λ_{OU} (°C)	-	0.81
σ_{OU} (°C)	-	0.05
μ_{OU} (°C)	-	0.057
Cure time	115 min	115.3 min
Temperature overshoot	40 °C	40.7 °C

4.6. RTM6 epoxy resin cure kinetics and thermal conductivity variability

Cure kinetics variability investigated in [37] can introduce significant variations in cure process outcomes reaching coefficients of variation of approximately 30%. The main parameters of the cure kinetics model presented in Eqs. (4.4)-(4.9) which show significant variations and thus considered as stochastic are the activation energy of the autocatalytic term (E_2), the autocatalytic order (m) and the initial degree of cure (α_0) [37]. The mean values and the corresponding standard deviation of stochastic cure kinetics parameters are presented in Table 4.9. Table 4.10 summarises the correlation matrix of cure kinetics stochastic objects in which significant positive correlation is observed between the reaction order and the activation energy. Cure kinetics stochastic parameters can be represented by a normal distribution [37].

The experimental scatter presented in the early stages of resin thermal conductivity characterisation, while the degree of cure is low, leads to significant uncertainty of the initial resin thermal conductivity estimation. The intercept k in Eq. (4.15) controls the overall level of conductivity representing the initial state of resin thermal conductivity. Therefore, the thermal conductivity intercept was considered as unknown stochastic parameter in the inversion scheme implementation of cure process which is presented in chapter 8.

Table 4.9 Stochastic properties of cure kinetics parameters [37].

Parameter	Average	Standard deviation
Initial degree of cure: α_0	0.033	0.006
Activation energy E_2 (J/mol)	57,820	600
Reaction order: m	1.29	0.094

Table 4.10 Correlation matrix of uncertain parameters [37].

Parameter	α_0	E_2	m
α_0	1	-0.09	0.55
E_2	-0.09	1	-0.84
m	0.55	-0.84	1

4.7. Variability of woven carbon fibre fabric permeability

Variations in fibre architecture due to handling and storage, nesting effects during lay-up and preform misplacement in the mould affect permeability significantly [19, 21]. The nominal values of longitudinal and transverse permeability of G0926 woven carbon fabric in the warp and weft direction corresponding to volume fraction of 57% respectively are reported in Table 4.11 [31]. Statistically characterisation of a glass fibre woven fabric principal permeabilities indicates a Gaussian distribution with a coefficient of variation of about 20% [12]. Therefore, considering the woven architecture of G0926 a normal distribution was assigned around the nominal value in order to result in a coefficient of variation of 20%. Preform permeability variability was represented as a scalar variable rather than a random field with autocorrelation structure [25]. This simplified approach does not consider the variations of preform permeability in local scale and spatial correlation; however, it results in a significant reduction of flow models dimensions enabling the construction of efficient surrogate models. The effective in-plane permeabilities of the G0926 fabric of the composite flat panel with the recessed edge and composite C spar described in sections 3.5.1.2 and 3.5.2.2 respectively were considered stochastic with average and standard deviations based on statistical properties of principal permeability values reported in Table 4.11.

4.8. Race tracking variability

Race tracking effects can be represented in flow simulation by an equivalent permeability [130] characterised by the race tracking strength, which is the ratio of equivalent race tracking permeability over fabric permeability in the same direction [35]. The RTM mould described in section 3.4.1 is sealed with silicone rubber along the edges which may cause compaction to the preform edges after closing the mould. This effect was represented by a lower limit of 0.5 in race tracking strength. Conversely, inaccuracies in fabric cutting or fabric misplacement may result in small gaps between the reinforcement and the seal which results in increasing the local permeability in the longitudinal direction of the gap. This potential effect was represented by adopting a maximum value of race tracking strength of 10. Variability in race tracking equivalent permeability is usually represented by a Weibull or a Gaussian distribution. In the present study, a normal distribution was selected with its statistical properties summarised in Table 4.11 utilised

in the filling simulation of carbon/epoxy composite flat panel with the recessed edge (FPR) described in sections 3.5.1.2.

Table 4.11 Nominal values of G0926 carbon fibre woven fabric [31] and the corresponding standard deviation [12] of principal permeabilities and the equivalent race tracking permeability statistical properties.

Parameter	Average	Standard deviation
Longitudinal permeability: K_1 (m^2)	$1.7\ 10^{-11}$	$3.4\ 10^{-12}$
Transverse permeability: K_2 (m^2)	$1.4\ 10^{-11}$	$2.6\ 10^{-12}$
Race tracking permeability: K_{Ri} (m^2)	$4\ 10^{-11}$	$1.5\ 10^{-11}$

4.9. Overview

Initial viscosity of RTM6 epoxy resin presents significant variability and is considered as a stochastic variable as well as the preform permeability and race tracking for the implementation of the inversion scheme in the RTM filling stage presented in chapters 6 and 7. Thermal boundaries conditions such as tool temperature and surface heat transfer coefficient present considerable variability. The stochastic objects developed representing are used in the inverse solution of the cure problem in chapter 8 and in the stochastic multi-objective optimisation framework described in chapter 9.

5. Dielectric sensor for process monitoring of carbon fibre composites manufacture

5.1. Introduction

Process monitoring techniques are used to follow critical parameters of manufacturing such as flow front position and cure reaction progress and to identify potential defects. Monitoring sensors, based on impedance spectroscopy, are considered beneficial due to the high response sensitivity, the efficiency and low cost of the data acquisition setup and the capability for incorporation on tooling. However, their applicability is limited by the influence of carbon reinforcement on the electrical signals. This chapter presents the development of a dielectric sensor capable of operating with the presence of carbon reinforcement. The main concept is used for the design of two sensor types; a lineal sensor used to monitor the flow front and a woven arrangement able to track the cure. Sensor signals are analysed using the corresponding equivalent circuits. The lineal sensor is validated in RTM filling of a carbon/epoxy composite flat panel, described in section 3.4.1, in different injection pressures. The cure sensor is evaluated in isothermal neat resin cure processing using the experimental set-up presented in section 3.3.3 and in VARTM processing of the carbon/epoxy composite flat part described in section 3.4.2.

5.2. Sensor set-up

5.2.1. Principle of operation

The design of the dielectric sensor developed in this work is illustrated in Figure 5.1a. It comprises two twisted solid copper wires coated by an insulator. The insulating coating prevents contact of the copper wire with the conductive fibres. An electric field is formed between the wires upon application of voltage. The field goes through the insulating coating and penetrates the gaps between the wires. The twisting increases the effective length as well as the air gaps between the wires resulting in stronger signal. Although the reinforcement can interfere with the fringing field, it only screens it partially. The sensor principle can be adapted to address both flow and cure monitoring applications.

A lineal sensor made using the twisted pair can be used to monitor the resin flow front position. An example of the configuration of the lineal sensor in an RTM tool is presented in Figure 5.1b. The measurement area of the sensor is divided into two parts: the wetted area impregnated by resin, which fills the gaps between the wires, and the dry area in

which the gaps are filled with air. As the flow process progresses the wetted area percentage increases, whilst the dry area decreases. The very large contrast in dielectric properties between liquid resin and air results in significant sensitivity of the sensor response to its covered length. The sensor can be placed either on the tool surface in contact with the carbon fabric or between two layers of reinforcement. One potential configuration is where the sensor is placed on the lower tooling in contact with the fabric as illustrated in Figure 5.1b, in which case the presence of the sensor only causes a small disturbance to the fibre architecture, similar in size to the diameter of the wires. The lineal sensor was made by twisting two solid insulated copper wires specified in section 3.2 using a hand drill. The pitch of the twist was 500 twists/m. A detailed view of the dielectric sensor is illustrated in Figure 5.2. The diameter of each wire is 127 μm which is smaller than the tow width. Therefore, the disturbance in reinforcement architecture can be considered similar to the resin rich channels that are present in the composite material,

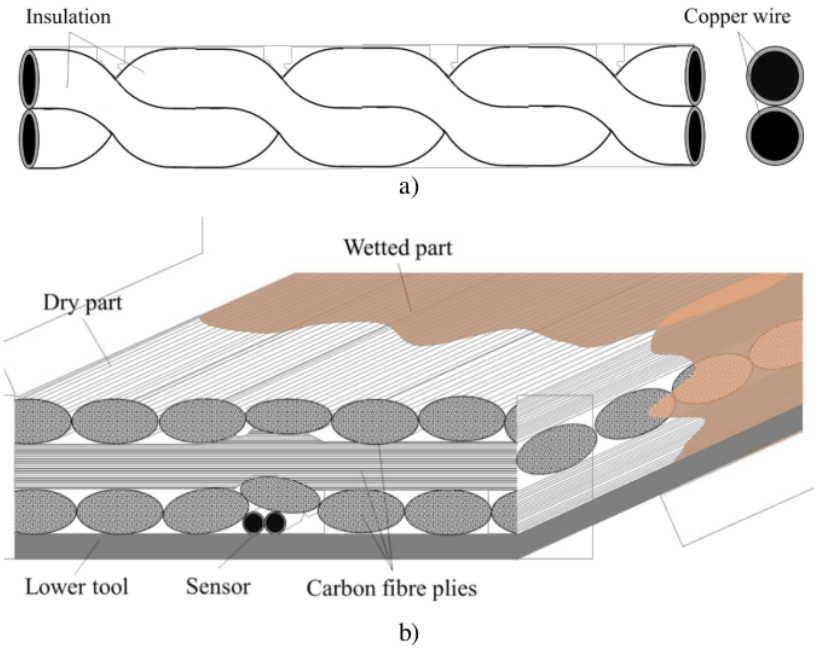

Figure 5.1 Lineal flow sensor: a) sensor geometry; b) schematic representation of the operational principle of the flow sensor.

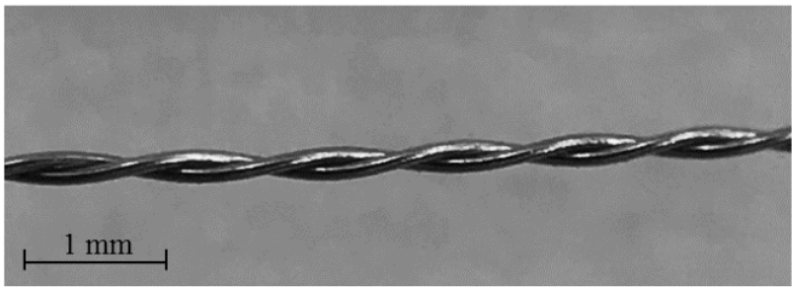

Figure 5.2 Detailed view of lineal flow sensor.

In the case of cure monitoring, the local material state is estimated based on the sensitivity of electrical properties on cure progress. For the sensing concept based on the twisted pair proposed here, the strength of the signal is governed by the total length of the sensor. A woven configuration of the dielectric sensor was utilised for the cure sensor concept implementation. The cure sensor was made using 1.2 m of twisted wire and a nominal weaving distance of 2 mm. The miniature loom illustrated in Figure 5.3a is made of ABS filament and was produced in a Lulzbot TAZ 5 3-D printer as detailed in section 3.2. Figures 5.3b and 5.3c present the sensor production and the resulting woven configuration with dimensions 20×20×0.25 mm. The woven configuration allows fitting a large length within a small area. This results in sufficient sensitivity combined with local cure sensing. The dielectric sensor design presented here overcomes the difficulties related to shorting in the presence of carbon fibre reinforcement. The presence of the insulation material precludes the use of glass cloths or veils on the dielectric sensor to ensure electrical insulation from the carbon fibre. The twisted pattern increases the available air pockets between the wires strengthening the signal and allowing the monitoring of resin state during cure. The relative small size of the sensor allows its implementation on complex geometries where other sensing systems such as pressure sensors require tool modifications as described in section 2.3.1.

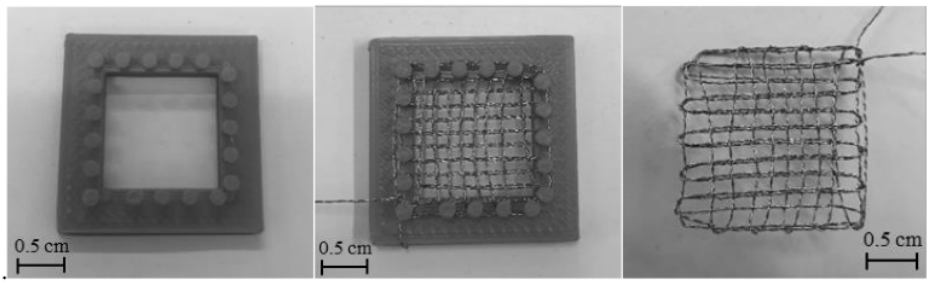

a) b) c)

Figure 5.3 Cure sensor: a) miniature loom; b) production of sensor and; c) woven sensor.

5.2.2. Analysis of lineal flow sensor signal

The lineal sensor response has been examined following the analysis in [44]. The electric circuit representing the sensor response is illustrated in Figure 5.4. The wetted and dry parts of the sensor are connected in parallel, whilst within each part the element corresponding to the gaps and the element corresponding to the coating are connected in series. The admittance per unit length of the wetted part is:

$$y_w = \frac{y_{wg} y_c}{y_{wg} + y_c} \tag{5.1}$$

and of the dry part

$$y_d = \frac{y_{dg} y_c}{y_{dg} + y_c} \tag{5.2}$$

where y_c is the admittance per unit length of the coating, y_{wg} the admittance per unit length of the filled gaps and y_{dg} the admittance per unit length of the dry gaps.

The admittance measured by the sensor is:

$$Y = L_w \frac{y_{wg} y_c}{y_{wg} + y_c} + (L - L_w) \frac{y_{dg} y_c}{y_{dg} + y_c} \tag{5.3}$$

where the length of the sensor is L and the length covered by resin L_w. Eq (5.3) can be rearranged as follows:

$$L_w = \frac{Y - Y_o}{Y_f - Y_o} L \tag{5.4}$$

where $Y_f = Ly_w$ is the admittance of the fully wetted sensor and $Y_o = Ly_d$ the admittance of the dry sensor.

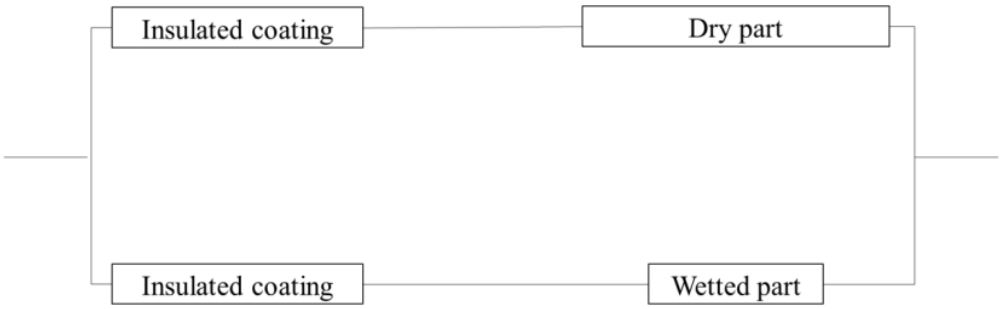

Figure 5.4 Electrical circuit representing the lineal sensor response.

Eq. (5.4) describes the linear response of the sensor to the flow front position and allows the online estimation of the length of sensor covered by resin using the measured admittance, the admittance of the dry sensor and the admittance of the fully wetted sensor. It should be noted that the latter two need to be determined for the conditions of the measurement, matching the reinforcement architecture and pressure applied during impregnation.

5.2.3. Analysis of cure sensor signal

In order to uncover the quantitative characteristics of the resin reaction during cure process it is necessary to translate the dielectric/impedance signal to information related to resin reaction state. The behaviour of a thermoset under AC electrical excitation is governed by three phenomena: dipolar relaxation, charge migration and electrode polarisation. These phenomena can be represented by the equivalent circuit illustrated in Figure 5.5a [151]. The circuit comprises two constant phase elements (CPE) representing the electrode-material interface connected in series with a sub-circuit corresponding to dipolar relaxation and migration charges. It is expected that the action of the insulating coating of the sensor developed in this work is incorporated into this part of the equivalent circuit coating, with the CPE representing both electrode effects and the capacitive response of the insulator. The presence of dipolar relaxation is represented by a capacitance (C_{sd}), in series with a resistance (R_{sd}) which correspond to static dipoles due to molecular asymmetry of the material, connected in parallel with a capacitance of the dipoles induced by electric field (C_{id}). The migrating charges mechanism is considered

by a resistor (R_m) connected in parallel with the sub-circuit of dipolar relaxation. The imaginary part of the complex impedance of the equivalent circuit can be expressed as follows:

$$Z'' = \frac{R_m[\omega^3 C_{sd}^2 R_{sd}^2 R_m C_{id} + \omega R_m (C_{id} + C_{sd})]}{\omega^2 (C_{sd} R_m + C_{sd} R_{sd} + C_{id} R_m)^2 + (\omega^2 C_{sd} R_{sd} R_m C_{id} - 1)^2} + \frac{2}{(A_e \omega)^{n_{CPE}}} \quad (5.5)$$

where A_e and n_{CPE} are coefficients of the constant phase element and ω the angular frequency.

For a lossy dielectric such as a curing epoxy resin with electrical behaviour dominated by migrating charges and a small contribution by dipolar relaxation, the equivalent circuit can be simplified by replacing the sub-circuit corresponding to dipolar relaxation and migration charges with a parallel R-C sub-circuit [80]. The simplification is possible in intermediate frequencies where the electrode polarisation and dipolar relaxations effect are negligible. The capacitive element C represents the overall ability of the material to store energy through polarisation, whilst the resistance $R \approx R_m$ includes all the dissipative contribution of migrating charges. Hence, Eq. (5.5) is transformed as follows:

$$Z'' = \frac{\omega C R^2}{1 + \omega^2 C^2 R^2} + \frac{2}{(A_e \omega)^{n_{CPE}}} \quad (5.6)$$

Figure 5.5b illustrates the imaginary impedance spectrum of the simplified equivalent circuit. The imaginary impedance decreases linearly in a log-log plot, with a slope equal to the exponent of the electrode polarisation and coating term (n_{CPE}) in the low frequency zone of the spectrum where this term dominates the signal. The peak region observed in intermediate frequencies is dominated by migrating charges. In this region the electrode polarisation effect is negligible and the corresponding term in Eq. (5.6) can be excluded. Consequently, the imaginary impedance can be rewritten as follows:

$$Z'' = \frac{\omega C R^2}{1 + \omega^2 C^2 R^2} \quad (5.7)$$

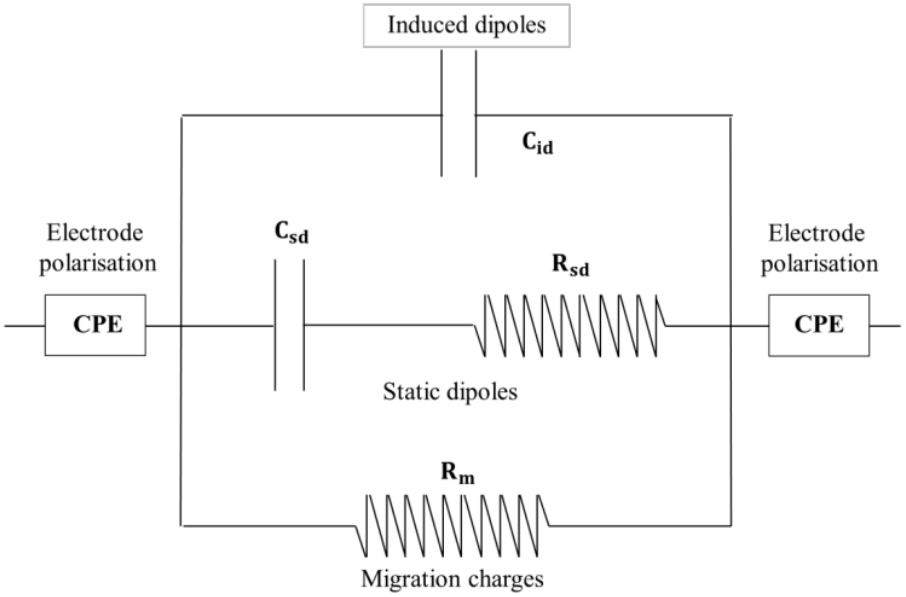

a)

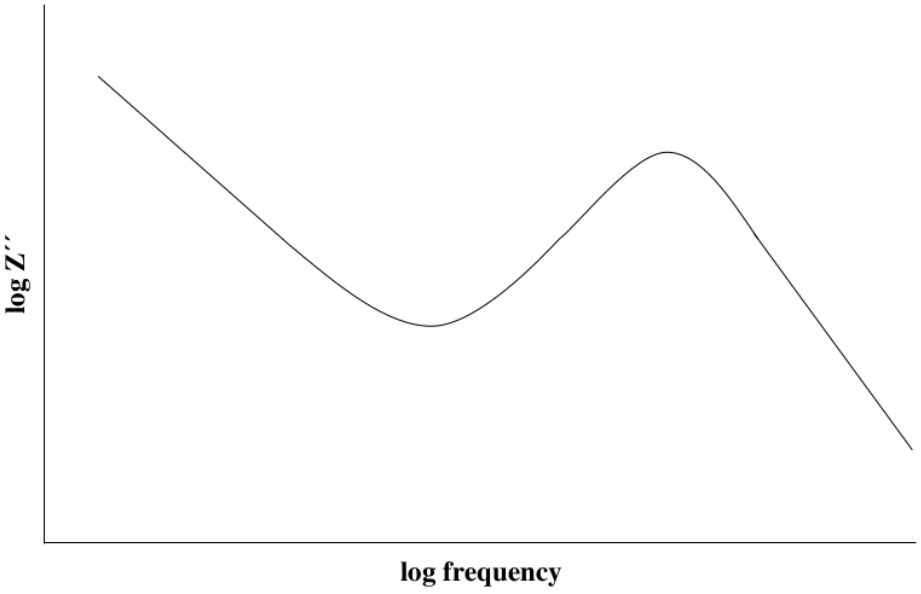

b)

Figure 5.5 a) Equivalent circuit representing the behaviour of a curing thermoset; b) Imaginary impedance spectrum of simplified equivalent circuit expressed by Eq. (5.6).

The derivative of Eq. (5.7) can be expressed as follows:

$$\frac{dZ''}{d\omega} = \frac{CR^2(1-\omega^2C^2R^2)}{(1+\omega^2C^2R^2)^2} \tag{5.8}$$

which has a root corresponding to the imaginary impedance maximum at:

$$\omega = \frac{1}{CR} \tag{5.9}$$

and the corresponding maximum imaginary impedance is:

$$Z''_{max} = \frac{R}{2} \tag{5.10}$$

The local imaginary impedance maximum (IIM) is related directly to the resistor corresponding to migrating charges as highlighted by Eq. (5.10) [80]. The high frequency zone is governed by the capacitive elements of the circuit, which in the case of the simplified spectrum expressed by Eq. (5.6) is manifested as a line with a slope of -1 in a log-log plot. In the case of the more complex behaviour represented by Eq. (5.5), the high frequency response incorporates a small shoulder corresponding to dipolar relaxation with a linear behaviour with a slop of -1 at very high frequencies.

The imaginary impedance maximum is used in practice to monitor the cure based on the dependence of resistivity on migrating charges mobility, which in turn depends on local material viscosity [152]. This can implemented through a normalised form of the IIM [74, 75, 80] or through treating its time derivative as a signal equivalent to heat flow in differential scanning calorimetry [153].

5.2.4. Evaluation of the signal of the dielectric sensor

The dielectric sensor signal was evaluated by placing it in different locations within the RTM assembly under vacuum. The RTM assembly comprises a carbon fibre composite flat panel with thickness 3.3 mm and the tool which consists of a steel metal cavity and a glass top plate allowing the visual monitoring of the filling stage as described in section 3.4.1. Three different setups were tested by evaluating the response prior to filling; the sensor placed between the tool cavity and the lower side of the preform, at preform mid thickness – between the carbon fibre layers - and between the glass top plate and the upper surface of the preform. For all three configurations impedance data were acquired over 31 frequencies swept logarithmically from 1 Hz to 1 MHz.

Figure 5.6 illustrates the imaginary impedance spectra for the three different sensor configurations alongside the spectrum of the lineal sensor in air. The imaginary impedance spectrum corresponds to a capacitive circuit in all cases. The air between the two copper wires operates as an insulation material thus forming a nearly ideal capacitor. The migrating charges effect present in resin and illustrated in Figure 5.5b is not manifested as the sensor is dry. The sensor response is identical in the three different placements configurations and in air.

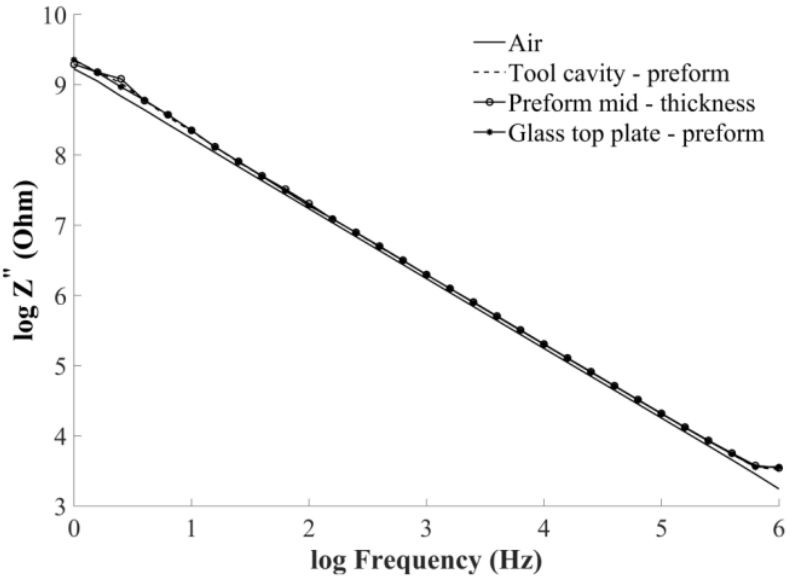

Figure 5.6 Imaginary impedance spectrum of dielectric sensor for different sensor placements in contact with carbon reinforcement.

The imaginary impedance evolution with time at a fixed frequency of 10 kHz is illustrated in Figure 5.7. The sensor signal does not present fluctuations over time showing stability under industrial manufacturing conditions. The results show that the sensor is not affected negatively by the presence of the electrical conductive carbon reinforcement. This allows the placement of the dielectric sensor in different locations within the RTM tool and preform. Therefore, the sensing system implementation can be modified according to different process conditions, especially where the complexity of the manufacturing process is increased and the available space options for the sensor installation are limited. The dielectric sensor developed here can be used in composites manufacturing processes

without affecting significantly process parameters decisions due to its geometrician flexibility and robustness.

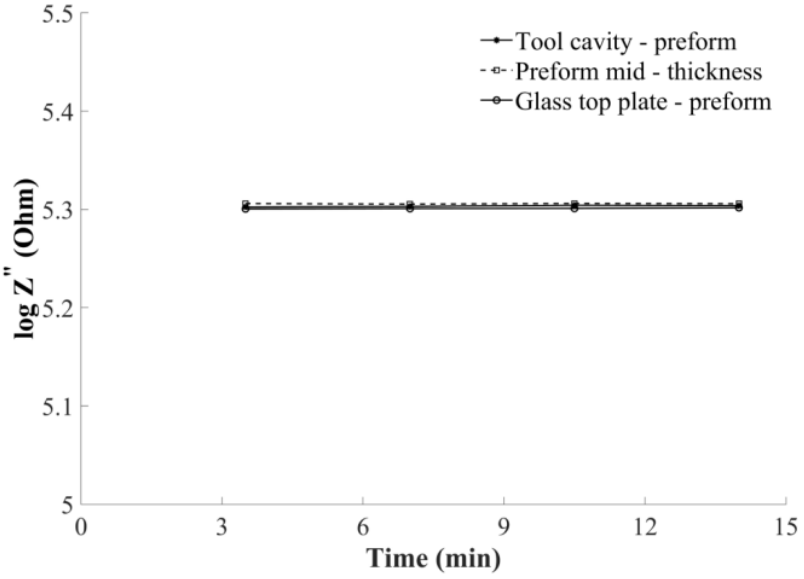

b)

Figure 5.7 Imaginary impedance evolution with time at 10 kHz for different sensor placements.

5.3. Flow monitoring

Two RTM runs of the carbon/epoxy composite flat panel (FP) presented in section 3.4.1 have been conducted for the validation of the lineal flow sensor. The RTM runs (FP_1, FP_2) were carried out using two different injection pressures; 2 and 3 bar. The sensor was placed centrally along the long direction of the mould in contact with the lower tool. More details regarding the process can be found in section 3.4.1. The evolution of the flow front for the case of FP_2 part is shown in Figure 5.8. It can be observed that there is race tracking on the sides of the mould, affecting the flow in a region extending to about 80 mm from the edge by the end of filling. The filling pattern is uniform in the central region of the mould where the sensor is placed. The filling pattern is similar in the case of the FP_1 part filling.

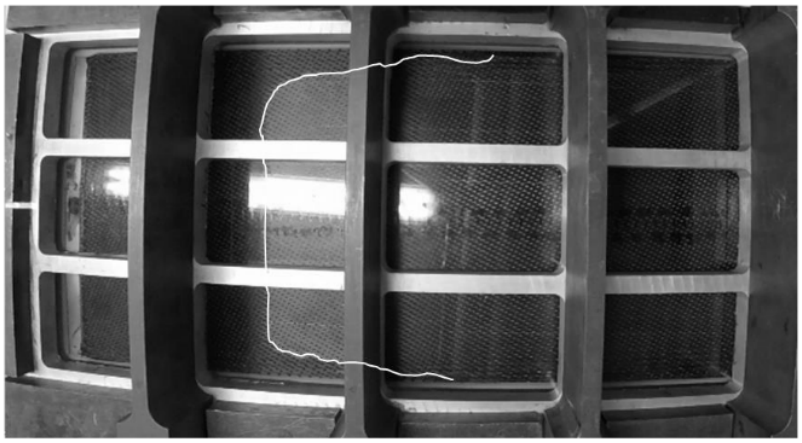

a)

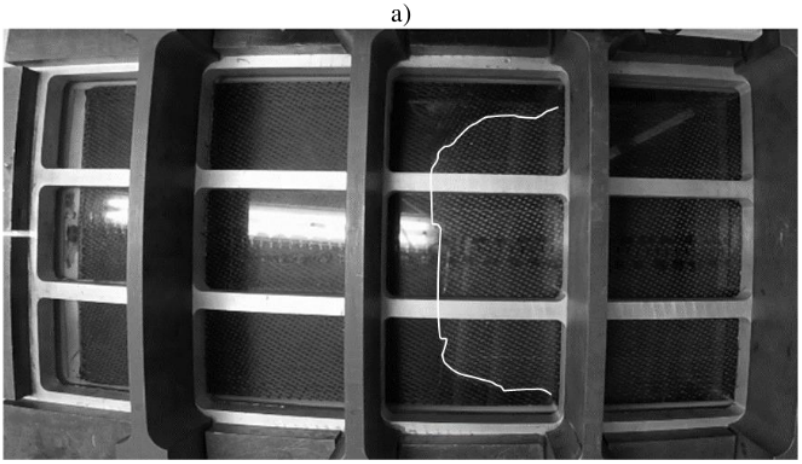

b)

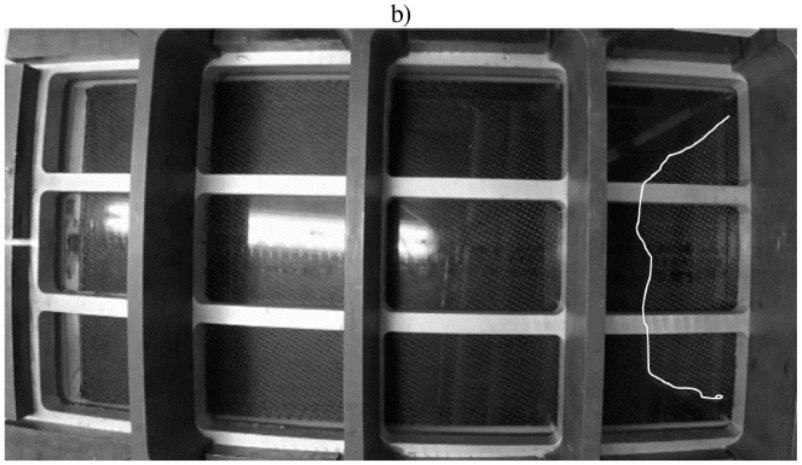

c)

Figure 5.8 Visual flow front evolution in the 3 bar RTM filling stage of epoxy/carbon composite flat panel (FP_2): a) 3 min; b) 8 min and; c) 16 min.

Figure 5.9 illustrates the lineal sensor response for the 2 and 3 bar RTM experiments and compares it with the visual flow front measurements. It can be observed that the sensor response, represented as real length using Eq. (5.4), follows closely the parabolic behaviour of the flow front position during the whole duration of the impregnation. The sensor signal is sensitive to changes in flow front speed with an error that never exceeds 3% of the actual front position measured visually.

According to Eq. (5.4) the length estimated using the admittance measurements is the ratio of two complex numbers. In an ideal situation, in which the sensor field, material state and environmental conditions are uniform across the length of the sensor, the numerator and denominator of the fraction are in phase resulting in a negligible imaginary part of the estimated length. Deviations from these ideal conditions, as well as measurement noise, cause higher values of imaginary length. Consequently, the sensor response provides a direct indication of measurement and analysis errors [44]. In the results presented in Figure 5.9 the imaginary impedance length in predominantly between -10 and 10 mm with a few extreme values reaching an absolute value of 25 mm. This is below 3% of the overall length, indicating a high quality estimation based on the real part of the length computed using Eq. (5.4).

The results obtained using the flow sensor show clearly that the concept developed in this work is applicable to liquid moulding of carbon composites under industrial conditions. The sensor withstands RTM level pressures, whilst its placement between the metal tool and the carbon fabric tested here is the worst case scenario in terms of potential interference by conductors as well as potential damage to the insulating coating. The lineal flow sensor provides similar signal stability when it is placed in different location in the RTM assembly. The lineal flow sensor flexibility overcomes practical complexities presented in flow dielectric sensors set-ups which use the conductive carbon reinforcement as one of the electrodes of the sensing system [49] and thus their operation requires electrical insulation of the reinforcement from the tooling assembly. The air/resin pockets formed around the sensor by the fabric are sufficient to guarantee high sensitivity to filling state. The disturbance in the fabric architecture caused by the presence of the sensor is minimal, whilst the sensor is easily removed after curing if it is placed on the surface. The fabric conforms around the sensor forming a groove with a maximum dimension of around 250 μm as illustrated in Figure 5.10. The dimension of the

disturbance is governed by the wire diameter, which can be minimised by selection of a thinner coated wire for the twisted pair.

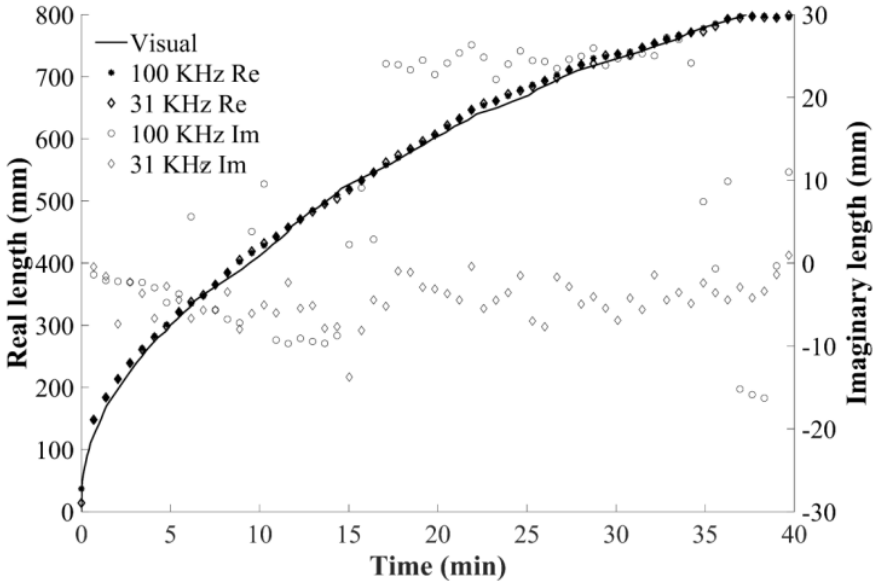

a)

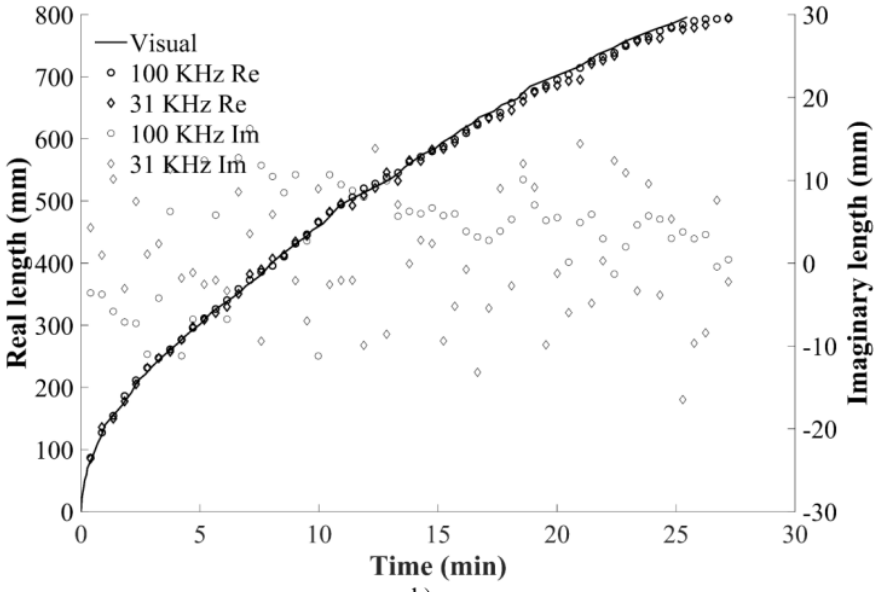

b)

Figure 5.9 Comparison of visual with dielectric flow measurement for RTM filling stage of epoxy/carbon fibre flat composite panel at a) 2 bar (FP_1) and; b) 3 bar (FP_2).

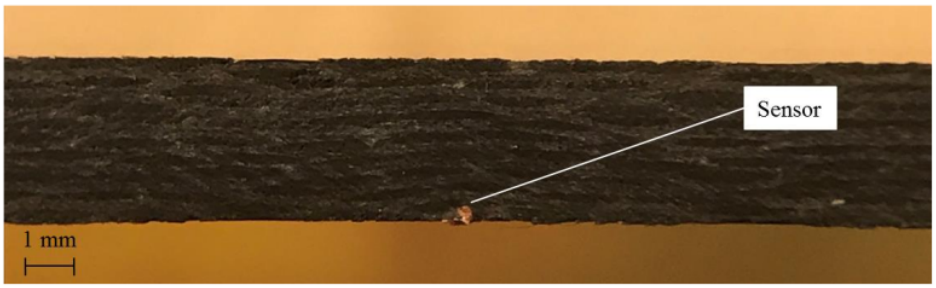

Figure 5.10 Microscopic view of the epoxy/carbon composite flat panel (FP_1) deformation caused by the flow sensor.

5.4. Cure monitoring

Isothermal cure runs of neat epoxy resin in different temperatures and a VARTM process were carried out for evaluation of the cure sensor. The isothermal cure processes of neat resin were conducted at 150 °C and 160 °C using the experimental set-up specified in section 3.3.3. The VARTM process involved the cure of a carbon fibre composite flat panel comprising six plies of carbon fibre woven fabric, whilst the matrix was RTM6 epoxy as described in section 3.4.2. The evolution of the imaginary impedance spectrum during the isothermal cure of neat resin at 150 °C and 160 °C is illustrated in Figures 5.11a and 5.111b respectively. A linear log-log reduction of imaginary impedance at low frequency is observed as expected. At intermediate frequencies the plot shows a shoulder at the location where the local imaginary impedance peak is expected, whilst at high frequency the plot reverts to a linear log-log behaviour. The manifestation of migrating charges as a shoulder in the spectrum instead of a peak, which is the case for standard sensors [153], can be attributed to the insulating coating of the twisted wires, which behaves as an additional - mostly capacitive - element acting alongside electrode polarisation resulting in a higher effective value of A_e in the equivalent circuit. In terms of physical phenomena, the presence of the coating limits direct charge migration towards the electrodes, with the migration mostly occurring up to the boundary of the coating and the curing material and limited by the polarisation of the insulating layer as the field alternates. As the curing progresses the spectrum shifts to lower frequency and higher impedance. This behaviour, which is the same as that observed with conventional sensing elements, is attributed to the effect of increasing viscosity during the cure, which results in reduced mobility of charge carriers and increased timescale in their response.

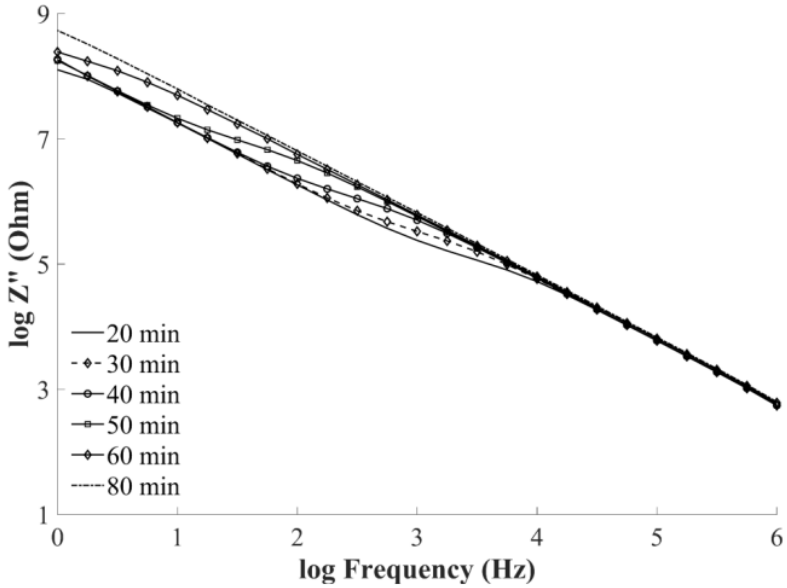

a)

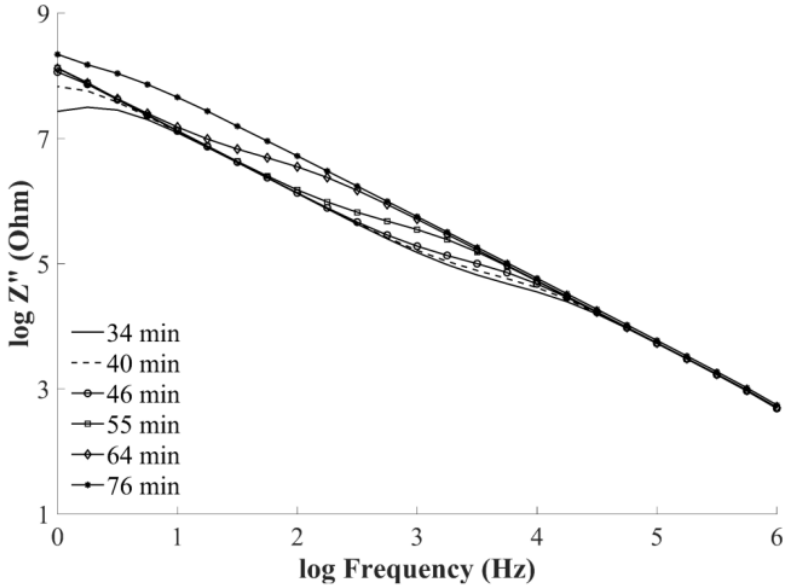

b)

Figure 5.11 Imaginary impedance spectra evolution during isothermal cure of neat epoxy resin at a) 150 °C and; b) 160 °C.

The manifestation of migrating charges as a shoulder instead of a peak in imaginary impedance does not allow use of the conventional analysis based on the IIM to monitor

progress of cure [74, 75, 80]. For the spectra obtained by the sensor presented here, this is carried out by estimating the values of A_e and n_{CPE} for the CPE element of the equivalent circuit from the low frequency response and subtracting the contribution of the constant phase element corresponding to electrode polarisation and the insulating coating from Eq. (5.6). The values of A_e and n_{CPE} were calculated for different times and using the log-log plot of imaginary impedance versus frequency at low frequencies and linear regression. As illustrated in Figures 5.12 and 5.13 the values of A_e and n_{CPE} for the CPE element can be considered constant during the experiments and equal to 100 MOhm/s$^{0.96}$ and 0.96 respectively. The resulting spectrum after subtraction of the constant phase element from Eq. (5.6), termed material impedance (Z''_m), is illustrated in Figure 5.14 alongside the original spectrum. The material impedance spectrum incorporates a pronounced peak which can be used instead of the IIM for estimating the state of cure.

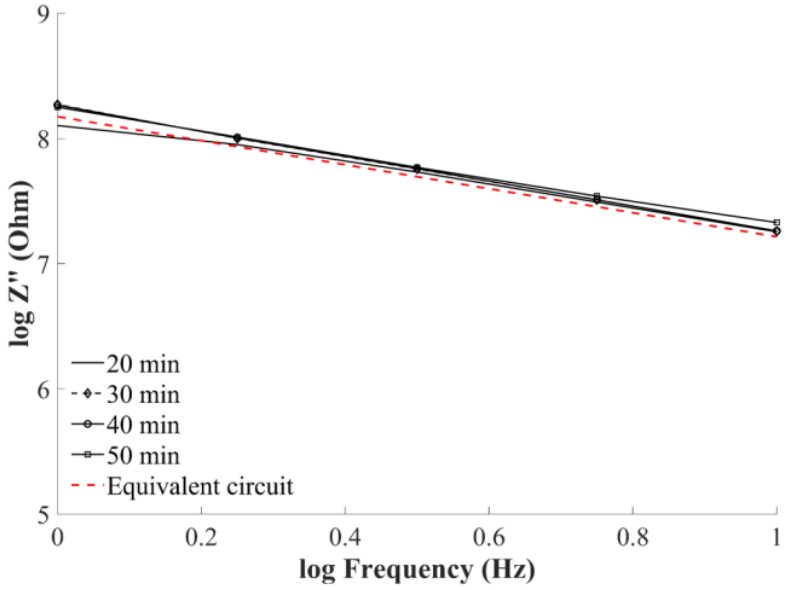

Figure 5.12 Imaginary impedance in low frequencies evolution during isothermal cure of neat epoxy and equivalent circuit response at 150 °C.

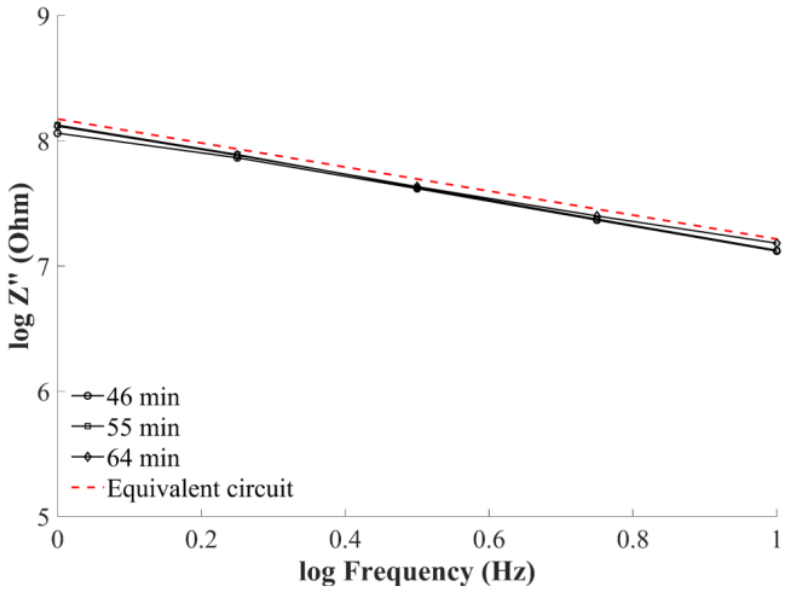

Figure 5.13 Imaginary impedance in low frequencies evolution during isothermal cure of neat epoxy and equivalent circuit response at 160 °C.

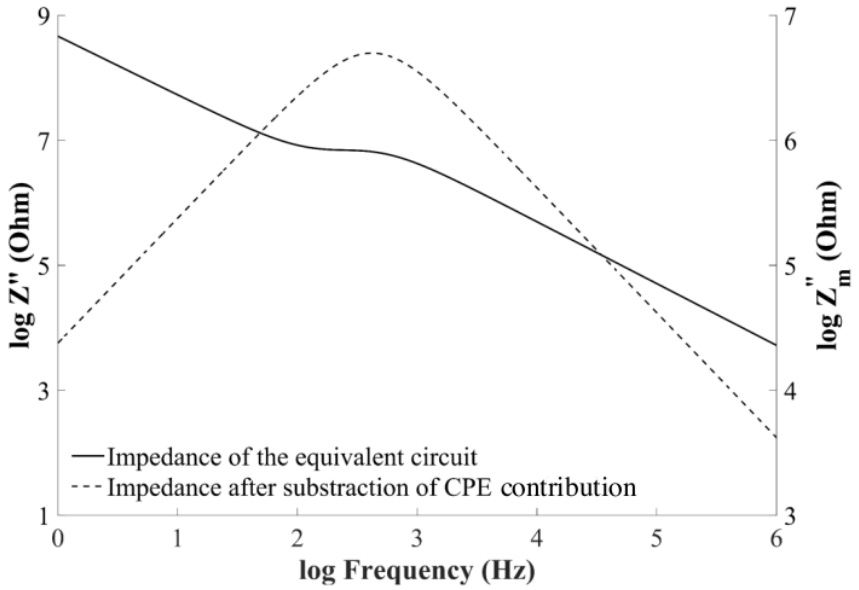

Figure 5.14 Imaginary impedance of equivalent circuit before and after subtraction of the CPE contribution: spectrum obtained at 64 min during the cure of neat RTM6 at 160°C.

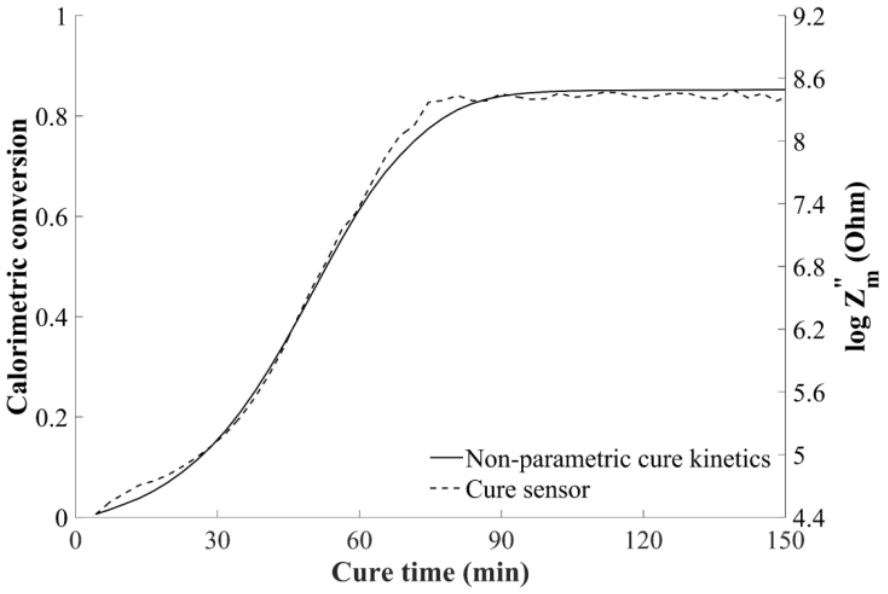

a)

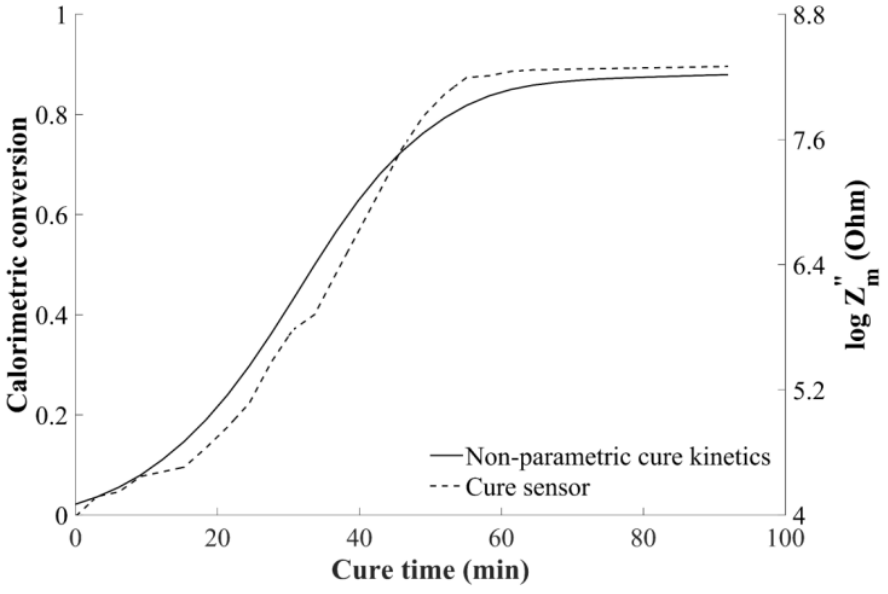

b)

Figure 5.15 Material impedance maximum evolution and comparison with fractional conversion computed using non-parametric kinetics for the isothermal cure of neat RTM6 epoxy resin at a) 150 °C and; b) 160 °C.

Figures 5.15a and b illustrate the evolution of the maximum of Z''_m for the two isothermal neat resin experiments and compare it with the results of a non-parametric cure kinetics model for the resin system of this study based on calorimetric data [134]. In both experiments the response of the cure sensor follows closely the resin reaction. The results highlight the cure sensor efficiency in terms of monitoring the degree of cure evolution during the whole process.

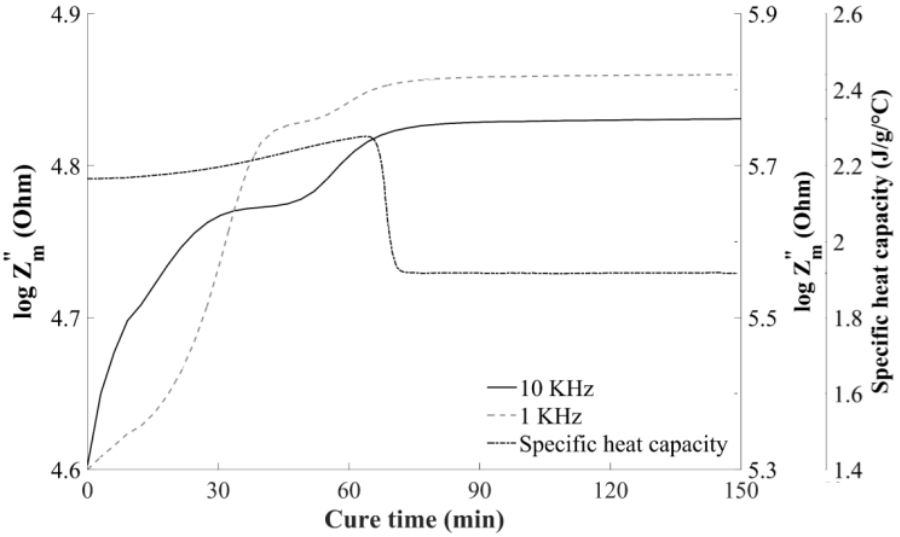

Figure 5.16 Imaginary impedance at fixed frequencies and comparison with the evolution of specific heat capacity for the isothermal cure of neat RTM6 epoxy resin at 150 °C.

Imaginary impedance spectroscopy can also be used for identifying the vitrification point of the resin during the cure. This follows from the influence of vitrification on dipolar relaxation and is manifested as a secondary shoulder in the evolution of imaginary impedance at fixed frequency [154]. Figures 5.16 and 5.17 illustrate the imaginary impedance evolution at 1 kHz and 10 kHz alongside the specific heat capacity for the isothermal curing of neat resin at 150 °C and 160 °C. The imaginary impedance at fixed frequency shows a two-step behaviour; the first major step corresponding to the effect of curing on migrating charges and the secondary step to vitrification. The vitrification is manifested at 50-70 min and 35-55 min at 150°C and 160°C respectively. This time can be compared with the vitrification time identified as a step change in specific heat capacity during the cure. The specific heat capacity for the resin system of this study was

calculated based on the results presented in [155] using the model reported in section 4.2.3. The step in specific heat capacity curves occurs at 65 min and 50 min at 150°C and 160°C respectively, which shows that the sensor identification of vitrification is in agreement with the calorimetric manifestation of the phenomenon. The comparison highlights the capability of the cure sensor to identify the vitrification of the resin during isothermal runs.

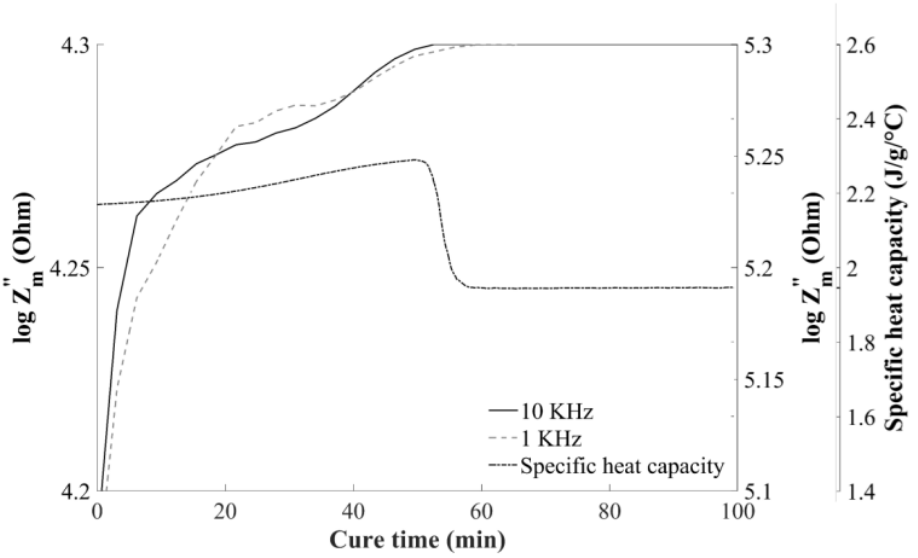

Figure 5.17 Imaginary impedance at fixed frequencies and comparison with the evolution of specific heat capacity for the isothermal cure of neat RTM6 epoxy resin at 160 °C.

The results of cure monitoring during VARTM processing of the carbon/epoxy composite flat panel described in section 3.4.2 are illustrated in Figures 5.18 and 5.19. The response is very similar to that of the neat resin, showing that the sensor monitors resin material changes in the presence of carbon reinforcement and is able to follow the cure. The reaction progress, as monitored by the cure sensor, is in very good agreement with the corresponding estimation of the cure kinetics model, as observed in Figure 5.18. The woven cure sensor allows the monitoring of resin reaction under industrial conditions in the presence of carbon fibre reinforcement. The disturbance caused by the cure sensor in the preform is small compared with other solutions where the sensor is covered with a permeable non-conductive material such as glass cloth or a polymer weave [72, 78, 83]. Figure 5.19 illustrates the imaginary impedance evolution at fixed frequencies alongside

the evolution of specific heat capacity during the cure of the carbon part. The vitrification is manifested as the second step of imaginary impedance during the cure process at 40-50 min. The signal sensitivity obtained for the length of twisted wire corresponding to the woven sensor is about 20% higher than the sensitivity of conventional interdigitated electrode sensors (Pearson Panke, GIA) [153]. More specifically, the sensitivity during the isothermal cure of neat resin is equal to 1 order of magnitude per 20% progress of cure and 1 order of magnitude per 25% progress of cure for the sensor presented here and a conventional interdigitated sensor respectively. Despite the fact that the insulation covers the sensor electrodes, increasing the contribution of the constant phase element, the resulting sensitivity is higher than a conventional sensor covering a similar area.

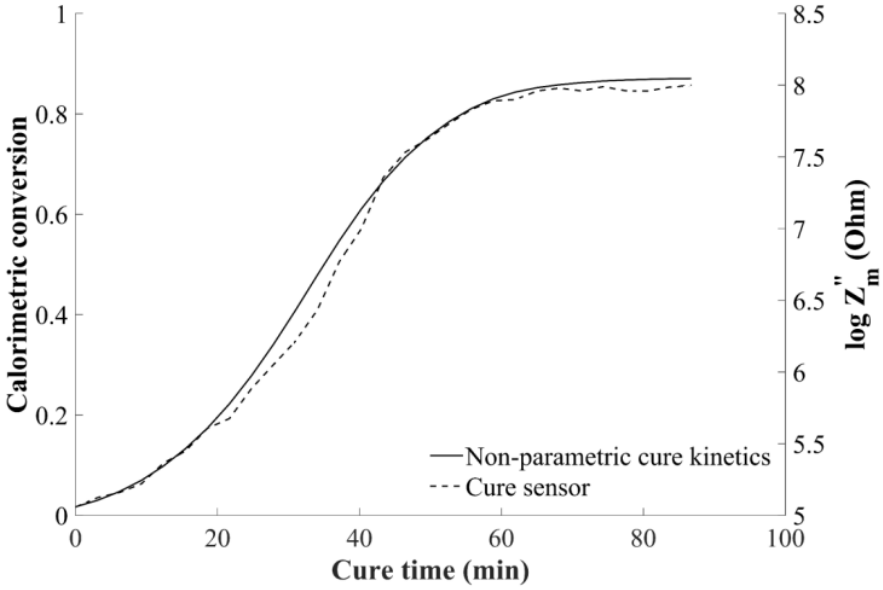

Figure 5.18 VARTM cure of epoxy/carbon composite flat panel: material impedance maximum evolution and comparison with fractional conversion computed using non-parametric kinetics.

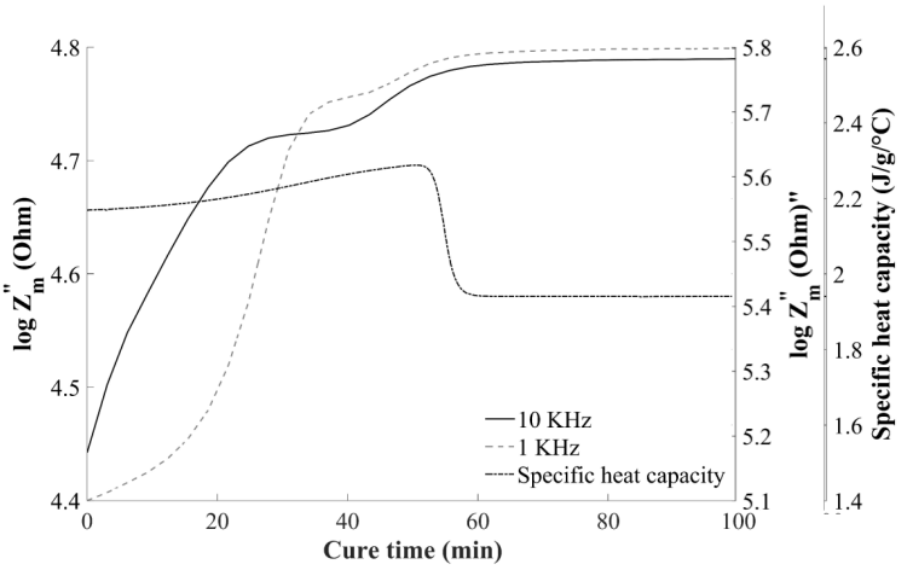

Figure 5.19 VARTM cure of epoxy/carbon composite flat panel: imaginary impedance evolution at fixed frequencies and comparison with the evolution of specific heat capacity.

The lineal flow sensor signal was evaluated after the completion of RTM filling of the RTM6 epoxy/carbon composite flat panel (FP) in order to investigate its cure monitoring capabilities. Figure 5.20 illustrates the imaginary impedance evolution of the lineal flow sensor at a fixed frequency of 3.16 kHz during cure at 160°C in RTM process. The vitrification is pronounced as a secondary step at 40 -50 min in imaginary impedance evolution and is in good agreement with the specific heat capacity step change. The lineal sensor response is noisy in comparison to the cure sensor, highlighting the improvements in terms of sensitivity due to the woven configuration of the cure sensor. The local character of cure sensor allows the monitoring of resin presenting uniform material state. In the case of lineal sensor, the interrogated material is distributed across the length of the sensor and potential dissimilarities in boundary conditions may affect the uniformity of the measured resin introducing noise.

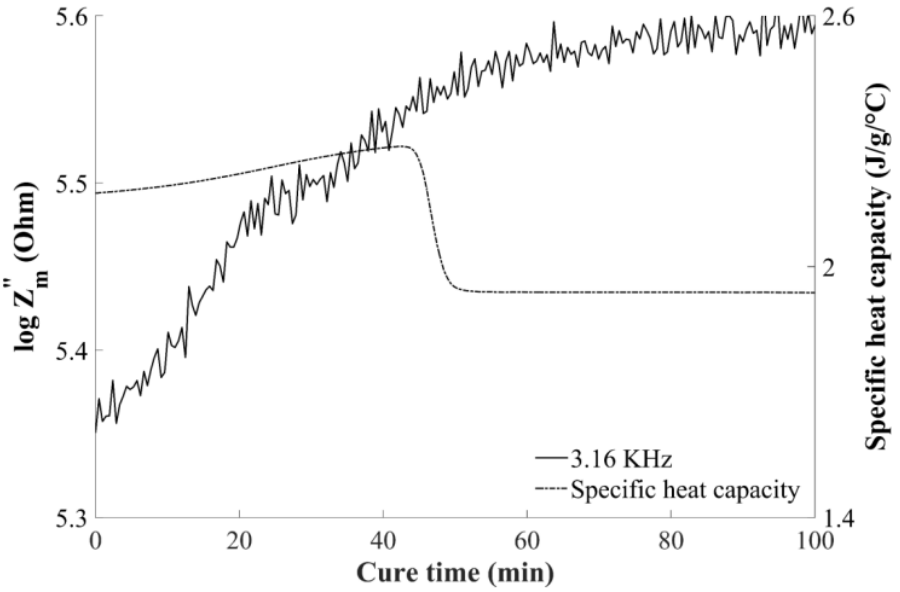

Figure 5.20 Lineal sensor imaginary impedance evolution at fixed frequency during RTM cure of epoxy/carbon composite panel and comparison with the evolution of specific heat capacity.

5.5. Overview

The new approach of dielectric sensing developed in this study overcomes limitations related to the presence of conductive carbon-fibre reinforcement monitoring the filling and curing stage of composites manufacture. The intrusiveness of the sensor in preform architecture is negligible due to its small size, whilst the sensor design allows its placement anywhere in composite part. Validation RTM tests have been conducted demonstrating the accuracy and robustness of the flow sensor with an error never exceeding 3%. The cure sensor evaluated in curing of neat resin and VARTM processing allows the monitoring of resin reaction progress, whilst it identifies the vitrification time in different isothermal runs. A set of lineal flow dielectric sensors are used as the process monitoring system in the RTM filling stage for the evaluation of the inversion procedure performance which is presented in chapter 6.

6. Inversion scheme development in the RTM filling of a carbon/epoxy composite flat panel with recessed edge

6.1. Introduction

The presence of uncertainty in composites manufacture [5] can lead to significant variations in filling duration and initiate process defects such as dry spots and voids resulting in rejected parts. Variability of resin viscosity, preform permeability and length of the distribution medium can introduce up to 20% variance in filling duration [25]. The inverse algorithm described in section 3.8 is implemented in the case of the RTM filling of a carbon/epoxy composite flat panel with recessed edge specified in section 3.4.1 for the probabilistic estimation of unknown stochastic parameters and the corresponding process outcomes. Lineal flow sensors, presented in chapter 5, are placed in strategic positions in the mould cavity providing data during the flow stage. Surrogate flow models are constructed based on the methodology described in section 3.6 to represent the response of sensors allowing the real time implementation of the inverse scheme. The stochastic objects presented in chapter 4 related to the filling stage were considered in this part of the work.

6.2. Surrogate flow models of carbon/epoxy composite flat panel construction and validation

Four surrogate models based on the methodology described in section 3.6 were constructed for the implementation of the inversion procedure. The surrogate models were constructed based on an initial sample generated using the flow model described in section 3.5.1.1. This represents the RTM filling stage of an epoxy/carbon composite flat panel with a recessed edge (FPR). Three surrogate models (FPR SM_1, FPR SM_2 and FPR SM_3) represent the covered lengths S_1 , S_2 and S_3 of the three sensors as function of the stochastic variables and time t. Sensors S_1 and S_3 were placed on the straight and recessed edge of the part respectively, whilst sensor S_2 was placed across the main flow. More details regarding the lineal flow sensor placement can be found in section 3.4.1. The fourth surrogate model (FPR SM_4) represents the filling duration (t_{fill}) as a function of the unknown stochastic parameters. The unknown stochastic parameters are the initial

reference viscosity (η_0), preform permeabilities (K_x, K_y) and the equivalent race tracking permeabilities (K_R).

Table 6.1 Sensitivity analysis parameter values and results for filling process of carbon/epoxy composite flat panel with recessed edge (FPR).

			Average relative difference		
Parameter	**Lower value**	**Upper value**	**Sensor 1**	**Sensor 2**	**Sensor 3**
K_x (m^2)	$1\ 10^{-11}$	$2.4\ 10^{-11}$	**38%**	**41%**	**40%**
K_y (m^2)	$9\ 10^{-12}$	$1.9\ 10^{-11}$	3%	2%	**22%**
K_{R1} (m^2)	$1\ 10^{-11}$	$7\ 10^{-11}$	**44%**	**28%**	**14%**
K_{R2} (m^2)	$1\ 10^{-11}$	$7\ 10^{-11}$	2%	2%	**65%**
K_{R3} (m^2)	$1\ 10^{-11}$	$7\ 10^{-11}$	3%	3%	3%
K_{R4} (m^2)	$1\ 10^{-11}$	$7\ 10^{-11}$	**8%**	**9%**	**30%**
K_{R5} (m^2)	$1\ 10^{-11}$	$7\ 10^{-11}$	1%	1%	**20%**
K_{R6} (m^2)	$1\ 10^{-11}$	$7\ 10^{-11}$	0.04%	0.05%	4%

The resulting high dimensional input space of the surrogate models requires a very large initial set of sampling points to ensure model accuracy compared to the PAM-RTM® model. A sensitivity analysis was carried out in order to reduce model dimensionality investigating the model response by altering each parameter by two positive and two negative standard deviations about their mean values. The initial reference viscosity affects the response of all sensors given the global role of viscosity in the evolution of filling. In contrast, the preform permeability and race tracking permeability have a local role and only affect significantly some of the sensor responses. Therefore, only the preform permeability and equivalent race tracking permeability were considered in the sensitivity analysis. The values of the parameters used in the analysis are reported in Tables 4.5 and 4.11. The PAM-RTM® model was utilised for the evaluation of the filling of carbon/epoxy composite flat panel for the 256 input parameter combinations. The average absolute relative difference of covered sensor length was computed for each of the input parameters as the average difference over all corresponding cases with the upper and lower value of the specific parameter. Table 6.1 summarises the results of the sensitivity analysis. An absolute relative difference of 10% in sensor response was considered as the threshold beyond which the sensor is considered sensitive to the

corresponding parameter. Sensors S_1 and S_2 are sensitive only to K_x, K_{R1} and K_{R4}, whereas S_3 to K_x, K_y, K_{R2}, K_{R4} and K_{R5}. The equivalent race tracking permeability K_{R3} does not affect significantly the response of any of the sensors since the flow front at that area is dominated by K_x. In the case of K_{R6}, the flow at the last section of recessed edge of the part is governed by K_y due to the presence of the recessed edge. Table 6.1 presents the parameters of each of the surrogate models and their corresponding ranges. Therefore, FPR SM_1 and FPR SM_2 result in an input vector of five variables, whilst FPR SM_3 in eight parameters. The surrogate model representing filling duration has a dimensionality equal to seven.

The surrogate models representing the flow front position of each sensor and the filling duration were evaluated against the PAM-RTM® flow model. Three different cases were tested for the surrogate models which correspond to sensor response. The surrogate model of S_1 was compared with the simulation for three different initial reference viscosity values with the preform permeability values equal to 1.7 10^{-11} and 1.3 10^{-11} m^2 respectively and race tracking permeability values equal to 1.3 10^{-11} m^2. The results are illustrated in Figure 6.1. The estimated flow front position of S_1 is in good agreement with the corresponding PAM-RTM® model results and reproduces trends of dependence on viscosity correctly. Figure 6.2 depicts the evolution of flow front position of the second sensor (S_2) as computed by the FPR SM_2 and PAM-RTM® models for three different K_x values, with K_y equal to 1.3 10^{-11} m^2, race tracking permeability values equal to 1.3 10^{-11} m^2 and initial reference viscosity equal to 0.15 Pas. The discrepancy between the two models is negligible with an average absolute error of about 15 mm.

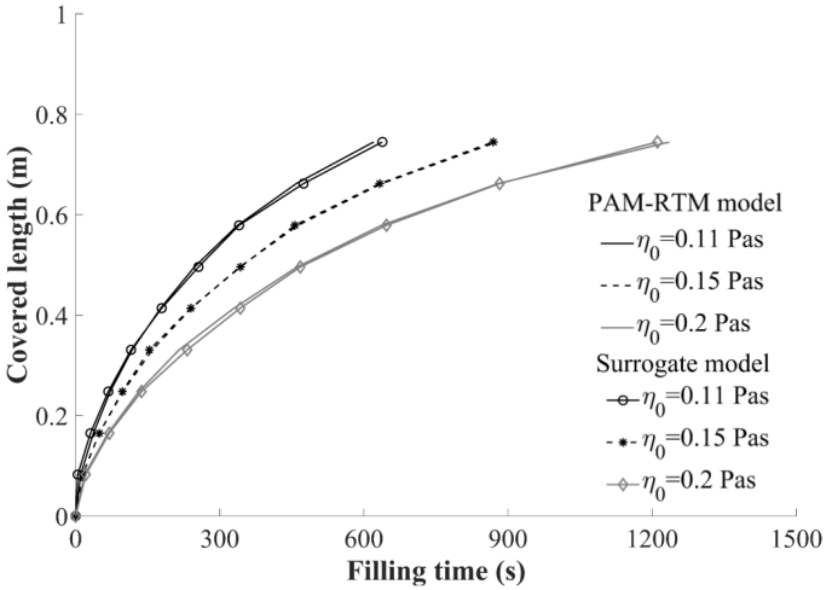

Figure 6.1 FPR SM_1 validation of RTM filling of carbon/epoxy composite flat panel with recessed edge (FPR) against the CV/FE simulation.

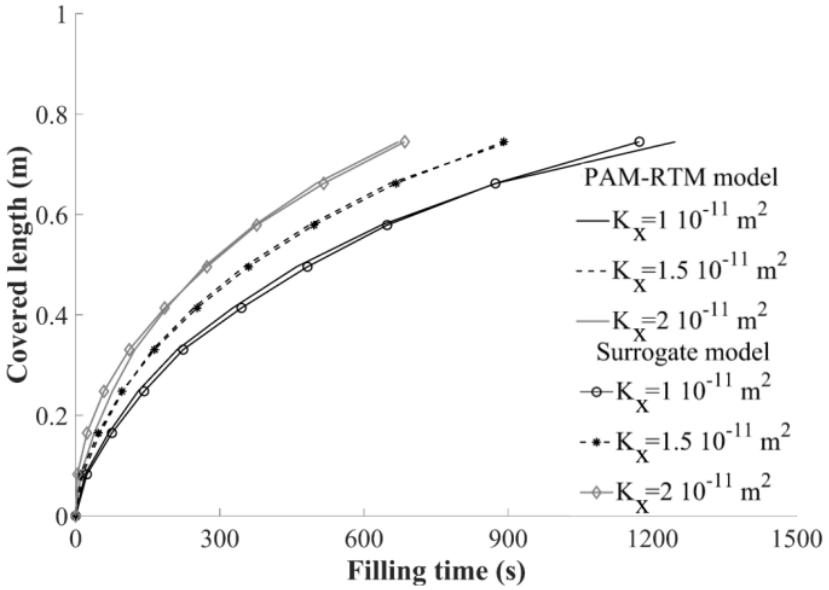

Figure 6.2 FPR SM_2 validation of RTM filling of carbon/epoxy composite flat panel with recessed edge (FPR) against the CV/FE simulation.

The response of FPR SM_3 corresponds to a total covered length greater than the other two models as this sensor covers the recessed edge of the part. Figure 6.3 illustrates S_3 for three different initial reference viscosity values with K_x and K_y equal to 1.7 10^{-11} and 1.3 10^{-11} m^2 respectively and race tracking permeability of 1.3 10^{-11} m^2 as estimated by the two models. The average absolute error of surrogate model is about 12 mm highlighting the accuracy of the surrogate model. Figure 6.4 illustrates the comparison between the filling duration surrogate model and the PAM-RTM® solution for different initial viscosity values with K_x and K_y equal to 1.7 10^{-11} and 1.3 10^{-11} m^2 respectively and race tracking permeability equal to 1.3 10^{-11} m^2. The estimated average absolute error is about 50 sec or less than 2% of the filling duration estimated using the simulation. The input parameters and the ranges of the validation cases are reported in Table 6.2.

Table 6.2 Input parameters values used for the construction of validation curves for the comparison of surrogate and CV/FE models of carbon/epoxy composite flat panel with recessed edge (FPR).

Parameter	FPR SM_1	FPR SM_2	FPR SM_3	FPR SM_4
K_x (m^2)	1.7 10^{-11}	**1 10^{-11} - 2 10^{-11}**	1.7 10^{-11}	1.7 10^{-11}
K_y (m^2)	-	-	1.3 10^{-11}	1.3 10^{-11}
K_{R1} (m^2)	1.3 10^{-11}	1.3 10^{-11}	1.3 10^{-11}	1.3 10^{-11}
K_{R2} (m^2)	-	-	1.3 10^{-11}	1.3 10^{-11}
K_{R4} (m^2)	1.3 10^{-11}	1.3 10^{-11}	1.3 10^{-11}	1.3 10^{-11}
K_{R5} (m^2)	-	-	1.3 10^{-11}	1.3 10^{-11}
η_0 (Pas)	**0.1 - 0.2**	0.15	**0.1 - 0.2**	**0.1 - 0.2**

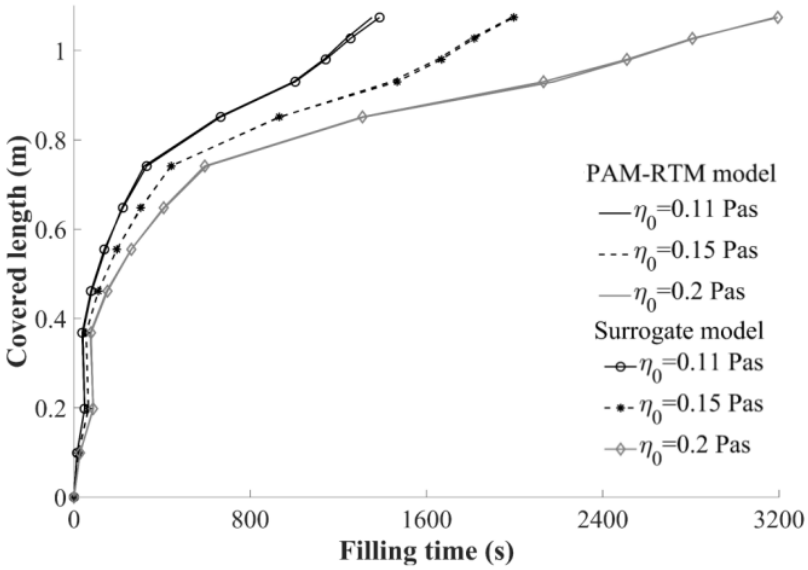

Figure 6.3 FPR SM_3 validation of RTM filling of FPR composite part against the CV/FE simulation.

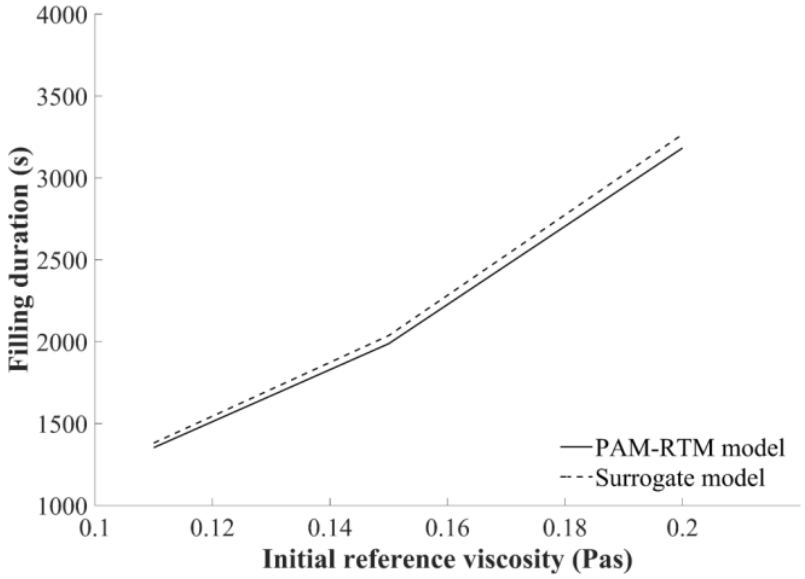

Figure 6.4 FPR SM_4 validation of RTM filling of carbon/epoxy composite flat panel with recessed edge (FPR) against the CV/FE simulation.

6.3. Stochastic simulation of RTM filling of carbon/epoxy composite flat panel with recessed edge (FPR)

A stochastic simulation of the RTM filling of FPR composite part (Figure 3.7) was carried out in order to investigate the influence of the stochastic input parameters on the filling process outcomes. The stochastic simulation is based on Monte Carlo and involves the generation of N_{MC} realisations of random input stochastic variables. The MC sampling points are generated using a set of normally distributed uncorrelated random variables. More details regarding the stochastic simulation are reported in section 3.7. The random variables considered in this study were the initial reference viscosity, preform permeability, equivalent race tracking permeability and the tool temperature as described in chapter 4. In each realisation, the flow model is executed calculating the filling duration and subsequently computing its first and second statistical moments using the overall set of realisations. A total of 400 realisations are required to ensure convergence in average and standard deviation.

The average and standard deviation evolution of filling duration are illustrated in Figure 6.5, whilst Figure 6.6 shows the cumulative probability. The mean value converges after 80 iterations to 2400 sec, whilst the standard deviation reaches a plateau of about 780 sec after 300 realisations. The filling duration presents high variability with a coefficient of variation of about 30%. This can be attributed mainly to the significant variations of the initial state of resin viscosity and preform permeability. Also, tool temperature uncertainty affects resin viscosity resulting in filling time variations. The results highlight the initial uncertainty existing before the initiation of the manufacturing process. Potential uncertainties in material properties and boundary conditions may lead to significant variations during the manufacturing process resulting in unexpected defects and long process cycles.

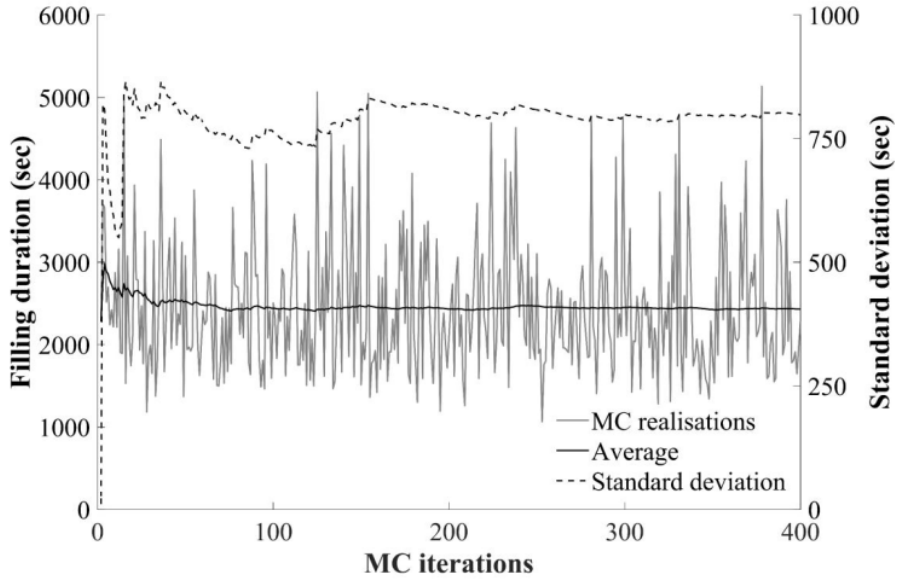

Figure 6.5 Stochastic simulation of RTM filling of carbon/epoxy composite flat panel with recessed edge (FPR): filling duration average and standard deviation evolution with MC iterations.

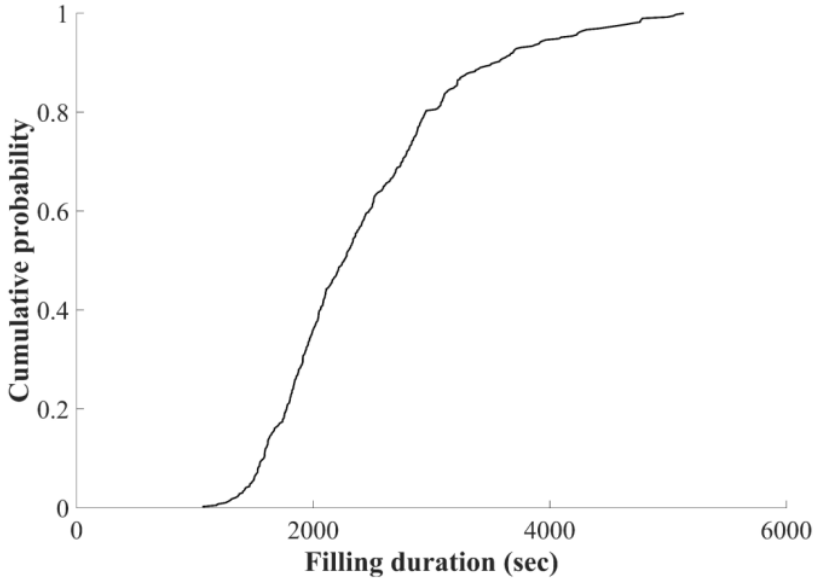

Figure 6.6 Stochastic simulation of RTM filling of carbon/epoxy composite flat panel with recessed edge (FPR): cumulative probability of filling duration.

6.4. Real time uncertainty estimation during filling stage of carbon/epoxy composite flat panel with recessed edge

6.4.1. Inversion procedure implementation

An inversion scheme was developed for the real time uncertainty estimation of the unknown stochastic parameters and the filling duration. Figure 6.7 summarises the inversion procedure framework. The analysis is initiated when the filling stage of the RTM process of FPR composite part takes place. The sensors monitor the covered lengths S_1, S_2 and S_3 at each time increment t_k. The inverse scheme integrates the monitoring data $\mathbf{Y_{exp}}(t_k) \in \mathbb{R}^{N_k \times 3}$, with N_k the number of experimental data which correspond to covered lengths of the three lineal sensors at times $t_1 \dots t_k$, in real time with the surrogate flow models $\mathbf{Y_m} = [S_1, S_2, S_3]$ using the MCMC method described in section 3.8 for the probabilistic prediction of the unknown stochastic parameters and the filling duration.

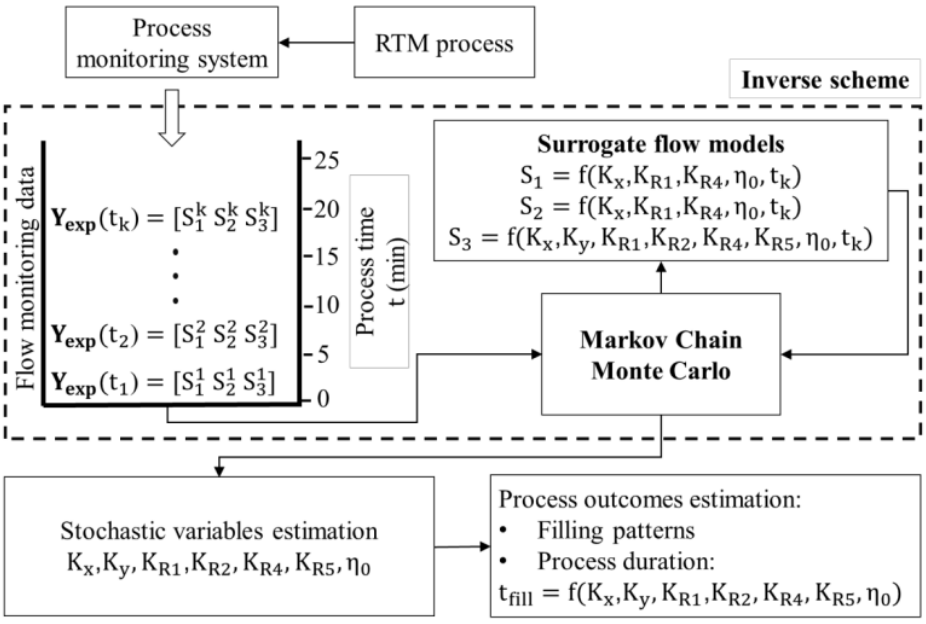

Figure 6.7 Inversion scheme implementation for the RTM filling stage of carbon/epoxy composite flat panel with recessed edge (FPR).

In the real time implementation of the inversion procedure the monitoring matrix $\mathbf{Y_{exp}}$ is updated every minute with a new batch of monitoring data. In this case, every new batch includes three data points corresponding to the three sensor responses. The number M of MCMC iterations carried out in the real time implementation of the inversion procedure in the filling of carbon/epoxy composite flat panel can be calculated based on the time of the execution of an MCMC iteration. The execution time of one iteration for the given computer increases with the increase of the size of $\mathbf{Y_{exp}}$. The number of MCMC iterations executed at the beginning of the process is about 2,500 points/min on the 4 cores @3.2 GHz computer used, whilst this number decreases gradually to about 170 point/min in the last stage of the process. The total number of MCMC iterations was approximately 20,000. Table 6.3 summarises inversion procedure parameters values.

Table 6.3 Inverse scheme parameters values of carbon/epoxy composite flat panel with recessed edge (FPR).

Parameter	Symbol	Value
Noise level ε_{K_x} standard deviation	$\sigma_{\varepsilon_{K_x}}$	3 10^{-13} m^2
Noise level ε_{K_y} standard deviation	$\sigma_{\varepsilon_{K_y}}$	3 10^{-13} m^2
Noise level $\varepsilon_{K_{R1}}$ standard deviation	$\sigma_{\varepsilon_{K_{R1}}}$	3 10^{-13} m^2
Noise level $\varepsilon_{K_{R2}}$ standard deviation	$\sigma_{\varepsilon_{K_{R2}}}$	3 10^{-13} m^2
Noise level $\varepsilon_{K_{R4}}$ standard deviation	$\sigma_{\varepsilon_{K_{R4}}}$	3 10^{-13} m^2
Noise level $\varepsilon_{K_{R5}}$ standard deviation	$\sigma_{\varepsilon_{K_{R5}}}$	3 10^{-13} m^2
Noise level ε_{η_0} standard deviation	$\sigma_{\varepsilon_{\eta_0}}$	0.001 Pas
Number of MCMC iterations	M	20,000 iterations
Number of monitoring data	N_k	96
Number of data batches	k_{tot}	32

6.4.2. RTM filling results of carbon/epoxy composite flat panel with recessed edge

Figure 6.8 depicts the flow front evolution of the RTM filling stage of FPR composite part presented in section 3.4.1. The duration of the filling was 32 min. Race tracking occurs at the recessed edge at the beginning of the process. In the straight edge, the flow is slightly slower than the main flow due to local compaction by the silicone rubber. The presence of the rectangular insert results in asymmetric flow in which the resin fills the straight edge of the part first and then the area close to the recessed edge. Figure 6.9 illustrates the flow monitoring results of the three lineal flow sensors. The flow front evolution of the first sensor (S_1) presents some noise potentially due to measurement effects or the presence of local reinforcement variations leading to non-uniform flow across the straight edge of the part. The latter can be attributed to the preparation of the preform and its placement in the mould resulting in variations of the gap size between preform and mould across the edge and in turn in variations of local edge permeability. The flow front curve of sensor 3 (S_3) indicates the different flow front velocities of each of the sub-sections of the recessed edge of the mould. At the beginning of the flow process the slope of the S_3 curve is greater than those of S_1 and S_2 implying a race tracking effect on the recessed edge of the mould, which is also observed by visual monitoring.

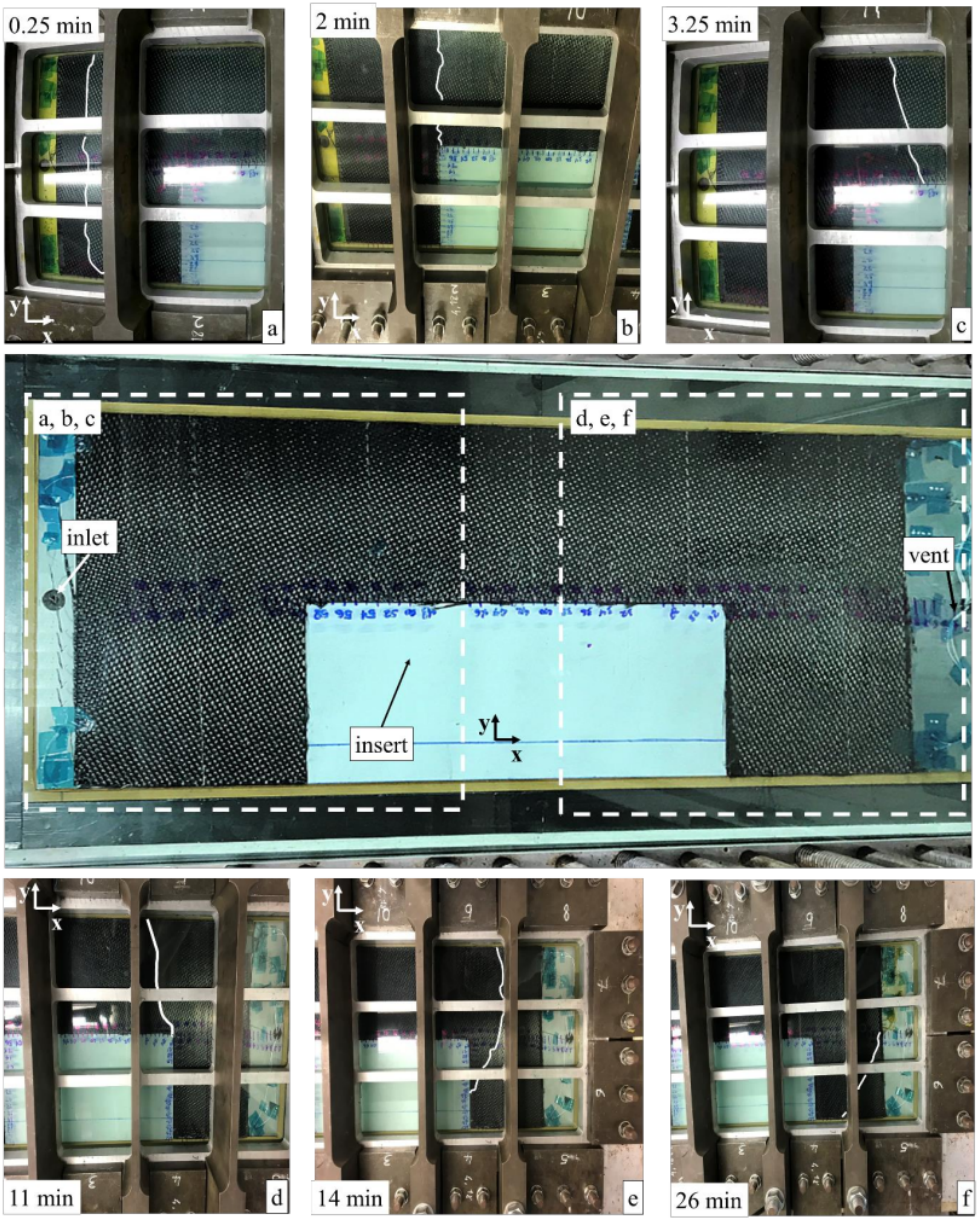

Figure 6.8 Flow front position during RTM filling process of carbon/epoxy composite flat panel with recessed edge (FPR) in different time frames: a) 0.25 min; b) 2 min; c) 3.25 min; d) 11 min; e) 14 min; f) 26 min.

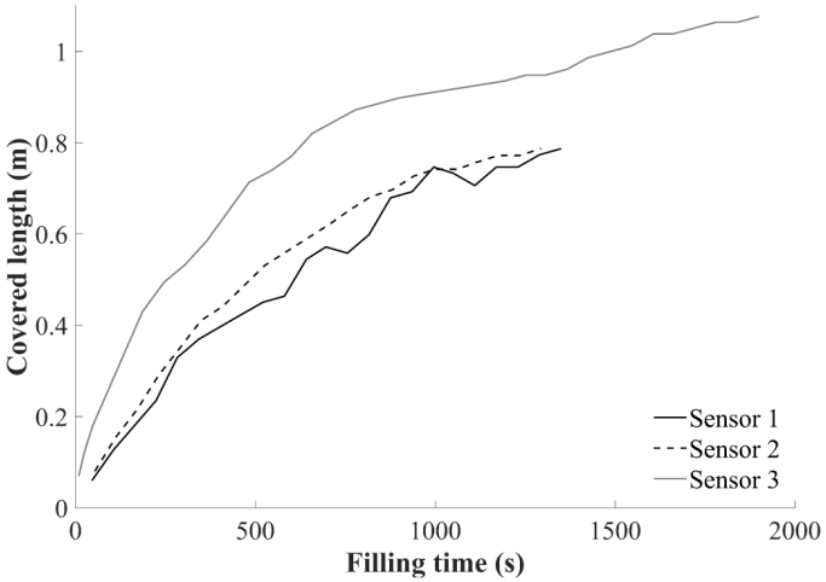

Figure 6.9 Flow monitoring results on the filling of carbon/epoxy composite flat panel with recessed edge (FPR).

6.4.3. Results of the inverse solution

The flow monitoring data were integrated into the inverse scheme for the real time uncertainty estimation of the stochastic parameters. The results of the inversion scheme for the unknown stochastic parameters and the filling duration are presented in Figures 6.10 - 6.13. The use of the surrogate models allows the execution of MCMC iterations as the filling process evolves. Consequently, the results are presented as a function of filling time, which corresponds to the monitoring data and inverse estimation up to the specific point in the filling process. The estimated preform permeabilities reach a plateau of 1.31 10^{-11} m^2 and 1.17 10^{-11} m^2 respectively after about 25 min from the beginning of the flow stage as depicted in Figure 6.10. Both parameters present significant variations in the initial stages of the inversion due to the limited monitoring data available at that time. As the inversion proceeds, the uncertainty is narrowed down.

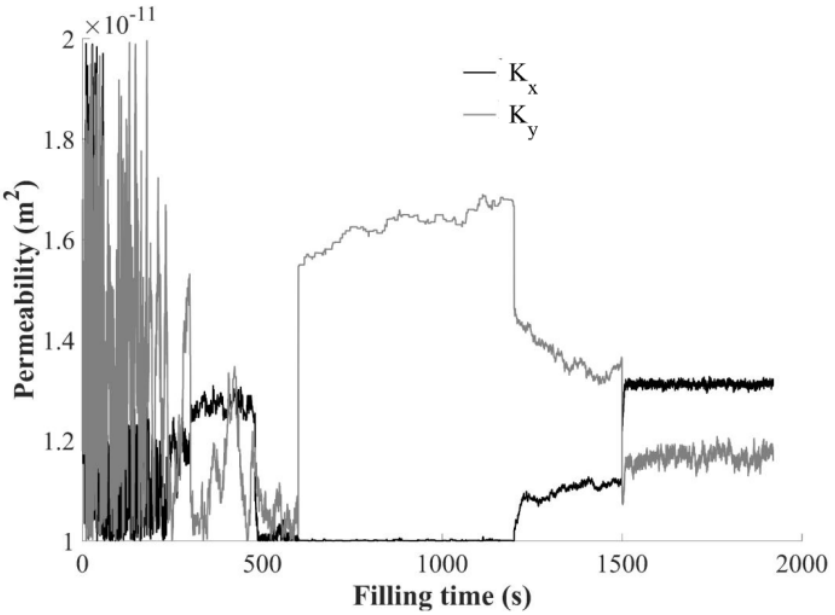

Figure 6.10 Unknown stochastic parameters estimation: preform permeabilities of the filling of carbon/epoxy composite flat panel with recessed edge (FPR).

The predicted K_{R1}, K_{R2} , K_{R4} and K_{R5} values present similar behaviour as depicted in Figure 6.11. The equivalent permeability of the straight edge (K_{R1}) converges after 5 min as the monitoring data of sensor 1 are sufficient to provide information regarding the flow front evolution in the corresponding region. The other three equivalent race tracking permeabilities (K_{R2}, K_{R4}, K_{R5}) are in the range of 4-6 10^{-11} m^2 and are mostly stabilised after about 10 min, highlighting the occurrence of race tracking effects in the recessed edge. The initial reference viscosity reaches a plateau of 0.17 Pas after about 25 min (Figure 6.12). Table 6.4 summarises the statistical properties of the estimated stochastic parameters. Parameters such as K_x, the equivalent permeability of race tracking channel 1 (K_{R1}) and the initial viscosity present lower variability than the other parameters due to the greater sensitivity of the monitoring dataset to these variables.

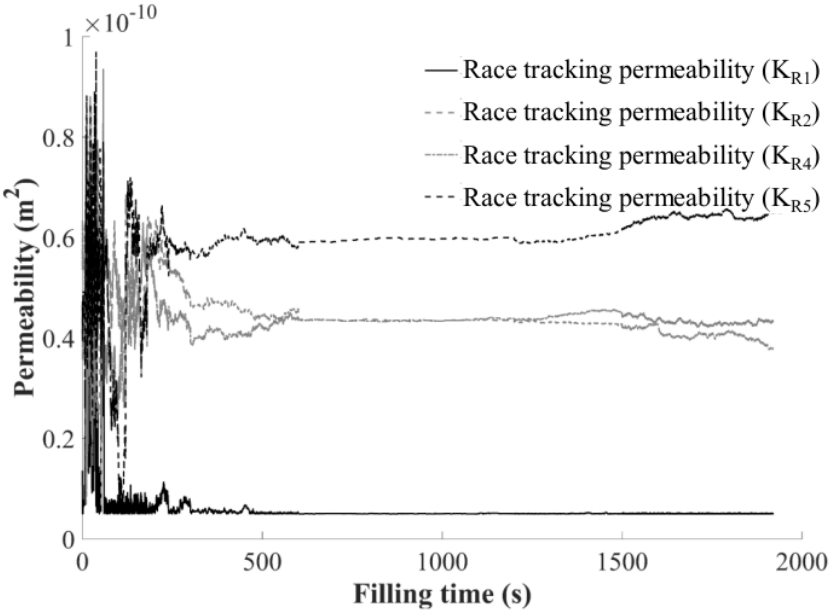

Figure 6.11 Unknown stochastic parameters estimation: equivalent race tracking permeabilities of the filling of carbon/epoxy composite flat panel with recessed edge (FPR).

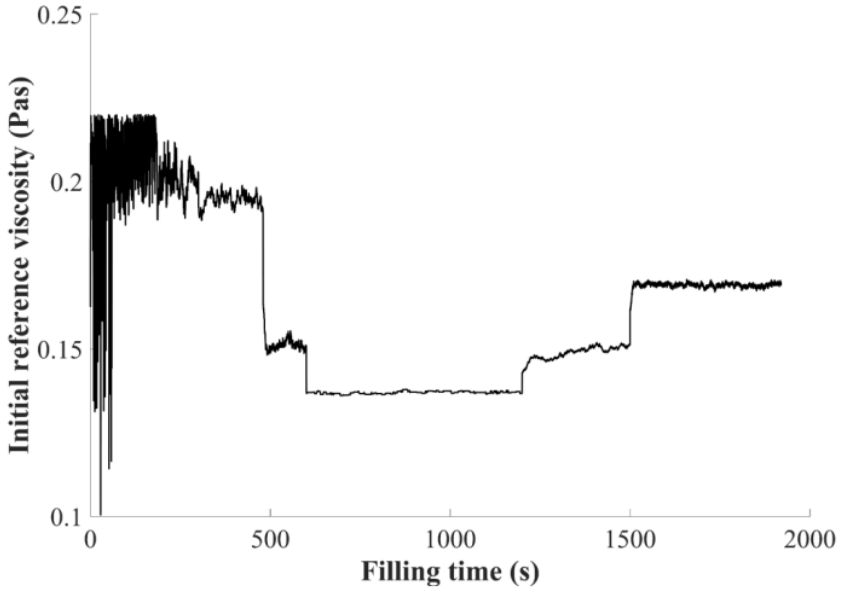

Figure 6.12 Unknown stochastic parameters estimation: initial reference viscosity of the filling of carbon/epoxy composite flat panel with recessed edge (FPR).

Table 6.4 Statistical properties of estimated parameters on the filling of carbon/epoxy composite flat panel with recessed edge (FPR).

Parameter	Average	Standard deviation
K_x (m^2)	$1.312\ 10^{-11}$	$4.52\ 10^{-14}$
K_y (m^2)	$1.168\ 10^{-11}$	$1.26\ 10^{-13}$
K_{R1} (m^2)	$5.044\ 10^{-12}$	$3.81\ 10^{-14}$
K_{R2} (m^2)	$4.056\ 10^{-11}$	$1.07\ 10^{-12}$
K_{R4} (m^2)	$4.318\ 10^{-11}$	$5.22\ 10^{-13}$
K_{R5} (m^2)	$6.422\ 10^{-11}$	$5.63\ 10^{-13}$
η_0 (Pas)	0.1691	$5\ 10^{-4}$

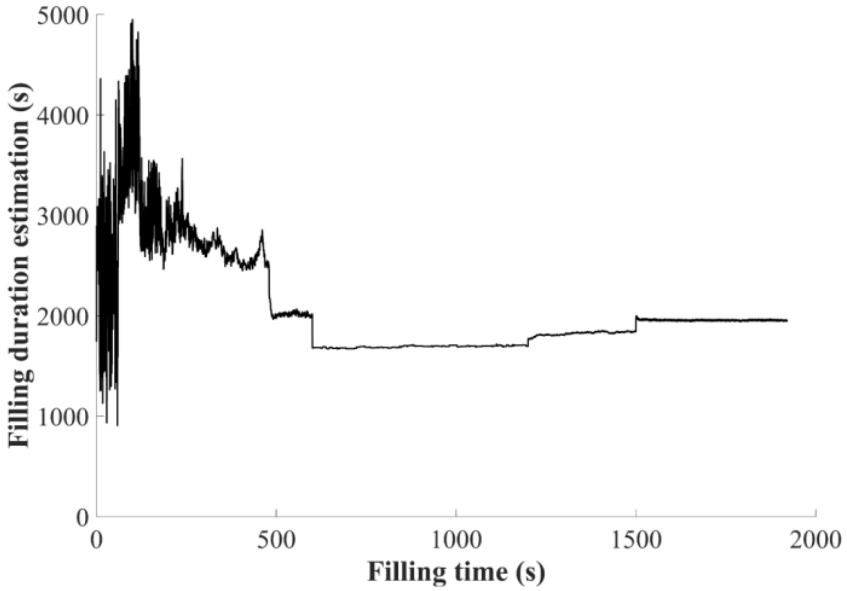

Figure 6.13 Unknown stochastic parameters estimation: filling duration estimation of carbon/epoxy composite flat panel with recessed edge (FPR).

It is possible to predict the duration of the filling as well as other features of the process, using the unknown parameter values estimated in real time by the inversion scheme. Figure 6.13 illustrates the estimation of filling duration as the filling stage evolves. Initially, the uncertainty of filling duration estimation is significant since the available monitoring data are insufficient for an accurate prediction with low uncertainty. However,

as the monitoring data are enriched, the probabilistic estimation of filling duration is narrowed down as illustrated in Figure 6.14. Initially, the coefficient of variation of the estimated filling duration is about 25%, whilst after about 20 min the uncertainty is reduced by 80% to a coefficient of variation of 5%. The predicted filling duration converges to an average of 31 min with a standard deviation of 1.5 min, whilst the actual filling takes 32 min.

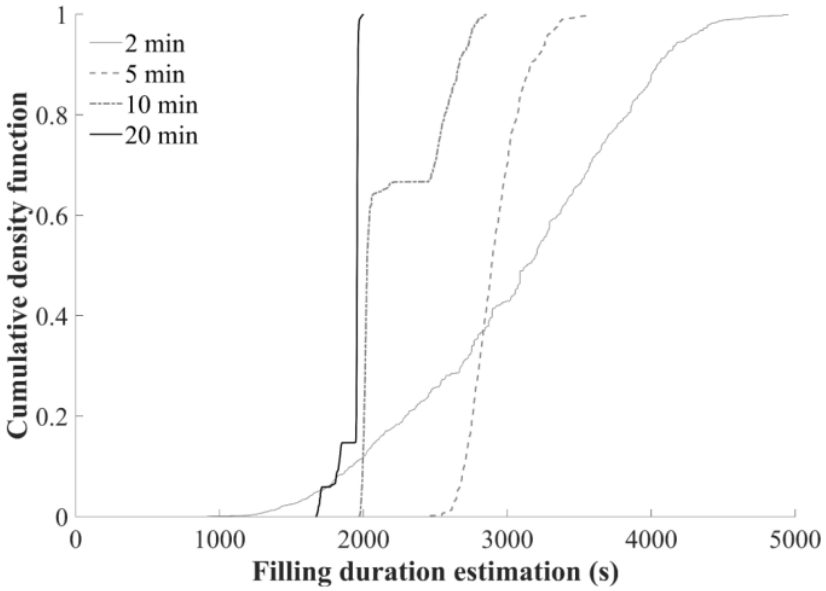

Figure 6.14 Cumulative density function evolution of estimated filling duration of carbon/epoxy composite flat panel with recessed edge (FPR).

Figures 6.15 - 6.17 illustrate the efficiency of the inversion procedure in terms of reducing the uncertainty of flow front estimation. The 95% confidence intervals of the response of the three sensors, illustrated in Figures 6.15a, 6.16a and 6.17a, were calculated considering the initial uncertainty of the input parameters (Table 6.1). The confidence intervals of the prior estimate are wide due to the initial uncertainty of the problem, whilst the coefficient of variation of the predicted filling duration is equal to 30%. Figures 6.15b, 6.16b and 6.17b illustrate the 95% confidence intervals of the three sensors calculated considering the inverse solution. The confidence intervals of the estimated covered lengths have been narrowed down significantly, whilst there is a good agreement between

posterior prediction and the actual covered length. The real time implementation of the inverse scheme is able to estimate the flow front evolution and filling duration with high accuracy. The discrepancies observed between FPR flow model predictions and sensor data are attributed to the fact that the scheme does not consider local flow phenomena such as nesting or preform imperfections, in contrast to sensors which are sensitive to local effects. The representation of preform permeability and race tracking variability with random fields [25] would result in estimations of local phenomena monitored by the sensing system. However, this approach increases significantly the dimensionality of the surrogate flow models causing practical difficulties related to computational resources requirements. The inversion procedure gives a probabilistic estimation of the main flow parameters such as preform permeability, viscosity and boundary conditions such as race tracking effects allowing the probabilistic on line prediction of the filling duration and flow front evolution.

The flow fronts corresponding to the 1st and 3rd quartiles of the prior estimate and using the outcome of the inversion scheme are illustrated in Figure 6.18 and compared to the flow front measured visually during RTM filling of FPR part. The uncertainty obtained by the prior estimate is high. The probabilistic estimations of the flow front with the initiation of the inverse scheme present low variations and are very close to the visual observations. There are small differences between the inverse scheme estimations and the actual flow front at the beginning of process mainly due to noise effects in the experimental data and the presence of local flow phenomena. As the flow evolves the estimated flow front follows closely the actual resin front position identifying potential disturbances such as race tracking effects at the part edges.

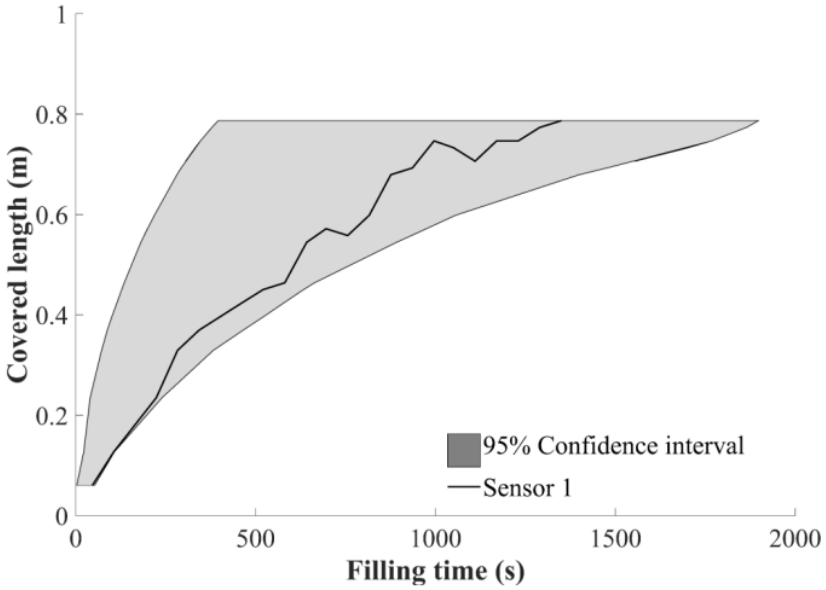

a)

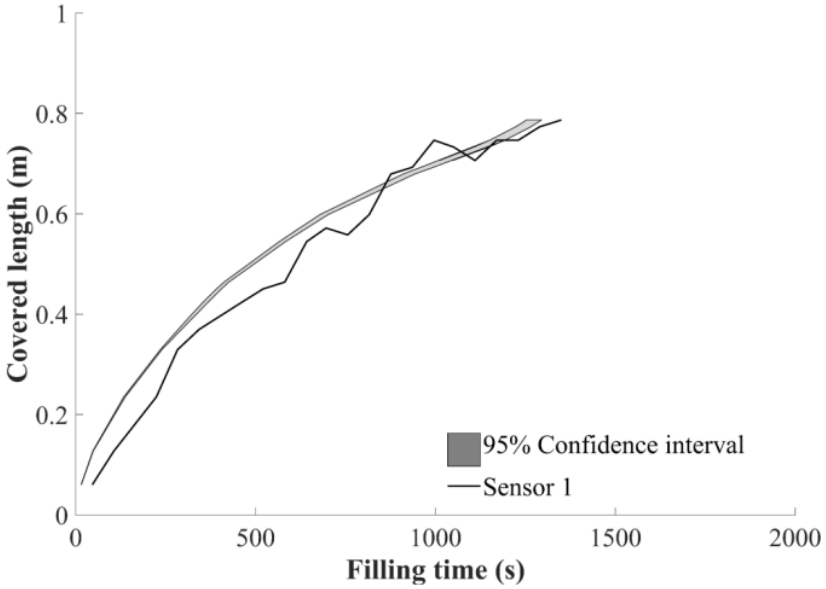

b)

Figure 6.15 Estimation uncertainty of covered length of a) sensor 1 before the filling; b) sensor 1 after 1500 s on the filling of carbon/epoxy composite flat panel with recessed edge (FPR).

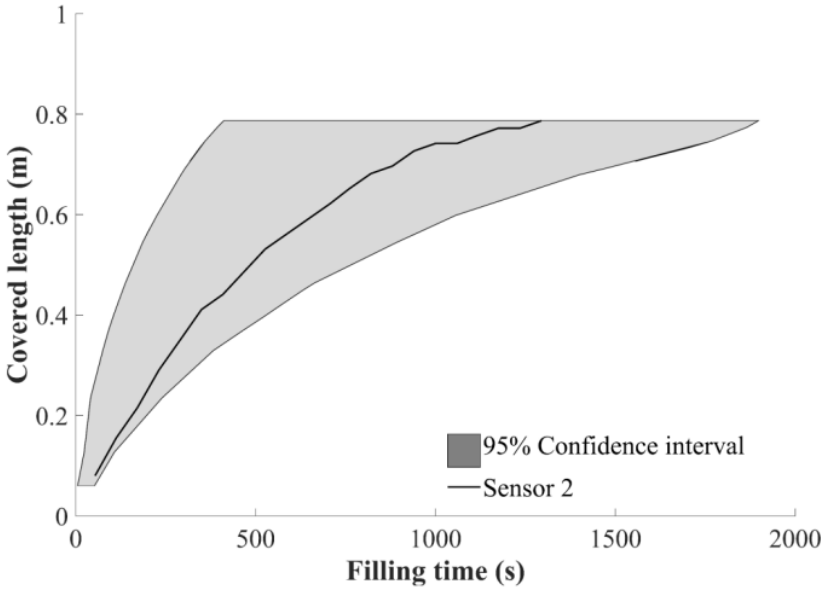

a)

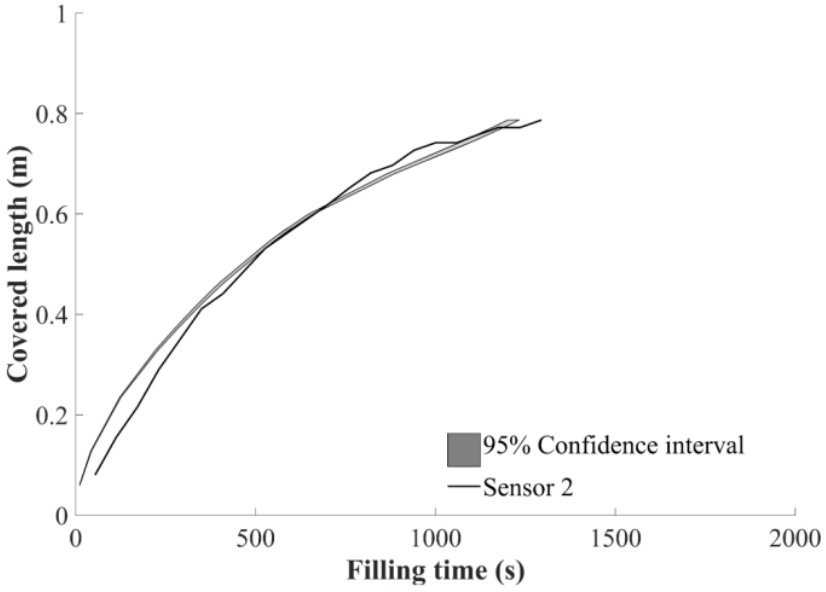

b)

Figure 6.16 Estimation uncertainty of covered length of a) sensor 2 before the filling; b) sensor 2 after 1500 s on the filling of carbon/epoxy composite flat panel with recessed edge (FPR).

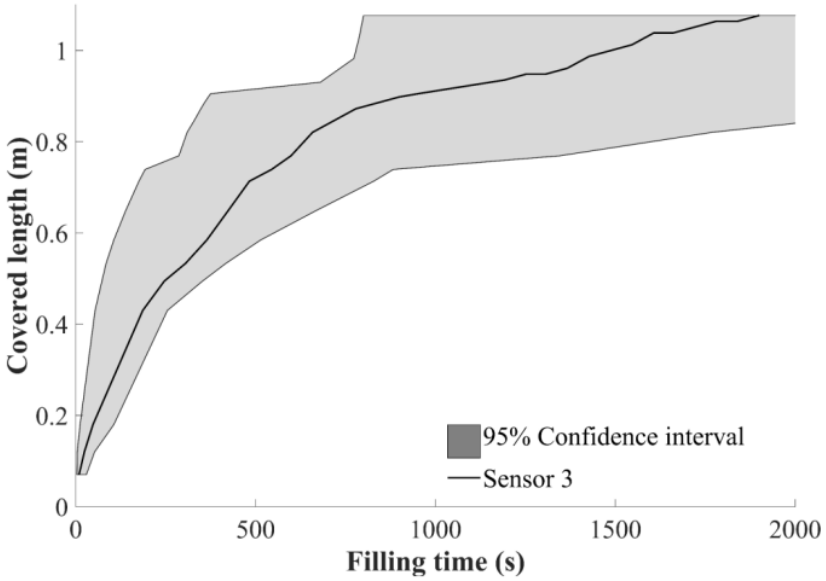

a)

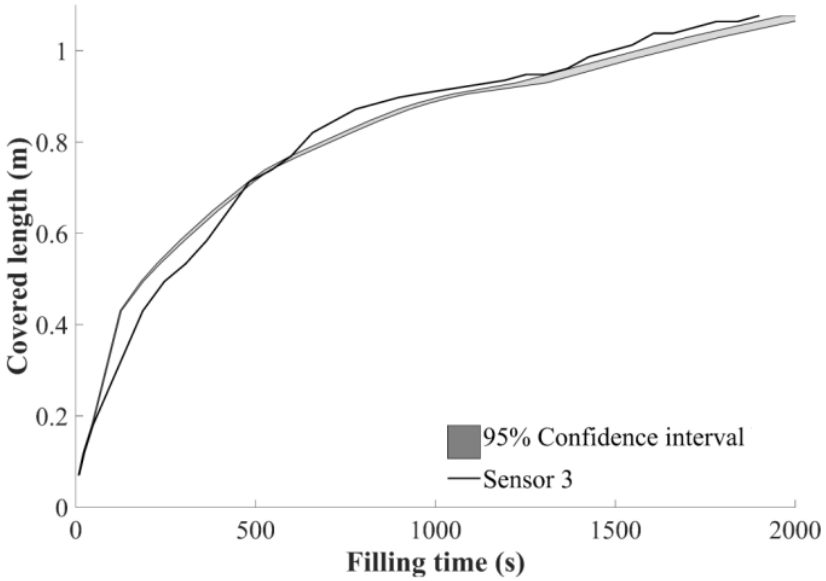

b)

Figure 6.17 Estimation uncertainty of covered length of a) sensor 3 before the filling; b) sensor 3 after 1500 sec on the filling of carbon/epoxy composite flat panel with recessed edge (FPR).

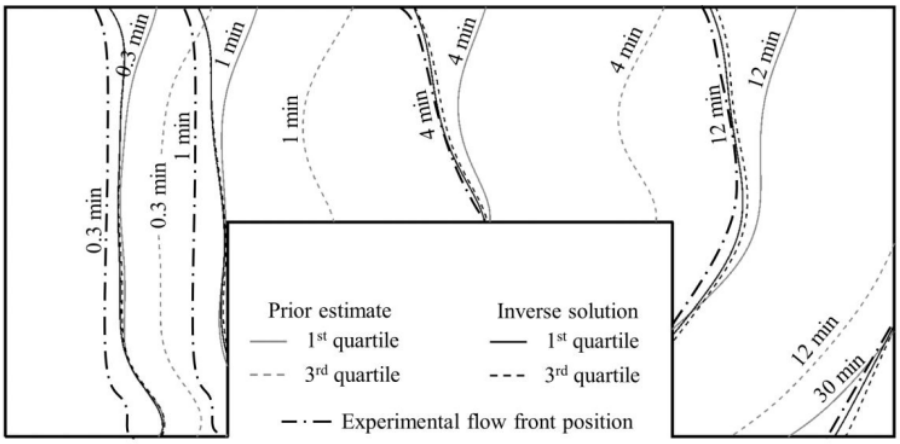

Figure 6.18 Experimental flow front and iso-probability contours at different times for prior and posterior flow front estimates of carbon/epoxy composite flat panel with recessed edge (FPR).

For the geometry examined here, the use of three lineal sensors in the mould is sufficient for the inverse scheme to predict accurately the resin flow front evolution and to identify potential flow disturbances and defects such as edge effects by estimating the equivalent race tracking permeability. The location of lineal sensors in the mould is crucial for the successful estimation of unknown parameters. In the general case, the number of sensors used needs to be selected considering the trade-off between minimising monitoring complexity and monitoring system intrusiveness and maximising the sensitivity of the data obtained to all stochastic parameters of interest. In this case, the utilisation of three sensors placed across part edges and the main flow allows the model to capture the main process parameters such as K_x, K_y and η_0 and provide sufficient information on race tracking phenomena.

6.5. Overview

The application of the inverse scheme in RTM filling of carbon/epoxy composite part with complex geometry reduces the initial uncertainty of the problem estimating the preform permeability values, initial viscosity, race tracking effects, filling duration and flow front evolution with significantly lower variability than prior estimates within a fraction of the process duration. In the experimental demonstration of the scheme presented here the inverse scheme is able to provide a low uncertainty real time prediction

of filling approximately 10 min after the initiation of the process, which corresponds to 30% of the whole duration. The utilisation of surrogate models allows the implementation of inversion in parallel with the RTM filling of the composite part. Furthermore, the strategic placement of flow sensors within the tool increases the sensitivity of the problem resulting in a faster convergence of the inverse solution. This is of importance, especially in cases of fast filling processes where the inversion scheme needs to find a solution in short time. The capability of the inverse algorithm to operate in short process cycles is investigated in the next chapter for the case of the artificial RTM filling of a carbon/epoxy composite C spar.

7. Inversion procedure development in the RTM filling stage of a carbon/epoxy composite C spar

7.1. Introduction

In chapter 6 the inversion procedure was applied and validated in the case of a filling process with a duration of about 30 min. In order to fully uncover the inversion scheme capabilities, the algorithm needs to be evaluated in a sort term filling stage. Therefore, the artificial RTM filling of the carbon/epoxy composite C spar described in section 3.5.1.2 was carried out. Artificial lineal sensors are placed in strategic positions in the mould cavity providing data during the flow stage. The methodology described in section 3.6 is employed in order to build computationally efficient surrogate models representing the flow front evolution of lineal sensors and the filling simulation described in section 3.5.1.2 is utilised for the construction of surrogate models.

7.2. Surrogate models of filling of carbon/epoxy composite C spar construction and validation

Five surrogate models (C spar SM_1 - C spar SM_5) were constructed to represent the response of sensors and the total filling time for the case of the C spar. The inputs of the surrogate models in the case of the C spar are the longitudinal and transverse permeability, the initial reference viscosity and the filling time, whilst the outputs are the covered length of the four artificial flow sensors and the filling duration. The resulting dimensional input space of the sensors surrogate models requires a large initial design space to ensure model efficiency compared to the PAM-RTM® model. The initial design input space and the corresponding responses were calculated using the PAM-RTM® model described in section 3.5.1.2 Table 7.1 summarises the input parameters of the four surrogate models and their ranges.

Table 7.1 Surrogate models parameters and their ranges of filling process of carbon/epoxy composite C spar.

Parameter	Ranges
Longitudinal permeability	$5\ 10^{-12}$-$2\ 10^{-11}$ m^2
Transverse permeability	$5\ 10^{-12}$-$2\ 10^{-11}$ m^2
Initial reference viscosity	0.11-0.22 Pas

The surrogate models corresponding to the response of the four flow sensors were compared to the PAM-RTM® flow model described section 3.5.1.2. Response surfaces were constructed using both the surrogate and the PAM-RTM® models representing the covered length as a function of filling time and unknown parameters, whilst the remaining inputs were assigned with the nominal values reported in Table 7.2. The results of surrogate models validation tests are presented in Figures 7.1-7.5. The covered length of sensors depends on initial reference viscosity as illustrated in Figures 7.1-7.3. The effect of resin viscosity on sensor covered length increases significantly as the resin flows away from the inlet as illustrated in Figures 7.1 and 7.3. This is attributed to the fact that, as the filling evolves the effect of injection pressure on flow front velocity decreases, whilst the role of resin viscosity becomes more dominant as indicated by Eq. (3.3). The longitudinal principal permeability does not affect the covered length of sensors 1, 2 and 4 as the presence of flow channels on the top surface of the C spar geometry (Figure 3.9) accelerates the flow front in the x direction reducing the role of K_1. Figure 7.4 illustrates the covered length evolution with time as a function of K_1 for artificial sensor 4 where the remaining inputs were assigned with the nominal values as reported in Table 7.2. A slightly faster flow front evolution can be observed in sensor 4 when the longitudinal permeability value increases.

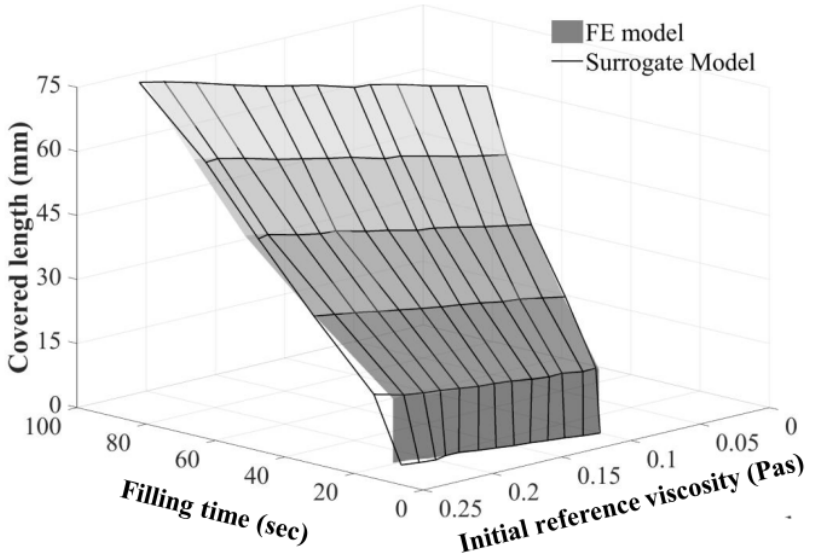

Figure 7.1 Response surfaces of surrogate model sensor 1 response and PAM-RTM model of carbon/epoxy composite C spar.

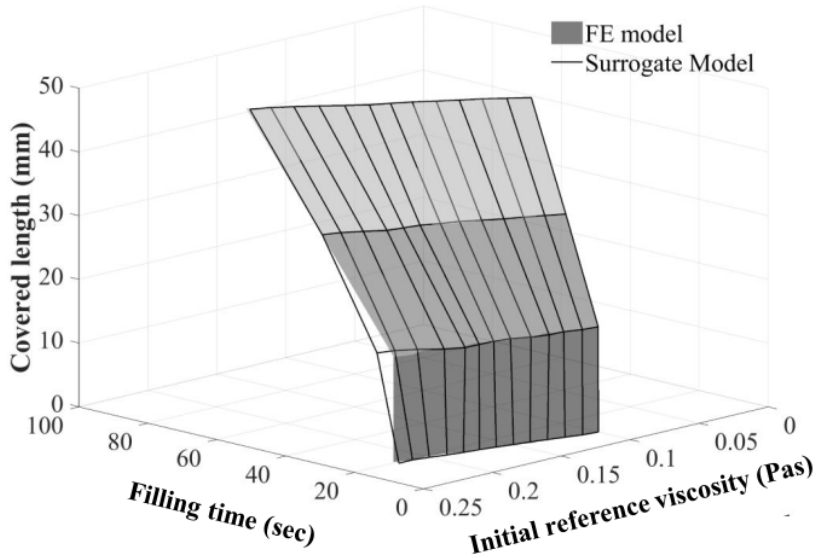

Figure 7.2 Response surfaces of surrogate model sensor 2 response and PAM-RTM model of carbon/epoxy composite C spar.

The discrepancies between the surrogate and PAM-RTM® models are negligible with an average square error equal to 10 mm. The error is more pronounced in the beginning of the flow process for high values of initial viscosity. In a more advanced flow state the error is significantly lower reaching a minimum error value of 0.01%. This can be attributed to the reduced estimation efficiency of the surrogate model in the boundaries of input parameters range, where the initial sampling points in which the surrogate model is based for its prediction are limited. Figure 7.5 depicts the filling duration as a function of initial reference viscosity as computed by the surrogate and the PAM-RTM® models. The rest of the input parameters are kept constant and are reported in Table 7.2. The viscosity affects the flow front position of each sensor as well as the total filling duration significantly. The filling duration increases in a linear manner with the initial reference viscosity with values in the 150-300 s range, whilst the comparison between the models highlight the efficiency of the surrogate model.

Table 7.2 Surrogate models validation cases input parameters.

Parameter	**Surrogate models validation cases**				
	C spar SM_1	C spar SM_2	C spar SM_3	C spar SM_4	C spar SM_5
Longitudinal permeability (m^2)	$1.7\ 10^{-11}$	$1.7\ 10^{-11}$	$1.7\ 10^{-11}$	**$1\text{-}1.9\ 10^{-11}$**	$1.7\ 10^{-11}$
Transverse permeability (m^2)	$1.5\ 10^{-11}$	$1.5\ 10^{-11}$	$1.5\ 10^{-11}$	$1.5\ 10^{-11}$	$1.5\ 10^{-11}$
Initial reference viscosity (Pas)	**0.11-0.22**	**0.11-0.22**	**0.11-0.22**	0.17	**0.11-0.22**

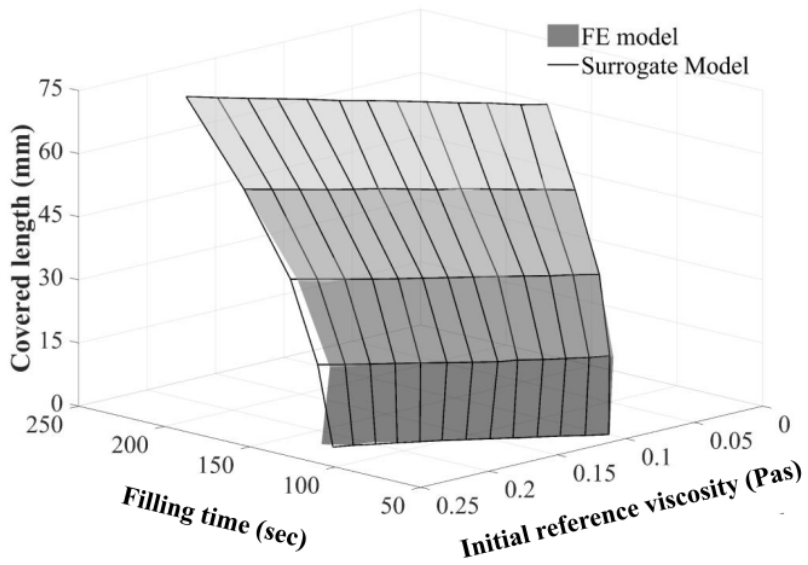

Figure 7.3 Response surfaces of surrogate model sensor 3 response and PAM-RTM model of carbon/epoxy composite C spar.

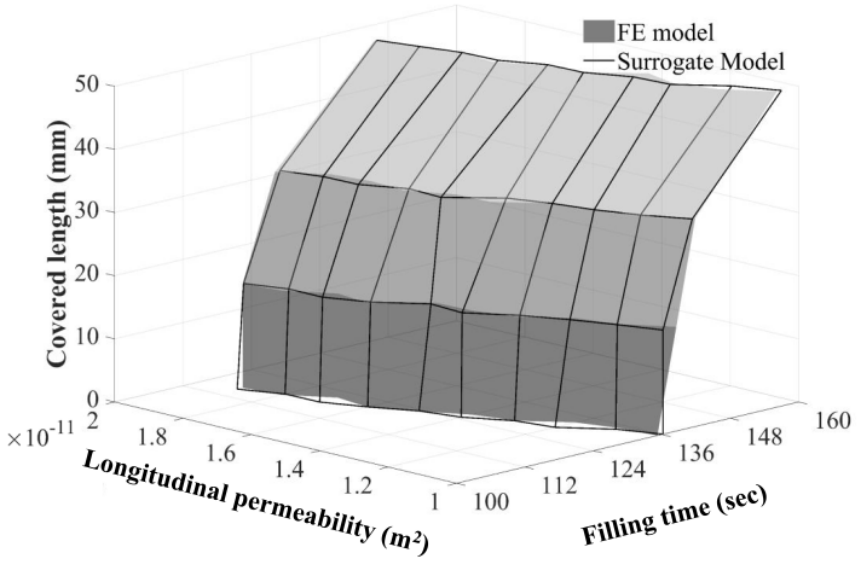

Figure 7.4 Response surfaces of surrogate model sensor 4 response and PAM-RTM model of carbon/epoxy composite C spar.

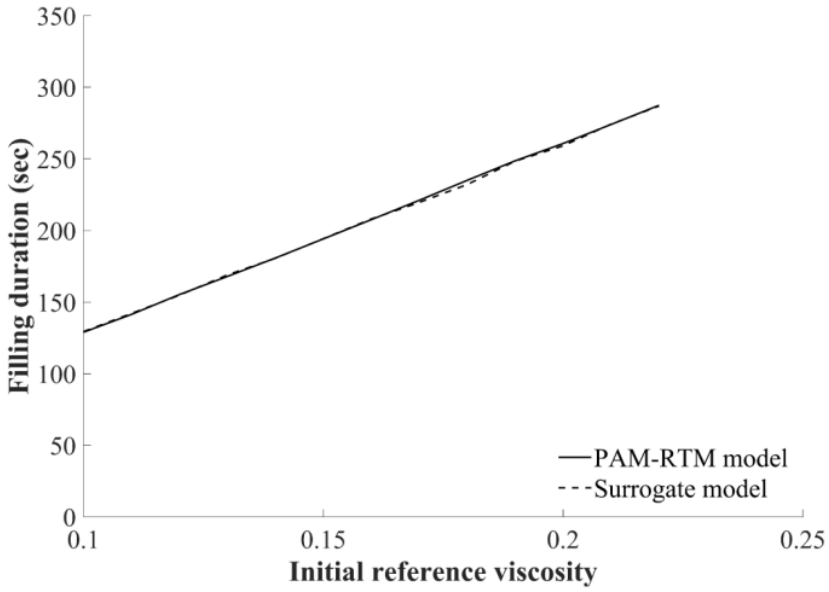

Figure 7.5 Filling duration surrogate model validation against CV/FE model as a function initial reference viscosity of carbon/epoxy composite C spar.

7.3. Real time uncertainty estimation during filling stage of carbon/epoxy composite C spar

7.3.1. Inversion procedure implementation for the filling of carbon/epoxy composite C spar

The inversion procedure described in section 3.8 was applied to the filling stage of the carbon/epoxy composite C spar. The inversion scheme runs in parallel with the filling stage updating the flow monitoring matrix every 30 sec with the four artificial flow monitoring datasets corresponding to the four artificial lineal sensors. The inversion scheme integrates the surrogate models with the flow monitoring data into the MCMC algorithm for the real time probabilistic prediction of unknown parameters and filling duration. The parameters of the MCMC algorithm are reported in Table 7.3. The total number of MCMC iterations was approximately 40,000.

Table 7.3 Inversion scheme parameters values for carbon/epoxy composite C spar.

Parameter	Symbol	Value
Likelihood distribution standard deviation	σ_{exp}	10 mm
Noise level ε_{K_1} standard deviation	$\sigma_{\varepsilon_{K_1}}$	3E-13 m^2
Noise level ε_{K_2} standard deviation	$\sigma_{\varepsilon_{K_2}}$	3E-13 m^2
Noise level ε_{η_0} standard deviation	$\sigma_{\varepsilon_{\eta_0}}$	0.001 Pas
Number of MCMC iterations	M	40,000 iterations
Number of monitoring data	N_k	19
Number of data batches	k_{tot}	6

7.3.2. Artificial flow monitoring results of filling stage of carbon/epoxy composite C spar

The artificial flow monitoring data were generated using the artificial flow sensors integrated in the PAM-RTM® model as described in section 3.5.1.2. The artificial filling process data generated using the PAM-RTM® model of the C spar utilised a set of unknown input parameters η_0, K_1, and K_2 randomly selected from their averages and standard deviations reported in Tables 4.5 and 4.11 respectively. The selected input parameters for the artificial filling are reported in Table 7.4. The artificial results of the filling of the carbon/epoxy C spar are illustrated in Figure 7.6. The duration of the filling stage was 230 s. The resin flow accelerated across the x direction due to the presence of the rectangular flow channel on top surface of C spar. The filling follows an elliptical pattern due to the presence of the rectangular flow channel and to the slight fabric anisotropy. The vacuum ports at the four corners of the C spar assist the resin flow to fill the preform without introducing dry spots.

Table 7.4 Artificial filling process of carbon/epoxy composite C spar input parameters.

Parameter	Value
Longitudinal permeability	1.45 10^{-11} (m^2)
Transverse permeability	1.12 10^{-11} (m^2)
Initial reference viscosity	0.175 (Pas)

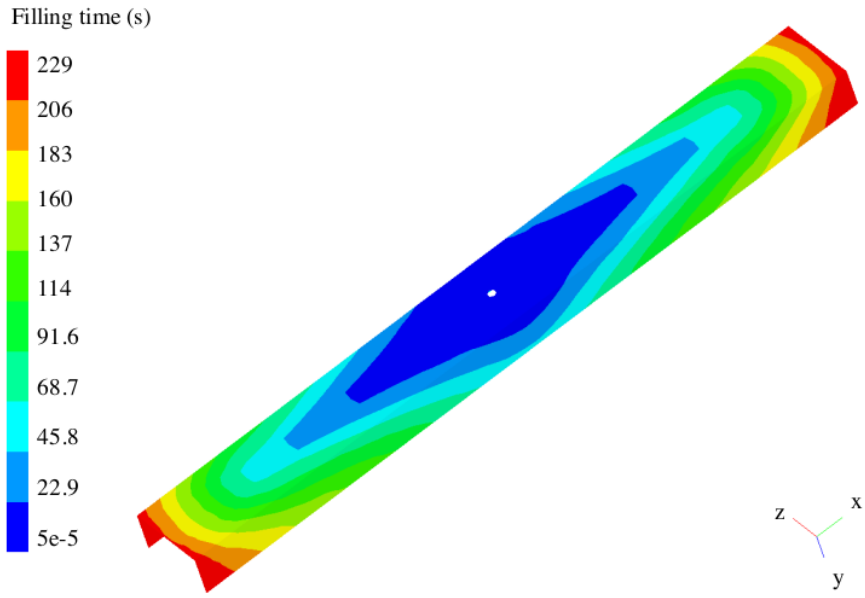

Figure 7.6 Artificial filling results of carbon/epoxy composite C spar.

An artificial noise was applied to the flow monitoring data points of each sensor as depicted in Figures 7.7-7.10 to simulate the effect of potential measurement error of the lineal flow sensors. The applied noise of each artificial data point was randomly selected from normal distributions with average equal to the nominal values and standard deviation equal to the real dielectric sensor error of about 10 mm reported in section 5.3. The first 20 mm of the length of the artificial flow sensors placed on the top surface of the C spar is covered in a short time due to the rectangular flow channel (Figure 3.9) which accelerates the flow in this region. The second slope observed is governed mainly by resin viscosity and transverse permeability. Sensors 1 and 2 are located closer to the inlet port and thus their filling times are lower than those of sensors 3 and 4.

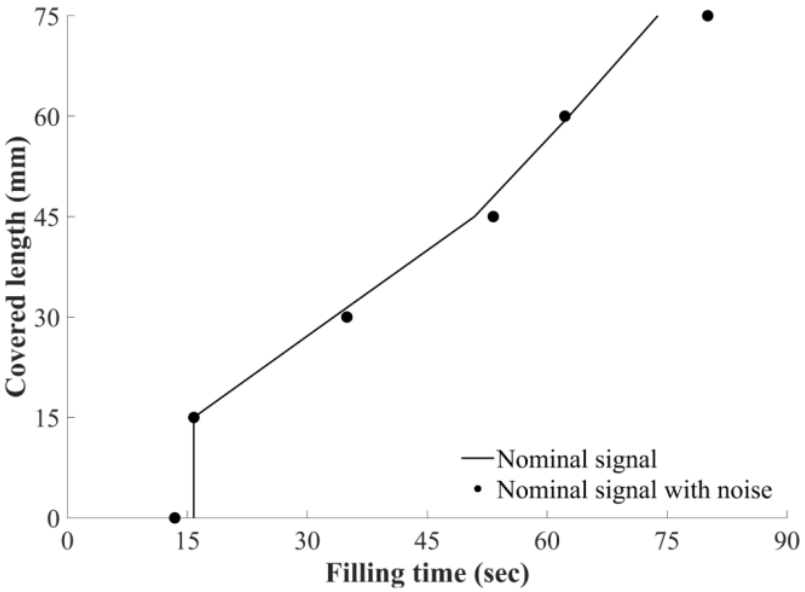

Figure 7.7 Artificial filling monitoring data with and without noise of sensor 1 of carbon/epoxy composite C spar.

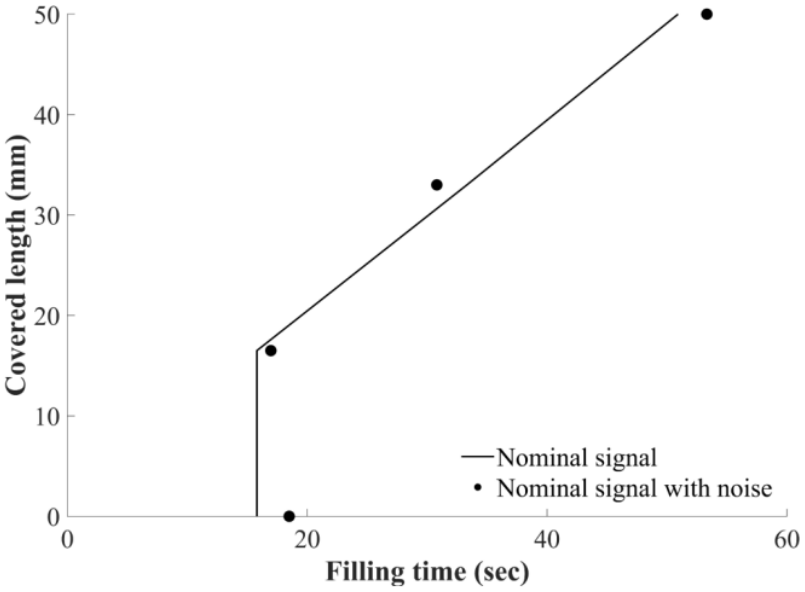

Figure 7.8 Artificial filling monitoring data with and without noise of sensor 2 of carbon/epoxy composite C spar.

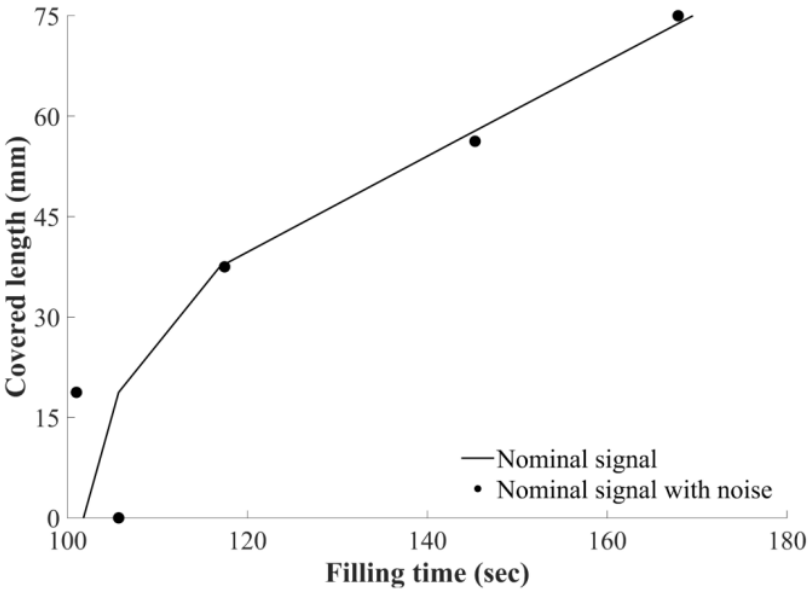

Figure 7.9 Artificial filling monitoring data with and without noise of sensor 3 of carbon/epoxy composite C spar.

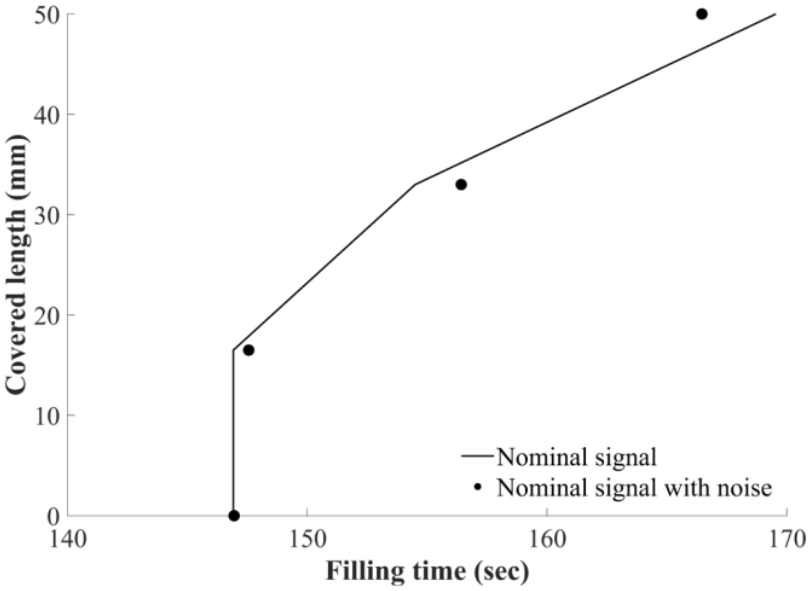

Figure 7.10 Artificial filling monitoring data with and without noise of sensor 4 of carbon/epoxy composite C spar.

7.3.3. Inverse solution results

Figures 7.11-7.14 illustrate the results of the inversion scheme for the real time estimation of the unknown stochastic parameters. The estimated longitudinal permeability reaches a plateau of 1.52 10^{-11} m^2 after about 150 s from the beginning of the filling process as depicted in Figure 7.11. The high variability of K_1, which is aligned to the C spar x direction, during the first 150 s is attributed to the fact that the resin flow speed is governed by the flow channel on the top surface of the C spar rendering the role of K_1 negligible. Sensor 3 is placed across the x direction right after the flow channel. The uncertainty in estimation of the longitudinal principal permeability is narrowed down when the first artificial data of sensor 3 are included in the flow monitoring dataset. The predicted transverse principal permeability illustrated in Figure 7.12 converges faster than K_1 to a value of 1.2 10^{-11} m^2 and the uncertainty in its estimation is narrowed down after 100 s. Sensors 1, 2 and 4 are placed across the y and z direction on the top and on the sides of the C spar respectively. Therefore, the flow monitoring set is updated with data directly related to K_2 allowing fast convergence of its estimate. The initial reference viscosity reaches a plateau of 0.174 Pas after about 40 s (Figure 7.13). This is attributed to the fact that the response of all sensors is sensitive to initial viscosity regardless of their location and orientation. Therefore, the scheme is able to converge to a plateau with few available monitoring data points.

Table 7.4 summarises the statistical properties of the estimated stochastic parameters. The transverse permeability and the initial viscosity present lower variability than K_1 due to the greater sensitivity of the monitoring data set to these variables. The predicted average viscosity is equal to 0.174 Pas which is very close to the input value of artificial filling 0.175 Pas. The longitudinal and transverse permeability present higher error of about 5% and 7% respectively compared to the input parameters of the artificial filling. The error of the inversion scheme predictions is attributed to the introduced noise in the nominal artificial data. The MCMC tries to maximise the posterior distribution considering the conditional probability of monitoring data, and the applied noise leads to deviation of the real solution. The uncertainties in inversion solution estimations can be reduced by increasing the acquisition rate of monitoring data. The increased coefficients of variation of K_1 and K_2 compared to that of initial reference viscosity are also associated with the lower sensitivity of artificial flow sensors to principal permeability values. The sensitivity

is directly related to the placement and the orientation of flow sensors. The strategic position of flow sensors contributes to the reduction of the overall number minimising the complexity of flow monitoring system [156].

The estimation of the filling duration of the filling of the composite C spar is illustrated in Figure 7.14. In the first 30 s the uncertainty in filling duration estimation is relatively high due to the limited flow monitoring data in that period. The inversion scheme yields a low uncertainty estimation after about 100 s with an average equal to 226 s and a standard deviation of 13 s. The predicted filling duration is in very good agreement with the actual filling duration with an absolute error of about 4 s or below 2%. The time frame within which the inversion scheme is capable of providing an accurate prediction with low uncertainty corresponds to 45% of the total filling stage. It should be noted that this is in a short filling time moulding, which corresponds to the most challenging conditions for the numerical scheme developed in this work. The early low uncertainty estimation provided by the inversion scheme allows potential control actions in order to avoid potential defects or to reduce the duration of the process.

Figure 7.15 illustrates the cumulative probability of filling duration with and without the estimation provided by the inversion scheme. The coefficient of variation of the estimated filling duration without inversion is about 25%, whilst after about 100 sec the uncertainty is reduced by 80% to a coefficient of variation of 5%.

Table 7.5 Statistical properties of estimated parameters of filling of carbon/epoxy composite C spar.

Parameter	Average	Standard deviation
K_1 (m^2)	$1.52\ 10^{-11}$	$1.96\ 10^{-12}$
K_2 (m^2)	$1.2\ 10^{-11}$	$1.28\ 10^{-12}$
η_0 (Pas)	0.174	0.009

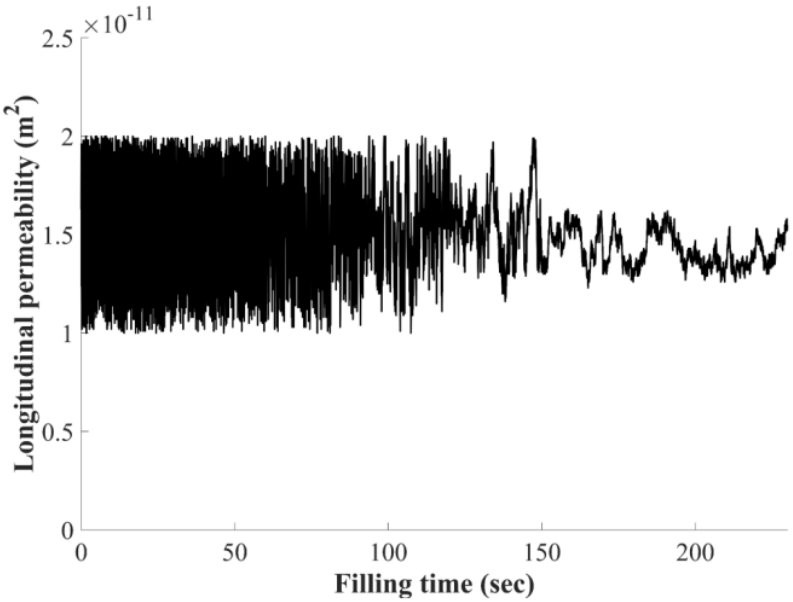

Figure 7.11 Unknown stochastic parameters estimation: longitudinal permeability of the filling of carbon/epoxy composite C spar.

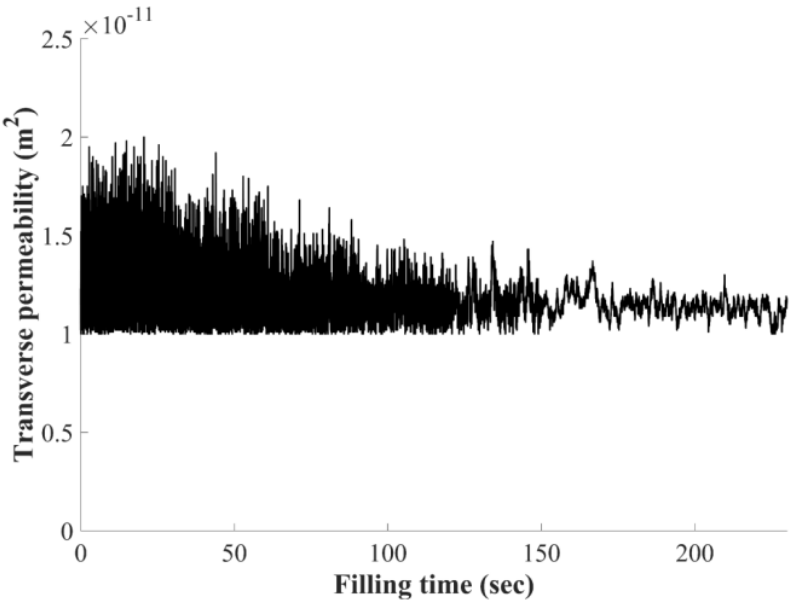

Figure 7.12 Unknown stochastic parameters estimation: transverse permeability of the filling of carbon/epoxy composite C spar.

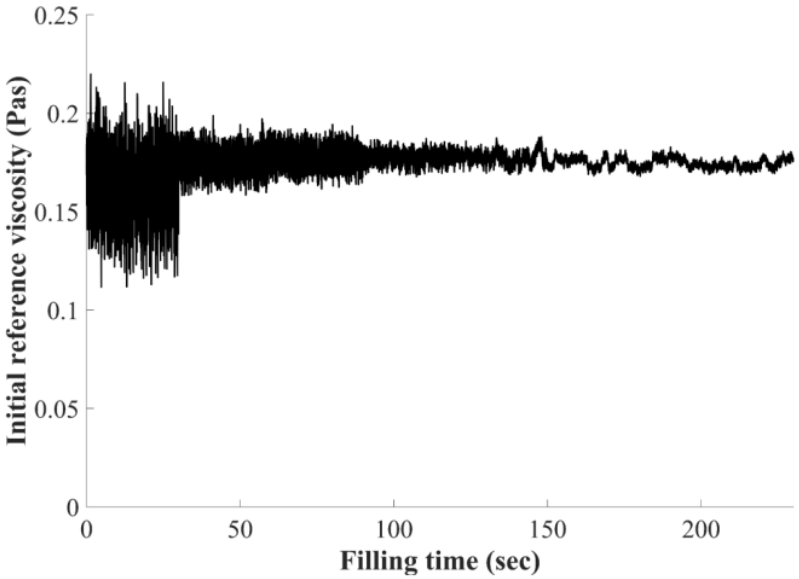

Figure 7.13 Unknown stochastic parameters estimation: initial reference viscosity of the filling of carbon/epoxy composite C spar.

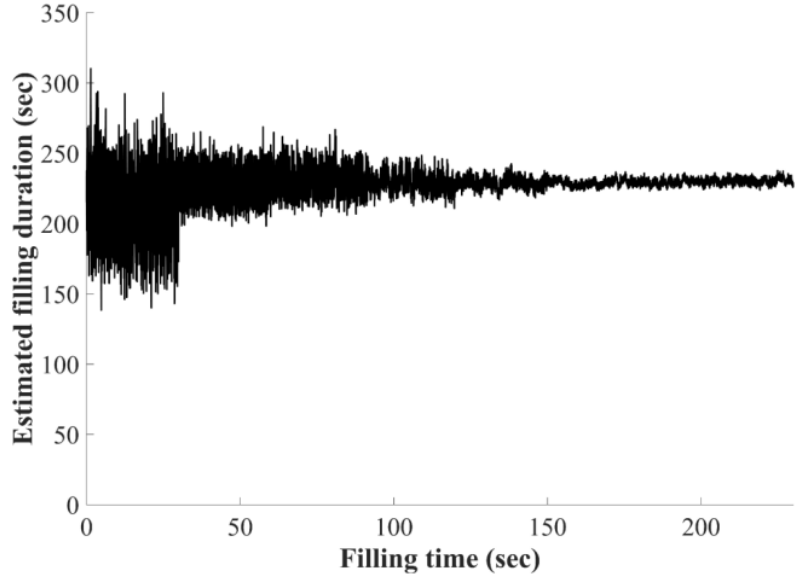

Figure 7.14 Unknown stochastic parameters estimation: filling duration estimation of carbon/epoxy composite C spar.

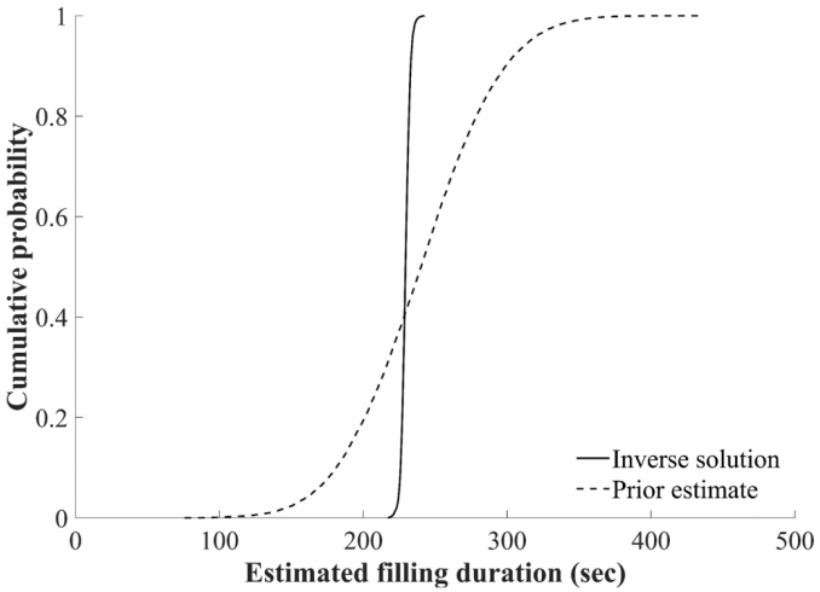

Figure 7.15 Cumulative density function evolution of estimated filling duration.

Figures 7.16a, 7.17a, 7.18a, and 7.19a illustrate the 95% confidence intervals of the four flow sensor responses calculated considering the initial variability of the input stochastic parameters. Figures 7.16b, 7.17b, 7.18b, and 7.19b illustrate the 95% confidence intervals of the four flow sensor responses calculated considering the inverse solution. The reduction of the width of the confidence intervals indicates the efficiency of the inversion scheme in providing accurate estimations of the unknown parameters with low uncertainty. The confidence intervals include the artificial flow monitoring data. The resulting spread is attributed mainly to the noise of artificial data. The confidence intervals of sensors 1-3 as estimated by the inversion are narrower than that of sensor 4. This is attributed to the fact that sensors 1-3 are more sensitive to transverse permeability and initial reference viscosity rather than to longitudinal permeability due to their placement. This results in lower uncertainty in estimation as the coefficient of variation of K_2 and η_0 is lower than that of K_1. The influence of longitudinal permeability is more pronounced in the response of sensor 4. Consequently, the uncertainty in the estimation of K_1 results in wider confidence intervals for sensor 4.

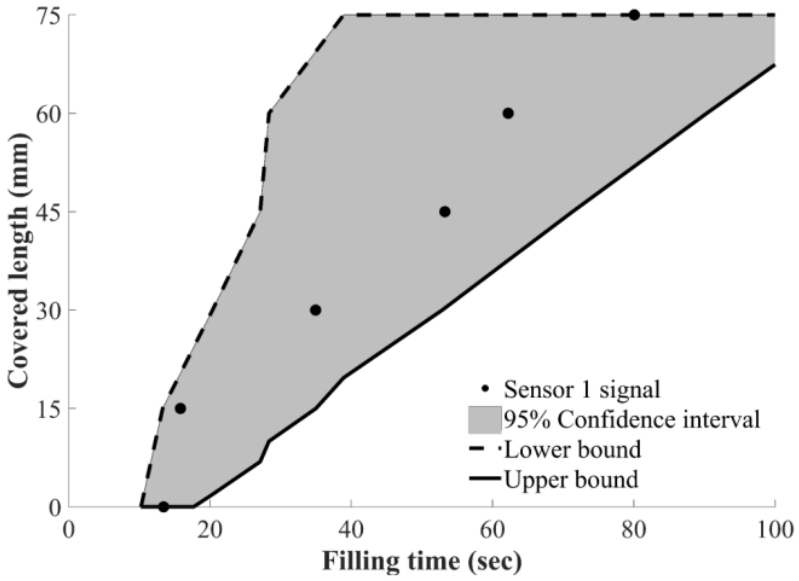

a)

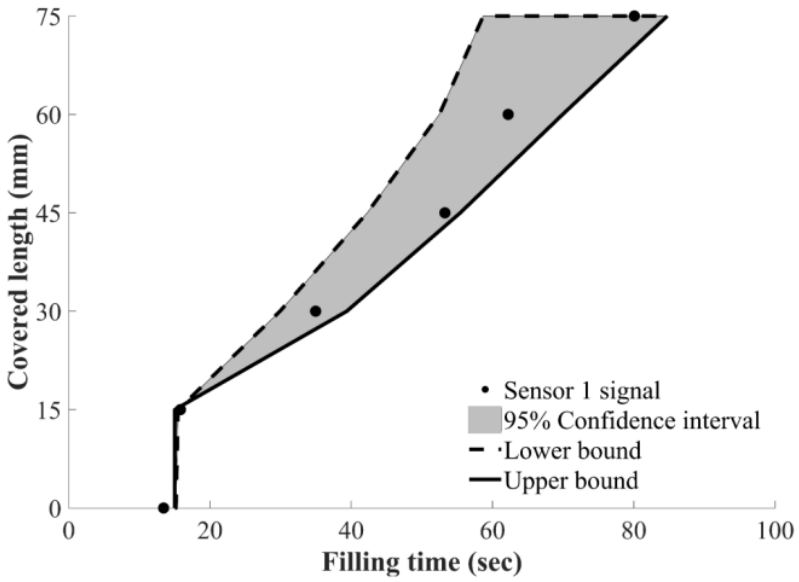

b)

Figure 7.16 Estimation uncertainty of covered length of a) sensor 1 before the filling; b) sensor 1 after 100 sec of carbon/epoxy composite C spar.

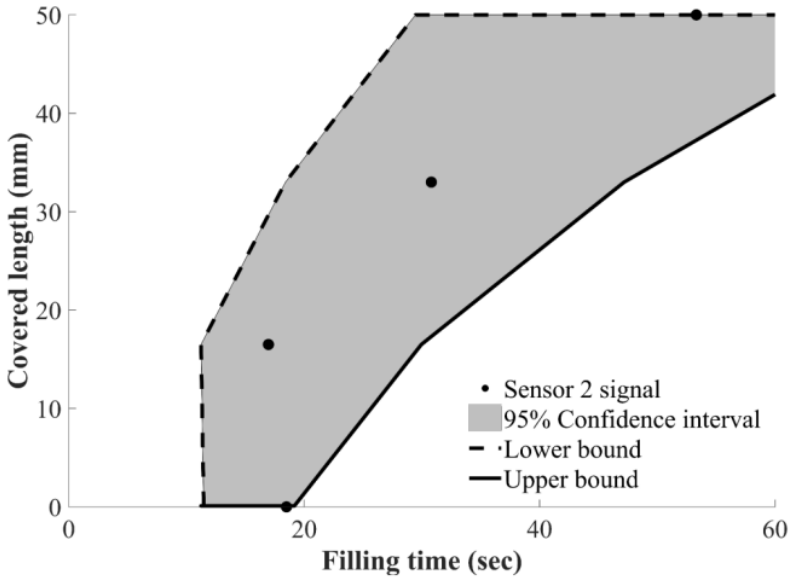

a)

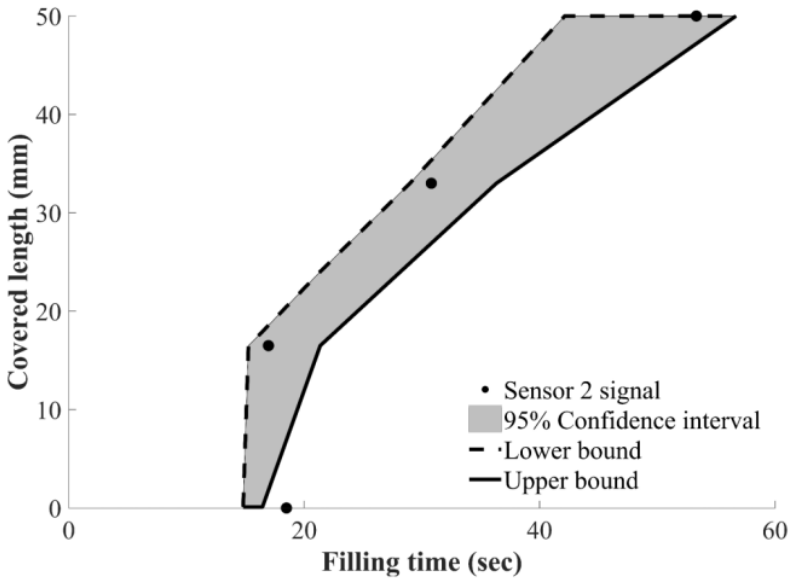

b)

Figure 7.17 Estimation uncertainty of covered length of a) sensor 2 before the filling; b) sensor 2 after 100 sec of filling of carbon/epoxy composite C spar.

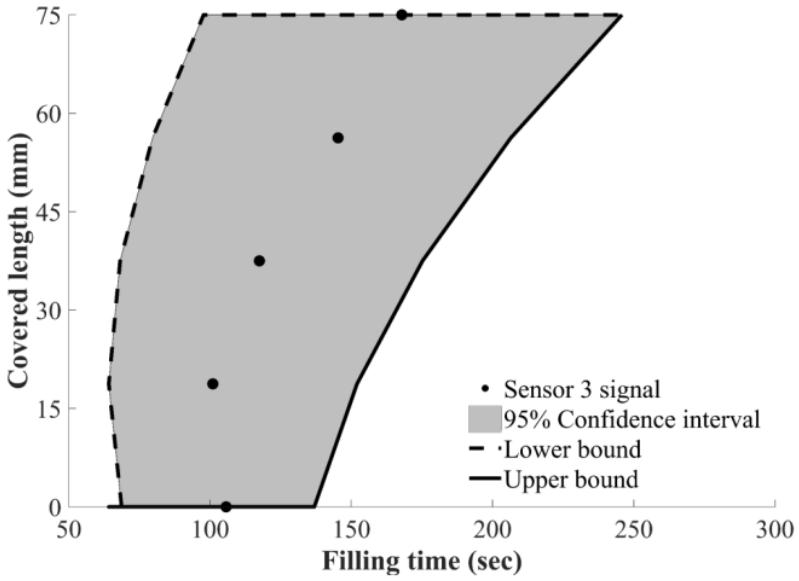

a)

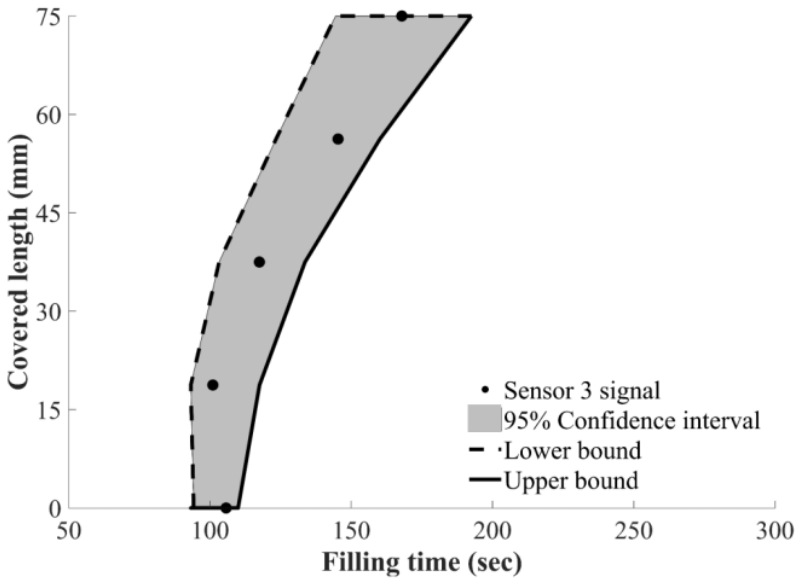

b)

Figure 7.18 Estimation uncertainty of covered length of a) sensor 3 before the filling; b) sensor 3 after 100 sec of filling of carbon/epoxy composite C spar.

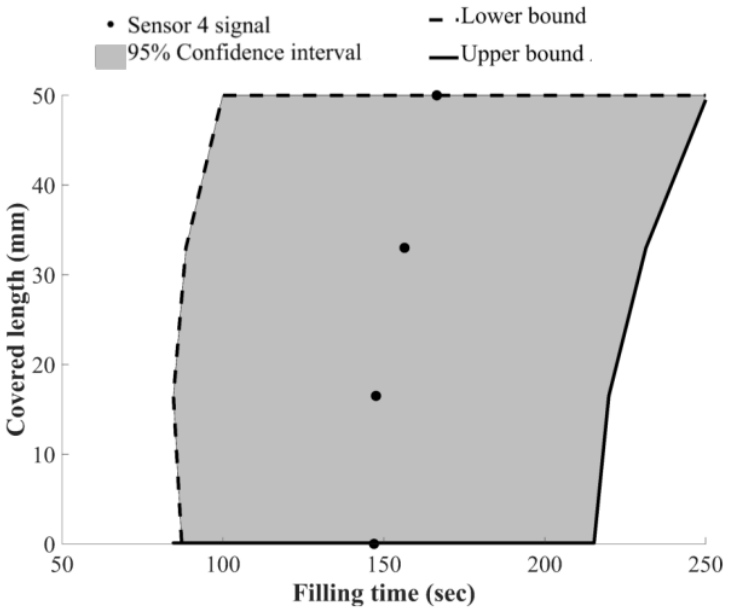

a)

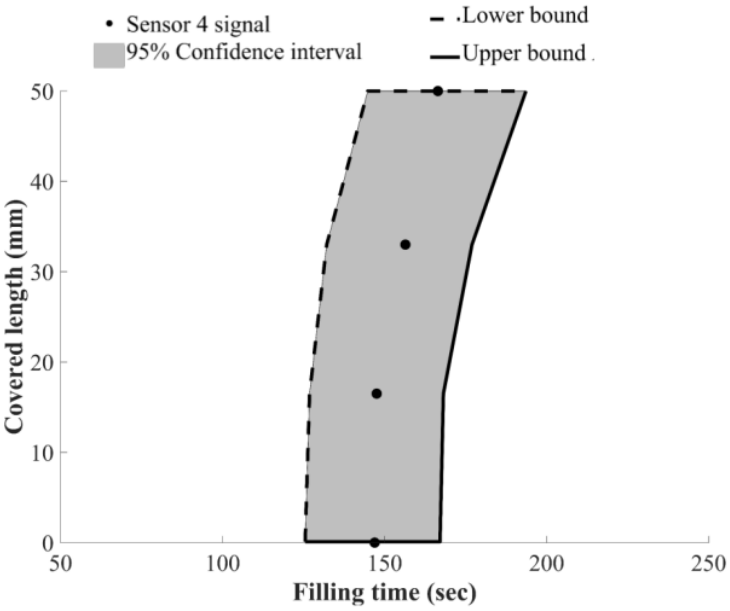

b)

Figure 7.19 Estimation uncertainty of covered length of a) sensor 4 before the filling; b) sensor 4 after 100 sec of filling of carbon/epoxy composite C spar.

Figures 7.20a and b illustrate the flow front positions at 20 s, 70 s and 120 s as estimated by the PAM-RTM® flow model using prior information for the lower and upper bounds of the 95% confidence intervals respectively. The filling pattern is qualitatively the same in these six cases. The filling times present significant differences due to the initial uncertainty of the problem. The 95% confidence interval of the filling duration is estimated from 120 s to 350 s which is considerably wide. The efficiency of the inversion scheme in narrowing down the uncertainty prediction is illustrated in Figures 7.21a and b. The 95% confidence interval of filling patterns at 20 s, 100 s, and 200 s as predicted using the inverse solution is relatively narrow, whilst the estimated filling duration of the lower and upper bound is between 200 s and 270 s, which is considerably lower compared to the prior estimate.

The inversion scheme results highlight that the utilisation of four lineal flow sensors in the C spar manufacture can yield low uncertainty estimates of unknown parameters and of the duration of the filling stage. Sensor placement and orientation plays a crucial role on how fast the simulation tool can reach a low uncertainty estimation. In this case, the placement of the four sensors results in a relative fast convergence of transverse permeability and initial viscosity in contrast to longitudinal which reaches a low uncertainty plateau at about 50% of the total duration of the filling process. The sensitivity of sensor response to unknown parameters needs to be taken into account in order to minimise the number of sensors and consequently the intrusiveness of the monitoring system. Maximising the sensitivity of the monitoring system can lead to early low uncertainty prediction and thus to potential control actions to prevent undesirable phenomena which will affect final part quality.

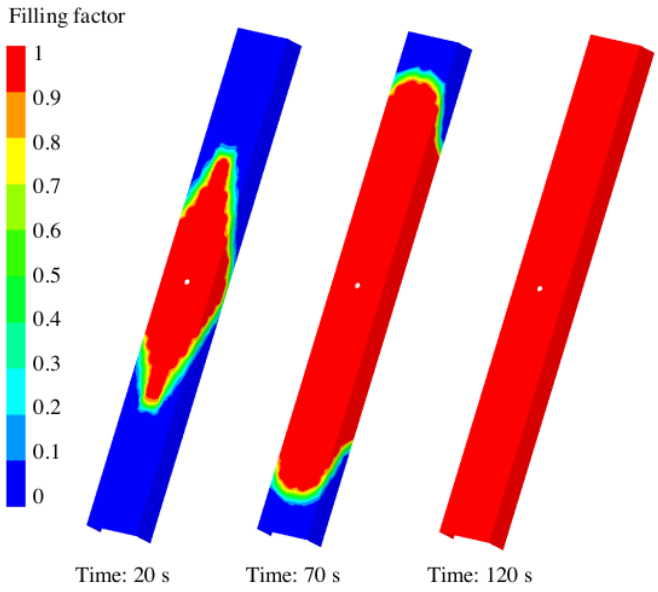

a)

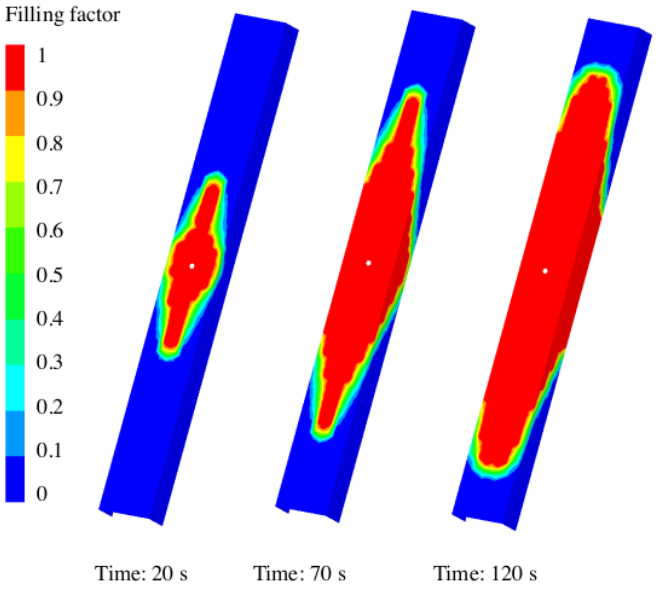

b)

Figure 7.20 Prior estimation of flow patterns of carbon/epoxy composite C spar: a) lower bound of 95% confidence intervals and; b) upper bound of 95% confidence intervals.

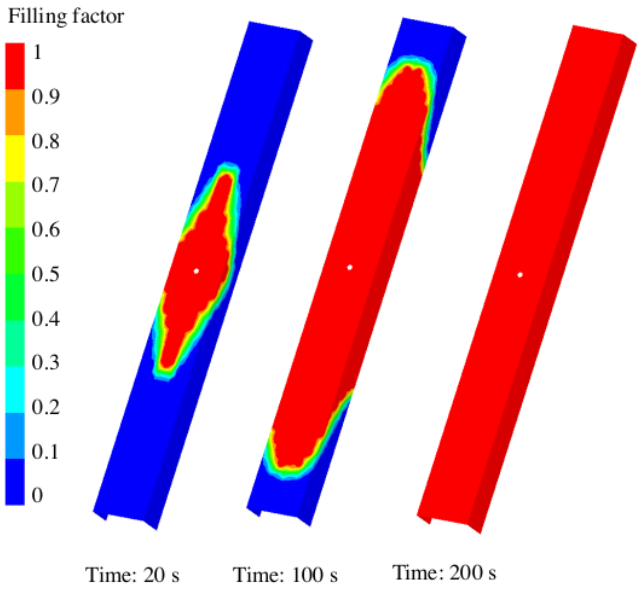

a)

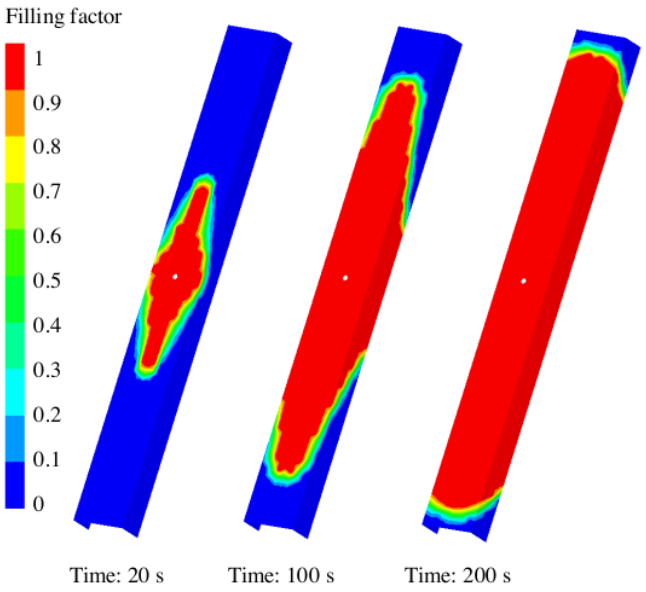

b)

Figure 7.21 Inverse solution of flow patterns of carbon/epoxy composite C spar: a) lower bound of 95% confidence intervals and; b) upper bound of 95% confidence intervals.

7.4. Overview

The inversion procedure was implemented in the RTM filling of a carbon/epoxy composite C spar using artificial flow monitoring data. The results highlight the efficiently of the inversion scheme to operate in different flow conditions either the filling is sort –below 5 min – or slow over 30 min as presented in chapter 6. The decision of the number of lineal flow sensors and their placement and orientation in the part plays a significant role since it affects the uncertainty of predictions. The solution provided by the inversion scheme presents errors up to 7% in predictions of unknown input parameters highlighting the influence of the applied noise to nominal artificial flow monitoring data. The inversion scheme is implemented in the case of cure heat transfer process of carbon/epoxy composite flat panel in the next chapter in order to evaluate its performance in a heat transfer problem which constitutes potentially an ill-posed problem with more complex and non-linear phenomena.

8. Inversion procedure development in the RTM curing of a glass/epoxy composite flat panel.

8.1. Introduction

The low uncertainty prediction capabilities of the inversion scheme have been investigated in two case studies of filling stage presented in chapters 6 and 7. In the case of the curing stage, the presence of resin thermal properties and boundary conditions variations, described in chapter 4, introduces significant variability in cure duration and exothermic effects reaching a coefficient of variation of 20% [38] and 30% [37] respectively. The inversion scheme developed in this work is applied in the RTM curing of a glass/epoxy composite flat plate (GFP), specified in section 3.5.2.1, to investigate its performance in a nonlinear heat transfer problem with potential ill-posedness. The inversion scheme integrates cure monitoring data with the cure model into the MCMC algorithm for the real time probabilistic estimation of unknown thermal property, boundary conditions and cure process outcomes.

8.2. Validation of surrogate models corresponding to inversion procedure cure process implementation.

The inversion procedure based on MCMC and described in section 3.8 requires thousands of cure model evaluations increasing significantly the computational time if an FE cure model is utilised. Surrogate cure models have been developed to reduce computational time allowing implementation of the inversion procedure in real time. Three surrogate models (GFP SM_1 - GFP SM_3) were constructed based on the implementation of Kriging as detailed in section 3.6. Figure 8.1 illustrates the surrogate model implementation for the cure process. The construction of the surrogate model requires a set of design points and their response as inputs. Latin Hypercube Sampling (LHS) was used for generating a sample of N input points, whilst the FE cure model was used to compute the response at these points. The FE cure model created in MSC.Marc simulates the RTM curing of the GFP composite part. More details regarding the cure model can be found in section 3.5.2.1. The input variables of the GFP SM_1 and GFP SM_2 surrogate models include the unknown stochastic parameters k and h of the cure process as described in chapter 4 and the cure time (t), whilst the outputs are the temperatures measured by the corresponding sensors. These are the temperature at mid-thickness (T_{mid}) and on the top surface (T_{top})

of the curing composite component. The third surrogate model (GFP SM_3) computes the minimum final degree of cure (α_{fmin}) as a function of the unknown stochastic variables k and h. The final minimum degree of cure is defined as the minimum degree of cure over the volume of the part at the end of the process. Its practical significance is related to the glass transition temperature reached at the end of the process, which governs the softening temperature of the composite material beyond which the component cannot play a structural role. Table 8.1 summarises the parameters of the surrogate cure models used in the inversion scheme implementation and their ranges. Considering the relative small dimensionality of the problem an initial sample of 2,000 points was selected.

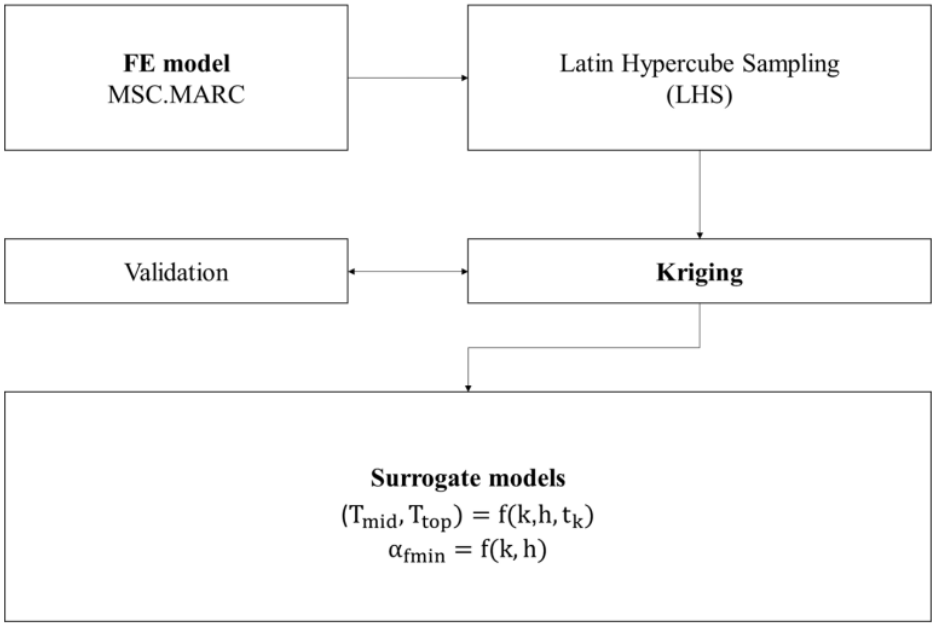

Figure 8.1 Surrogate models methodology.

Response surfaces, expressing the relationship between models outputs and inputs, were constructed to compare the surrogate model with the FE model results. Figures 8.2 and 8.3 illustrate the dependence of GFP SM_1 and GFP SM_2 outputs (T_{mid}, T_{top}) on inputs (k and h) at 60 min in the cure process. It can be observed that the heat transfer coefficient causes greater changes in T_{mid} and T_{top} than the thermal conductivity level. This is attributed to the fact that the response surface corresponds to a time at which the tool temperature has reached a plateau and the influence of the thermal conductivity has been reduced. The temperature at the top of the part is more sensitive to parameter changes

than the temperature at mid-thickness. The temperature decreases when the surface heat transfer coefficient increases and the thermal conductivity level decreases. Figure 8.3 illustrates the relationship of minimum final degree of cure with the underlying parameters of the surrogate model. The minimum final conversion decreases with increasing surface heat transfer coefficient and decreasing thermal conductivity level. A pronounced steep decrease of the final degree of cure occurs when the thermal conductivity level is in the range between 0.01-0.05 W/m/°C. In this area, the minimum final conversion reaches values as low as 0.7.

The three surrogate models are in very close agreement with the FE model with the average absolute difference being equal to 0.2°C for GFP SM_1 and GFP SM_2 and 3×10^{-6} for GFP SM_3. The surrogate model execution time is approximately 4 ms on the 4 cores @3.2 GHz computer used, whilst the FE model takes 30 sec to solve the cure problem. This difference in execution times, which is about 4 orders of magnitude, highlights the efficiency of the surrogate model on estimating cure models outputs within the input domain, whilst the very short computation required for the surrogate model allows its utilisation in real time computational processing.

Table 8.1 Surrogate models parameters and their ranges

Parameter	Symbol	Range
Thermal conductivity level	k ($Wm^{-1}°C^{-1}$)	0.01-0.2
Heat transfer coefficient	h ($Wm^{-2}°C^{-1}$)	3-21
Cure time	t (min)	0-110

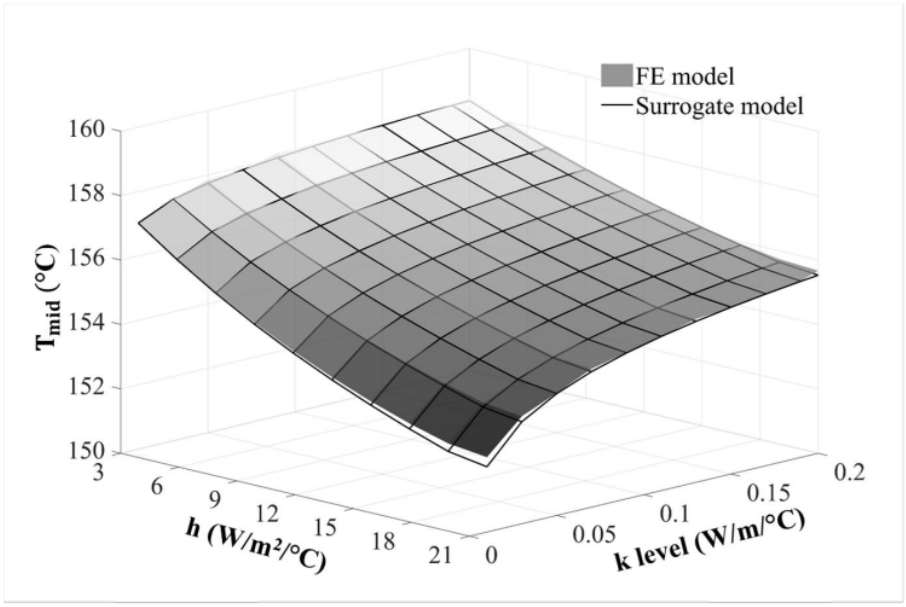

Figure 8.2 GFP SM_1 validation case: response surface of temperature at mid thickness as a function of the heat transfer coefficient and the thermal conductivity level at 60 min during the cure of a 3.3 mm thick glass/epoxy panel (GFP).

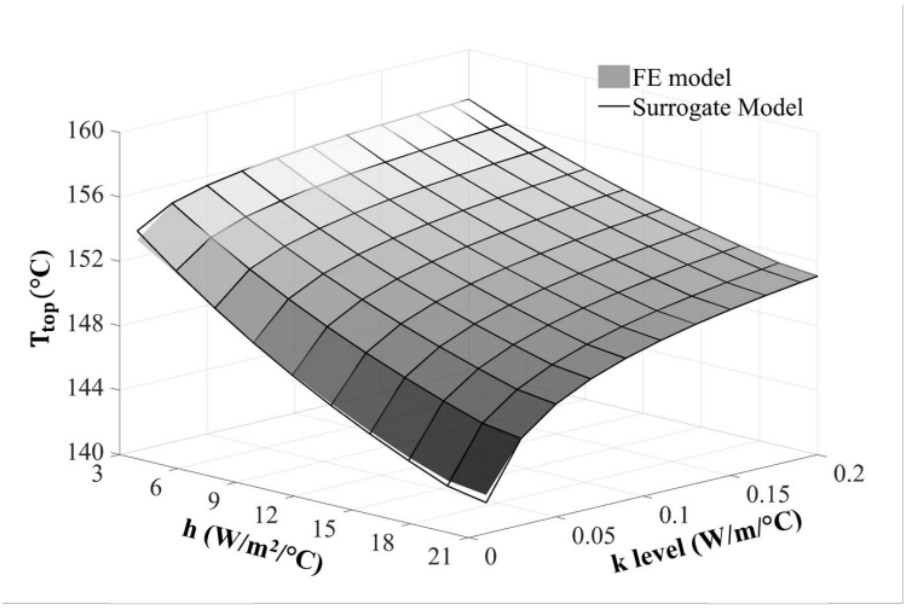

Figure 8.3 GFP SM_2 validation case: response surface of temperature on the top as a function of the heat transfer coefficient and the thermal conductivity level at 60 min during the cure of a 3.3 mm thick glass/epoxy panel (GFP).

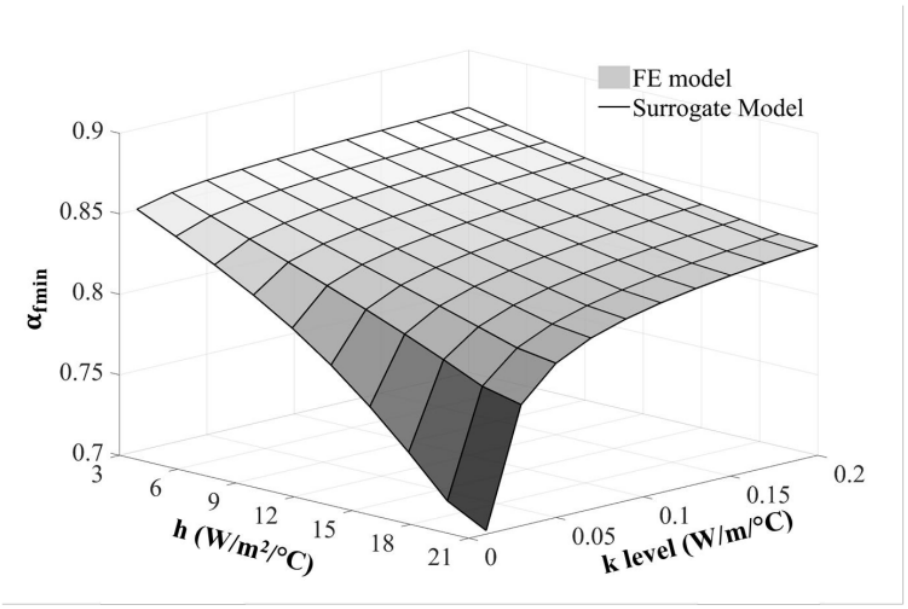

Figure 8.4 GFP SM_3 validation case: response surface of minimum final degree of cure as a function of the heat transfer coefficient and the thermal conductivity level during the cure of a 3.3 mm thick glass/epoxy panel (GFP).

8.3. Real time uncertainty estimation of during the cure stage.

8.3.1. Inversion procedure implementation

The inversion procedure integrates cure monitoring data with surrogate cure modelling for the on line probabilistic estimation of the unknown thermal properties and boundary conditions and the corresponding process outcomes such as the minimum final degree of cure. The inverse algorithm framework is illustrated in Figure 8.5. The setup includes an RTM moulding of an glass/epoxy composite flat panel (GFP) in which three K-type thermocouples are placed on the bottom, at the mid-thickens and on the top of the part measuring the temperature evolution with time. More details on the process implementation and the corresponding datasets can be found in [125]. The inverse analysis starts when the first cure monitoring data arrive and uses this information to predict k and h and consequently the minimum final degree of cure in real time. The MCMC is executed, while the monitoring matrix $\mathbf{Y_{exp}}(t) = [\,\mathbf{T_{mid}}\ \mathbf{T_{top}}\,] \in \mathbb{R}^{\mathbf{N_k}\times 2}$ is updated with new data every minute, which in this case is a matrix representing the temperatures at mid-thickness and on the top surface of the composite part at the time t_k.

The standard deviation σ_{exp} used in the likelihood term in Eq. (3.21) represents the accuracy level of experimental data and is assigned a small value taking into account the low noise levels of thermocouple signals. In the case of K-type thermocouples the error can reach up to 2 °C [144]. The standard deviation vector of the Gaussian variable $\boldsymbol{\sigma_\varepsilon} = [\sigma_{\varepsilon_k}, \sigma_{\varepsilon_h}], \boldsymbol{\sigma_\varepsilon} \in \mathbb{R}^2$, presented in Table 3.4, was adjusted by performing a short sequence of MCMC iterations every minute after acquisition of the new data in order to achieve the desirable acceptance probability in the range of 30-50%. The initial noise ($\boldsymbol{\varepsilon}$) standard deviation ($\boldsymbol{\sigma_\varepsilon}$) was set equal to the standard deviation of the prior distributions of k and h. The MCMC parameter values for the inverse glass/epoxy cure solution reported in Table 8.2.

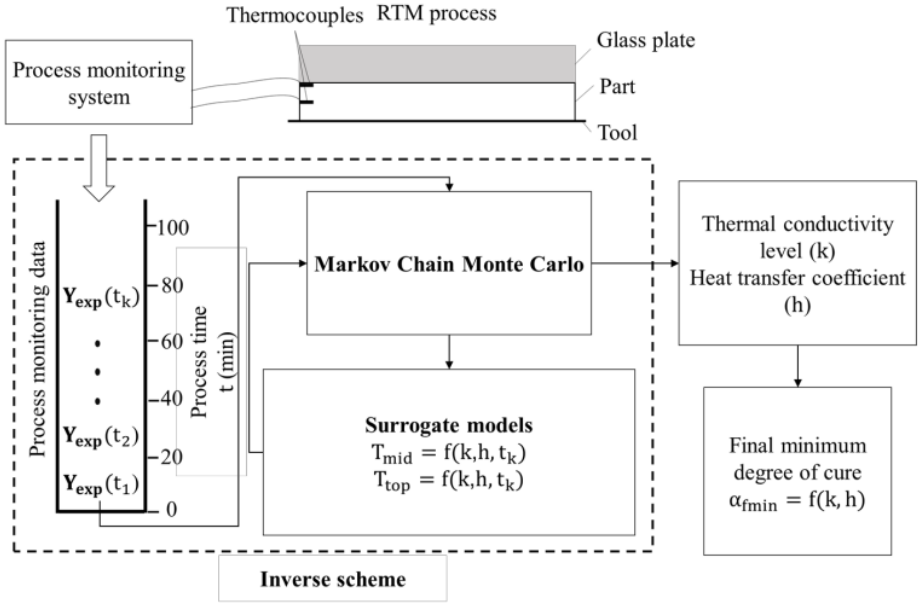

Figure 8.5 Real time uncertainty estimation framework.

The number of MCMC iterations in real time depends on the execution time of a single iteration. The execution time increases with increasing experimental data. In the beginning of the process the rate of MCMC iterations was about 20,000 per minute for the computer used, whilst towards the end of the process the rate decreased to about 500

iterations per minute. The total MCMC iterations of the inversion procedure were approximately 210,000. Table 8.2 reports the inverse algorithm parameters values.

Table 8.2 MCMC parameters values for the inverse glass/epoxy flat panel (GFP) cure solution.

Parameter		Value
Likelihood distribution standard deviation	σ_{exp}	1 (°C)
Thermal conductivity prior mean value	μ^{k}_{prior}	0.12 ($Wm^{-1}°C^{-1}$)
Heat transfer coefficient prior mean value	μ^{h}_{prior}	8.5 ($Wm^{-2}°C^{-1}$)
Thermal conductivity level prior standard deviation	σ^{k}_{prior}	0.02 ($Wm^{-1}°C^{-1}$)
Heat transfer coefficient prior mean value	σ^{h}_{prior}	1.5 ($Wm^{-2}°C^{-1}$)
Initial noise (ε_k) standard deviation	σ_{ε_k}	0.02 ($Wm^{-1}°C^{-1}$))
Initial noise (ε_h) standard deviation	σ_{ε_h}	1.5 ($Wm^{-2}°C^{-1}$)
Initial thermal conductivity level	k_0	0.12 ($Wm^{-1}°C^{-1}$))
Initial heat transfer coefficient	h_0	8.5 ($Wm^{-2}°C^{-1}$)
Total number of MCMC iterations	M	210,000
Total number of experimental data	N_k	220
Total number of data batches	k_{tot}	110

8.3.2. Results obtained by the inverse glass/epoxy cure solution

Figure 8.6 illustrates the process monitoring results obtained during the cure of the glass/epoxy composite flat panel [125]; the temperature evolution with cure time at the lower surface, at mid-thickness and on the top of the curing composite. It can be observed that the temperature is lower away from the heated tool surface reaching a plateau after 60 min from the beginning of the cure process. Temperature overshoots due to the exothermic nature of the resin reaction are not detected due to the small thickness of the composite part. The measurement noise is small observed at 18-22 min and 8-10 min in the temperature of the lower surface and mid-thickness respectively.

Figure 8.7 illustrates the evolution of thermal conductivity level, surface heat transfer coefficient and minimum final conversion of the cold chain during the process. The thermal conductivity level converges faster than the surface heat transfer coefficient reaching a plateau after 20 min in the cure. This can be attributed to the fact that in the first 20 min the tool temperature increases, and transient phenomena governed by thermal

conductivity dominate the evolution of the thermal field. The surface heat transfer coefficient and minimum final degree of cure converge after 70 min as depicted in Figures 8.8 and 8.9, showing a step decrease/increase pattern as a result of the periodic updating of monitoring data. At about 70 min the top surface temperature reaches a plateau of 155 °C and the thermal response becomes more sensitive to the surface heat transfer coefficient.

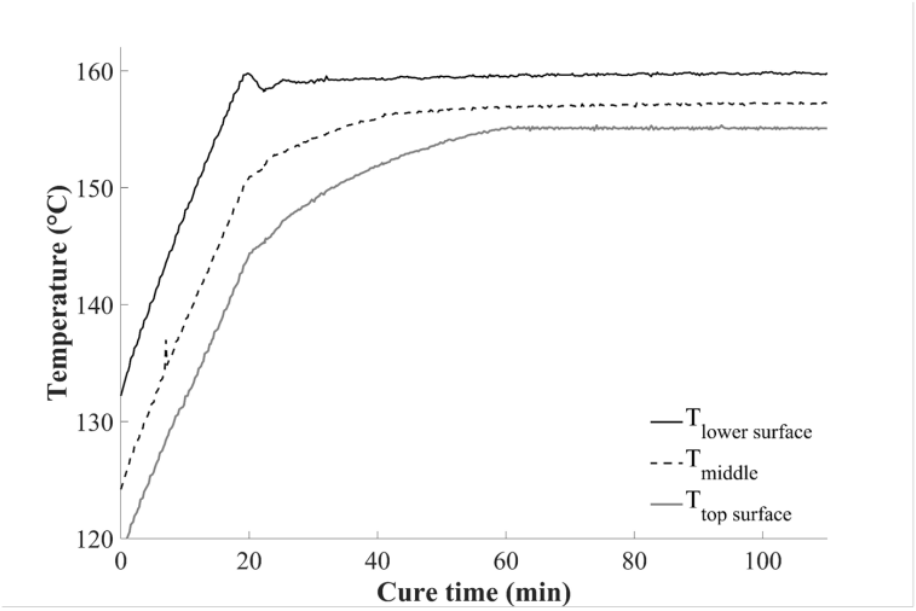

Figure 8.6 Temperature evolution with time at the bottom, mid-thickness and top surface of glass/epoxy composite flat panel (GFP) [125].

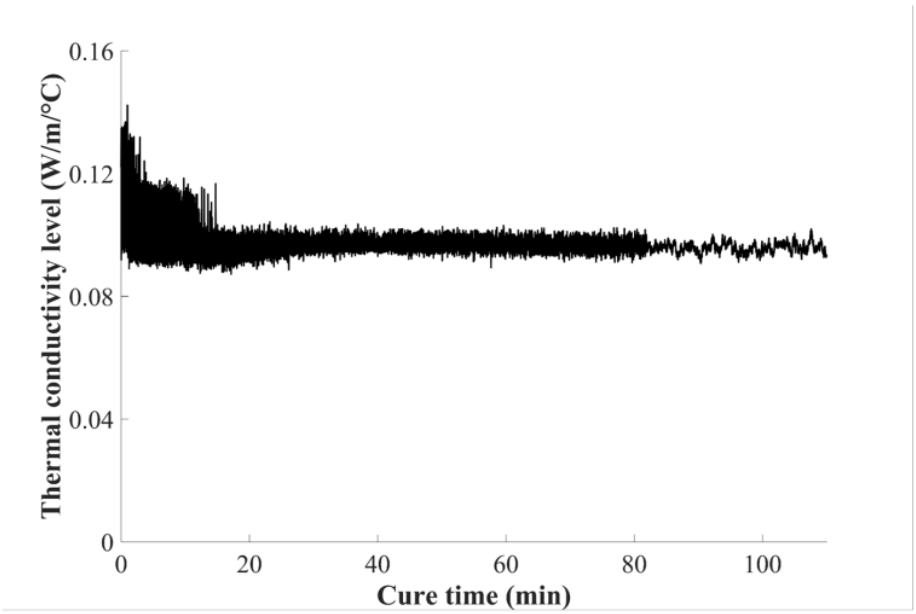

Figure 8.7 Real time evolution of thermal conductivity level during the cure of glass/epoxy composite flat panel (GFP).

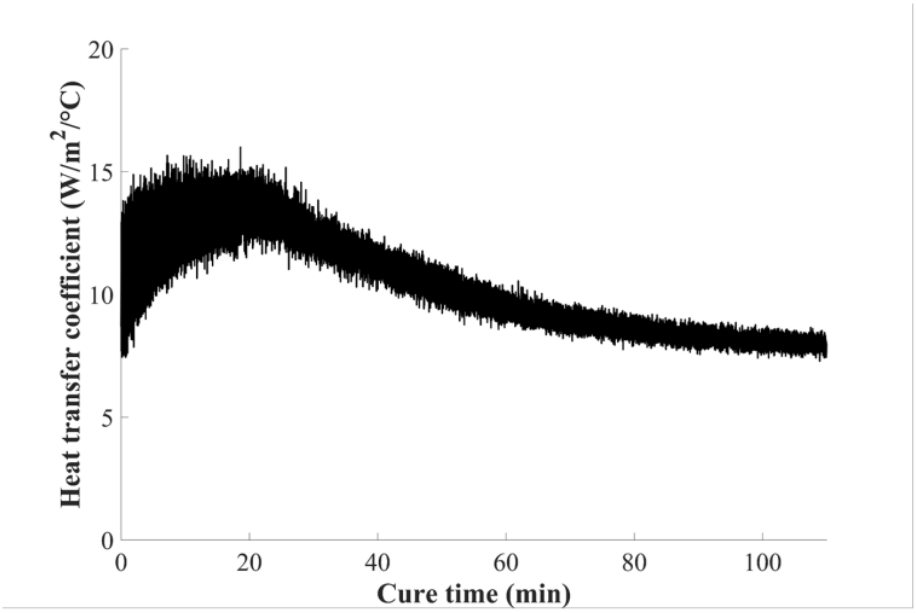

Figure 8.8 Real time evolution of surface heat transfer coefficient during the cure of glass/epoxy composite flat panel (GFP).

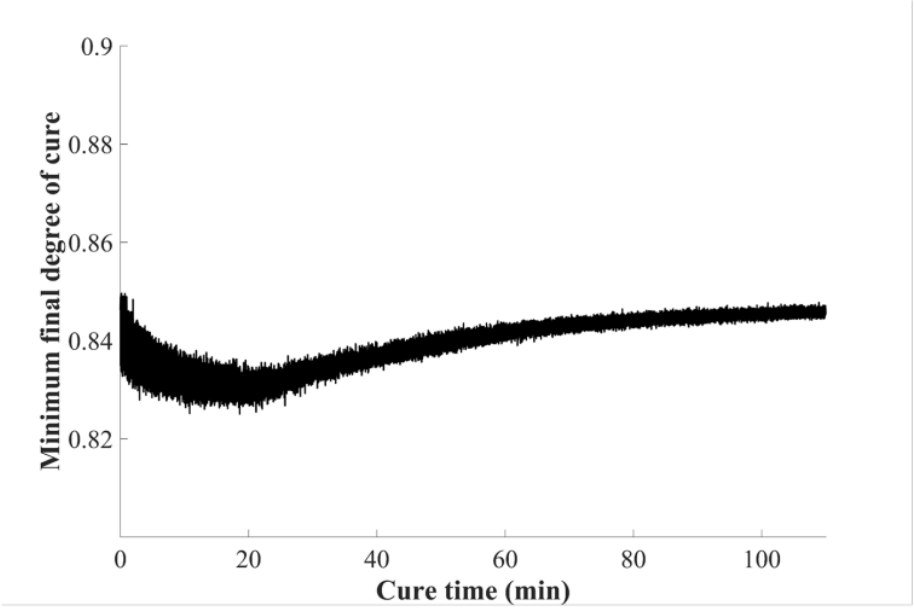

Figure 8.9 Real time evolution of minimum final degree of cure of glass/epoxy composite flat panel (GFP).

The sample after convergence can be used to calculate the statistical properties of variables of interest. The values within the stationary sequence are highly correlated due to the nature of the MH algorithm. Consequently, a step size calculated considering the autocorrelation structures of the initial sampling of the k, h and α_{fmin} was used for thinning the sample. Figure 8.10a shows the autocorrelation structure of the thermal conductivity level. The autocorrelation reaches a relatively small value after 400 samples indicating a strong correlation between the drawn samples. The autocorrelation structures of heat transfer coefficient and final minimum degree of cure present similar behaviour reaching a plateau after about 10 samples as illustrated in Figure 8.10b and 8.11. Therefore, a step size of 400 and 10 was selected for k and h, α_{fmin} respectively.

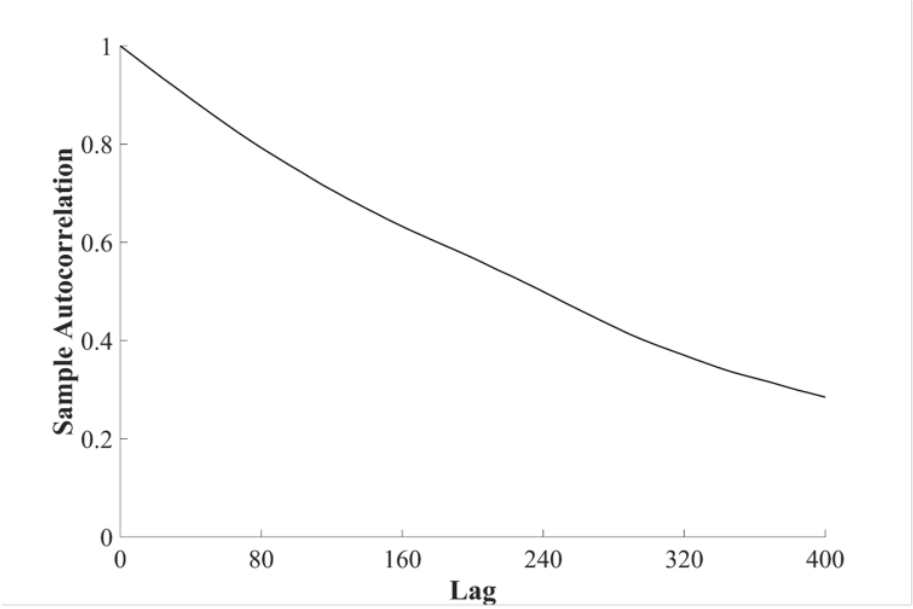

a)

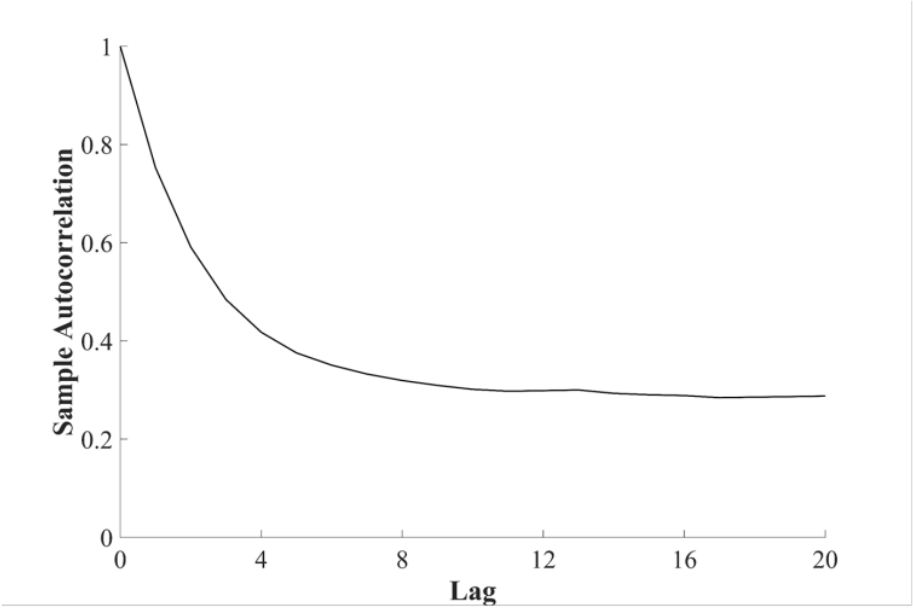

b)

Figure 8.10 Sample autocorrelation a) thermal conductivity level b) heat transfer coefficient of glass/epoxy composite flat panel (GFP).

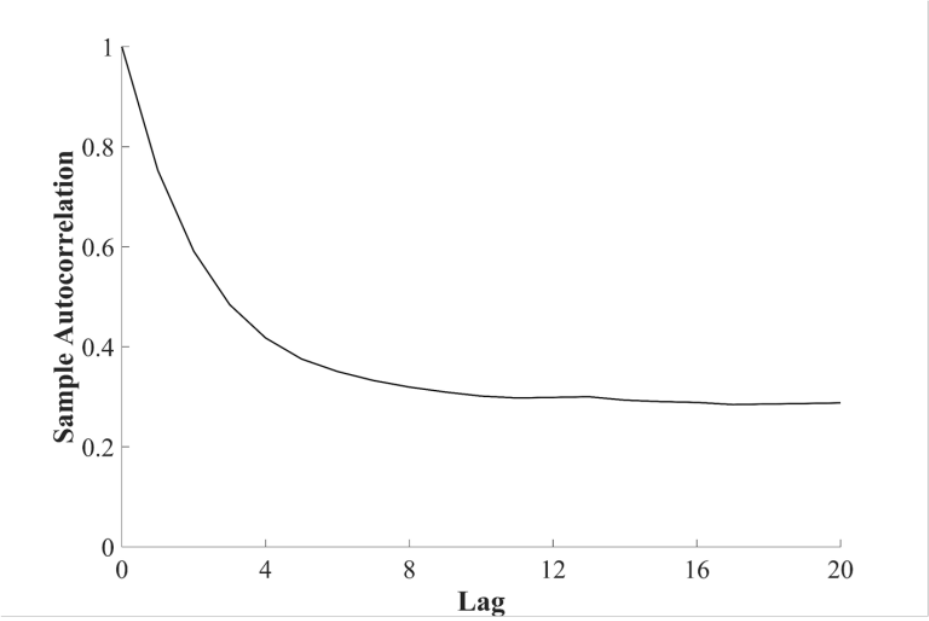

Figure 8.11 Sample autocorrelation of minimum final degree of cure of glass/epoxy composite flat panel (GFP).

Figures 8.12, 8.13 and 8.14 depict the prior estimate and inversion solution cumulative probabilities of the thermal conductivity level, heat transfer coefficient and minimum final degree of cure respectively. The mean value of thermal conductivity level is 0.095 W/m/°C, which is relatively close to the prior mean value of 0.12 W/m/°C, whilst the standard deviation is very low and equal to 0.002 W/m/°C. The heat transfer coefficient average is 8.2 W/m^2/°C with a standard deviation of 0.2 W/m^2/°C, whereas the nominal value is 8.5 W/m^2/°C. In terms of variability, the inversion procedure reduces the estimation uncertainty of surface heat transfer coefficient lowering its coefficient of variation from 18% [38] to 3%. In the case of the estimated minimum final degree of cure the mean value is 0.845 with standard deviation of 7 10^{-4} resulting in a 0.08% coefficient of variation.

A Monte Carlo simulation has been carried out using the prior statistical properties of the unknown stochastic variables to estimate the minimum final degree of cure without the information acquired from process monitoring system. The results of this simulation are illustrated in Figure 8.14. Prior estimates result in a wide range of minimum final conversion values of 0.82 - 0.86. This uncertainty may result in variations of final glass

transition temperature potentially affecting high temperature performance. The estimated minimum final degree of cure variability was reduced by 90% as a result of the inversion procedure. The low uncertainty prediction of the minimum final conversion during the curing stage allows control decisions to be made preventing undesirable effects such as under cure.

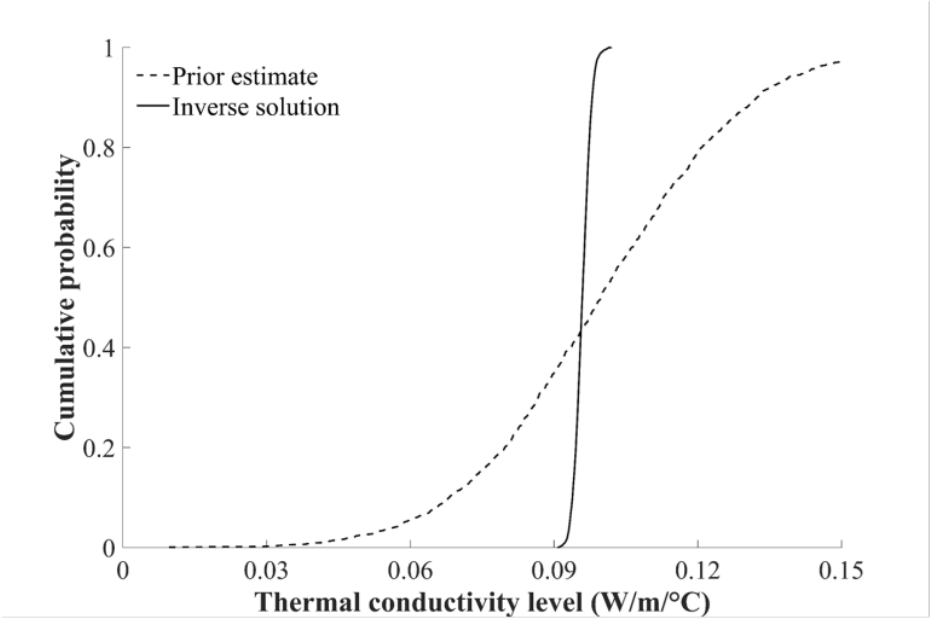

Figure 8.12 Cumulative probabilities before and after inverse analysis of thermal conductivity level of glass/epoxy composite flat panel (GFP).

Figure 8.15a illustrates the experimental measurements on the lower surface, the mid-thickness and the top of the curing glass/epoxy composite flat panel alongside the 95% confidence intervals of model response estimated using the prior statistical properties of thermal conductivity level and surface heat transfer coefficient (Table 8.2). The confidence intervals of model prior estimations are wide, highlighting the influence of stochastic variables on the through thickness temperature distribution. These results indicate the benefits of estimating the resin thermal conductivity level and surface heat transfer coefficient from the real time data. After inverse analysis the confidence intervals are narrowed down, and the model approximations of measured temperatures calculated with the estimated mean values of unknown variables are in close agreement with the experimental data with an average error of 1 °C (Figure 8.15b). The inversion procedure

runs simultaneously with the manufacturing process, estimating in real time the process outcomes by updating the cure model with the upcoming monitoring data.

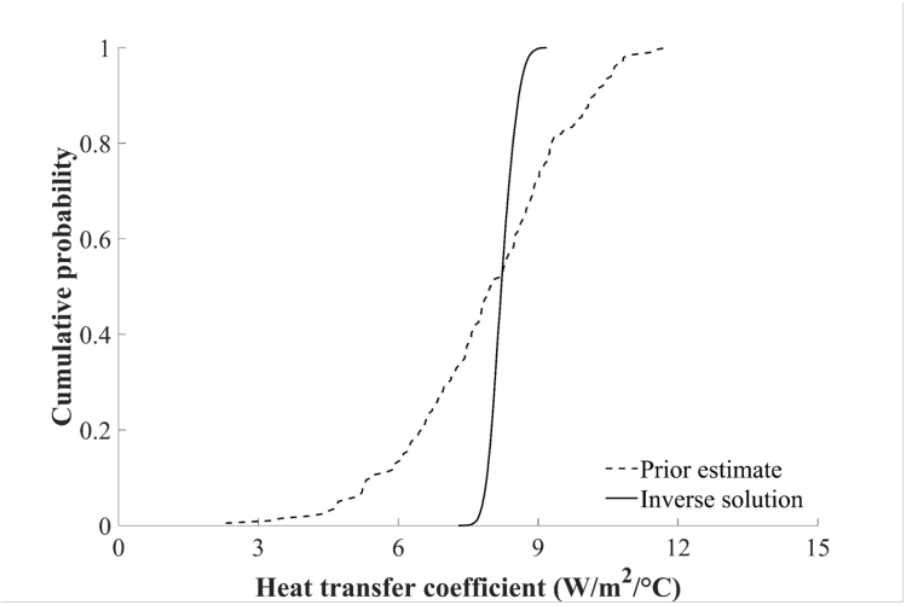

Figure 8.13 Cumulative probabilities before and after inverse analysis of heat transfer coefficient of glass/epoxy composite flat panel (GFP).

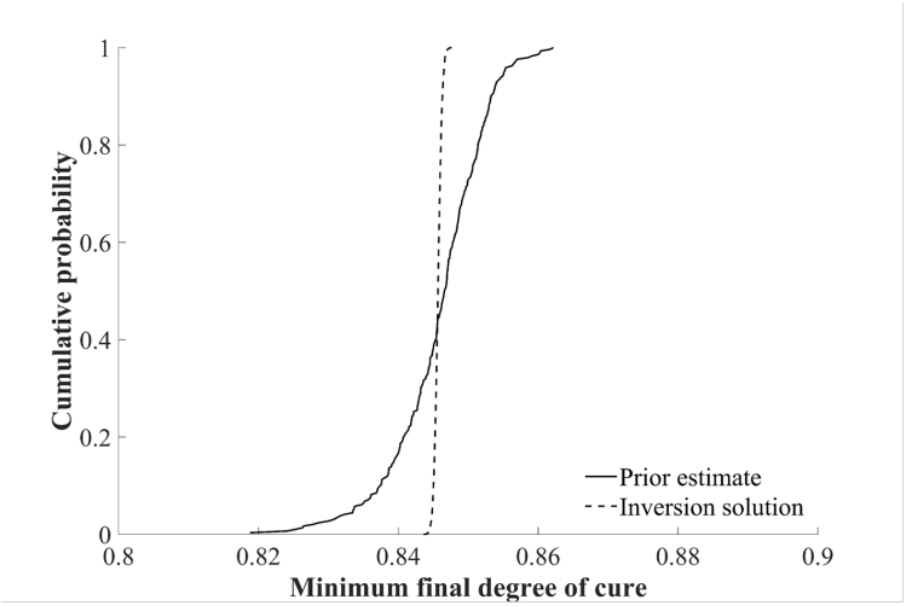

Figure 8.14 Cumulative probabilities before and after inverse analysis of minimum final degree of cure of glass/epoxy composite flat panel (GFP).

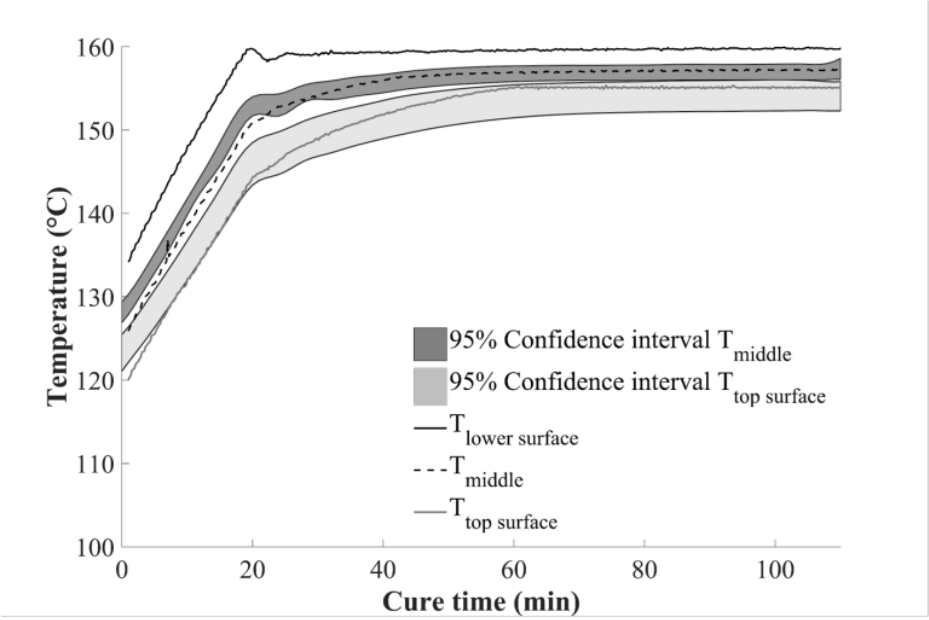

a)

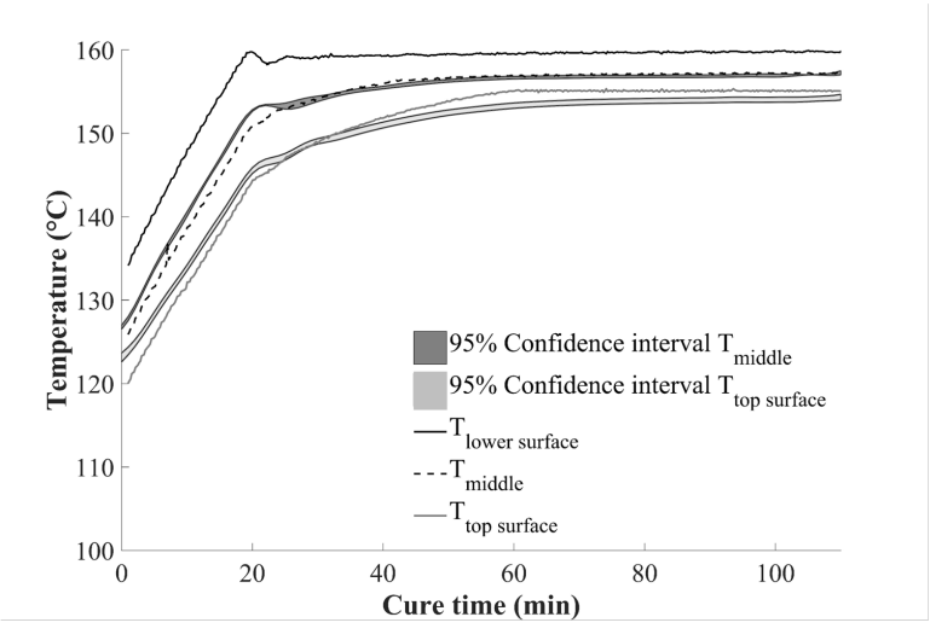

b)

Figure 8.15 Experimental data and probabilistic model response comparison: a) prior knowledge; b) estimated values of glass/epoxy composite flat panel (GFP).

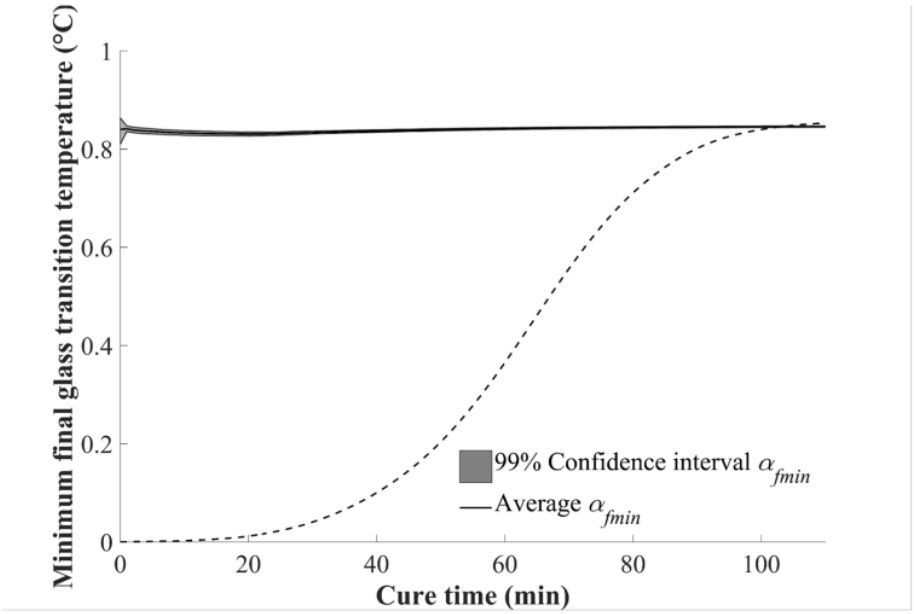

Figure 8.16 Evolution of minimum degree of cure and 99% confidence intervals of estimated minimum final degree of cure with time (GFP).

Figures 8.16 and 8.17 depict the evolution of the 99% confidence intervals of the minimum final degree of cure estimation and actual minimum degree of cure with time and the corresponding results for the evolution of the final minimum predicted glass transition temperature of glass/epoxy composite flat panel. The evolution of the actual minimum degree of cure was calculated using a non-parametric cure kinetics model for the epoxy resin system of this study [134] considering as an input the top surface temperature evolution with time and the glass transition temperature based on Eq. (4.9). The comparison of the predicted with the actual minimum final conversion indicates the estimation capabilities of the cure model during the inversion scheme. The estimated error is approximately 0.9%. The final glass transition estimate involves uncertainty of about 4 °C. This is reduced as a result of taking into account the monitoring data to about 1 °C. This, as well as the potential correction of glass transition temperature levels using monitoring data, can have significant implications in the high temperature performance of the produced composite. The overall scheme allows the continuous updating with new monitoring data sets enhancing the cure model fidelity on predicting the unknown parameters and consequently the desirable process outcomes with low uncertainty.

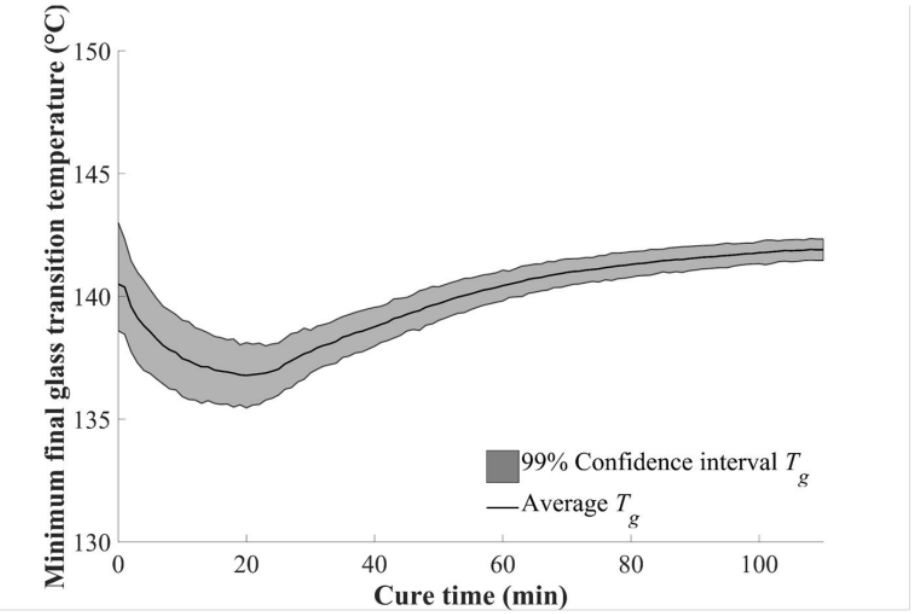

Figure 8.17 99% confidence intervals of estimated minimum final glass transient temperature with time of glass/epoxy composite flat panel (GFP).

8.4. Overview

The findings of the application of the inversion scheme to curing highlight the effectiveness of the MCMC method in terms of reducing the inherent uncertainty of the process and of predicting the process outcomes and their uncertainty using the results of process monitoring. The inversion scheme predicts the minimum final degree of cure with very low uncertainty with an error of about 0.9%. This accuracy is translated directly to an accurate estimate of the final glass transition of the material. The real time inversion procedure demonstrated in chapters 6, 7 and 8 can forms the basis of a control strategy that takes into account the prediction of process outcomes and their variability. This necessitates the use of an optimisation algorithm that can, in light of estimated current variability of process inputs, identify modifications of process parameters that maximise process efficiency and robustness. As a first step in this direction a stochastic multi-objective optimisation scheme is developed and implemented in chapter 9 to identify optimal cure process designs.

9. Stochastic multi-objective optimisation of the curing of a thick carbon/epoxy composite flat panel

9.1. Introduction

The inversion scheme presented in chapters 6-8 narrows down initial problem variability estimating unknown process parameters and their variability as well as their evolution during the process. The increased process simulation fidelity achieved as a result of the real time application of the inverse algorithm can be utilised in the context of the stochastic multi-objective optimisation scheme described in section 3.9 to identify efficient and robust process parameter adjustments that can potentially lead to process control. This can be accomplished in real time since the inversion provides fast low uncertainty estimation of process outcomes. In the present chapter a stochastic multi-objective optimisation framework is developed and demonstrated for the cure stage of composite manufacture based on the curing of a thick carbon/epoxy composite flat panel described in section 3.5.2.2. This is carried out off line considering only the known variability at the beginning of the cure process. The stochastic objects related to cure process such as cure kinetics and thermal boundary conditions described in chapter 4 are considered. This development is a first step in the integration of the inverse scheme developed in this work with process optimisation and control.

9.2. Surrogate cure models of curing of thick carbon/epoxy composite part

Surrogate models TFP SM_1, TFP SM_2 representing the cure process outcomes for the thick carbon/epoxy composite flat panel (TFP) were constructed based on the Kriging technique described in section 3.6. Figure 9.1 summarises the methodology of surrogate model construction used for the stochastic multi-objective optimisation of curing of the TFP. These models are based on an initial cloud of sampling points at which the cure model responses are known. The FE cure model, described in section 3.5.2.2, was used in order to generate the initial sample points and the corresponding responses. The FE cure model represents the cure of thick carbon/epoxy composite flat panel with thickness of 15.6 mm. A sample of 30,000 points was selected taking into account the dimensionality and the nonlinear character of the problem and following preliminary testing of the behaviour of the surrogate model. The input variables of the surrogate model

include the optimisation parameters such as first and second dwell temperature, heating ramp and dwell time, described in section 3.9, and the stochastic variables of the cure kinetics model i.e. initial degree of cure, reaction order and activation energy and boundary conditions i.e. tool temperature and surface heat transfer coefficient presented in sections 4.6 and 4.4 respectively.

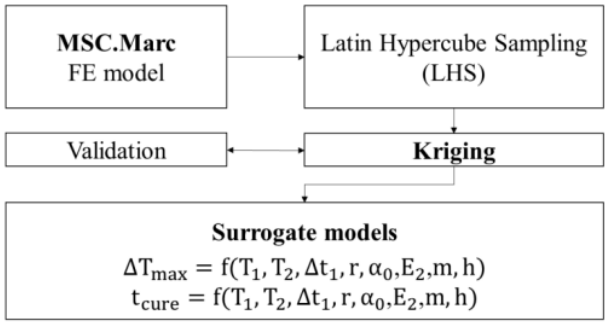

Figure 9.1 Surrogate model construction methodology.

Response surfaces, representing the relationship between process outputs and inputs, for two different cases detailed in Table 9.2, were constructed to assess the accuracy of the surrogate model. The response surface of t_{cure} over the space of T_1 and T_2 is illustrated in Figure 9.2a for constant values for the rest of the input parameters (Δt_1, r, h, m, E_2, α_0) as reported in Table 9.3 (Case 1). It can be observed that, for the values of parameters considered, increasing T_1 reduces cure time significantly, whilst the effect of T_2 is weaker. The reduction of cure time is non-linear with increasing temperature as a consequence of the non-linear nature of cure. The negligible influence of the second dwell temperature on cure time in the region of high first dwell temperatures is attributed to the fact that the cure process is already completed before the second dwell. The contribution of T_2 is of importance when the first dwell temperature is below 165 °C, in which case the cure time is decreasing with increasing T_2. The comparison of the two surfaces shows that the surrogate model is an accurate representation of the FE cure simulation. The mean absolute difference between the two is 0.9 min, which corresponds to a very small percentage of cure time (0.5% to 2%). Figure 9.2b illustrates the probability density function (PDF) of absolute difference between the FE and surrogate models. The region with the highest probability is between 0 and 0.7 min, with probability becoming very small over 1.2 min.

Table 9.1 Range and role of surrogate model input parameters of the cure of thick carbon/epoxy composite flat panel (TFP).

Parameter	Symbol (unit)	Range	Optimisation variable	Stochastic variable
First dwell temperature	T_1 (°C)	$135 - 175$	Yes	Yes
Second dwell temperature	T_2 (°C)	$175 - 215$	Yes	Yes
Duration of first dwell	Δt_1 (min)	$33 - 300$	Yes	No
Heating rate	r (°C/min)	$1 - 4$	Yes	No
Convection coefficient	h ($W/m^2/°C$)	$14 - 22$	No	Yes
Activation energy	E_2 (KJ/mol)	$56 - 60$	No	Yes
Autocatalytic reaction order	m	$1 - 1.6$	No	Yes
Initial degree of cure	α_0 (%)	$1.5 - 5.1$	No	Yes

Table 9.2 Input parameters values used for the construction of the response surfaces of the two validation test cases for surrogate and FE models comparison.

	T_1 (°C)	T_2 (°C)	Δt_1 (min)	r (°C/min)	h ($W/m^2/°C$)	E_2 (KJ/mol)	m	α_0 (%)
Case 1	135-175	175-215	84	2	17.8	57.8	1.29	3.3
Case 2	135-175	195	84	1-4	17.8	57.8	1.29	3.3

Figure 9.3a illustrates the dependence of ΔT_{max} on T_1 and r for constant values for the rest of the parameters (T_2, Δt_1, h, m, E_2, α_0) as reported in Table 9.2 (Case 2) during the cure of a thick carbon/epoxy composite flat panel. The agreement between the surrogate model and the simulation is very good. The temperature overshoot increases with increasing T_1. In the region of low heating ramp and high first dwell temperature, the temperature overshoot decreases with increasing first dwell temperature as a result of the occurrence of maximum reaction during the ramp. The PDF of absolute error (Figure 9.3b) indicates that the region of high probability is from 0 to 0.8 °C. The mean absolute error is 0.9 °C, whilst the probability of error greater than 1.6 °C is negligible.

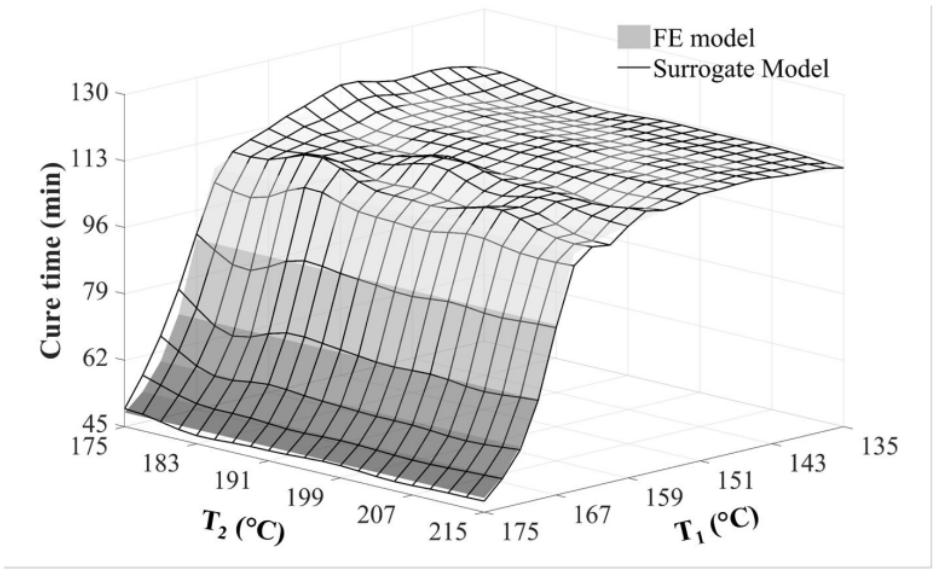

a)

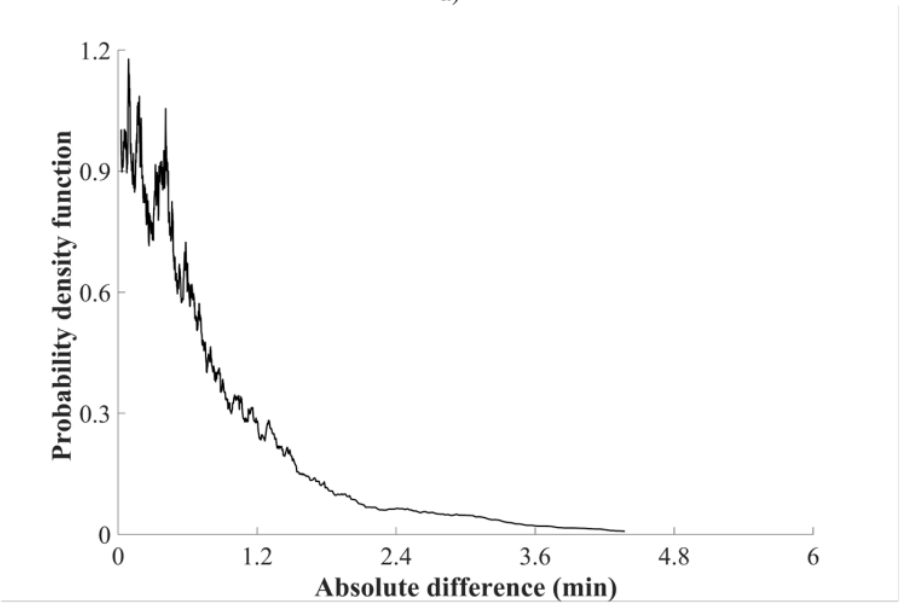

b)

Figure 9.2 FE and surrogate model response surfaces: a) Case 1 (Table 9.1) cure time as a function of the first and second dwell temperature; b) PDF of absolute differences between surrogate and FE model for Case 1 of the curing of thick carbon/epoxy composite flat panel (TFP).

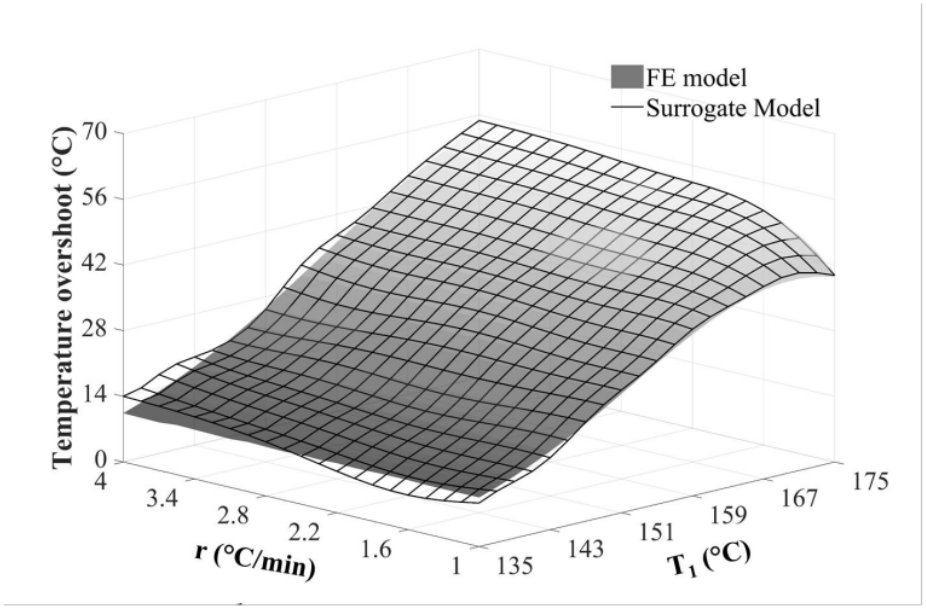

a)

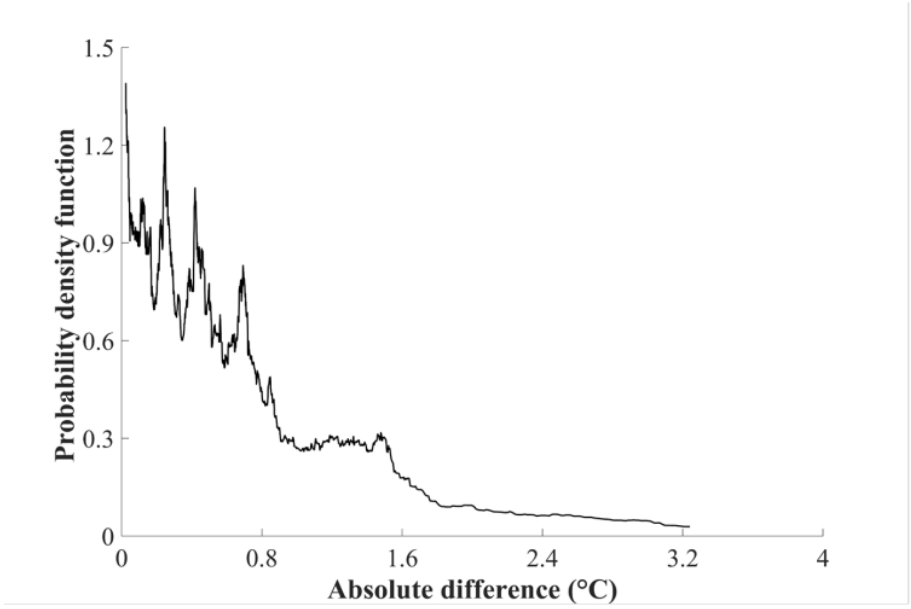

b)

Figure 9.3 FE and surrogate model response surfaces: c) Case 2 (Table 9.1) temperature overshoot as a function of first dwell temperature and ramp; d) PDF of absolute differences between surrogate and FE model for Case 2 of the curing of thick carbon/epoxy composite flat panel (TFP).

The surrogate model accuracy was also tested in the case of the MC simulation implementation presented in section 3.7.2. A standard two dwell cure profile applied during the cure of the thick carbon/epoxy composite flat panel with first dwell temperature of 160 °C for 75 min and second dwell temperature of 180 °C [28] was simulated using 400 realisations. Figure 9.4 illustrates the cumulative density function (CDF) of temperature overshoot as computed by the FE and surrogate models. The average temperature overshoot is 37 °C, whilst the standard deviation is 4.5 °C implying a coefficient of variation equal to 12 %. It can be observed that the two CDFs are in very close agreement. The computational time of stochastic simulation is reduced significantly with the use of the surrogate model. The stochastic simulation using FE takes 420 min on the 4 cores @3.2 GHz computer used, whilst the surrogate model based solution needs 3 min. This represents a reduction by more than 99%.

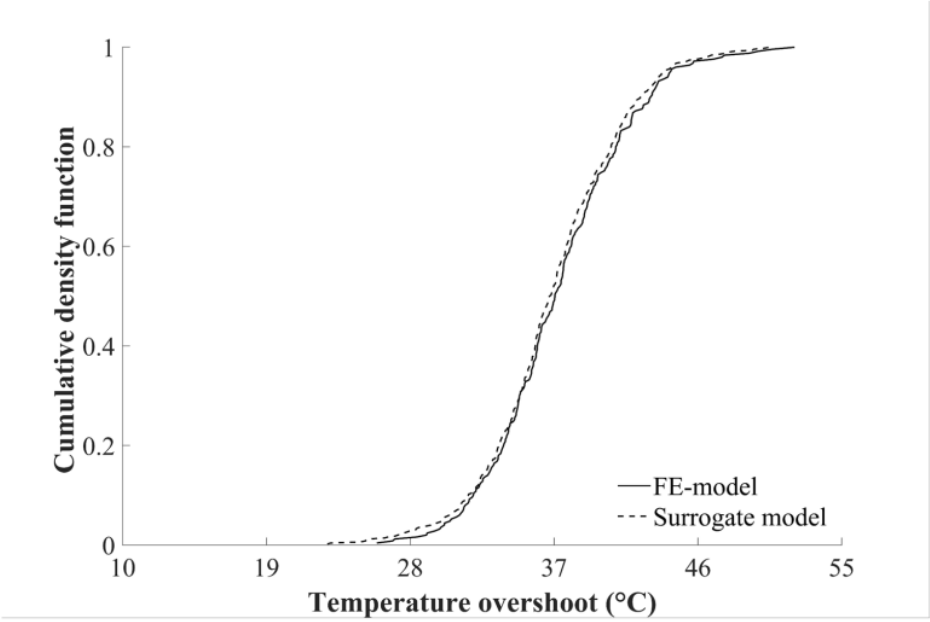

Figure 9.4 Cumulative density function (CDF) of a standard cure profile of temperature overshoot of thick carbon/epoxy composite flat panel (TFP).

9.3. Results of stochastic multi-objective optimisation of curing of thick carbon/epoxy composite flat panel

Stochastic multi-objective optimisation incorporates the MC method into a GA minimising cure time and temperature overshoot average and their corresponding uncertainty during the cure process of a thick carbon/epoxy composite flat panel as described in section 3.9. The evolution of the GA population during stochastic multi-objective optimisation run is illustrated in Figure 9.5 in terms of mean cure time and temperature overshoot. As the stochastic optimisation progresses, the population sample is improved compared to populations of previous generations. The GA converges – i.e. the Pareto set is stabilised – between 7 and 12 generations.

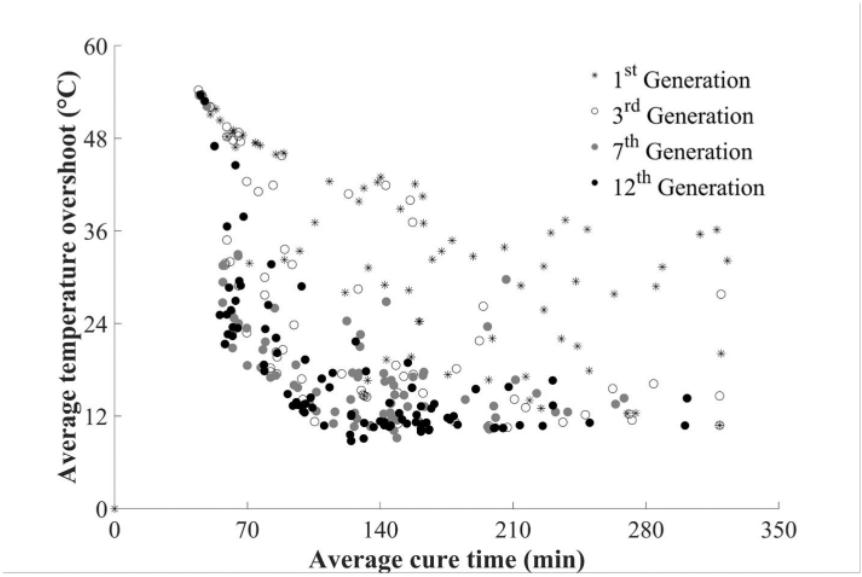

Figure 9.5 Population evolution of stochastic multi-objective optimisation on the cure of thick carbon/epoxy composite flat panel (TFP).

Figure 9.6 shows the average cure time-average temperature overshoot cross section of the stochastic Pareto front, with the variability with respect to both variables presented in box plots. The deterministic Pareto front is also illustrated with a solid line. The Pareto fronts of both the stochastic and deterministic optimisation are in the form of an L-shape curve comprising two regions: (i) a horizontal region in which cure time can be reduced significantly without considerable changes in temperature overshoot; and (ii) a vertical region in which high temperature overshoots occur with small changes in cure time. The

majority of the stochastic Pareto points are shifted up compared to the deterministic Pareto front. The stochastic Pareto set includes points in which the mean values are dominated by other optimal points, but they dominate them in terms of variability resulting in a 4-D front. In contrast, in the deterministic case the domination ranking occurs only in terms of nominal values and consequently the Pareto front is 2-D.

Deterministic optimisation schemes address only the minimisation of process duration and defects formation without considering the associated variability [120]. However, the benefits offered by the exploration of the design space by numerical optimisation can be accompanied by relative instability of some of the solutions with respect to perturbations of nominal process parameters leading to potential risks. This can be problematic, especially in cases where the deterministic optimisation exploits high sensitivity areas of the landscape. For example, optimal points in the vertical region of the deterministic Pareto set can be highly sensitive to variations resulting in temperature overshoots significantly different than predicted by the simulation. This possibility necessitates the use of more conservative cure profiles. In order to demonstrate this weakness of deterministic optimisation and the way the stochastic optimisation can overcome it, two points of the vertical region of deterministic and stochastic Pareto front with similar cure time and temperature overshoot were selected and analysed. The details of these design points are reported in Table 9.3. Table 9.3 also summarises the results of the stochastic simulation for these points. The average cure time and temperature overshoot of deterministic and stochastic point are similar, whilst the cure time coefficient of variation is about 2.5 % in both cases. The standard deviation of temperature overshoot of the point of deterministic optimisation is 6.6 °C, which is approximately twice that of the stochastic point. Furthermore, the nominal overshoot determined by deterministic simulation is lowered by 7°C compared to the average computed by stochastic simulation. Consequently, deterministic simulation provides a biased estimate of average overshoot underestimating risks. This explains the upward shift of the stochastic Pareto front with respect to the deterministic points observed in Figure 9.6. The temperature overshoot in the deterministic case is 9 °C - 43 °C, whilst the stochastic one is in the range of 15 °C - 30 °C. The sensitivity of the deterministic point can be attributed to the higher first dwell temperature of its cure profile. These differences highlight the high sensitivity of deterministic optimal points and the robustness offered by stochastic optimal points.

Table 9.3 Sensitivity analysis of deterministic and stochastic optimal points of cure process of thick carbon/epoxy composite flat panel (TFP).

Parameter	Stochastic optimal point	Deterministic optimal point
1st dwell temperature (°C)	144	152
2nd dwell temperature (°C)	214	214
Dwell duration (min)	35	33
Heating ramp (°C/min)	3.7	3.8
Average cure time (min)	58	55
Average temperature overshoot (°C)	21	27
Cure time standard deviation (min)	1.3	1.9
Temperature overshoot standard deviation (°C)	3.6	6.6

The stochastic Pareto front contains some points with cure time values twice as high as that of deterministic solutions. These points are located at the end of the horizontal region of the stochastic Pareto front and present low variations with standard deviations of 0.4 min and 2.5 °C for cure time and temperature overshoot respectively. These individuals are generated using conservative cure profiles with low first dwell temperature and long first dwell time. In these cases, overshoots are negligible and the cure process long. The vertical region of the stochastic Pareto front includes two points with temperature overshoot higher than 50 °C, a low cure time below 50 min and significant variations especially in the case of temperature overshoot with standard deviation of 4-4.5 °C.

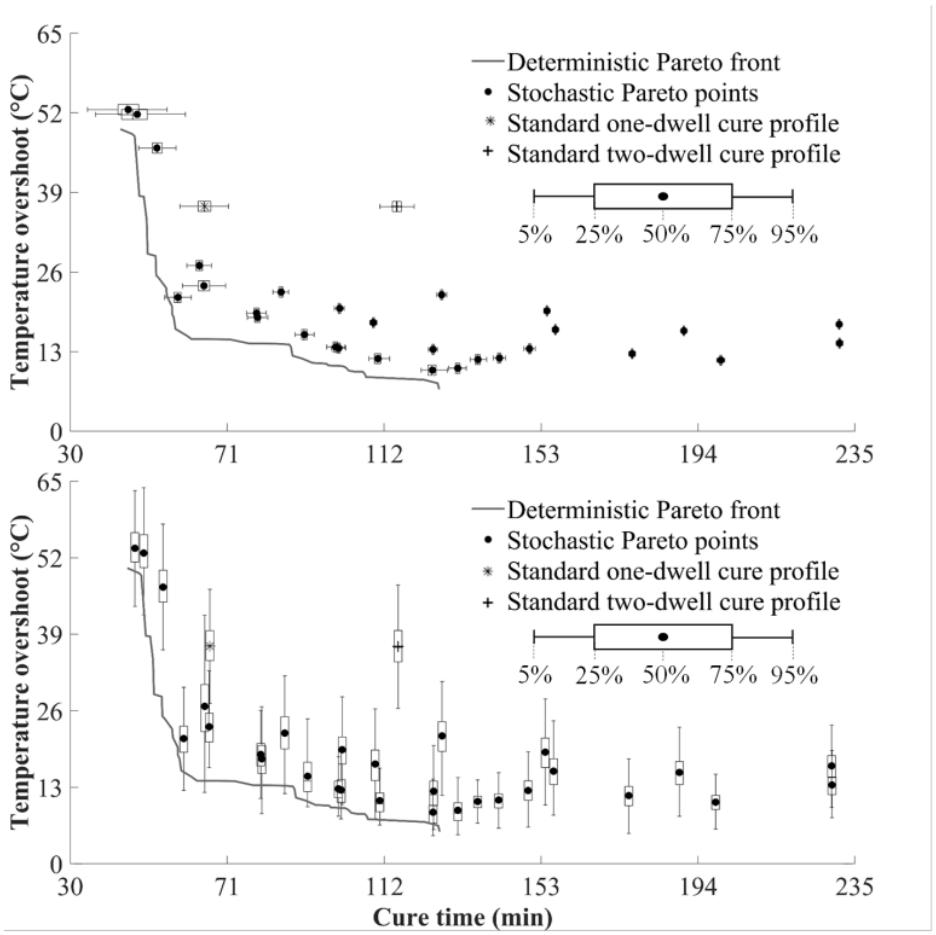

Figure 9.6 Pareto front of stochastic and deterministic multi-objective optimisation a) cure time box plots; b) temperature overshoot box plots of cure process of thick carbon/epoxy composite flat panel (TFP).

The variations of cure time in extreme points in the vertical region of the 4-D Pareto front can be observed clearly in Figure 9.7 which depicts the Pareto front of average cure time with the corresponding standard deviations. The Pareto front presents an L shape trade off, with a vertical region corresponding to aggressive cure profiles with high temperature overshoot and a horizontal region with more conservative profiles resulting in higher cure times. The variability is high for aggressive cure profiles and can reach up to 6 min. However, for cure times above 65 min the corresponding variability reaches a plateau with a standard deviation of 0.3-1.5 min.

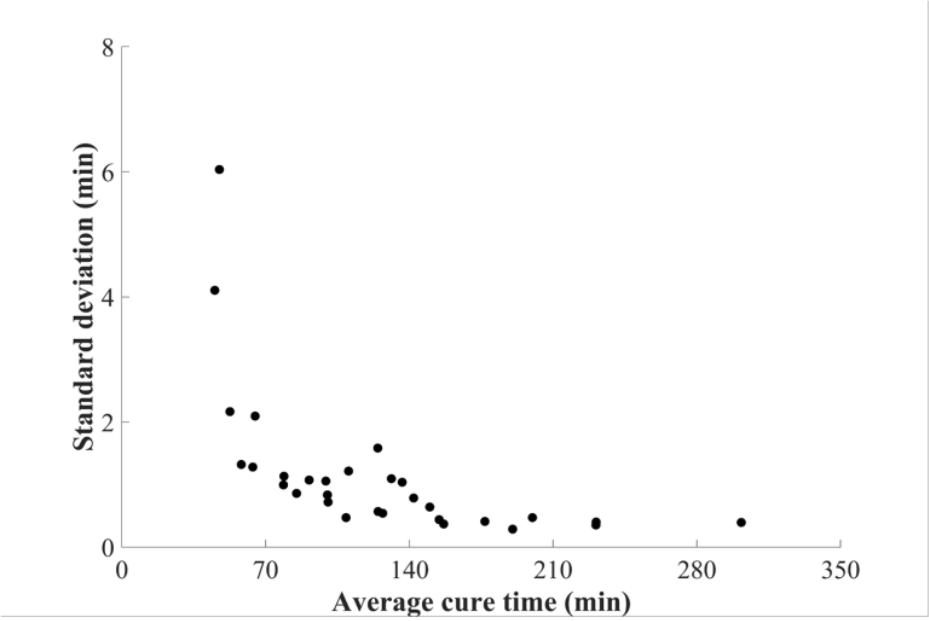

Figure 9.7 Pareto front of average cure time and the corresponding variability in the case of carbon/epoxy thick composite flat panel (TFP).

MC simulation of the two standard cure profiles of thick carbon/epoxy composite flat panel has been carried out. The first profile comprises two dwells at 160 °C and 180 °C [157] and the second one dwell at 180 °C [121]. A detailed analysis of the cure process has been performed to uncover the qualitative characteristics of two optimal points with short and intermediate dwell profile and compare them with the standard cure profiles. Table 9.4 reports the inputs of this analysis. Figures 9.8-9.11 illustrate the evolution of temperature and degree of cure at the tooling side and in the middle of the laminate for the three realisations. In the mean realisation stochastic variables (T_1, T_2, h, m, E_2, α_0) are equal to the mean values reported in Table 4.7 and 4.9. Aggressive and conservative realisations correspond to the cases where each stochastic variable was shifted by two standard deviations in the positive and negative direction according to the influence of each on cure time and overshoot. The aggressive realisation represents an extreme scenario in which all stochastic variables have values resulting in acceleration of the process, whilst the conservative realisation corresponds to values leading to a slower cure.

Table 9.4 Comparison of optimal and standard cure profiles and their response under aggressive and conservative uncertainty scenarios of thick carbon/epoxy composite flat panel (TFP) curing.

		Short dwell optimal profile	Intermediate dwell optimal profile	Standard one dwell profile	Standard two dwell profile
Cure profile	T_1 (°C)	147	139	180	160
	T_2 (°C)	189	209	-	180
	Δt_1 (min)	38	56	120	75
	r (°C/min)	3	2	1	1.5
Mean realisation	T_1 (°C)	147	139	180	160
	T_2 (°C)	189	209	-	180
	h (W/m^2/°C)	17.8	17.8	17.8	17.8
	E_2 (J/mol)	57,820	57,820	57,820	57,820
	m	1.29	1.29	1.29	1.29
	α_0	0.033	0.033	0.033	0.033
	Cure time (min)	65	90.6	66	115
	Overshoot (°C)	22	12	37.3	37
Aggressive realisation	T_1 (°C)	150	142	183	163
	T_2 (°C)	192	212	-	183
	h (W/m^2/°C)	15.1	15.1	15.1	15.1
	E_2 (J/mol)	56,162	56,162	56,162	56,162
	m	1.48	1.48	1.48	1.48
	α_0	0.049	0.049	0.049	0.049
	Cure time (min)	59	90.7	60	112
	Overshoot (°C)	36	25	45	52
Conservative realisation	T_1 (°C)	144	136	177	157
	T_2 (°C)	186	206	-	177
	h (W/m^2/°C)	20.5	20.5	20.5	20.5
	E_2 (J/mol)	59,477	59,477	59,477	59,477
	m	1.1	1.1	1.1	1.1
	α_0	0.017	0.017	0.017	0.017
	Cure time (min)	73	97	76	118
	Overshoot (°C)	32	18	34	22
Standard deviation	Cure time (min)	2	1	2.6	1
	Overshoot (°C)	3.3	3.1	3.8	4.4

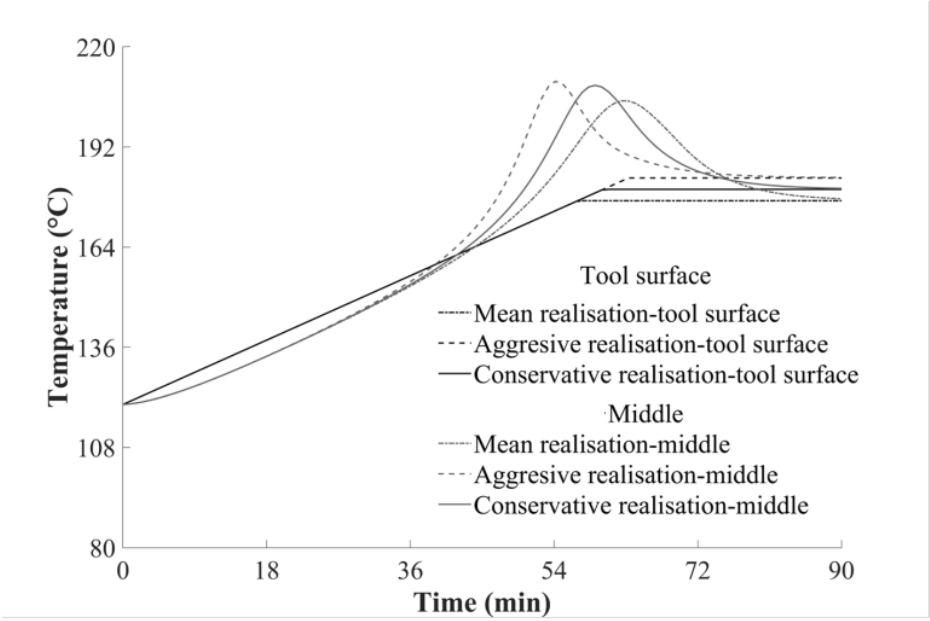

a)

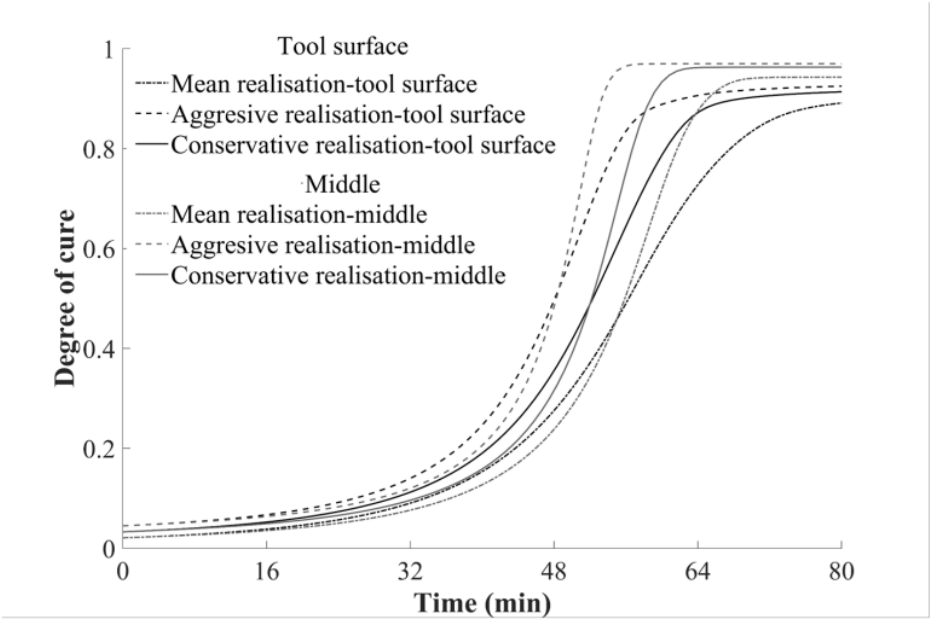

b)

Figure 9.8 One dwell standard profile: a) temperature evolution; b) degree of cure evolution of thick carbon/epoxy composite flat panel (TFP).

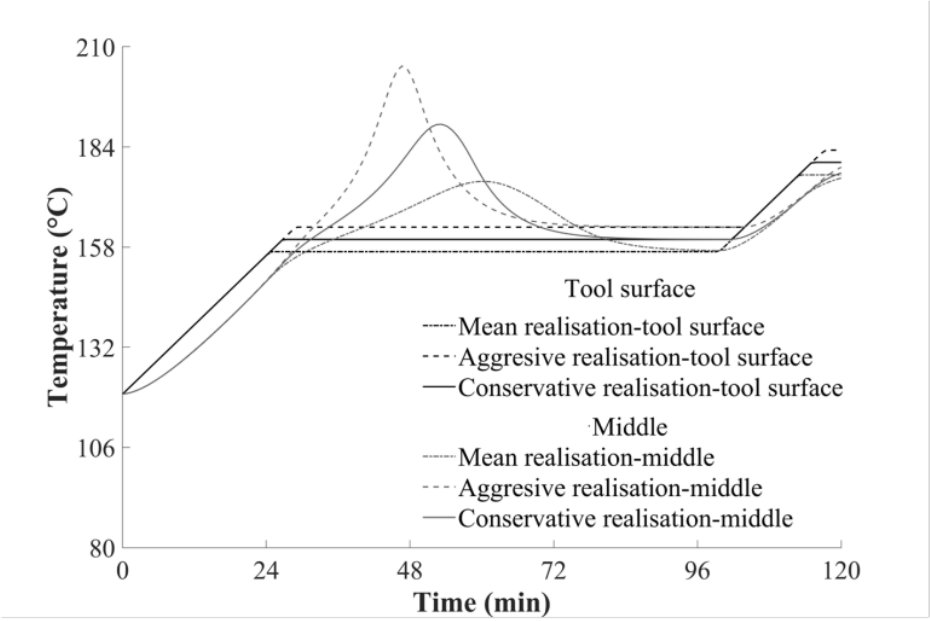

a)

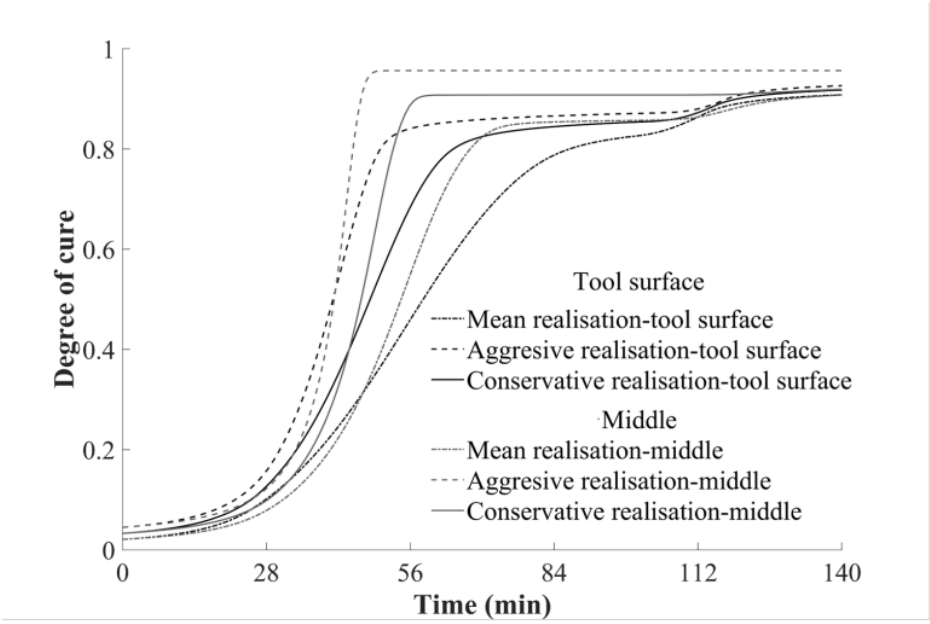

b)

Figure 9.9 Two dwell standard profile: a) temperature evolution; b) degree of cure evolution of thick carbon/epoxy composite flat panel (TFP).

The results obtained at the optimal points illustrate the significant improvements in terms of minimising both the mean value and the standard deviation of cure time and temperature overshoot in comparison with standard cure profiles as reported in Table 9.4. In the intermediate dwell optimal profile, the average and the standard deviation of cure time were reduced by about 20% and 30% respectively compared to the standard two dwell profile. In addition, the optimal point presents a decrease of 60% in average temperature overshoot in comparison with both the one and two dwells standard profile. A higher first dwell temperature (Figure 9.8a) results in an early reaction rate peak in the case of the one dwell standard profile. Consequently, the maximum temperature overshoot occurs during the first dwell. The selection of a cure profile with high first dwell temperature results in low cure time and causes significant temperature overshoots that can reach up to about 50 °C in the aggressive realisation (Figures 9.8a, 9.9a). The temperature evolution of the different realisations, as illustrated in Figure 9.10a, highlights the stability of the intermediate optimal profile. The first dwell temperature is lower than that of the standard profiles reducing significantly exothermic effects and resulting in relative uniformity of temperature across the thickness. Also, the cure occurs almost at the same time in the three realisations, as shown in Figure 9.10b, whereas for the standard profiles there are significant variations in cure duration between realisations (Figures 9.8b and 9.9b). The short dwell optimal profile results in slightly faster cure (Figure 9.11b) than the standard one-dwell profile and approximately 40% reduction of cure time in comparison to the standard two dwell profile. The evolution of degree of cure through the thickness is more uniform for all realisations in the case of optimal profiles in comparison to standard profiles. This can be attributed to the fact that the cure reaction in the optimal solutions occurs more gradually than in the standard profiles, in which the high first dwell temperature accelerates aggressively the exothermic reaction. The average temperature overshoot of the short dwell optimal profile is lowered by about 40%, whilst the standard deviation by about 20% and 10% compared to the standard one and two dwell profiles respectively.

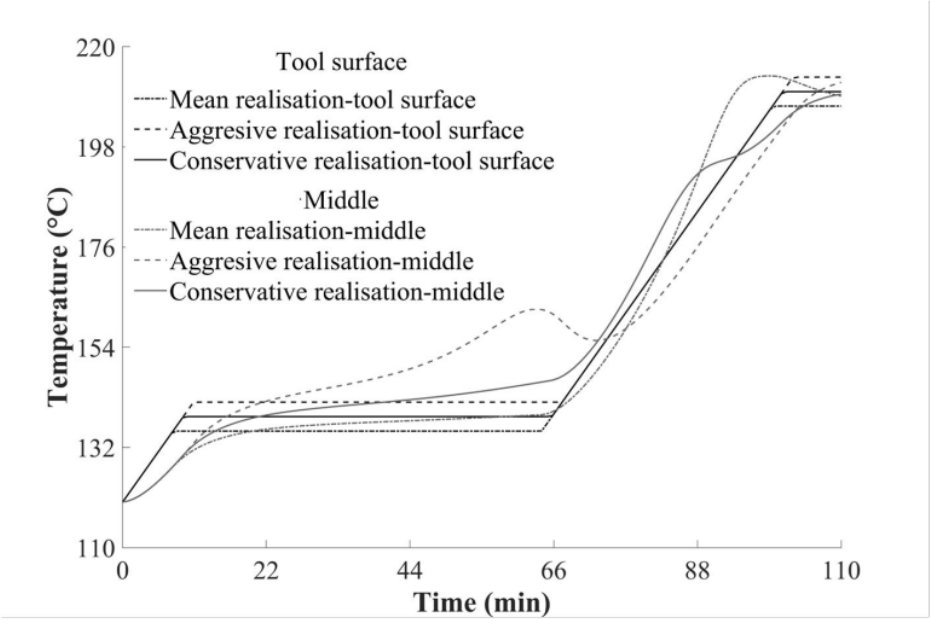

a)

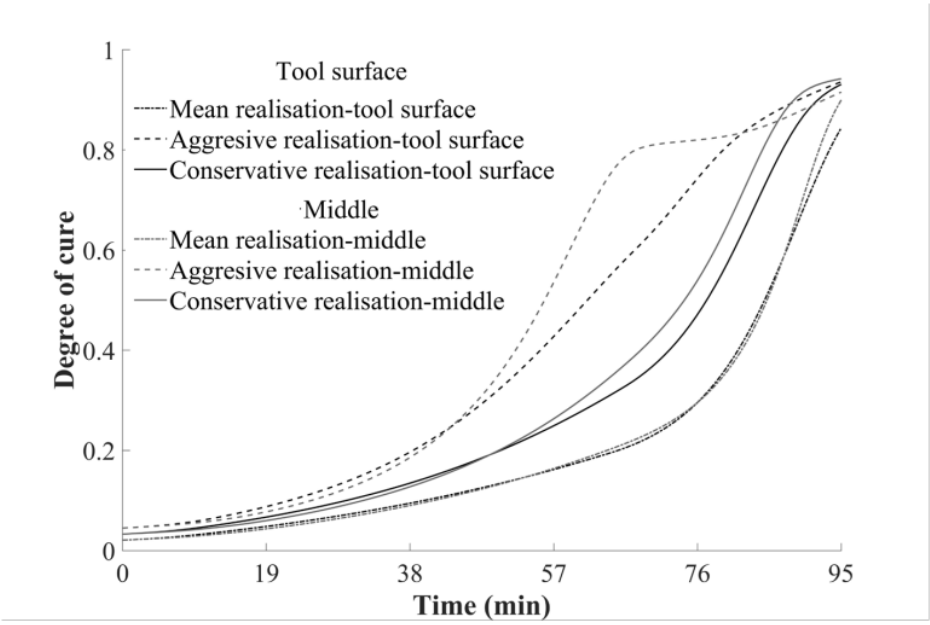

b)

Figure 9.10 Intermediate dwell optimal profile: a) temperature evolution; b) degree of cure evolution of thick carbon/epoxy composite flat panel (TFP).

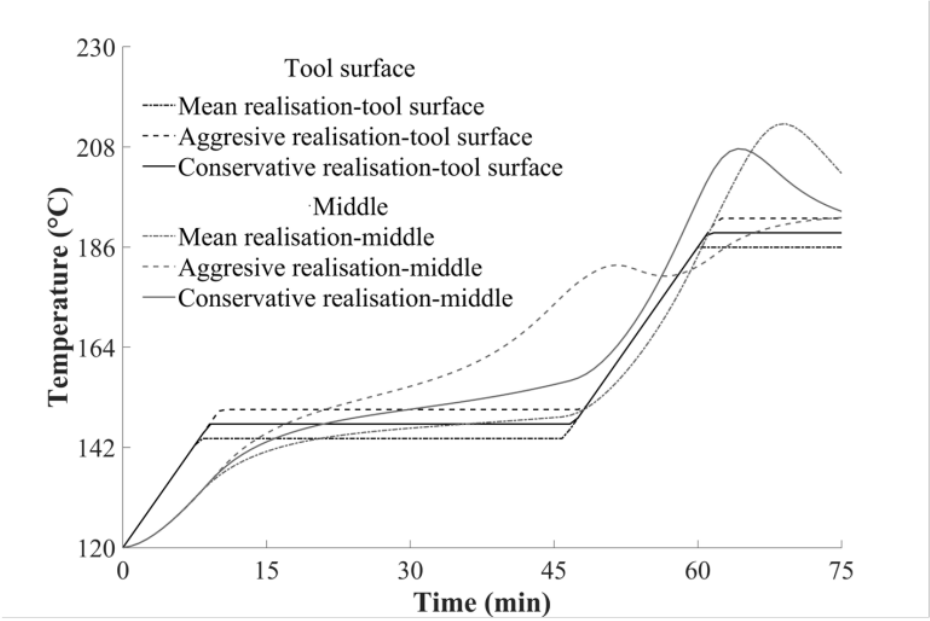

a)

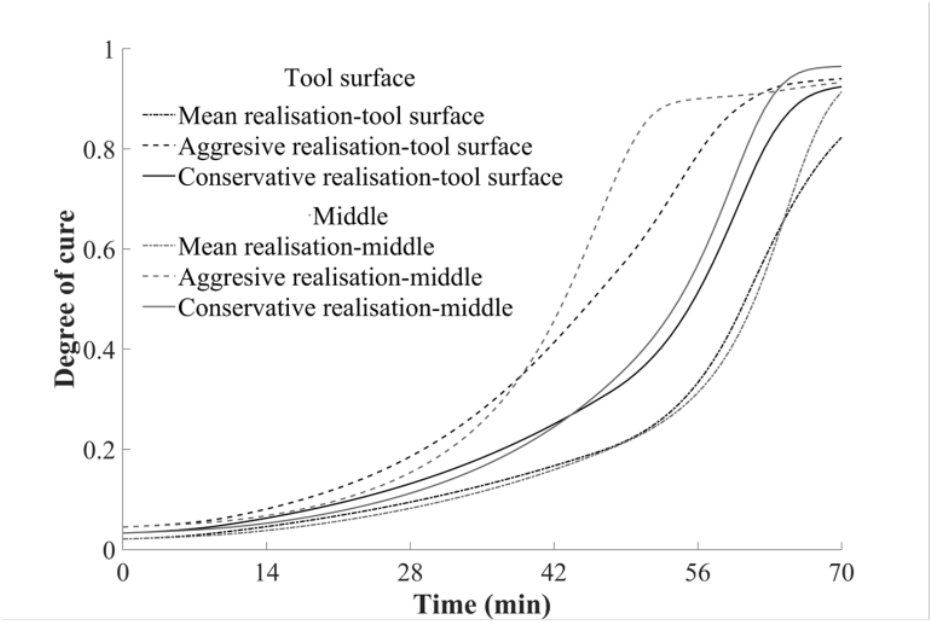

b)

Figure 9.11 Short dwell optimal profile: a) temperature evolution; b) degree of cure evolution of thick carbon/epoxy composite flat panel (TFP).

Stochastic multi-objective optimisation yields a multi-dimensional Pareto front with optimal profiles that can be chosen based on the relative weightings of the different objectives relevant to specific applications. These are usually implied in the manufacturer's choices; e.g. in thick high cost components a low overshoot long cure process might be prioritised, whilst in inexpensive non-critical components a short and relatively unstable process might be preferred. In this sense, in an application in which duration is not prioritised, cure cycles such as the intermediate dwell optimal case can be implemented with process duration of about 1.5 h and temperature overshoots in the range of 10 °C - 20 °C. In the case of high throughput lower specification composite parts, the short optimal profile can be chosen resulting in faster cure cycles of about 1 h, associated with temperature overshoots in the 20 °C - 35 °C range.

9.4. Overview

The stochastic multi-objective optimisation methodology presented in this chapter accounts for different sources of uncertainty by implementing a Monte Carlo simulation integrated into a GA to minimise temperature overshoot, cure time and their variability. Current deterministic optimisation methodologies generate optimal solutions that are sensitive to variations of the input parameters. The findings highlight the efficiency of stochastic optimisation in minimising cure time and temperature overshoot uncertainty in comparison with the standard cure profiles. The stochastic multi-objective optimisation can be applied to composite manufacturing processes alongside with the inversion scheme described in chapters 6-8. The utilisation of surrogate models which reduce significantly computational time enables the implementation of the stochastic multi-objective optimisation framework in real time. The inversion procedure can provide low uncertainty estimations of unknown stochastic input parameters to the stochastic optimisation tool in order to find optimal solutions which minimise the process duration, potential defects and the corresponding variability on line. Consequently, control actions can be taken based on the outcomes of on line optimisation during the manufacturing process preventing undesirable phenomena which can be detrimental for final part quality. In the case of cure the coupling of inversion with stochastic optimisation can lead to optimal cure profiles which result in low cure duration and temperature overshoot, whilst their corresponding uncertainty can be reduced by inversion alongside the optimisation. The stochastic multi-objective optimisation can be applied to the case of the

filling stage identifying optimal design parameters such as inlet/outlet ports number and position, flow channels and applied pressure gradient to minimise filling times and induced defects as well as variability. Furthermore, control actions, such as switching of gates and vents, applied pressure or flow rate levels changes can be activated based on the results of optimisation obtained in conjunction with a real time inverse scheme like the ones described in chapters 6 and 7.

10. General discussion

10.1. Introduction

The present study achieved the development and implementation of an inversion scheme integrating process monitoring with process modelling for the real time uncertainty estimation in composites manufacture. In the current state of the art, it has been demonstrated that the variability of material properties and boundary conditions affects composites manufacture inducing significant variations in process outcomes [5]. This inherent uncertainty of input parameters leads to estimations with wide confidence intervals, reducing the predictive fidelity of process simulation models. The method put forward in this study narrows down the uncertainty in model predictions in the filling and curing stage of composites manufacture. The sensors developed are capable of monitoring the flow and cure process in the presence of carbon fibre reinforcement. The incorporation of real time process monitoring into the inverse algorithm provides reliable data related to phenomena occurring during the process, enhancing the predictive capabilities of models. The real time application of the inversion scheme was accomplished by developing fast surrogate models replacing computationally expensive conventional FE process models. The approaches presented here progress the state of the art significantly towards the minimisation of the mismatch between stochastic simulation estimations and real phenomena in composites manufacturing processes. The following sections discuss the main outcomes of the work, with a focus on progress beyond the state of the art and its implications for further development and industrial application.

10.2. Uncertainty quantification in composites manufacture

Uncertainty in the filling stage has been experimentally investigated in then literature focusing on preform permeability. This variability is attributed to fibre imperfections in the preform, such as tow misalignment and nesting effects. Resin viscosity variability has not been examined in the literature and only assumptions have been made for its incorporation in stochastic flow simulations [24]. Hypothesising the levels of resin viscosity variability can lead to inaccurate estimations of process outcomes. This gap was addressed in this study by conducting a series of rheology tests to quantify the variability of a high performance epoxy resin viscosity. All resin samples were within self-life as recommended by the supplier. The results show significant variability of about 30% in initial resin viscosity. This is attributed to the dependence of resin viscosity on storage conditions. Resin conditioning governs viscosity variability since the initial viscosity increases by up to 80% with increasing days of exposure

at ambient temperature. Stochastic objects have been developed in this work to represent initial resin viscosity variability. Stochastic flow simulations have demonstrated that variations in resin viscosity introduce variability in the filling duration of about 30%. The resulting variability highlights the importance of resin viscosity uncertainty.

The quantification of resin viscosity uncertainty advances the current state of the art providing a greater insight regarding the sources of variability in the filling stage. The selection of a uniform distribution for the initial resin viscosity reflects accurately the dependence of initial material state on storage conditions considering an even probability of resin usage within the recommended time range. Resin viscosity plays a dominant role in the filling stage. Therefore, stochastic simulations focused on filling should consider viscosity variability alongside with preform permeability and boundary conditions variations. The characterisation of material properties and boundary conditions variability and their integration into stochastic simulations offer a solution in terms of bridging the gap between real phenomena and process simulation allowing a more efficient process design.

The cost of composites manufacture and the final part quality are of importance and are governed by material properties and process design. A process design that does not consider the existence of variability in material properties and boundary conditions can result in inaccurate estimations of process outcomes potentially leading to increases amounts of scrap due to unexpected process induced defects. The utilisation of resin, conditioned as recommended by the supplier, may lead to variations in process outcomes, such as the filling duration and presence of defects. The application of a control plan in resin storage conditions can reduce variations related to viscosity resulting in more uniform filling process eliminating unanticipated defects. This is of importance in manufacturing of high performance parts, such as the C spar investigated in chapter 7, in which the tolerances are narrow and the probability of rejected parts due to process parameters variability high.

In the case of preform permeability and race tracking, variability has been modelled in this study as a scalar variable in order to reduce the dimensionality of the flow model. This approach does not consider local scale variations and autocorrelation. Local scale phenomena were observed in the results of the lineal flow sensor placed across the tool edge during RTM filling, where the monitored resin flow front presented some noise attributed mainly to the nonuniformity of the gap size between the preform and tool across the edge and in turn in variations of local edge permeability. Using this simplified approach, the process models can provide estimations of output scalar variables, such as the filling duration but may result in accuracies in estimations of outcomes linked to local scale phenomena such as micro/macro

voids percentage. Local variations and autocorrelation of preform permeability have been quantified extensively in literature [24, 25] and modelled with random fields, whilst race tracking has been modelled only as a scalar variable [36]. The investigation of race tracking variability can be expanded to develop a more comprehensive representation. In the case of RTM processing, race tracking variability and its spatial correlation across the tool edge can be quantified by measuring the size of the gap between the preform and tool edges. This information can be captured in 1-D stochastic objects.

10.3. Fast surrogate flow and cure process models

Fast surrogate models have been developed in this work based on Kriging estimating the filling and curing stage outcomes as a function of design and/or stochastic input parameters. Surrogate models provide accurate estimations of process outcomes 99% faster than conventional FE analysis models. The comparison between surrogate and FE models highlights the accuracy of surrogate models with an average error below 2%. The fast execution of surrogate models advances the state of the art on process simulation by making feasible the implementation of computational iterative methods requiring a large number of models evaluation such as inverse algorithms, stochastic simulation and optimisation. Especially in the case of stochastic multi-objective optimisation, the required model executions can reach up to $2\ 10^6$ due to the integration of MC into a GA. In this case, the utilisation of FE models introduces significant limitations making the implementation of stochastic multi-objective optimisation method computationally cumbersome. The methodological approach presented in this study offers an easy way to construct robust surrogate models representing different phenomena in each stage of the manufacturing process. The number of initial sampling points, needed for the construction of surrogate models, depends on the complexity and the dimensionality of the problem and should be carefully selected to achieve the desirable accuracy. The computational efficiency of surrogate models allows the incorporation of process modelling into the production line through integration with process monitoring and control equipment. This is of great importance, since control actions can be taken not only based on process monitoring signals but also on robust real time process modelling predictions related to process outcomes i.e. duration and occurrence of defects.

The developed surrogate model methodology faces limitations in cases of problems with high dimensionality of input variables. The initial points required for the construction of surrogate models based on Kriging has a nonlinear dependence on dimensionality of the problem. In this study the maximum number of input parameters were eight, in which case 30,000 initial points

were required to achieve the desirable accuracy. Further increase of model dimensions makes the application of Kriging difficult due to the large number of required initial points and the corresponding computational resources needed for the estimation of Kriging parameters. Dimensionality reduction methods such as Principal Component Analysis (PCA) [29] can be used to treat problems with high dimensionality. PCA transforms a large set of correlated variables into a smaller number of uncorrelated variables. This capability will allow the incorporation of surrogate models into stochastic simulations that represent input parameters variability with random fields, i.e. fibre imperfections [8, 10], preform local permeability variations [25, 30].

Process monito

related to the final part quality. The ability to scale down the size of the sensor -currently at about 250 μm can enhance the non-intrusive character of the concept

The form of the sensing element lends itself to direct incorporation in fabrics, offering potential routes for producing smart materials with process monitoring capabilities. Self-sensing multi-functional composites can be developed by tufting the lineal dielectric sensor within the preform. The use of copper wire as tufted through thickness reinforcement has been demonstrated successfully [158] showing significant improvements in electrical and mechanical properties as well as lighting strike performance [159]. Furthermore, a local dielectric sensor can be tufted in the preform making a spot cure sensor for the monitoring of curing. The integrated sensing system has also the potential provide health monitoring information related to potential defects induced during service life.

10.5. Real time uncertainty estimation in composites manufacture

The on-line integration of process simulation models with process sensing systems requires successful implementation of an inverse solution scheme. Activity in this area in the literature has focused on off-line property identification such as preform permeability and thermal properties. Stochastic simulation, performed prior to process, provide predictions with high uncertainty up to 30% considering the full input process parameters variability. The developed inversion methodology overcomes limitations presented in deterministic approaches, addressing successfully potential ill-posedness of inverse flow and cure problems considering the prior distribution of stochastic variables. The capabilities of the inversion scheme have been demonstrated in both filling and curing of LCM processing providing low uncertainty real time estimations of process duration at a fraction of the process duration. The methodology presented in this study is the first comprehensive attempt to integrate process monitoring with process modelling in real time for uncertainty estimation in composites manufacture. The use of fast surrogate models is a major enabler of this approach. The successful online implementation of the inversion procedure eliminates the gap between stochastic simulation and manufacturing process.

These findings highlight the importance of combining process simulations with process monitoring for the reduction of the uncertainty of off-line estimations. The design of the monitoring system setup with respect to the number and position of monitoring sensors within the part plays a significant role in the convergence behaviour of the inverse solution. Inefficient design of the embedded sensing system can result in low sensitivity and convergence issues. Increasing the number of sensors increases the complexity and intrusiveness of the monitoring

system. An optimisation scheme can be applied identifying the optimal trade-off between the number of embedded sensors and the sensitivity of the monitoring system.

The inversion procedure contributes towards the development of a probabilistic hybrid twin for composites manufacture. The integration of models and monitoring within an inverse solution allows the on-line estimation of the evolution of the process and its uncertainty. This can be utilised to carry out control and corrective actions during manufacturing, potentially increasing process efficiency, improving part quality and reducing process failures and defects. The integration of the inversion scheme with control can be achieved by developing the framework illustrated in Figure 10.1. The inversion scheme is fed by monitoring data predicting the probability of defects formation, such as micro/macro voids, distortion or exotherms and the final degree of cure, within the part. At the end of each estimation cycle the results of the inversion scheme are imported into a control system calculating the actions needed to prevent or correct potential undesirable effects. The updated process parameters such as activation/deactivation of injection/outlet ports, cure profile changes or tool geometry adjustments, applied to manufacturing process by appropriate actuators, are inserted back to the inverse algorithm as inputs to estimate the process outcomes considering at the same time the new monitoring data batch. This loop continues until the completion of the process, where the final inverse solution, which includes probabilistic estimations of defects formation within the part, is imported into the quality inspection equipment. Non-destructive testing can be focused on areas of the part with high probability of defects formation as identified by the inversion scheme. This will result in improved quality and significant savings of inspection time.

Figure 10.1 Framework for integration of the inversion scheme with control system and

ports, applied pressure and/or flow rate and tool temperature can be identified which can lead to minimisation of the filling duration and presence of defects with minimum variance.

Stochastic multi-objective optimisation identifies a set of optimal solutions forming a trade-off between the process duration and defects formation alongside with the corresponding variability. The selection of an optimal solution among the others in the Pareto set is crucial and should be tailored according to each application type. The consideration of process outcomes variability as objective in optimisation scheme can provide additional paths for the decision of design process parameters. In cases of high performance parts, where the specifications of part quality are strict, the focus can be placed on optimal solutions which result in defect occurrence below the tolerance thresholds with minimum variance. In processes where the production rate is the highest priority, optimal solutions corresponding to sort process cycles would be preferred. The identification of optimal solutions with the minimum variance is particularly important in processes in which the variability is higher due to the use of lower specification materials and tooling equipment.

The stochastic multi-objective optimisation approach developed in this study can be implemented in real time as a means of process control. The proposed framework illustrated in Figure 10.1 can be expanded incorporating the stochastic multi-objective optimisation scheme. In the framework depicted in Figure 10.2 the stochastic multi-objective optimisation scheme is incorporated between the inversion scheme and the control system. The stochastic optimisation scheme can identify optimal and stable using the low uncertainty estimates provided by the inverse algorithm. The identified optimal solution, which includes the updated process design parameters, can be applied to the manufacturing process directly through control actions leading to faster process cycles and improved final part quality. The proposed development would result in a multi-functional automated tool optimising the manufacturing process in real time considering unexpected phenomena occurring during the process.

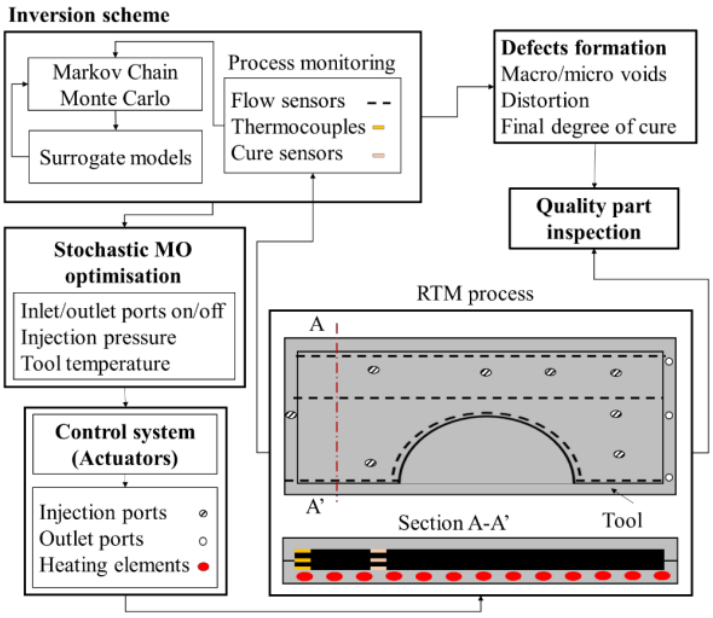

Figure 10.2 Framework for real time uncertainty prediction, stochastic multi-objective optimisation and control in composites manufacture.

10.7. Overview

The findings presented in this study highlight the importance of integrating process monitoring techniques with process modelling for real time low uncertainty estimations of process duration and defects formation. Resin viscosity uncertainty, quantified in this study, affects significantly the filling process introducing variations in filling duration up to 30%. This uncertainty is narrowed down during the manufacturing process by the inversion scheme enhancing the predictive capabilities of process models. The inverse algorithm based on MCMC method takes into account the prior distributions of stochastic variables addressing successfully potential ill-posedness of inverse problems of the filling and curing process. The use of fast surrogate models makes the real time implementation of the inversion procedure computationally feasible. The dielectric sensor developed here presents significant efficiency in terms of monitoring flow and cure process phenomena in LCM processing of carbon composites. The flexibility and the small size of the lineal sensor allow its implementation in manufacture of complex composites parts without affecting preform architecture significantly. The stochastic multi-objective optimisation methodology put forward in this study identifies process design parameters which leads to advanced stability of process outcomes in variations of input parameters. The inversion scheme and stochastic multi-objective optimisation, presented in this

study, can be combined with control to develop an automated optimisation tool operating in real time.

11. Conclusions

The main conclusions of this study are as follows:

- Viscosity variations present in high performance epoxy resins, attributed to discrepancies in initial material state, introduce variability in filling duration of typical composite parts of about 30%.
- Surrogate flow and cure models based on the Kriging technique provide accurate estimations 99% faster than FE models with 2% error, allowing the real time implementation of computational methods with large number of model evaluations such as Monte Carlo, Markov Chain Monte Carlo and Genetic Algorithms.
- Lineal dielectric sensors comprising two twisted insulated copper wires monitor flow successfully in the filling stage of LCM of carbon composites with an error lower than 3%.
- A woven arrangement of two twisted insulated copper wires can be used to monitor the reaction progress and identify vitrification time during the cure of carbon fibre reinforced composites with a signal sensitivity increased by 25% compared to conventional interdigitated dielectric sensors.
- An inversion scheme integrating on line process monitoring data and surrogate models can be applied to the filling and cure stages of composites manufacturing process in real time, reducing the estimation uncertainty computed by stochastic simulation by 80% and 90% respectively.
- The real time estimation of material properties and boundary conditions in the filling stage of LCM leads to prediction of the filling patterns and duration with 97% accuracy compared to experiments.
- The inversion scheme applied to the cure stage provides real time predictions with 0.9% error compared to experiments at approximately 70% of cure process completion.
- The incorporation of monitoring sensors within the manufacturing tool results in faster convergence of the inverse solution at about 50% of process duration.
- The integration of a stochastic simulation into a multi-objective optimisation framework implemented in the curing stage allows the identification of optimal points with improved stability in terms of corresponding variability by about 20% compared to deterministic optimal solutions.

12. Suggestions for further investigation

Suggestions for further work that can expand the outcomes of this work and also lead to industrial application are presented in the following order of importance:

- Integration of stochastic multi-objective optimisation scheme with the inversion procedure and process control into a single tool operating in parallel with the manufacturing process to identify stable optimal solutions leading to fast and effective process cycles.
- Development of efficient surrogate models representing high dimensionality problems such as fibre orientation random fields. Dimensionality reduction methods such as Principal Component Analysis can be used to capture a large number of correlated variables in a two or three dimensional space.
- Development of self-sensing composites by tufting dielectric sensing lines within the preform. Tufting can provide effective monitoring of in plane flow front evolution and the increase of though the thickness mechanical and electric properties.
- Uncertainty quantification of race tracking effects in LCM processing. Quantification of gap size between the preform and tool edges and its autocorrelation structure using image analysis can provide the datasets required for the development of a one dimensional stochastic object of race tracking permeability. Similarly, the variability of porous media permeability for flexible tooling LCM process variants can be quantified as a random field.
- Development of an optimisation scheme for the selection of the number and position of lineal flow sensors within the part minimising monitoring system intrusiveness while maximising sensitivity.
- Application of the stochastic multi-objective optimisation framework to the filling stage, setting as objectives the minimisation of the filling duration and presence of defects with respect to variability using the number and position of inlets/outlets, the injection pressure and flow rate and the applied tool temperature as design parameters.

References

[1] Hale J. Boeing 787 from the ground up. Aero 2006;4:17–24.

[2] Marsh G. Airbus A350 XWB update. Reinf Plast 2010;54(6):20–4.

[3] Airbus S.A.S. Airbus in Illescas delivers first A350 XWB Wing Lower Cover to Airbus in Broughton. https://www.airbus.com/newsroom/press-releases/en/2011/09/airbus-in-illescas-delivers-first-a350-xwb-wing-lower-cover-to-airbus-in-broughton.html/ 2011, (accessed 07 January 2019).

[4] Skordos AA, Partridge IK. Inverse heat transfer for optimization and on-line thermal properties estimation in composites curing. Inverse Probl Sci Eng 2004;12(2):157–72.

[5] Mesogitis TS, Skordos AA, Long AC. Uncertainty in the manufacturing of fibrous thermosetting composites: A review. Compos Part A Appl Sci Manuf 2014;57(2):67–75.

[6] Potter KD. Understanding the origins of defects and variability in composites manufacture. In: Proceedings of 17th Int. Conf. Compos. Mater. Edinburgh, UK, July, 2009, p. 1–19.

[7] Potter K, Khan B, Wisnom M, Bell T, Stevens J. Variability , fibre waviness and misalignment in the determination of the properties of composite materials and structures. Compos Part A Appl Sci Manuf 2008;39(9):1343–54.

[8] Mesogitis TS, Skordos AA, Long AC. Stochastic simulation of the influence of fibre path variability on the formation of residual stress and shape distortion. Polym Compos 2015;38(12):2642–52.

[9] Yu WR, Harrison P, Long AC. Finite element forming simulation of NCF considering natural variability of fiber direction. In: Proceedings of 8th Int. ESAFORM Conf. Mater. Form. Cluj-Napoca, Romania, April, 2005, p. 1–4.

[10] Skordos AA, Sutcliffe MPF. Stochastic simulation of woven composites forming. Compos Sci Technol 2008;68(1):283–96.

[11] Endruweit A, McGregor P, Long AC, Johnson MS. Influence of the fabric architecture on the variations in experimentally determined in-plane permeability values. Compos Sci Technol 2006;66(11–12):1778–92.

[12] Pan R, Liang Z, Zhang C, Wang BEN. Statistical characterization of fiber permeability for composite manufacturing. Polym Compos 2000;21(6):996–1006.

[13] Vanaerschot A, Cox BN, Lomov S V, Vandepitte D. Stochastic framework for quantifying the geometrical variability of laminated textile composites using micro-

computed tomography. Compos Part A Appl Sci Manuf 2013;44(1):122–31.

[14] Vanaerschot A, Cox BN, Lomov S V, Vandepitte D. Stochastic multi-scale modelling of textile composites based on internal geometry variability. Comput Struct 2013;122(6):55–64.

[15] Skordos AA, Aceves CM, Sutcliffe MPF. A simplified rate dependent model of forming and wrinkling of pre-impregnated woven composites. Compos Part A Appl Sci Manuf 2007;38(5):1318–30.

[16] Avgoulas EI, Mulvihill DM, Endruweit A, Sutcliffe MPF, Warrior NA, Focatiis DSA De, et al. Frictional behaviour of non-crimp fabrics (NCFs) in contact with a forming tool. Tribol Int 2018;121(5):71–7.

[17] Cao J, Akkerman R, Boisse P, Chen J, Cheng HS, de Graaf EF, Gorczycad JL, Harrisone P, Hivetc G, Launayc J, Leea W, Liud L, Lomovf SV, Longe A, Luyckerc E, Morestinc F, Padvoiskisa J, Penga XQ, Sherwoodd J, Stoilovaf TZ, Taog XM, Verpoestf I, Willemsf A, Wiggerse J, Yug TX, Zhug B. Characterization of mechanical behavior of woven fabrics: Experimental methods and benchmark results. Compos Part A Appl Sci Manuf 2008;39(6):1037–53.

[18] Belov EB, Lomov S V, Verpoest I, Peters T, Roose D, Parnas RS. Modelling of permeability of textile reinforcements : lattice Boltzmann method. Compos Sci Technol 2004;64(7–8):1069–80.

[19] Hoes K, Dinescu D, Sol H, Parnas RS, Lomov S. Study of nesting induced scatter of permeability values in layered reinforcement fabrics. Compos Part A Appl Sci Manuf 2004;35(12):1407–18.

[20] Li C, Potter K, Wisnom MR, Stringer G. In-situ measurement of chemical shrinkage of MY750 epoxy resin by a novel gravimetric method. Compos Sci Technol 2004;64(1):55–64.

[21] Hoes K, Dinescu D, Sol H, Vanheule M, Parnas RS, Luo Y, Verpoest I. New set-up for measurement of permeability properties of fibrous reinforcements for RTM. Compos Part A Appl Sci Manuf 2002;33(7):959–69.

[22] Endruweit A, Gommer F, Long AC. Stochastic analysis of fibre volume fraction and permeability in fibre bundles with random filament arrangement. Compos Part A 2013;49(6):109–18.

[23] Stenberg R, Bergstro R. In-plane permeability measurements: a nordic round-robin study. Compos Part A Appl Sci Manuf 2000;31(1):29–43.

[24] Guilleminot J, Deléglise M, Binetruy C, Krawczak P. Stochastic modeling of resin flow

in fibrous media in liquid composite molding. In: Proceedings of 16th Int. Conf. Compos. Mater. Kyoto, Japan, July, 2007, p. 1–8.

[25] Zhang F, Cosson B, Comas-Cardona S, Binetruy C. Efficient stochastic simulation approach for RTM process with random fibrous permeability. Compos Sci Technol 2011;71(12):1478–85.

[26] Markicevic B, Heider D, Advani SG, Walsh S. Stochastic modeling of preform heterogeneity to address dry spots formation in the VARTM Process. Compos Part A Appl Sci Manuf 2005;36(6):851–8.

[27] Yun M, Carella T, Simacek P, Advani S. Stochastic modeling of through the thickness permeability variation in a fabric and its effect on void formation during Vacuum Assisted Resin Transfer Molding. Compos Sci Technol 2017;149(9):100–7.

[28] Yun M young, Simacek P, Binetruy C, Advani S. Random field generation of stochastically varying through the thickness permeability of a plain woven fabric. Compos Sci Technol 2018;159(5):199–207.

[29] Yun M young, Lopez E, Chinesta F, Advani S. Manifold embedding of heterogeneity in permeability of a woven fabric for optimization of the VARTM process. Compos Sci Technol 2018;168(11):238–45.

[30] Park M, Tretyakov M V. Stochastic resin transfer molding process. SIAM/ASA J Uncertain Quantif 2016;5(1):1110–35.

[31] Friedrich M, Exner W, Wietgrefe M. Sensitivity analysis of influencing factors on impregnation process of closed mould RTM. CEAS Aeronaut J 2014;2(1–4):195–202.

[32] Endruweit A, Long AC. Influence of stochastic variations in the fibre spacing on the permeability of bi-directional textile fabrics. Compos Part A Appl Sci Manuf 2006;37(5):679–94.

[33] Kracke C, Nonn A, Koch C, Nebe M, Schmidt E, Bickerton S, Gries T, Mitschang P. Interaction of textile variability and flow channel distribution systems on flow front progression in the RTM process. Compos Part A Appl Sci Manuf 2018;106:70–81.

[34] Li J, Zhang C, Liang R, Wang B. Statistical characterization and robust design of RTM processes. Compos Part A Appl Sci Manuf 2005;36(5):564–80.

[35] Lawrence JM, Barr J, Karmakar R, Advani SG. Characterization of preform permeability in the presence of race tracking. Compos Part A Appl Sci Manuf 2004;35(12):1393–405.

[36] Li J, Zhang C, Liang Z, Wang B. Stochastic simulation based approach for statistical analysis and characterization of composites manufacturing processes. J Manuf Syst

2006;25(2):108–21.

[37] Mesogitis TS, Skordos AA, Long AC. Stochastic simulation of the influence of cure kinetics uncertainty on composites cure. Compos Sci Technol 2015;110(4):145–51.

[38] Mesogitis TS, Skordos AA, Long AC. Stochastic heat transfer simulation of the cure of advanced composites. J Compos Mater 2016;50(21):2971–86.

[39] Padmanabhan SK, Pitchumani R. Stochastic analysis of isothermal cure of resin systems. Polym Compos 1999;20(1):72.

[40] Acquah C, Datskov I, Mawardi A, Zhang F, Achenie LEK, Pitchumani R, Santos E. Optimization under uncertainty of a composite fabrication process using a deterministic one-stage approach. Comput Chem Eng 2006;30(6–7):947–60.

[41] Padmanabhan SK, Pitchumani R. Stochastic modeling of nonisothermal flow during resin transfer molding. Heat Mass Transf 1999;42(16):3057–70.

[42] Ghanem RG, Spanos PD. Stochastic Finite Element Method: Response Statistics. Stoch. Finite Elem. A Spectr. Approach, Springer; 1991, p. 101–19.

[43] Huang S, Mahadevan S, Rebba R. Collocation-based stochastic finite element analysis for random field problems. Probabilistic Eng Mech 2007;22(2):194–205.

[44] Skordos AA, Karkanas PI, Partridge IK. A dielectric sensor for measuring flow in resin transfer moulding. Meas Sci Technol 2000;11(1):25–31.

[45] Kueh SRM, Advani SG, Parnas RS. Sensor placement study for online flow monitoring in liquid composite molding. Polym Compos 2000;21(3):436–49.

[46] Dominauskas A, Heider D, Gillespie JW. Electric time-domain reflectometry sensor for online flow sensing in liquid composite molding processing. Compos Part A Appl Sci Manuf 2003;34(1):67–74.

[47] Barooah P, Sun J. Lineal sensors for flow sensing in liquid injection molding of composites. J Mater Process Manuf Sci 1999;7(4):416–27.

[48] Luthy T, Ermanni P. Linear direct current sensing system for flow monitoring in liquid composite moulding. Compos Part A Appl Sci Manuf 2002;33(3):385–97.

[49] Skordos AA, Partridge IK. Dielectric flow sensing in resin transfer moulding of carbon fibre reinforced composites. Plast Rubber Compos Process Appl 2000;29(8):391–4.

[50] Buchmann C, Filsinger J, Ladstätter E. Investigation of Electrical Time Domain Reflectometry for infusion and cure monitoring in combination with electrically conductive fibers and tooling materials. Compos Part B Eng 2016;94(6):389–98.

[51] Gupta N, Sundaram R. Fiber optic sensors for monitoring flow in vacuum enhanced resin infusion technology (VERITy) process. Compos Part A Appl Sci Manuf

2009;40(8):1065−70.

[52]

[64] Mijovic J, Andjelic S. A study of reaction kinetics by near-Infrared Spectroscopy. 1. Comprehensive analysis of a model epoxy/amine system. Macromolecules 1995;28(8):2787–96.

[65] Mijović J, Andjelić S. In situ real-time monitoring of reactive systems by remote fibre-optic near-infra-red spectroscopy. Polymer 1995;36(19):3783–6.

[66] Fernando GF, Liu T, Crosby P, Doyle C, Martin A, Brooks D, et al. A multi-purpose optical fibre sensor design for fibre reinforced composite materials. Meas Sci Technol 1997;8(10):1065–79.

[67] Mijović J, Andjelić S. Monitoring of reactive processing by remote mid infra-red spectroscopy. Polymer 1996;37(8):1295–303.

[68] Levy RL, Schwab SD. Monitoring the composite curing process with a fluorescence-based fiber-optic sensor. Polym Compos 1991;12(2):96–101.

[69] Stroeks A, Shmorhun M, Jamieson AM, Simha R. Cure monitoring of epoxy resins by excimer fluorescence. Polymer 1988;29(3):467–70.

[70] Wang FW, Lowry RE, Fanconi BM. Novel fluorescence method for cure monitoring of epoxy resins. Polymer 1986;27(10):1529–32.

[71] Liu YM, Ganesh C, Steele JPH, Jones JE. Fiber optic sensor development for real-time in-situ epoxy cure monitoring. J Compos Mater 1997;31(1):87–102.

[72] Maistros GM, Partridge IK. Monitoring autoclave cure in commercial carbon fibre/epoxy composites. Compos Part B Eng 1998;29(3):245–50.

[73] Bellucci F, Valentino M, Monetta T, Nicodemo L, Kenny J, Nicolais L, Mijovic J. Impedance spectroscopy of reactive polymers. 1. J Polym Sci Part B Polym Phys 1994;32(15):2519–27.

[74] Mijović J, Andjelic S, Fitz B, Zurawsky W, Mondragon I, Bellucci F, Nicolais L. Impedance spectroscopy of reactive polymers. 3. Correlations between dielectric, spectroscopic, and rheological properties during cure of a trifunctional epoxy resin. J Polym Sci Part B Polym Phys 1996;34(2):379–88.

[75] Day DR. Dielectric determination of cure state during non-isothermal cure. Polym Eng Sci 1989;29(5):334–8.

[76] Levita G, Livi A, Rolla PA, Culicchi C. Dielectric monitoring of epoxy cure. J Polym Sci Part B Polym Phys 1996;34(16):2731–7.

[77] McIlhagger A, Brown D, Hill B. Development of a dielectric system for the on-line cure monitoring of the resin transfer moulding process. Compos Part A Appl Sci Manuf 2000;31(12):1373–81.

[78] Maistros GM, Partridge IK. Dielectric monitoring of cure in a commercial carbon-fibre composite. Compos Sci Technol 1995;53(4):355–9.

[79] Mijović J, Kenny JM, Maffezzoli A, Trivisano A, Bellucci F, Nicolais L. The principles of dielectric measurements for in situ monitoring of composite processing. Compos Sci Technol 1993;49(3):277–90.

[80] Mijovic J, Yee CFW. Use of complex impedance to monitor the progress of reactions in epoxy/amine model systems. Macromolecules 1994;27(25):7287–93.

[81] Maïstros GM, Block H, Bucknall CB, Partridge IK. Dielectric monitoring of phase separation during cure of blends of epoxy resin with carboxyl-terminated poly(butadiene-co-acrylonitrile). Polymer 1992;33(21):4470–8.

[82] Li C, Cao M, Wang R, Wang Z, Qiao Y, Wan L, Tian Q, Liu H., Zhang D, Liang T, Tang C. Fiber-optic composite cure sensor: Monitoring the curing process of composite material based on intensity modulation. Compos Sci Technol 2003;63(12):1749–58.

[83] Kim J-S, Lee DG. On-line cure monitoring and viscosity measurement of carbon fiber epoxy composite materials. J Mater Process Technol 1993;37(1):405–16.

[84] Maffezzoli A, Quarta E, Luprano VAM, Montagna G, Nicolais L. Cure monitoring of epoxy matrices for composites by ultrasonic wave propagation. J Appl Polym Sci 1999;73(9):1969–77.

[85] Shepard DD, Smith KR. A new ultrasonic measurement system for the cure monitoring of thermosetting resins and composites. J Therm Anal 1997;49(1):95–100.

[86] Lionetto F, Maffezzoli A. Monitoring the cure state of thermosetting resins by ultrasound. Materials 2013;6(9):3783–804.

[87] Fomitchov PA, Kim YK, Kromine AK, Krishnaswamy S. Laser ultrasonic array system for real-time cure monitoring of polymer-matrix composites. J Compos Mater 2002;36(15):1889–901.

[88] Papadakis EP. Monitoring the moduli of polymers with ultrasound. J Appl Phys 1974;45(3):1218–22.

[89] Schmachtenberg E, Schulte Zur Heide J, Töpker J. Application of ultrasonics for the process control of Resin Transfer Moulding (RTM). Polym Test 2005;24(3):330–8.

[90] Mitra B, Booth DJ. Remote cure monitoring of epoxy materials using optical techniques. Ultrasonics 1998;35(8):569–72.

[91] Harrold RT, Sanjana ZN. Acoustic waveguide monitoring of the cure and structural integrity of composite materials. Polym Eng Sci 2004;26(5):367–72.

[92] Pineda U, Montés N, Sánchez F, Domenech1 L. Experimental evaluation of heat transfer

measurements during LCM processes by intrusive and non-intrusive heat flux sensors. In: Proceedings of 18th Int. Conf. Compos. Mater., Jeju Island, Korea, Aug, 2011, p. 1–6.

[93] Lai L, Carman G, Chiou S, Kukuchek P, Echternach D. Processing monitoring of carbon/phenolic composites using smart sensors. Smart Mater Struct 1995;4(2):118–25.

[94] Perry MJ, Lee LJ, Lee CW. On-Line Cure Monitoring of Epoxy/Graphite Composites Using a Scaling Analysis and a Dual Heat Flux Sensor. J Compos Mater 1992;26(2):274–92.

[95] Pineda U, Bensadoun F, Ruiz E, Montés N, Sánchez F. Experimental analysis by thermography and heat flux sensors of the curing stage of composite parts made by resin infusion. In: Proceedings of 15th Eur. Conf. Compos. Mater. Venice, Italy, June, 2012, p. 24–8.

[96] Di Fratta C, Klunker F, Trochu F, Ermanni P. Characterization of textile permeability as a function of fiber volume content with a single unidirectional injection experiment. Compos Part A Appl Sci Manuf 2015;77(10):238–47.

[97] Konstantopoulos S, Grössing H, Patrick H, Weninger M, Schledjewski R. Determination of the unsaturated through-thickness permeability of fibrous preforms based on flow front detection by ultrasound. Polym Compos 2018;39(2):360–7.

[98] Nielsen DR, Pitchumani R. Control of flow in resin transfer molding with real-time preform permeability estimation. Polym Compos 2002;23(6):1087–110.

[99] Bai-Jian W, Yu-Sung C, Yuan Y, Jun F. Online estimation and monitoring of local permeability in resin transfer molding. Polym Compos 2016;37(4):1249–58.

[100] Musavi Naeenian SM, Sefidgar M, Pourshaghaghy A. The inverse estimation of kinetic parameters of composite materials without using DSC data. Mech Compos Mater 2008;44(4):379–88.

[101] Scott EP, Beck J V. Estimation of Thermal Properties in Epoxy Matrix/Carbon Fiber Composite Materials. J Compos Mater 1992;26(1):132–49.

[102] Tikhonov AN. On the solution of ill-posed problems and the method of regularization. Dokl. Akad. Nauk 1963;151(3):501–4.

[103] Xiong XT, Shi WX, Hon YC. A one-dimensional inverse problem in composite materials: Regularization and error estimates. Appl Math Model 2015;39(18):5480–94.

[104] Wang J, Zabaras N. Using Bayesian statistics in the estimation of heat source in radiation. Int J Heat Mass Transf 2005;48(1):15–29.

[105] Wang J, Zabaras N. A Bayesian inference approach to the inverse heat conduction

problem. Int J Heat Mass Transf 2004;47(17):3927–41.

[106] Kaipio JP, Fox C. The Bayesian framework for inverse problems in heat transfer. Heat Transf Eng 2011;32(9):83.

[107] Matveev M, Endruweit A, Long A, Iglesias M, Tretyakov M. Part I: Bayesian inversion algorithm for estimation local variations in permeability and porosity of reinforcements using experimental data. 2018.

[108] Iglesias M, Park M, Tretyakov M V. Bayesian inversion in resin transfer molding. Inverse Probl 2018;34(10):105002.

[109] Matveev M, Endruweit A, Long A, Iglesias M, Tretyakov M. Part II: Algorithms for active control of resin infusion in RTM process with uncertainties. 2018.

[110] Ruiz E, Achim V, Soukane S, Trochu F, Bréard J. Optimization of injection flow rate to minimize micro/macro-voids formation in resin transfer molded composites. Compos Sci Technol 2006;66(3):475–86.

[111] Li M, Tucker CL. Optimal curing for thermoset matrix composites: Thermochemical and consolidation considerations. Polym Compos 2002;23(5):739–57.

[112] Ruiz E, Trochu F. Multi-criteria thermal optimization in liquid composite molding to reduce processing stresses and cycle time. Compos Part A Appl Sci Manuf 2006;37(6):913–24.

[113] Pantelelis NG. Optimised cure cycles for resin transfer moulding. Compos Sci Technol 2003;63(2):249–64.

[114] Skordos AA, Sutcliffe MPF, Klintworth JW, Adolfsson P. Multi-objective optimisation of woven composite draping using genetic algorithms. 27th Int. Conf. SAMPE Eur., Paris, France, March, 2006, p. 1–6.

[115] Ratle F, Achim V, Trochu F. Evolutionary operators for optimal gate location in liquid composite moulding. Appl Soft Comput J 2009;9(2):817–23.

[116] Okabe T, Oya Y, Yamamoto G, Sato J, Matsumiya T, Matsuzaki R, Yashiro S, Obayashi S. Multi-objective optimization for resin transfer molding process. Compos Part A Appl Sci Manuf 2017;92(1):1–9.

[117] Baran I, Tutum CC, Hattel JH. Optimization of the thermosetting pultrusion process by using hybrid and mixed integer genetic algorithms. Appl Compos Mater 2013;20(4):449–63.

[118] Tutum CC, Baran I, Deb K. Optimum design of pultrusion process via evolutionary multi-objective optimization. Int J Adv Manuf Technol 2014;72(9–12):1205–17.

[119] Tutum CC, Baran I, Hattel J. Utilizing multiple objectives for the optimization of the

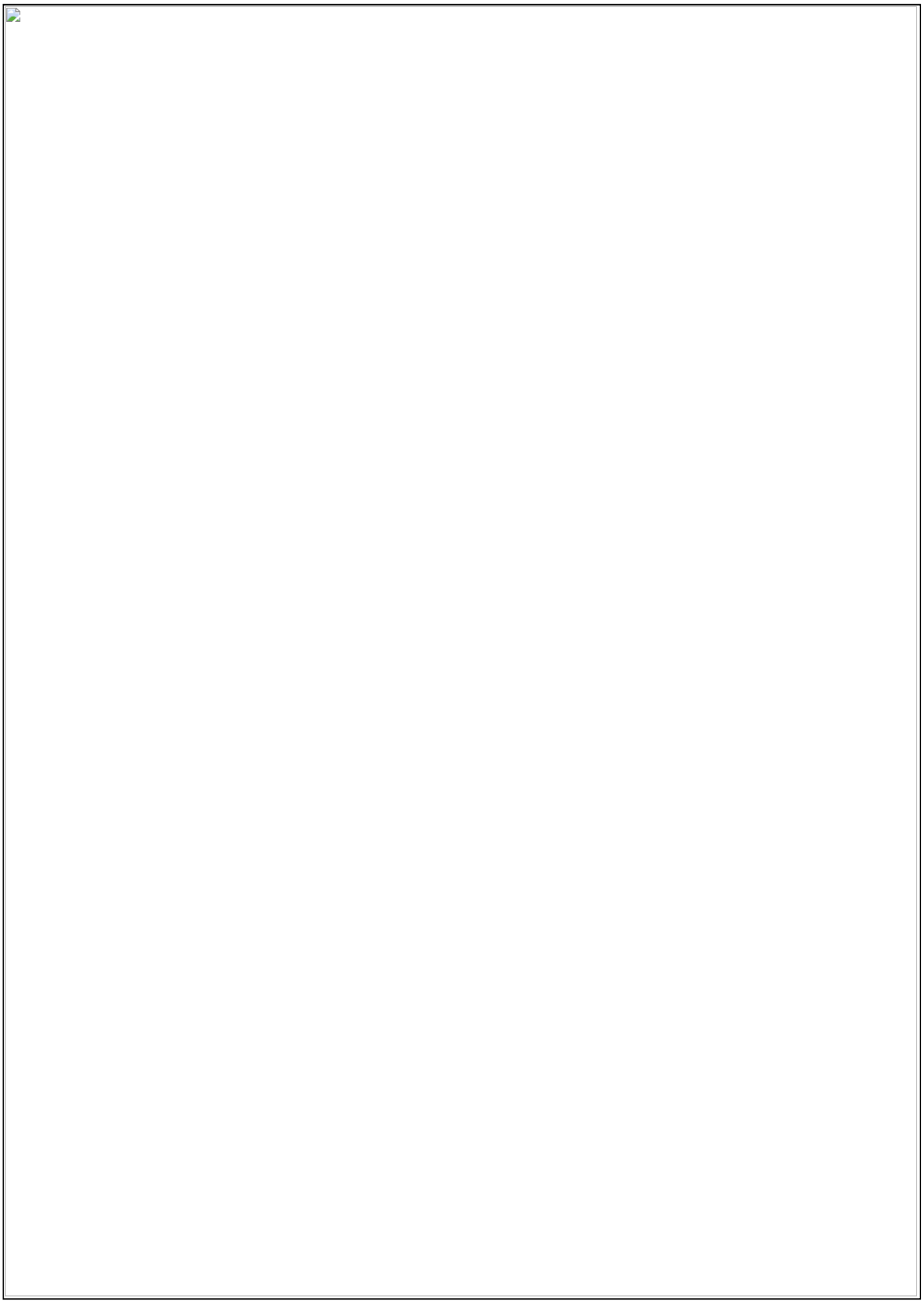

Sci 1989;4(4):409–35.

[138] Santner T, Williams B NW. The design and analysis of computer experiments. New York: Springer-Verlag New York; 2003.

[139] Lophaven SN, Nielsen HB, Søndergaard J. DACE-A Matlab Kriging toolbox, version 2.0. 2002.

[140] Smith W. On the simulation and estimation of the mean- reverting Ornstein-Uhlenbeck process. 2010.

[141] Matsumoto M, Nishimura T. Mersenne Twister: A 623-dimensionally Equidistributed Uniform Pseudo-random Number Generator. ACM Trans Model Comput Simul 1998;8(1):3–30.

[142] Gregory P. Bayesian Logical Data Analysis for the Physical Sciences: A Comparative Approach with Mathematica® Support. Cambridge: Cambridge University Press; 2005.

[143] Roberts GO, Gelman A, Gilks WR. Weak convergence and optimal scaling of random walk Metropolis algorithms. Ann Appl Probab 1997;7(1):110–20.

[144] Kollie TG, Horton JL, Carr KR, Herskovitz MB, Mossman CA. Temperature measurement errors with type K (Chromel vs Alumel) thermocouples due to short-ranged ordering in Chromel. Rev Sci Instrum 1975;46(11):1447–61.

[145] Barati R. Application of excel solver for parameter estimation of the nonlinear Muskingum models. KSCE J Civ Eng 2013;17(5):1139–48.

[146] Karkanas PI, Partridge IK. Cure modeling and monitoring of epoxy/amine resin systems. I. Cure kinetics modeling. J Appl Polym Sci 2000;77(7):1419–31.

[147] Pascault JP, Williams RJJ. Relationships between glass transition temperature and conversion. Polym Bull 1990;24(1):115–21.

[148] Farmer JD, Covert EE. Thermal conductivity of a thermosetting advanced composite during its cure. J Thermophys Heat Transf 1996;10(3):467–75.

[149] Box GEP, Jenkins GM, Reinsel GC, Ljung GM. Time series analysis: forecasting and control. John Wiley & Sons; 2015.

[150] Frigo M, Johnson SG. FFTW: An adaptive software architecture for the FFT. In Acoustics, Speech and Signal Processing, 1998. Proceedings of the 1998 IEEE International Conference. Seattle, Washington, USA, May, 1998. vol. 3. p. 1381-1384..

[151] Kazilas MC, Skordos AA, Partridge IK. Parameter estimation in equivalent circuit analysis of dielectric cure monitoring signals using genetic algorithms. Inverse Probl Sci Eng 2005;13(2):157–76.

[152] Fournier J, Williams G, Duch C, Aldridge GA. Changes in molecular dynamics during

bulk polymerization of an epoxide-amine system as studied by dielectric relaxation spectroscopy. Macromolecules 1996;29(22):7097–107.

[153] Skordos AA, Partridge IK. Determination of the degree of cure under dynamic and isothermal curing conditions with electrical impedance spectroscopy. J Polym Sci Part B Polym Phys 2004;42(1):146–54.

[154] Andjelić S, Mijović J, Bellucci F. Impedance spectroscopy of reactive polymers. 5. Impedance as a measure of chemical and physical changes in glass formers. J Polym Sci Part B Polym Phys 1998;36(4):641–53.

[155] Struzziero G, Remy B, Skordos AA. Measurement of thermal conductivity of epoxy resins during cure. J Appl Polym Sci 2018;47015(8):1–10.

[156] Kueh SRM, Advani SG, Parnas RS. Sensor placement study for online flow monitoring in liquid composite molding. Polym Compos 2000;21(3):436–49.

[157] Hexcel HexFlow® RTM6 epoxy system for Resin Transfer Moulding monocomponent system Product Data. www.hexcel.com. 2009.

[158] Lombetti DM. Tufting of complex composite structures. Cranfield University, 2015.

[159] Lombetti DM, Skordos AA. Lightning strike and delamination performance of metal tufted carbon composites. Compos Struct 2019;209(2):694–9.

Appendix

List of publications

Journal publications:

1. Tifkitsis KI, Mesogitis TS, Struzziero G, Skordos AA. "Stochastic multi-objective optimisation of the cure process of thick laminates", Composites Par A. Applied Science and Manufacturing, 2018; **112**:383-94.
2. Tifkitsis KI, Skordos AA. "A novel dielectric sensor for process monitoring of carbon fibre composites manufacture", Composites Part A. Applied Science and Manufacturing, 2018 (under review).
3. Tifkitsis KI, Skordos AA. "Real time uncertainty estimation in filling stage of RTM process", Composites Part A. Applied Science and Manufacturing, 2018 (under review).
4. Tifkitsis KI, Skordos AA. "Real time inverse solution of the composites cure heat transfer problem under uncertainty", Numerical Heat Transfer, Part A: Applications, 2018 (under review).

Conference publications:

1. Tifkitsis KI, Skordos AA. "On line uncertainty estimation in composites manufacturing", 9th International Conference on Inverse Problems in Engineering, Waterloo, Canada, 2017.
2. Tifkitsis KI, Skordos AA. "Stochastic multi-objective optimisation of composites manufacturing process", UNCECOMP 2017 - 2nd International Conference on Uncertainty Quantification in Computational Sciences and Engineering, Rhodes island, Greece, 2017
3. Tifkitsis KI, Skordos AA. "Real time uncertainty estimation in flow process of composites manufacturing", 14th International Conference on Flow Processing in Composite Materials, Lulea, Sweden, 2018.
4. Tifkitsis KI, Skordos AA. "Integration of stochastic process simulation and real time process monitoring of LCM", SAMPE Europe Conference, Southampton, UK, 2018.
5. Tifkitsis KI, Skordos AA. "A novel dielectric sensor for process monitoring of carbon fibre composites manufacturing", 11th International Conference on Manufacturing of Advanced Composites, Nottingham, UK, 2018.